STUDY OF STELLAR STREAMS IN THE GALAXY

A THESIS

SUBMITTED FOR THE DEGREE OF

DOCTOR OF PHILOSOPHY

IN

THE FACULTY OF SCIENCE

CALICUT UNIVERSITY

BY

RAMYA P

INDIAN INSTITUTE OF ASTROPHYSICS
BANGALORE - 560 034, INDIA

FEBRUARY 2014

In loving memory of my most beloved Grand Father,
Late Shri. Pezhumkattil Kuttan Nair

DECLARATION

I hereby declare that the thesis entitled **"Study of stellar streams in the Galaxy"** is the result of investigations carried out by me at the Indian Institute of Astrophysics (IIA), Bangalore, under the joint supervision of Prof. B Eswar Reddy (IIA) and Dr. M M Musthafa (University of Calicut). This thesis has not been submitted for the award of any degree, diploma, associateship, fellowship etc. of any University or Institute.

Ramya P
(Ph.D candidate)

CERTIFICATE

This is to certify that the thesis entitled **"Study of stellar streams in the Galaxy"** submitted to the University of Calicut by Ms. Ramya P for the award of the degree of Doctor of Philosophy in the Faculty of Science, is based on the results of investigations carried out by her under our joint supervision and guidance, at the Indian Institute of Astrophysics. This thesis has not been submitted for the award of any degree, diploma, associateship, fellowship etc. of any University or Institute.

Dr. M M Musthafa
(Co-Supervisor)

University of Calicut
Calicut

Prof. B Eswar Reddy
(Thesis Supervisor)

Indian Institute of Astrophysics
Bangalore

ACKNOWLEDGEMENTS

During my Ph.D work at IIA, many people helped me in one way or the other. I sincerely thank all of them. A few of them are particularly mentioned here.

First of all, I am deeply indebted to my thesis supervisor Prof. B Eswar Reddy, for introducing the exciting field of *stellar streams* to me for my Ph.D thesis. He supported me throughout my thesis, with his patience, great scientific intuitions and knowledge of the field. He always encouraged me to work independently, while at the same time providing me with timely guidance whenever needed. This thesis would not have happened, without his sincere efforts and time. I am extremely thankful to my co-guide Dr. M M Musthafa, Department of Physics, University of Calicut, for his support and encouragement throughout. I owe many thanks to Prof. David L. Lambert, McDonald Observatory, Texas, USA, for many insightful discussions and for the spectra he obtained for this work.

I thank IIA and its administration for providing facilities and maintaining academic environment at IIA. I take this opportunity to thank all the Faculty members of IIA for the interesting discussions on various topics and all my course instructors for giving a wonderful learning experience during the first year of Ph.D. I thank Prof. Gajendra Pandey and my doctoral committee members - Prof. Sunetra Giridhar and Prof. Annapurni Subramaniam for the useful suggestions and feedbacks. My sincere thanks to the library staff and the system support staff of IIA, for all the timely assistance provided to me. Special thanks goes to Dr. B A Varghese, for his time spent for me in solving various software related issues. I express my gratitude to the staff of Vainu Bappu Observatory, Kavalur, for the support provided during my observations using VBT. I offer my gratitude to the Faculty members of the Department of Physics, the staff members of both Directorate of Research and the office of Head of the Physics department, of University of Calicut, for all the help.

I sincerely thank all my dear teachers at Sree Krishna College, Guruvayur, Little Flower College, Guruvayur, St. Mary's G.H.S Chowwannur, Holy Child Convent G.U.P.S, Cherlayam and Emmanuel L.P.S, Alathur for having played an important role in my life, by inspiring me to pursue my dreams. At this point, I heartfully thank all my friends and class mates of school days and college days especially of graduation and post-graduation at Sree Krishna College, Guruvayur, Kerala, who gave me the confidence to face the challenges.

I thank all the staff members at CREST campus of IIA, who made my stay so comfortable during the one year of research traineeship over there. I am grateful to Prof. T P Prabhu, Prof. G C Anupama and Prof. B C Bhatt for all their support given to me during this period. My special thanks to Prof. D K Sahu, from whom I learned the first lessons of telescope operations and CCD data analysis. I thank all my friends - Naslim, Brinda, Roopa, Ravi, Sasi, Manju, Viswanath and Vyas, with a special mention to my very dear friend Aman, who made my first ever hostel life at CREST enjoyable and worth remembering. I thank Rumpa, Blesson, Uday and Bharat for the useful discussions and special thanks to Ramya S, for all the care and help given to me, during my time at CREST.

Coming back to my Ph.D years at IIA, its time to thank all of them, who made my life at IIA, especially at Bhaskara Guest House, a memorable one. First of all, I am truly blessed to have a wonderful friend like Arjo (Arya Dhar), who was there for me, in all the good and bad times, with his famous smile and care. My heartfelt gratitude to him, and to his parents for their affection towards me. I extend my gratitude to my office mate Smitha, for her care and affection for me, and for critically reading the early draft of this thesis. Special thanks to Jessy, Honey, Drisya, Sreejith, Susmitha and Bhavya for being there, as my strong support. I thank Rathna for all the useful discussions and all other batch mate friends - Sindhuja, Indu, Hema, Prashant, Dinesh, Krishna and Sudhakar for giving me such a wonderful company. I thank all my junior and senior friends - Anantha, Samyaday, Avijeet, Vineet, Sajal, Arun, Sreeja, Madhulita, Ananta, Girjesh, Veeresh, Vigeesh, Tapan, Jayashree, Swati, Koshy, Nataraj, Nagaraju, Amit, Joby, Smitha Rao, Maya, Preethi, Nirmal, Avinash, Annu, Ambily, Anand, Joice, Prasanna Deshmukh, Sreenivas Prasanna, Manpreet, Chandrasekhar and Rubi, who made my life at Bhaskara, a cherishable experience.

I feel nervous and run out of words, as I am going to say *thank you* to my family members, without whom I am nothing. I am extremely grateful to my parents, my dear Amma & Achan (Mrs. Anitha & Mr. Radhakrishnan) and my brother Kannan for *everything*. I am indebted to my dear Ammamma & Muthachan (Grand Parents) for their unconditional love and support. I thank all the members of my family, the list is too long to be listed here, for making my world so beautiful. Finally, let me conclude by saying *thank you Lord for being with me all the way*.

Ramya

TABLE OF CONTENTS

Abstract

Our Galaxy, also called the Milky Way, is a spiral galaxy consisting of three major distinct components: bulge, disc and halo. They differ from each other in their structural as well as kinematical and chemical properties. Bulge contains both the young and old stars, and large amounts of gas and dust. The region is known for high star formation rate. On the other hand halo is very sparse containing mostly old stars (>10 Gyr) and stars from accreted satellite galaxies. Disc of the Galaxy contains stars of very young age (few Myrs) and stars as old as 10 Gyr. Spiral structure of the Galaxy forms the disc. Apart from the large scale structures, the Milky Way has small scale structures which include open clusters, OB associations, globular clusters, and star forming regions. Some of these structures are gravitationally tightly bound in a smaller region in the space (globular clusters, Open Clusters) and some are loosely bound in relatively larger regions (OB associations etc). As they rotate about the center of the Galaxy, the spatially coherent groups disintegrate over time due to interactions with large structures such as molecular clouds. Probably, most of the stars in the field were once part of the spatially coherent groups. Also, there may be stars in the field resulting from the disintegrated merged satellite galaxies. The field stars are spatially unbound.

The subject of our study is not of the spatially bound or unbound stars but of stars of kinematically coherent groups. There are stars in the field which are spatially incoherent but coherent in their kinematics. In general, field stars within the disc or in the halo are expected to exhibit random motion such as three dimensional Schwarzschild velocity distribution. Contrary to this general expectation, it has been known in the literature for more than a century, there exist stars that form clumps in the velocity space sharing common motion. The kinematically coherent groups are known as moving groups or stellar streams. Stellar streams are defined as the tight clumps or over-densities of stars present in the velocity space over and above the large scale structure that Schwarzschild distribution can reproduce in the solar neighborhood. The pioneering work of identification of such moving groups in the Galaxy was done by O. J. Eggen (Eggen 1996 and references therein) who thought the moving groups are the resultant of cluster disintegration or cluster dispersion. Thus, many of the moving groups are named after the clusters or bright stars in the sky which share kinematics with the moving group stars. For example, the Sirius moving group is named after a bright star Sirius and the Hyades moving group is named after a young open cluster Hyades.

Though, the concept of stellar streams has been around in the literature for long, their origin and evolution within the Galaxy remained very poorly understood. There are three

principal hypothesis for the existence of the moving groups: a) cluster disruption, b) satellite accretion, c) dynamical perturbations. According to cluster disruption hypothesis, open clusters while orbiting around the Galactic center get disrupted due to encounters with the giant molecular clouds. The dispersed cluster members retain parental kinematics, thus forming moving groups in the Galaxy. As per the satellite accretion scenario, the Milky Way accretes its dwarf satellite galaxies and the debris of such accreted satellites remain in the Galaxy as stellar streams or moving groups. Finally, dynamical perturbation scenario says that the dynamical perturbations introduced by non-axisymmetric components of the Galaxy such as the bar and/or spiral arms or the merging satellite galaxies produce moving groups.

In this thesis we studied a few identified moving groups based on chemical tagging of their member stars. The chemical tagging of stars (Freeman & Bland-Hawthorn 2002) is an innovative method to understand stars' past history as their chemistry remains unaltered, to a large extent, from the chemical composition of the natal clouds from which the stars formed. We performed abundance analysis of member stars of the moving groups in search of clues to their origin. Understanding of the moving groups has far reaching significance in decoding the chronological evolution of the Galaxy.

We chose five well defined moving groups for this study. Of which two moving groups (Arcturus and AF06) belong to the thick disc and three (Hercules, Hyades and Sirius moving groups) belong to the thin disc component of the Galaxy. Main sequence member stars of the moving groups of the thick disc are chosen from the study of Arifyanto & Fuchs (2006). The Red giant member stars of the moving groups of the thin disc are chosen from the study of Famaey et al. (2005). All together, a total of 169 stars (44 main sequence dwarfs and 125 red giants) are subjected to the abundance study.

Chemical tagging of stars requires accurate photospheric elemental abundance determination which in turn requires high resolution spectra of individual stars. The high resolution (R $\sim$ 60,000) and high quality (S/N $\geq$ 100) spectra of member stars of the selected moving groups are obtained using two telescopes - 2.7 m Harlan J. Smith Telescope, located at the McDonald Observatory, Texas, USA and the 2.3 m Vainu Bappu Telescope located at the Vainu Bappu Observatory, Kavalur, India. The raw spectral data are reduced and calibrated using various spectral image processing tools.

Determination of stellar abundances requires determination of photospheric parameters : the effective surface temperature (T_{eff}), the surface gravity (log g), microturbulent velocity (ξ_t), and the metallicity ([Fe/H]). The parameters are determined using both photometry and spectroscopy. The photometric determinations involve optical and in-

frared colours and empirical colour-temperature relations (Alonso et al. 1996, Alonso et al. 1999). Spectroscopic determination of stellar atmospheric parameters require the equivalent widths measured from high resolution spectra, atomic data, stellar theoretical model atmosphers (Kurucz 1998) and spectral synthesis and analysis package. Parameters determined from photometry and spectroscopy agree very well within uncertainties. For the abundance study we adopted parameters determined from spectroscopy. For each member star, abundances of 16 elements of different nucleosynthesis groups- Fe-peak, α-process, and s-process are obtained. Ages are estimated using colour-luminosity diagram and the computed stellar evolutionary tracks (Demarque et al. 2004).

To extract clues of the origin of moving groups, we combined the abundance information with the kinematic information. The kinematic motion (U, V, W) for each of the member star is derived using radial velocity derived from the observed spectrum and the astrometry (parallax and proper motion) taken from HIPPARCOS catalogue (van Leeuwen 2007). Here, the velocity U is the radial component towards or away from the Galactic center, V is the tangential component, positive in the direction of Galactic rotation, and W is the vertical component, positive towards the North Galactic Pole. Distribution of member stars in the velocity spaces ($U - V$, $W - V$ etc.) studied in comparision with the member stars of the background thick and thin disc. Other parameters such as angular momentum components per unit mass - J_x, J_y and J_z are derived to segregate groups more easily. The orbital parameters - The apogalactic distance (R_{max}), perigalactic distance (R_{min}), the maximum and minimum distances away from the Galactic plane (Z_{max} and Z_{min}), eccentricity of the orbit (e) are calculated by integrating U, V, W components of the stars over the Galactic potential. The probabilities with which stars belong to any one of three major components of the Galaxy (thin disc, thick disc, halo) are calculated using derived kinematic motion and the recipe given in Reddy et al. (2006) (see references there in).

Arcturus stream and AF06 stream are high velocity streams. Kinematic results show that member stars of both the moving groups belong to the thick disc. Abundance results show that member stars of Arcturus and AF06 are metal poor and very old (10-14 Gyr). Other abundance trends ([Fe/H] versus [X/Fe], where X is any element other than Fe) are very similar to the background thick disc stars. Wide range in metallicity and ages rule out the possibility of the stars originated from the dispersed open clusters. Kinematics and abundance results suggest that the two streams might have formed as a result of resonant interactions of spirals/bar with stellar orbits. Moving groups being originated from accreted satellite dwarf galaxies is also unlikely as none of the nearby dwarf galaxies

abundances are similar to abundances of the moving groups.

Hercules, Hyades-Pleiades and Sirius are the low velocity streams. Kinematic results show that the groups revolve around the Galactic center in near circular orbits and belong to the thin disc component of the Galaxy. Abundance results suggest relatively a wide range of metallicity and ages compared to what one would expect for member stars of spatially coherent groups such as open clusters and associations. However, we find a fraction of stars exhibiting very similar ages and abundances which are characteristics of open clusters. For example, many of the Sirius moving group stars seems to be originated from the Sirius super cluster which is in a particular stage of disintegration. Contrary to the recent results, results in this study suggest that the Hercules moving group consists of only thin disc stars and not a mixture of thin and thick disc stars. Results also suggest that it is highly unlikely that any of the streams originated outside of the Milky Way. It is very likely that dynamical perturbations caused either by external forces and/or by interactions of bar and spirals with stellar orbits within the Galaxy are playing the role in creating moving clusters. In that sense, the moving groups may be a transient phenomenon.

The major findings of the thesis are :

1. None of the five streams studied here show chemical homogeneity and coevality, the defining properties of spatially coherent groups.
2. None of the streams studied here show any sort of similarity with the dwarf satellite galaxies of the Milky Way galaxy.
3. Abundance patterns are indistinguishable from that of the background Galactic disc (thin or thick disc) field stars.
4. A fraction of member stars of the moving groups (in particular Sirius, Hyades) seems to be originated from the cluster dispersion.

List of Publications

- **Refereed Journals**

  Chemical compositions of stars in two stellar streams from the Galactic thick disc, P. Ramya., Bacham E. Reddy., David L. Lambert., 2012, MNRAS, 425, 3188

- **In preparation**

  The abundance pattern of Hercules stream,
  P. Ramya., Bacham E. Reddy., David L. Lambert. (To be submitted)

- **Conference proceedings/Non refereed publications**

  Moving groups in the Galactic disc
  P. Ramya and Bacham E. Reddy., Proceedings of the IAU Symposium No. 298 on Setting the scene for GAIA and LAMOST - the current and next generations of surveys and models, held during 20-24, May, 2013 (In Press)

  Moving groups in the Galactic thin disc
  P. Ramya and Bacham E. Reddy., Proceedings of the 30th Meeting of the Astronomical Society of India, held during 20-22 February 2013. To be published as ASI Conference series

  Stellar streams in the Galactic thick disk: preliminary results
  P. Ramya and Bacham E. Reddy., Proceedings of the International Workshop on Stellar Spectral Libraries, held during 5-11, December, 2011. ASI Conference Series, 2012, Vol. 6, pp 125-131 , Edited by Ph. Prugniel & H. P. Singh

  Arcturus stream : A case study
  P. Ramya and Bacham E. Reddy., Proceedings of the 29th Meeting of the Astronomical Society of India, held during 23-25 February, 2011. ASI Conference Series, Vol. 3, Edited by P. Khare and C.H. IshwaraChandra, 2011, p. 120

LIST OF FIGURES

LIST OF TABLES

CHAPTER 1

INTRODUCTION

1.1 Our Galaxy : Early Developments

Our galaxy also known as the *Milky Way*, with reference to a Greek word *galaktos* meaning *milk*, is the most studied galaxy. It is also referred as *the Galaxy*. A part of it can be seen on clear dark nights as a faint white band of light stretching across the sky. Study of its constituent *stars* will help to understand its structure and evolution. The structure of it is the intense subject of many studies for the last four centuries. A brief account of it is given here.

In 1610s, Galileo Galilei using the 3 cm refractor suggested that the luminous band seen as the Milky Way is in fact consists of a number of bright stars. Based on star counting, Sir William Herschel (Herschel 1784, Herschel 1785) suggested that the Milky Way is a flattened elliptical system (5:1 axis ratio) with the Sun being very near to the center. About a century later, similar conclusion was arrived by Jacobus Kapteyn (Kapteyn & van Rhijn 1920, Kapteyn 1922) based on photographic data of star counts, proper motions and distances. He concluded that the Milky Way is a flattened spheroidal system of around 15 kpc wide and 3 kpc thick, and the Sun is located slightly out of the plane at a distance of about 650 pc. It was Harlow Shapley who from his study of globular clusters (GC) suggested that the center of the Galaxy lies towards Sagittarius as the distribution of GCs peaked in that direction. He also noted that, the Sun is not the center of the Milky Way and is 15 kpc (Shapley & Shapley 1919) away from the center. In all of these studies interstellar medium (ISM) and its absorption of star light was not taken into account. This led to overestimation of distances. By comparing photometric distances of open clusters with those measured using angular diameter (which is independent of extinction) Trumpler (1930) discovered an evidence of existence of absorbing medium. This led to better

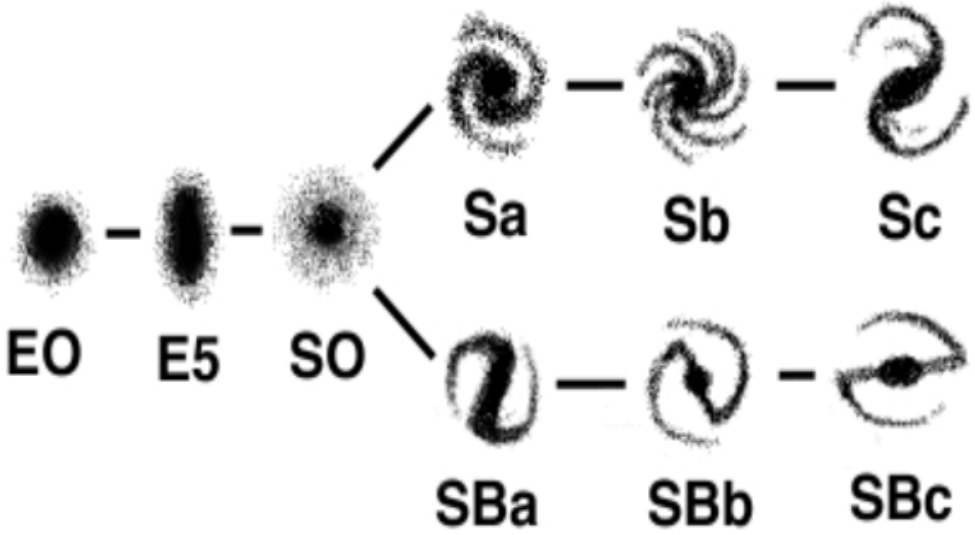

Figure 1.1: Hubble's tuning fork diagram.
Credit : *http://btc.montana.edu/ceres/html/Galaxy/galhubble.html*

understanding of the Galaxy structure.

Another major development was the discovery in 1920 by Edwin Hubble that the Galaxy is not unique, and there are many such galaxies in the universe. Studying the Cepheid variables, using the then largest telescope the Mount Wilson telescope of 2.5 m aperture, Hubble estimated their distances of about 300 kpc and noted that they are too far to be inside the Galaxy. This led to the studies of extragalactic astronomy. Also, Hubble morphologically classified galaxies into spirals, ellipticals and irregulars (lenticular) and placed them in a certain order, which is known as Hubble tuning fork diagram (see Figure 1.1). Elliptical galaxies (E) appear smooth and structureless. They are relatively less active with very little or no gas. Spiral galaxies have a centrally condensed bulge, halo and a flattened disc containing spiral arms. They contain large amount of gas and dust. Depending on the presence or absence of a bar, a spiral is classified as a barred spiral (SB) and a normal spiral (S) respectively. Spiral galaxies are further subclassified depending on how tightly the spiral arms are wound. Sa galaxies have their arms tightly wound and have conspicuous bulges, whereas Sc galaxies have open arms. Lenticular galaxies (S0) are intermediate between ellipticals and spirals in the tuning fork diagram. They have disc

and flattened bulge, but they lack gas and dust and spiral arms. Our galaxy is a barred spiral, classified as SBbc. It has got around 10^{11} stars in it.

1.2 Stellar Kinematics in the Galaxy : Basic Definitions

The space motion or kinematics of a star can be estimated from knowing star's astrometry (positon, distance, proper motion) and radial velocity.

To specify position of stars in the sky, different coordinate systems such as Horizontal, Equatorial, Ecliptic and Galactic coordinate systems are being used. The equatorial coordinate system, centered at the center of the earth, is the most widely used system in modern astronomical observations. The coordinates in the systems are: − Right Ascension (α) and Declination (δ) which are measured in hours and degrees, respectively. The distance to the stars is one of the fundamental parameters. It is measured mostly by parallax (π) method. As the earth moves around the Sun, the nearby stars appear to move with respect to more distant background stars. The apparent motion gives rise to stellar parallax, which is the angle subtended at the star by the mean radius of the earth's orbit around the Sun. Parallax is usually expressed in units of arc second. Another component is the proper motion (μ) which is star's velocity perpendicular to our line of sight, expressed in units of arcsecond per year. This has as two components $\mu_\alpha \cos\delta$ and μ_δ, representing changes in α and δ of the star, respectively. Similarly, the linear velocity of the star perpendicular to the line of sight is expressed as $V_t = \frac{4.75\mu}{\pi}$. Radial velocity ($V_r$) is the component of a star's velocity parallel to our line of sight, expressed in units of km s^{-1}. Radial velocity is determined from the Doppler shift of spectral lines of a star. Hence, the magnitude of total space velocity of a star can be written as $V_{tot} = \sqrt{V_t^2 + V_r^2}$.

For a given star, using its position, distance, proper motion and radial velocity, its space motion in the Galaxy can be expressed as components of velocity along three mutually perpendicular directions − radial, tangential and vertical directions in the Galaxy (see Figure 1.2). In general, it is customary to use U for the radial component towards or away from the Galactic center, V for the tangential component in the direction of Galactic rotation, and W for the vertical component perpendicular to the Galactic plane. The components can be expressed with respect to the Sun (heliocentric) or the Local Standard of Rest (LSR), or the Fundamental Standard of Rest (FSR). The Galactic center defines the Fundamental Standard of Rest (FSR). Local Standard of Rest (LSR) is a hypothetical, perfectly circular orbit around the center of the Galaxy passing through the present location of the Sun. LSR has no radial or vertical components of motion, as it is in perfectly

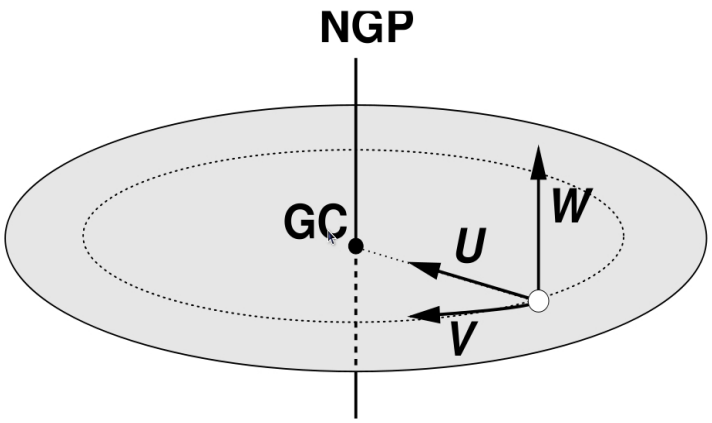

Figure 1.2: The stellar velocity components. Credit : *Thesis of T Bensby*

circular motion. The components of LSR's motion with respect to FSR is (U_0, V_0, W_0 = 0, 220, 0) km s^{-1}. The velocity of LSR is generally determined as the average velocity of stars in the solar neighborhood including the Sun, and the value V_0 = 220 km s^{-1} for LSR is recommended by International Astronomical Union (IAU). The total space velocity of a star with respect to LSR is generally called the peculiar velocity of a star. The space motion (UVW) is calculated using the recipe given in Johnson & Soderblom (1987).

1.3 Large Scale Structures of the Galaxy

The Galaxy contains many substructures each of them differs from other in their kinematics, structure, chemistry etc. There are four large structures : nucleus, bulge, disc and halo.

Nucleus is the innermost part of the Galaxy. It is a very small region of a size of the order of 3 pc which is known to host a black hole. Bulge is a spherical system surrounding the nucleus with a radius of the order of 2-3 kpc. Bulge contains old (RR Lyrae etc) as well as young stars with a wide range in metallicity (see the review, Wyse et al. 1997). The disc of the Galaxy hosts the spiral arms, and much of the gas (atomic and molecular hydrogen) and dust (graphite, silicates etc). Spiral arms are the sites of vigorous star formation (H II regions) with very young stars (dominated by O type and B type stars). In general, disc is occupied by stars having a range of age and metallicity from young metal rich stars to old metal poor stars. The disc is rotationally supported. The rotation curve, a graphical representation of rotational velocity as a function of distance from

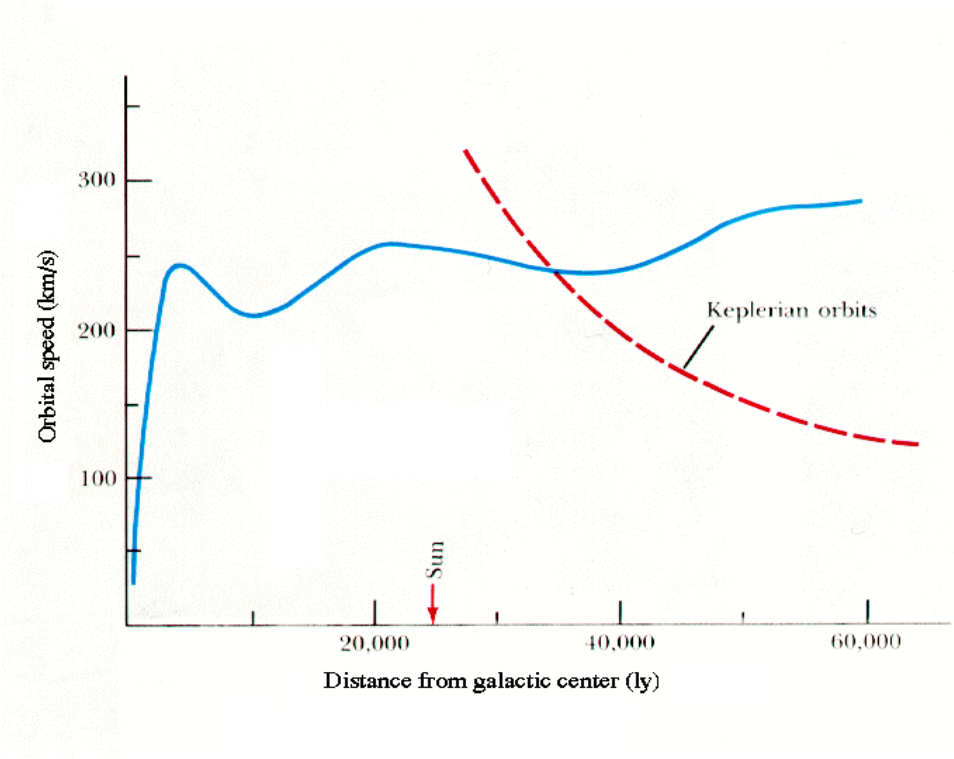

Figure 1.3: The rotation curve of the Galaxy
Credit : *http://abyss.uoregon.edu/ js/ast123/lectures/lec16.html*

the Galactic center, is shown in Figure 1.3. The flat region suggests differential rotation for the disc. In differential rotation, angular velocity $\Omega = \frac{v}{r}$ decreases radially outwards (with increasing r), while rotational velocity v remains constant. The rotation curve of the Galaxy is obtained by tracing the rotation of gas component (CO, H I etc) in the Galaxy. The flat rotation curve of the Galaxy suggests large amount of dark matter in the Galaxy. Since our study is focussed on stellar streams in the disc, it is relevant to have more discussion on the disc structure.

The disc of the Galaxy is known to have two distinct components: the thin disc and the thick disc. Stellar populations within the thick disc are metal poor, older and have hotter kinematics compared to stellar populations in the thin disc. The suggestion that the disc contains two different structures emerged from the study of brightness distribution of edge-on galaxies (Burstein 1979). The two-component structure for the Milky Way's disc was confirmed by performing star count analysis method using photometric data of a large sample of stars (Gilmore & Reid 1983). The star count or stellar density as a function of distance away from the plane of the Galaxy showed two distinct components as shown in

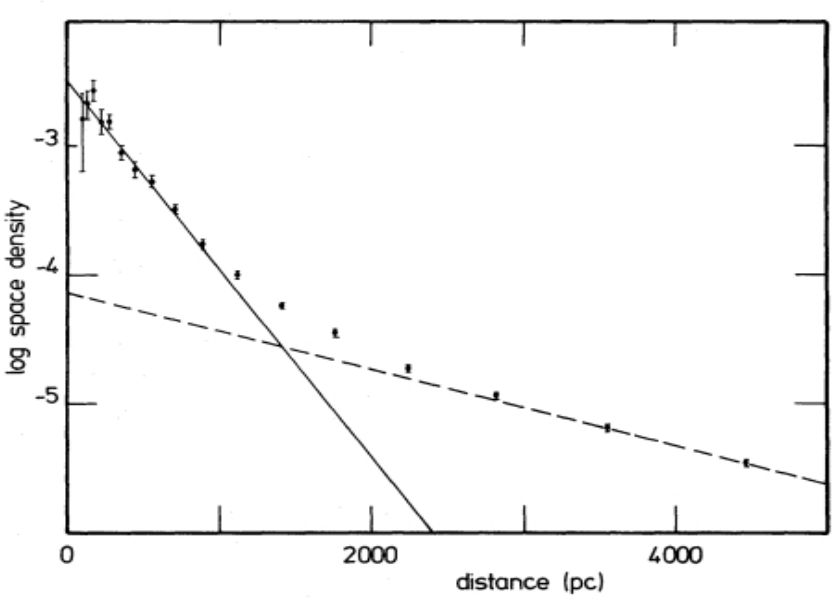

Figure 1.4: The density distribution for stars in the disc (Gilmore & Reid 1983)

the figure (see Figure 1.4, taken from Gilmore & Reid 1983). Two exponential fits (solid and broken lines) are used to best match the observed distribution. The solid line with scale height of $\sim$ 300 pc corresponds to the thin disc (sometimes also referred as the 'old disc′) and the broken line with scale height of $\sim$ 1350 pc corresponds to the so called 'thick disc′. There exists no clear boundary between the two discs. As the figure implies, thin disc stars dominate upto a distance of 1 kpc, from the plane of the Galaxy, beyond which the thick disc stars dominate (Reddy 2010).

Halo is a large, almost spherical system surrounding the whole visible Galaxy. It may extend upto 30 kpc or more in radius. There is no clear separation between the bulge and the halo. It has no gas or dust, hence no star formation in it. It contains old metal poor stars such as RR Lyrae variables, subdwarfs and globular clusters. As there is negligible extinction, even outer halo can be accessed with present large telescopes (see the review, Helmi 2008).

1.4 Schwarzschild Distribution and Velocity Ellipsoid

Kinematical properties of any stellar population can be characterized by specifying their mean velocity, velocity dispersion and the deviation from the LSR velocity. Given the kinematics, one could estimate the probability of a star being a part of a particular stellar

population with certain kinematic distribution. Below we outline the procedure to tag stars to different stellar agregates in the Galaxy.

The kinematic distribution of an unbiased group of stars follows a form of Schwarzschild distribution. Schwarzschild distribution is a three dimensional Gaussian distribution in all the three directions (U, V, W), with different dispersions ($\sigma_U \neq \sigma_V \neq \sigma_W$) in different directions. U, V and W are a set of orthogonal axes, which may or may not coincide with the standard radial (U), tangential (V), and vertical (W) velocity components shown in Figure 1.2. The probability that the velocity components (U, V, W) of a star lie in the elemental velocity space ($dUdVdW$), is expressed as a Schwarzschild distribution as given below,

$$P(U,V,W)dUdVdW = \frac{dUdVdW}{2\pi^{3/2}\sigma_U\sigma_V\sigma_W} \exp\left(-\left(\frac{U^2}{\sigma_U^2}+\frac{(V-V_a)^2}{\sigma_V^2}+\frac{W^2}{\sigma_W^2}\right)\right) \qquad (1.1)$$

Where, V_a is the asymmetric drift which is defined as the velocity deviation by which stellar population lags the LSR in the direction of Galactic rotation (V-component). For young stars, (e.g. spiral arm population) which are in near circular orbits, the asymmetric drift is very small, while for halo stars, it is maximum (for e.g. $V_a \sim -220$ km s^{-1}). The term asymmetric drift is the addition to the original form of Schwarzschild distribution, in order to reproduce the characteristic asymmetry of the stellar population. The functional form of the distribution is akin to that of an ellipsoid of semi axes lengths σ_U, σ_V and σ_W. It is also called Schwarzschild velocity ellipsoid, and the density of stars in the velocity space is constant on ellipsoidal surfaces.

As a result of interaction of stars and molecular clouds in the disc, velocity dispersion of stars in the disc tend to increase with time. Observations show, velocity dispersion is least for very young stars, and high for older stars. In general, disc kinematics imply large tangential or rotational velocity around the Galactic center, small velocity dispersion and small asymmetric drift. The spiral arm populations, Galactic clusters etc show disc kinematics, and are usually called disc populations. On the other hand, halo kinematics imply least rotational velocity, large velocity dispersions, large asymmetric drift with respect to LSR, and highly eccentric orbits. The very old metal poor stars like globular clusters, RR Lyrae stars etc., show halo kinematics, and are generally called halo populations. The halo population makes only a very small percentage of the solar neighborhood stars, and they make up most of the so called high velocity stars in the solar neighborhood. The velocity dispersions (σ_U, σ_V, σ_W) and the asymmetric drifts V_a of the thin disc, the thick disc, and the halo are given in Table 1.1 (see Reddy et al. 2006 and references therein).

Table 1.1: Thin disc, Thick disc and Halo - Kinematic characteristics

Component	σ_U	σ_V	σ_W	V_a
Thin disc	43	28	17	-9
Thick disc	67	51	42	-48
Halo	131	106	85	-220

1.5 Stellar Populations and Solar Neighborhood

The concept of stellar populations is known for over six decades (Baade 1944). Based on properties like age, metallicity, kinematics, and spatial distribution of stars in the Galaxy, Baade classified stars into two distinct populations − Population I and II. Population I stars are young with ages less than 10 Gyr and reside in the disc. They include Galactic clusters (open clusters), Cepheid variables, spiral arm population of very young, metal rich and massive O and B type stars. Population II stars are located in the spheroidal components of the Galaxy, mainly in the halo, and to some extent in the Galactic bulge. They are old with ages more than 10 Gyr and metal poor. Population II includes globular clusters, RR Lyrae variables etc. There is also a third catagory of stars called population III which are extremely metal poor, and are known to have formed in the very early epochs of the Galaxy formation. These are very massive and lived very short duration about a few Myrs. Over the period, the meaning of stellar populations has changed considerably (see the review Ivezić et al. 2012). Any sample of stars that share some common property that is appropriate for mapping the Galaxy in the space of various observables is considered to be a population. For example, a group of stars with common spatial, kinematic, chemical, luminosity, and/or age distributions.

Solar neighborhood is a term loosely used in the literature, to refer to the region near to the Sun and taken roughly as the spherical volume centered around the Sun. The Sun is located in the Galactic disc at a radial distance of around 8.5 kpc from the Galactic center. The extent of solar neighborhood is not a well defined parameter. Generally, solar neighborhood is small compared to the size of the entire Galaxy. So it may vary from 10 pc even upto 1-2 kpc, depending on the objects of study. The stellar content of solar neighborhood ranges from old metal poor halo population stars to young metal rich disc population stars. In other words, it is a mixture of thin disc, thick disc and

halo populations. The relative numbers of thin disc, thick disc, and halo stars in the solar vicinity are found to be $f_1 = 0.93$, $f_2 = 0.07$, and $f_3 = 0.006$, respectively (see Reddy et al. 2006 and references therein). It is possible to get accurate three dimensional distribution of solar neighborhood stars in position and velocity spaces, as it is the most accessible region to us.

1.6 Small Scale Structures in the Galaxy

There exist many smaller structures within the major structures. The smaller structures such as open clusters, OB associations, globular clusters differ from one another in one or more properties such as size, shape, kinematics and chemistry. A brief account of each of these smaller structures are given below which are relevant to our study of moving groups in the Galaxy.

1.6.1 Open Clusters

Open clusters are groups of stars, physically bound together by mutual gravitational attraction. They generally have irregular shapes, with stars in them are only loosely bound to each other. They are found in the plane of the Galaxy, mostly in the dusty spiral arms and are also called galactic clusters. Open clusters typically contain few tens to few thousands of stars. They show chemical homogeneity, as they formed from the same molecular cloud. The formation of an open cluster takes relatively short time as compared to the life time of the cluster, and hence the member stars are considered to be coeval. Open cluster members share the same space motion to within the internal velocity dispersion of the cluster (a few tenths of a km s^{-1}). In general, they are young with an age much less than 10 Gyr. Mostly, they are metal rich and are classified as population I stars. Open clusters may have stars of all spectral types with a range of masses. They show disc like kinematics, moving in almost circular orbits around the Galactic center. There are about 1200 open clusters which are known to exist in the Galaxy. However, the expected number of open clusters in the Galaxy is about 100,000. Hyades and Pleiades are examples of well studied young open clusters in the Galaxy.

Open clusters that are very old are rare. As they are loosely bound, they get dispersed with time due to interactions with moecular clouds and spiral arms. However, one may find older open clusters in the outer disc or well above or below the Galactic plane where the concentration of the molecular clouds is less, and hence less encounters which is more favourable for longer survival of open clusters (Carraro et al. 2013a, Carraro et al. 2013b).

1.6.2 OB Associations

OB associations are unbound expanding stellar systems, first defined and recognized by Ambartsumian (1947). They contain hundreds to thousands of massive stars of spectral class O and B which are sparsely populated, typically between a few tens and a few hundreds of light years across. They form in the cores of Giant Molecular Clouds (GMC) in the dusty spiral arms. The powerful winds of the early type stars and the shock waves from the supernova explosions blow away the surrounding gas and dust, making the association to expand away from the same common center, presumably their birth place. In general, they survive for about 30 Myr as coherent entities in the space (Blaauw 1964, Briceño 2009). OB associations form coherent structures in the velocity space, as they share common space motion, which can be perceived as a convergence of the proper motions of the member stars towards a single point on the sky. Also, their internal velocity dispersion is small of the order of few km s^{-1}. They are young population I objects with a stellar mass density < 0.1 $M_{\odot}$ pc^{-3}. They have circular orbits around the Galactic center. A well known example for OB association is the Scorpius-Centaurus Association, the nearest one to us. Although more than 1000 OB associations are expected to be present in the Milky Way, the detected number is less than 70.

1.6.3 Star Forming Regions

Star forming regions are dominated by massive O and B type stars, although they may contain stars of all the spectral classes and masses. The star forming regions are generally referred to as H II regions (Ionized Hydrogen regions). The intense radiation from the young massive stars causes the molecular hydrogen to ionize. Because of high concentration of gas and dust, the regions are optically opaque to us, and are observed in IR and radio wavelengths (see the review Lada & Lada 2003). The star forming regions are associated with spiral arms in the Galaxy, and have highly circular orbits. They may have very high matter density of the order of 100 particles per cm^3, and their size may reach as big as 100 light years and mass upto 6 million solar masses. The well known Orion nebula is the nearest star forming region to us.

1.6.4 Globular Clusters

Globular clusters are compact group of stars held together by strong gravitational attraction. They are spherically symmetric in shape and contain a large number of stars (of the order of millions of stars) with high concentration at the center. They are in highly eccen-

tric orbits. The stars in globular clusters are very metal poor and belong to population II. They are old with age > 10 Gyr. Recent studies suggest some of the globular clusters host heterogeneous stellar population (Gratton et al. 2004, D'Antona et al. 2013). Globular clusters are seen symmetrically distributed around the Galactic center, and most of them are found in the Galactic halo. Also, the thick disc component is known to have globular cluster (e.g. 47 Tuc). In general, stars within the globular cluster exhibit very similar chemical composition, but the composition may differ from one to another globular cluster. As of now, about 140 of globular clusters have been found in the Galaxy. Globular clusters are the oldest and most distant objects in the Galaxy (upto even 30-40 kpc). They contain information regarding the formation and early evolution of the Galaxy.

1.6.5 Stellar Streams

Stellar streams are the groups of stars essentially on the same orbits in the Galactic potential. They can be observed as overdensities in the velocity distribution of solar neighborhood stars. The velocity distribution of such clumps peaks over and above the large scale structure that the Schwarzschild ditribution reproduces. They exhibit very low velocity dispersion, typically of the order of few km s^{-1} or less. They are gravitationally unbound (field stars) and are scattered all over the sky, and can not be observed as physically bound structures like open clusters, OB associations, globular clusters etc. Stellar streams are also known as *moving groups*, although, in literature, the term moving group is widely used to refer to any entity having common kinematics. Sophisticated statistical techniques are deviced to detect such clumps in the space of various parameters. The genuine structures associated with the stellar streams can be detected in different samples of stars, using different techniques. A detailed discussion about the moving groups follows.

1.7 Moving Groups : Early Development

The phenomenon of neighboring stars with similar motions in parallel directions was noticed much early (Mädler 1846). In 1869, Richard A. Proctor, reported in his paper titled "Preliminary Paper on certain Drifting Motions of the Stars" that, in parts of the sky some stars exhibit a well marked tendency to drift in a definite direction (Proctor 1869).

In 1908, Lewis Boss studied a group of field stars moving together in parallel direction, in Taurus constellation, centered on Hyades cluster. He deviced a method known as the convergent point method to determine a possible radiant or convergent point (in terms of the Right Ascension and Declination- (A, D)) of stars (BOSS 1908). He used 39

stars (reported in Preliminary General Catalogue) showing the streaming motion, which he called the Taurus stream (see Figure 1.5). Boss also remarked that five stars (β, γ, δ, ϵ and ζ) of the constellation Ursa Major (Great Bear) have approximately equal proper motion and they move in parallel directions. In 1909, Hertzsprung demonstrated that many widely separated bright stars including Sirius (α Canis Majoris − the brightest star in the night sky) shared the motion of the five co-moving Big Dipper* stars (Hertzsprung 1909). He also proposed many widely separated stars sharing the motion of the Hyades cluster. The convergent point method was put to use by many to predict the existence of

*Big Dipper is a famous asterism, part of Ursa Major constellation

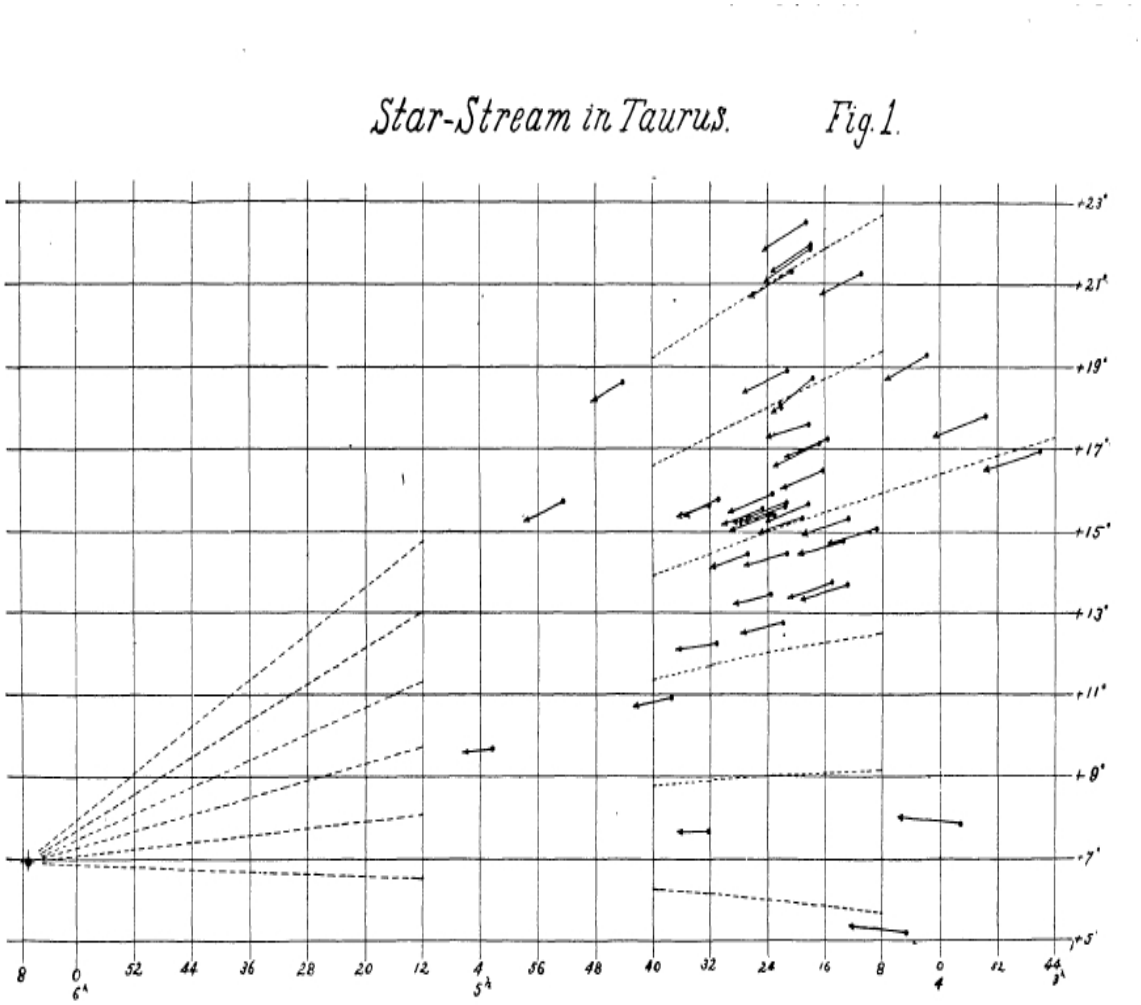

Figure 1.5: The converging proper motions of stars in the Taurus stream (BOSS 1908)

a number of new star streams, many of which got proved to be false detections later. Vela moving cluster (Kapteyn 1914) and Corona Borealis moving group (Ali 1940) were some examples for such spurious group detections.

Much of the modern work on the Galactic streams owe to O. J. Eggen who over the span of $\sim$ 50 years discovered a number of streams and studied them in detail. In 1950s, O. J. Eggen started re-examining the reality of star streams using the suitably modified convergent point method, and ended up in the detection of new star streams. If the group (stream) was associated with a cluster, or shared the motion of the cluster, the name of the cluster was given to it, or else the name of the defining star, whose motion was shared by the stream. Eggen's pioneering work started with the much discussed Hyades group and Ursa Major Group or Sirius group. To assign group membership, the first step was to find out the convergent point (A, D). If the streaming motion was associated with a cluster, the convergent point was found out from the convergence of the proper motions of the defining cluster (for example Hyades stream shares the motion of Hyades cluster). If there was no such defining cluster, the convergent point was found out from the position, radial velocity, proper motion and parallax of the defining star (for example Sirius stream shares the motion of the star Sirius or α Canis Majoris). Stars were admitted to candidacy for membership in a group if the observed position angle of the proper motion, θ_0, agreed with that computed from the group motion (θ_c) to the extent that $\Delta\theta_c \sin\lambda < X$ degree, where λ is the angular distance of the star from the (A, D) of the group motion and X is an arbitrarily chosen tolerance limit. The candidates were then admitted to group membership, only if the difference $(\rho_0 - \rho_c)$ between the observed radial velocity, ρ_0, and that computed from the group motion, ρ_c, was less than or equal to Y km s^{-1}, the chosen tolerance limit.

For the convergent point method to be successful, the velocity components U, V and W for all of the group stars must be precisely the same. But, as the Galactic potential varies more rapidly in the vertical direction than in the plane, the mixing in the direction away from the disc is much more efficient than mixing in the plane of the disc. Hence, the groups of stars can share a similar motion in the components of the velocity in the plane of the disc much longer time than they can do in the direction out of the plane. As a result, the W-motions may be uncoupled from those in (U, V).

To overcome some of the drawbacks of convergent point method, the (U, V, W) components of the space motion were used for assigning group membership. A preferrable method of selecting group members would be computing space motion vectors for a large number of stars and then selecting those having a common motion (mostly giving less

weightage to W-component of the velocity) with their defining cluster or a star. The calculation of U, V, W requires parallax, proper motion and radial veocity, in addition to the position which were lacking in Eggen's period. Hence, after shortlisting the candidates using the previously described procedure, the space motion vectors (U, V, W) were computed for a range of reasonable values of the parallax[†] using the spectral type as the only guide. If, for any value of the parallax, the resulting values of (U, V) could be matched with those of the defining cluster or star within say ± 3 km s^{-1} in both coordinates, the star was accepted as a candidate for membership in the group. The W-component was completely ignored and no star was removed from the list of candidates on the basis of the W-velocity. The group parallax was then computed for these candidates from the relation,

$$\pi_g = \frac{4.7\mu}{45 sin\lambda} \tag{1.2}$$

where, λ is the angular distance of the candidate from the convergent point of the defining cluster. Then, using the luminosity computed from the group parallax, each star was plotted in a color-magnitude diagram (CMD). If the star fell within about 1 magnitude of any sequence of CMD of the defining cluster, it was accepted as a group member. In this way, Eggen confirmed the existence of many moving groups in the solar neighborhood and catalogued (see Table 1.2).

Over a period of time, many other membership criteria were developed for assigning stars to the moving groups. This led to the detection of many new groups apart from the Eggen's groups. The newly detected groups and their adopted membership criteria are discussed in section 1.9.

Table 1.2: The moving groups detected by O. J. Eggen. UVW are heliocentric.

Name of Group	U, V, W km s^{-1}	Defining star/cluster	Reference
	Young disc		
Hyades (Taurus)	-40, -18, -2	Hyades cluster	Eggen (1984)
γ Leonis	-78, -4, -1	γ Leonis (double star system)	Eggen (1959)
Sirius (Ursa Major)	15, 1, -11	Sirius	Eggen (1998e)
Pleiades (Local association)	-9, -27, -12	Pleiades cluster	Eggen (1998d)
IC2391 group	-21, -16, -8.5	IC 2391 cluster	Eggen (1995)

[†]parallaxes were not available for most of the stars

	Old disc		
Arcturus	25, -115, -3	Arcturus	Eggen (1998a)
Wolf 630	25, -33, 13	Wolf 630 (multiple star system)	Eggen (1986)
61 Cygni	-90, -53, -8	61 Cygni (binary system)	Eggen (1971b)
Hercules	-52, -47, -27	ζ Hercules	Eggen (1971a)
ε Indi	-78, -38, 4	ε Indi (star system)	Eggen (1971d)
η Cephei	-33, -97, 10	η Cephei	Eggen (1971d)
σ Puppis	-75, -88, -21	σ Puppis (binary star system)	Eggen (1971d)
HR1614	-4, -58, -11	HR 1614	Eggen (1998a)
	Halo		
Groombridge 1830	+227, -157, -14	Groombridge 1830 (HIC57939)	Eggen (1977)
Kapteyn's	+19, -288, -53	Kapteyn's star	Eggen (1996)
Ross 451	-89, -346, -37	Ross 451 (HIC 56936)	Eggen (1997)

1.8 Formation Scenarios of Moving Groups

Though the modern concept of stellar streams is known in the literature for about five decades, their origin and evolution within the Galaxy is very poorly understood. Here, we provide a brief review of different scenarios that were put forward to explain the origin of stellar streams.

1.8.1 Open Cluster Disruption

It was O. J. Eggen who suggested that stellar streams could be due to cluster disruption (Eggen 1996). Open clusters that reside in the disc, orbit the Galactic center in the quasi circular epicyclic orbits. During their orbits they may encounter giant molecular clouds and/or face tidal forces in the Galactic gravitational field which contribute to the disruption of the cluster over a period of time. The dispersed member stars which are

gravitationally unbound will not be recognizable spatially as cluster members. However, they retain the parental kinematics and form a tube like structure, referred to as *super-clusters* by Eggen. Stars that formed at the same place and time, and stayed together in the disc for a few Galactic rotations are expected to have the same period of revolution (Woolley 1961), and hence the common V-velocities. If the Sun happens to fall inside this tube-like structure, some of the dispersed member stars appear to us scattered all around, but identifiable as a group in the phase space by their common space velocities. Such a group, which is the subset of the supercluster was named as a 'moving group′.

The classical open clusters have ages that span a range of 10^6 to 10^8 years (Lada 2010). The lifetime of open clusters in the Galactic disc is typicaly a few hundred million years (Wielen 1971). There are very few old clusters known confidently, such as Berkeley 17 (~ 12 Gyr ; Phelps 1997), NGC 188 (~ 7 Gyr ; Sarajedini et al. 1999), NGC 6791 (~ 8 Gyr ; Chaboyer et al. 1999). The very old open clusters (> a few G yrs) are found away from the Galactic plane. Since open clusters are loosely bound systems compared to the globular cluster they may dissociate relatively much easier and faster as they encounter molecular clouds and tidal forces (Carraro et al. 2013a). The reason we find relatively old open clusters away from the plane is probably due to less frequent encounters with molecular clouds. HR1614 is an example of the moving group to have formed by the disruption of open cluster (De Silva et al. 2007). However, recent studies based on accurate astrometry contradict the hypothesis that the moving groups are only due to disruption of open clusters.

1.8.2 Satellite Accretion

Currently, the most widely accepted theory of how the structures, including galaxies, formed is the λCDM model (λ Cold Dark Matter). The λCDM model is a cosmological model, according to which structure formation in the universe relies on a hierarchial process driven by gravitational forces of the large scale distribution of cold dark matter. After the Big Bang, local density enhancements in the cold dark matter got amplified and collapsed resulting in the dark matter halos. These structures then merged together to form larger dark matter halos, and became the sites of galaxy formation, driving the baryonic matter into it. This process of merging is an ongoing process, giving rise to larger structures in the universe (see the review Freeman & Bland-Hawthorn 2002).

In the λCDM model, galaxies evolve through mergers which can be of major and/or minor types. In major mergers, two large galaxies of comparable mass and size collide, losing their gas and dust, ultimately losing their identity. The presence of the thin disc,

constraints the major merger history of the Milky Way (Kazantzidis et al. 2008, Navarro 2004). Major mergers are relatively violent processes in which the role of dynamical friction is very efficient, and it takes only a very few number of peri-galactic passages for the complete merger to happen. In the case of minor mergers (mass ratio ~ 1:10), larger galaxies accrete and destroy the smaller galaxies. The debris of the smaller ones become part of the halo, bulge or disc of the larger galaxy. Such remnants of accreted satellites remain as stellar streams in the host galaxy, and are called *tidal streams*. In literature, the name tidal stream is sometimes used to describe streams arising from any disrupting cluster of stars. Minor mergers are relatively slow, as the orbital decay of satellite galaxies is slow (see Figure 1.6). The debris of a tidal stream will remain in the original orbit long after the satellite itself has disappeared. The tidal disruption time scale will depend on the mean density of the satellite and that of the host galaxy.

The Milky Way is a member of the Local Group, and has many satellite galaxies like Canis Major Dwarf, Sagittarius Dwarf, Large Magellanic Cloud, Small Magellanic Cloud etc., gravitationally bound to it. Ibata et al. (1994) discovered that the Galaxy is currently accreting Sagittarius dwarf spheroidal galaxy. However, it has not yet well mixed with the Galactic halo, either spatially or in the velocity space. The tidal stream associated with it wraps around the Galaxy nearly perpendicular to the Galactic plane (Ibata et al. 2001, Belokurov & Zucker 2006, Majewski et al. 2003). This serves as an excellent example for the Galaxy's accretion of its dwarf satellite galaxies. Tidal streams popularly known as *halo streams* can also be found in the disc. Arcturus stream present in the thick disc of the Galaxy was suggested to be originated by merger events (Navarro et al. 2004).

1.8.3 Dynamical Perturbation

Substructures or the moving groups in the disc are also thought of due to dynamical perturbation in the Galaxy either due to spiral arms or due to the Galactic bar. Bar or spiral arms can interact with stellar orbits resulting overdensities in a particular orbit. Stars in the disc, in general, perform epicyclic motions or radial oscillations with an angular frequency κ along with orbital motion with an angular velocity Ω around the center of the Galaxy. The disc is in a state of differential rotation where Ω decreases radially outwards.

The bar is in-plane with the disc extending upto ~ 4 kpc. If we perturb the axisymmetric potential of the rotating disc with that of a small non-axisymmetric component such as the bar we can label the bar rotation as pattern speed Ω_p. The bar can interact with the Galactic material and distort the Galactic orbits. A resonance happens if the dynamical

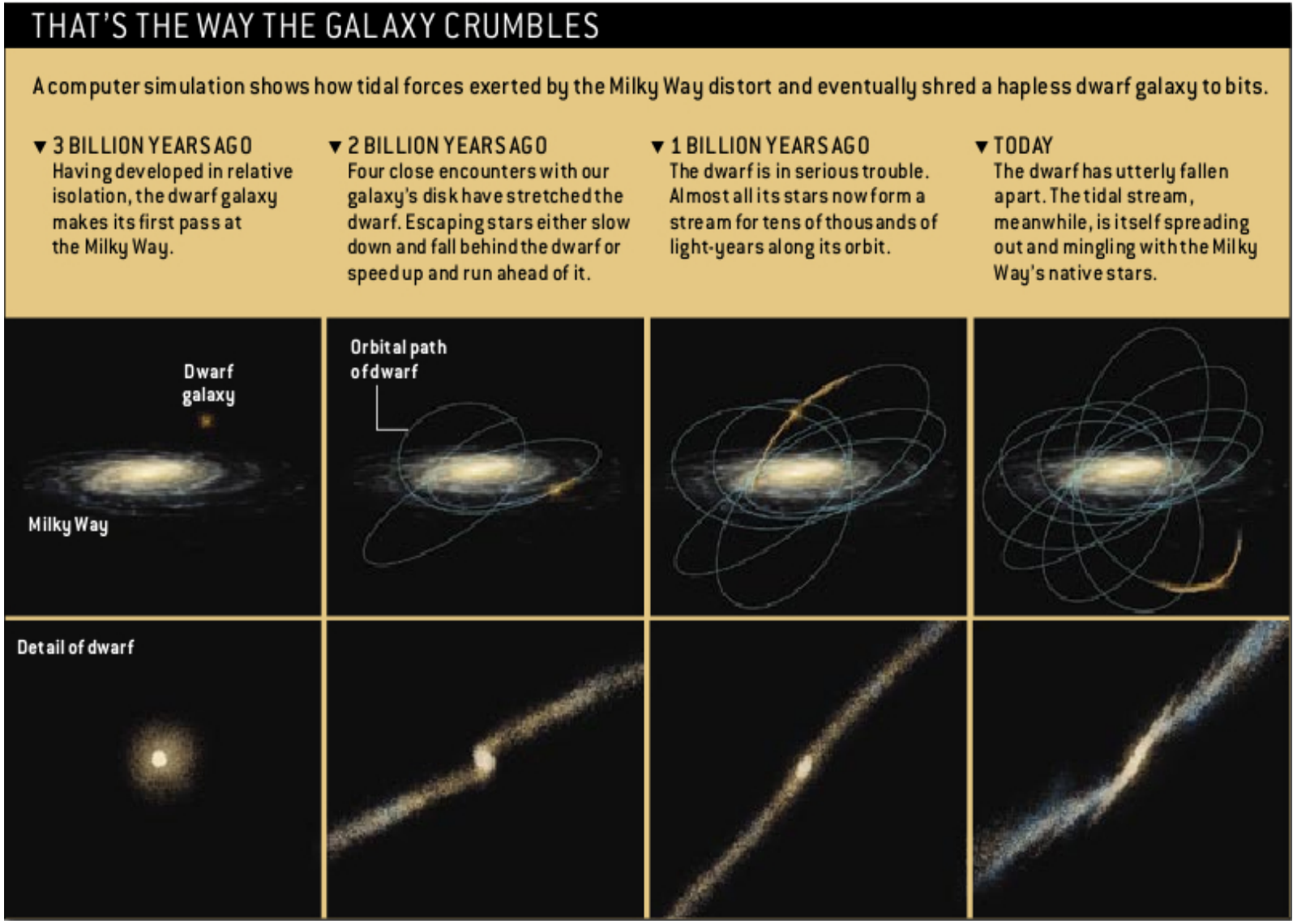

Figure 1.6: Image taken from 'The Ghost of Galaxies Past' by Rodrigo Ibata and Brad Gibson, published in Scientific American April 2007

frequencies of the stellar orbit and the angular frequency of the rotating bar satisfy certain conditions. In the rotating frame of the bar, the effective angular velocity of an object is $\Omega - \Omega_p$. In certain regions of the Galaxy, where $\Omega - \Omega_p = \kappa\frac{n}{m}$ (n and m are integers), the stellar orbits close themselves after n revolutions around the center and m radial oscillations or epicycles. The stars in the corresponding orbits are aligned with the perturbation. They interact with the perturbation always with the same sign, and hence resonates with it. These are called the Lindblad resonances in general. As the bar is a bisymmetric perturbation, the most important resonances in a realistic disc galaxy are those for m=2. The Inner Lindblad resonance (ILR) corresponds to n=+1, in which case $\Omega - \Omega_p = \frac{\kappa}{2}$, $(\Omega > \Omega_p)$. At this, stars rotate faster than the bar and appear as prograde. Outer Lindblad Resonance (OLR) corresponds to n=−1, corresponding to $\Omega - \Omega_p = \frac{-\kappa}{2}$, $(\Omega < \Omega_p)$, where stars rotate slower than the bar appear as retrograde. One also finds a situation where objects' rotation matches with the bar's rotational speed i.e $\Omega - \Omega_p = 0$. This is known as corotation resonance which occur at coradius R. The perturbations introduced by the Galactic bar are believed to be the cause for overdensities or moving groups in the solar neighborhood. Hercules stream is shown as due to dynamical perturbations in a number of studies (Kalnajs 1991, Raboud et al. 1998, Fux 2000, Fux 2001, Dehnen 1999, Dehnen 2000).

Similar to the case of Galactic bar, the steady and transient spiral arms have been proposed to explain the existence of moving groups (Mayor 1972). According to the Density wave theory (Lin et al. 1969 and references therein), the spiral pattern in the Galaxy is a density wave, rotating through the Galaxy at a fixed angular speed called the pattern speed Ω_s. Maps of the Milky Way, based on Cepheids, H I, CO and Far-Infrared observations suggest that the disc contains a four-armed tightly wound structure (Vallée 2002). The arms being Norma, Scutum-Centaurus, Sagittarius and Perseus. The Sun is located in a minor arm named the Orion Arm, or the Orion Spur, which lies between the Sagittarius and Perseus Arms. The near IR observations of the Galaxy suggested a dominant two-armed spiral structure in it (Drimmel & Spergel 2001). It was also suggested that the Milky Way spiral pattern is the superposition of a dominant two-armed and weak four-armed structure (Amaral & Lepine 1997).

De Simone et al. (2004) found that heating by strong transient spirals can also explain the presence of moving groups in the solar neighborhood. Like the bar, spirals also interact with stellar orbits, and introduce orbital resonance. In addition to the corotation resonance ($\Omega = \Omega_s$), resonances at ILR and OLR also occur at $\Omega - \Omega_s = \pm\frac{\kappa n}{m}$. Lindblad resonances with spiral density waves can cause structures in the velocity distribution by

exciting large epicyclic perturbations, allowing stars from distant locations to reach the solar neighborhood, providing a promising explanation to the existence of moving groups in the solar neighborhood. Quillen & Minchev (2005) could explain the existence of some of the moving groups (Hyades-Pleiades, Coma Berenicas) with models in which the Sun is in the outer limits of the 4:1 Inner Lindblad Resonance (4 radial oscillations in one orbital motion; n=1, m=4) of the spirals. It was also suggested that, the combined effect of the bar and spiral structure acting separately and simultaneously in the Galactic disc can explain the moving groups in the solar neighborhood (Quillen 2003, Chakrabarty 2007).

Other than the bar and/or spirals, external agents are also suggested to cause dynamical perturbations in the Galaxy. It was shown that the relatively massive minor-merger events can perturb the Galactic disc (mainly the thick disc) and generate substructure in the velocity field of disc stars located in the solar neighborhood resulting high velocity streams such as Arcturus (Minchev et al. 2009, Gómez et al. 2012).

1.9 Moving Group Detection and Membership Criteria

Moving groups in the era of pre HIPPARCOS mission, were, in general, identified based on the common proper motions of individual stars (see review Antoja et al. 2010). In his series of papers (see Eggen 1996 and references therein) Eggen used the best available proper motions and photometry (from which absolute magnitude and distance modulus were derived) to compute space motion V_{tot} to identify moving groups. Obvisouly, these were frought with large uncertainties, and, in fact, many of the groups identified in this way were later found to be incorrect (Kapteyn 1914, Ali 1940).

Streams in the Disc:

The launch of HIPPARCOS space mission in the late 1990s by European Space Agency (ESA) made a significant contribution to understand the Galactic structure. HIPPARCOS measured astrometry: proper motions and parallaxes for about 100,000 stars with an unprecedented accuracy. The accurate astrometry combined with radial velocity data from large surveys such as RAVE, CORAVEL made it possible to construct a 6-dimensional view (x, y, z, U, V, W) of the solar neighborhood. To extract the structures, many a techniques were developed: wavelet analysis, parametric techniques, non-parametric techniques using kernel estimator, cluster analysis, Schwarzschild decomposition etc., which used variety of parameter-spaces to reveal the substructures (Chen et al. 1997, Asiain et al. 1999, Skuljan et al. 1999, Bienaymé 1999, Chereul et al. 1998, Chereul et al. 1999,

Chereul et al. 1998). Many of these studies reported highly structured velocity distribution of the solar neighborhood with overdensities confirming many moving groups that were proposed earlier and detecting many more new ones.

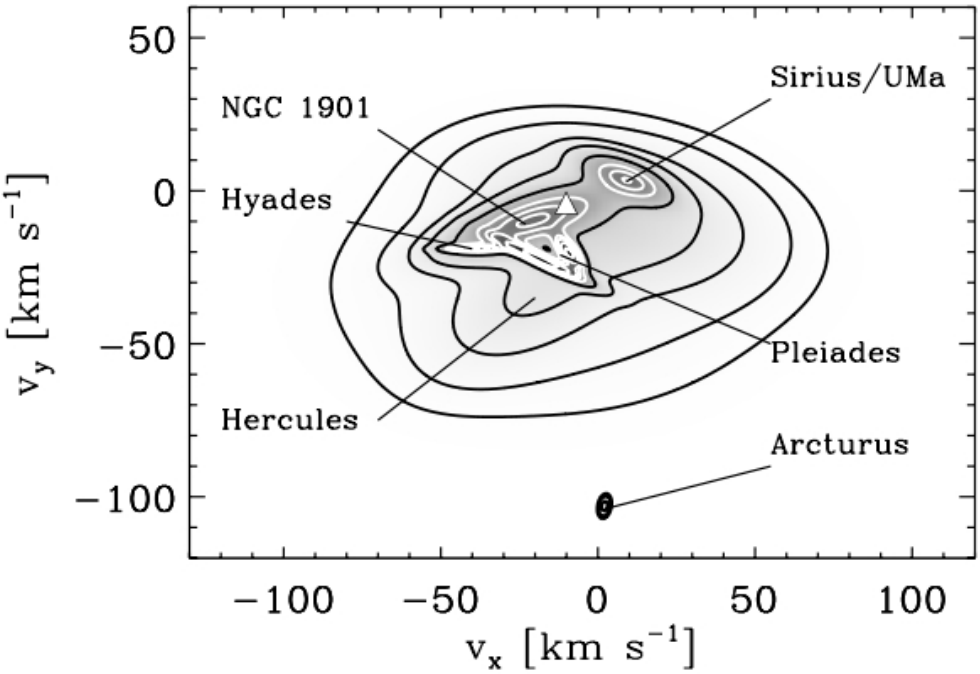

Figure 1.7: Moving Group Detection (Bovy et al. 2009)

Based on kinematic motion, the membership of the known moving groups is refined (Famaey et al. 2005, Antoja et al. 2008, Zhao et al. 2009). For example, the Geneva-Copenhagen Survey (Nordström et al. 2004) included ∼ 14,000 F and G dwarfs with HIPPARCOS astrometry and radial velocity data from CORAVEL database (Baranne et al. 1979, Mayor 1985) to decode nearby Galactic structure. To this data, Famaey et al. (2005) applied a maximum-likelihood method based on Bayesian approach, and cluster analysis to identify groups in the parameter-space $U - V$, and found 6 moving groups including Hyades-Pleaides, Sirius and Hercules. On the other hand, applying kernel estimator and wavelet technique to the U and V components, Zhao et al. (2009) detected 22 moving groups in the solar neighborhood of which 11 were new detections, the rest included Hercules, Sirius, Hyades, Castor group, Pleiades stream, and IC 2391 group etc. Using wavelet transform and wavelet deionising techniques in the four dimensional $U - V - age - [Fe/H]$ space of more than 24,000 stars in the solar neighborhood, Antoja

et al. (2008) detected many of the above moving groups. See Figure 1.7 taken from Bovy et al. (2009), for moving group detection which modelled the underlying velocity distribution of solar neighborhood stars as a mixture of three dimensional Gaussian distribution and detected the classical moving groups.

Streams in the Halo:

The λCDM model (Peebles 1974, White & Rees 1978, Blumenthal et al. 1984) suggests at least part of the halo might have been formed from disrupted accreted systems implying substructures in the phase space distribution of stars in the halo of the Galaxy (Bullock & Johnston 2005). The structures associated with the remnants of accretion in the outer halo (at large distances from the Sun) were detected in many studies (Doinidis & Beers 1989, Arnold & Gilmore 1992, Majewski et al. 1996). The most spectacular detection was that of Sagittarius dwarf galaxy as a clump in the radial velcity space of K and M giants (Ibata et al. 1994). The release of data from the large scale photometric surveys like 2MASS (Skrutskie et al. 2006), SDSS (Stoughton et al. 2002) improved the detection. The low stellar density in the outer halo enables relatively easy identification of larger tidal streams as stellar spatial overdensities, in particular, in the large photometric surveys like SDSS. Because of the large dynamical time scale > 1 Gyr in the outer halo, the phase-mixing of the tidal streams happen very slowly. The Orphan stream (Belokurov & Zucker 2006), and the Monoceros stream (Newberg et al. 2002, Yanny et al. 2003) are examples of halo streams (tidal streams) detected from SDSS survey.

It is understood from mumerical simulations that the accreted satellites spread their tidal debris on eccentric orbits. The debris slowly drifts into the inner halo (Helmi & White 1999) as a result of dynamical friction. Dynamical friction can drag satellites even to the plane of the Galactic disc. They can deposit significant fraction of their stars in the disc, if the accretion happens coplanar with the disc at a low inclination angle (Abadi et al. 2003a, Abadi et al. 2003b). They also claim that many of the oldest stars in the disc, and the thick disc itself, originated in satellites accreted on low inclination orbits (Abadi et al. 2003a, Abadi et al. 2003b, Meza et al. 2005). Hence, one may expect remnants of tidal streams or halo streams to be present in the solar neighborhood, and can be detected by analysing the dynamical and chemical properties of solar neighborhood halo stars.

Studies of Galactic structure got a boost with the release of the Radial Velocity Experiment (RAVE) survey (Steinmetz et al. 2006) and SEGUE[‡] survey data (Yanny et al.

[‡]The Sloan Extension for Galactic Understanding and Exploration (SEGUE) Survey obtained 240,000 moderate resolution (R ~ 1800) spectra from 3900 Å to 9000 Å of fainter Milky Way stars (14.0 < g <

2009). The large data set helped to detect remains of the satellite accretion in the disc. Unlike in the halo, stream-like spatial overdensities have not been observed in the Galactic disc where the stellar density is very high and the spatial coherence is lost very quickly. Due to the conservation of phase-space density, at each point along a stream, the velocity dispersion decreases inversely with time, with some periodic oscillation (Helmi & White 1999). Hence, velocity space is important to detect tidal streams, even after the spatial coherence is lost. The tidal stream stars passing the solar neighborhood have very similar azimuthal frequencies, equivalently, angular momenta implying a narrow distribution of azimuthal velocities. In this way, they behave very similar to the classical moving groups in the solar neighborhood. However, moving halo groups often have a distinct banana-shaped (U, V) velocity distribution, which is a consequence of their eccentric orbits (Helmi & White 1999, Helmi et al. 2006, Villalobos & Helmi 2009, Williams et al. 2009). Compared to in situ thick disc stars, accreted stars mostly occupy the outskirts of the (U, W) distribution (Villalobos & Helmi 2009). But due to their short dynamical time scales (orbital time scales) near the disc, a single progenitor can dispose multiple streams in the solar neighborhood in a short period of time, leading to several hundreds of cold (with $\sigma \leq 5$ km s^{-1}) stellar streams (Helmi & White 1999, Helmi et al. 2003, Gould 2003). As a result, the average phase space density in the finite observational volume, includes the contribution from multiple streams of a single progenitor known as phase mixing. Because of phase mixing, in a given volume, the stellar density of tidal debris from a satellite decreases, and its velocity dispersion increases with time. This would make it very difficult to separate out individual streams in velocity space.

To avoid the problem of phase mixing, the space of Intergrals of Motion was used for detecting halo streams. An integral of motion is a function of the phase space coordinates that is constant along any stellar trajectory in phase space, and it does not depend on time, for e.g. energy, angular momentum etc. The small satellite galaxy will have very similar values for the integrals of motion, which will ensure that they are tightly clumped in the corresponding spaces even after phase mixing has produced a spatial distribution that is effectively featureless. The advantage of using integrals of motion space is that the number of clumps detected in this way will represent the total number of accretions/merging events (Helmi & de Zeeuw 2000).

20.3) of a wide variety of spectral types, both main-sequence and evolved objects, with the goal of studying the kinematics and populations of our Galaxy and its halo.

Detection of Tidal Streams in the Solar Neighborhood

The presence of tidal streams in the solar neighborhood was first detected by Helmi & White (1999). They discovered two streams in the local halo, in the parameter space of (J_z - $J_\perp$) using 97 metal deficient red giants and RR Lyrae stars within 1 kpc vicinity of the Sun. J_z is the z-component of the total angular moemntum J, $J_\perp = \sqrt{J_x^2 + J_y^2}$, where J_x and J_y are the x and y components of the total angular momentum J. Further modification to this, Helmi & de Zeeuw (2000) proposed that the space of energy, z-component of the angular momentum and the total angular momentum (E, J_z, J) are well suited for identifying debris from disrupted satellites. J is not a conserved quantity as the Galactic potential is not spherical but axisymmetric, but J_z is conserved in axisymmetric potential. Similarly, energy E, whose computation requires the knowledge of Galactic potential, is also not a conserved quantity, as the stars lost in different passages end up in different energy levels. Hence, Helmi et al. (2006) suggested a new parameter space of orbital apocentre-pericentre-J_z ($A - P - J_z$ space) to look for the debris of accreted satellites in the solar neighborhood. Generally, stars from the same satellite cluster in the APJ_z space along a line of constant eccentricity. Using APJ_z combined with Geneva-Copenhagen survey data, they found three halo streams with distinct ages and metallicity distributions along with several known moving groups such as Sirius, Hyades-Pleiades, and Hercules. Similarly, the search for stars with constant eccentricity was undertaken to find the halo streams by Arifyanto & Fuchs (2006), Klement et al. (2009), Klement et al. (2008) and Dettbarn et al. (2007). There are many novel ways to detect individual halo streams some of which are discussed in Klement (2010) and Helmi (2008).

1.10 Nucleosynthesis and Chemical Tagging

It is understood that the first few elements such as hydrogen (H^1 or H), its isotope deuterium (H^2 or D), helium, lithium and their isotopes formed in the very beginning, when the universe was cooled to form stable protons and neutrons. These are often called as primordial elements, and the process is called the Big Bang Nucleosynthesis or the primordial nucleosynthesis. Heavier elements beyond Li are mostly synthesized either in the interiors of stars or during stellar explosions. These are called stellar nucleosynthesis and explosive nucleosynthesis, respectively. Kind of elements and their production depends on the initial mass of the stars.

Massive stars ($M > 8\ M_\odot$), can synthesize elements till Iron (Fe) through a series of nuclear reaction cycles: CNO cycle, triple alpha reaction, carbon burning, neon burning,

Table 1.3: Properties of nuclear burning stages in a 15 $M_\odot$ star (Woosley et al. 2002)

Burning stage	T (10^9 K)	ρ (g/cm^3)	fuel	Main products	time scale
Hydrogen	0.035	5.8	H	He	1.1×10^7 yr
Helium	0.18	1.4×10^3	He	C, O	2.0×10^6 yr
Carbon	0.83	2.4×10^5	C	O, Ne	2.0×10^3 yr
Neon	1.6	7.2×10^6	Ne	O, Mg	0.7 yr
Oxygen	1.9	6.7×10^6	O, Mg	Si, S	2.6 yr
Silicon	3.3	4.3×10^7	Si, S	Fe, Ni	18 days

oxygen burning and silicon burning. Nuclear burning stages in the interior of a 15 $M_\odot$ star computed in Woosley et al. (2002) is given in Table 1.3. The nucleosynthesis inside a massive star eventually leads to an onion skin structure of different layers consisting of heavier nuclei at increasing depth, separated by burning shells as shown in Figure 1.8. Beyond Fe formation, there is no net release of energy and hence no outward pressure. When the inert core exceeds the Chandrasekhar limit of 1.4 $M_\odot$ stellar equilibrium breaks down, and gravity prevails leading to core collapse. The inward collapse will be halted by neutron degeneracy leading to outward explosion. The core collapse explosion is called Type II supernova, during which neutron captures (mainly rapid neutron capture or *r*-process, which requires high neutron number densities in short time scales) on Fe seed nuclei build heavier and heavier elements. Much of α-elements (O, Mg, Si, S, Ca, Ti) and *r*-process elements like Eu, Nd are formed during the massive star SN II explosions. The elements thus formed get ejected into the interstellar medium making it rich in heavy elements. Stars formed out of this enriched ISM will be rich in heavier elements. Since massive stars live much shorter compared to less massive stars, rate of SN II was much higher in the earlier epochs than now. Measurement of heavier elements trace the earlier epochs of the Galaxy where SN II occured.

Nucleosynthesis in the less massive stars ($M < 8\ M_\odot$) is long and complicated. During the main sequence phase, hydrogen burns to form helium through P-P chain reactions. Once H is exhausted, stars evolve through Red Giant Branch (RGB). At the tip of the Red Giant Branch, the degenerate He core begins burning via triple alpha and carbon-Helim fusion reactions forming carbon-oxygen core. Afterwards, stars pass through the phases of Horizontal Branch (HB), Asymptotic Giant Branch (AGB), Post AGB and Planetary Nebulae (PN) and finally, end up as a white dwarf. Depending on the mass range, and hence the core temperature of the stars, the nucleosynthesis can stop at various stages: He

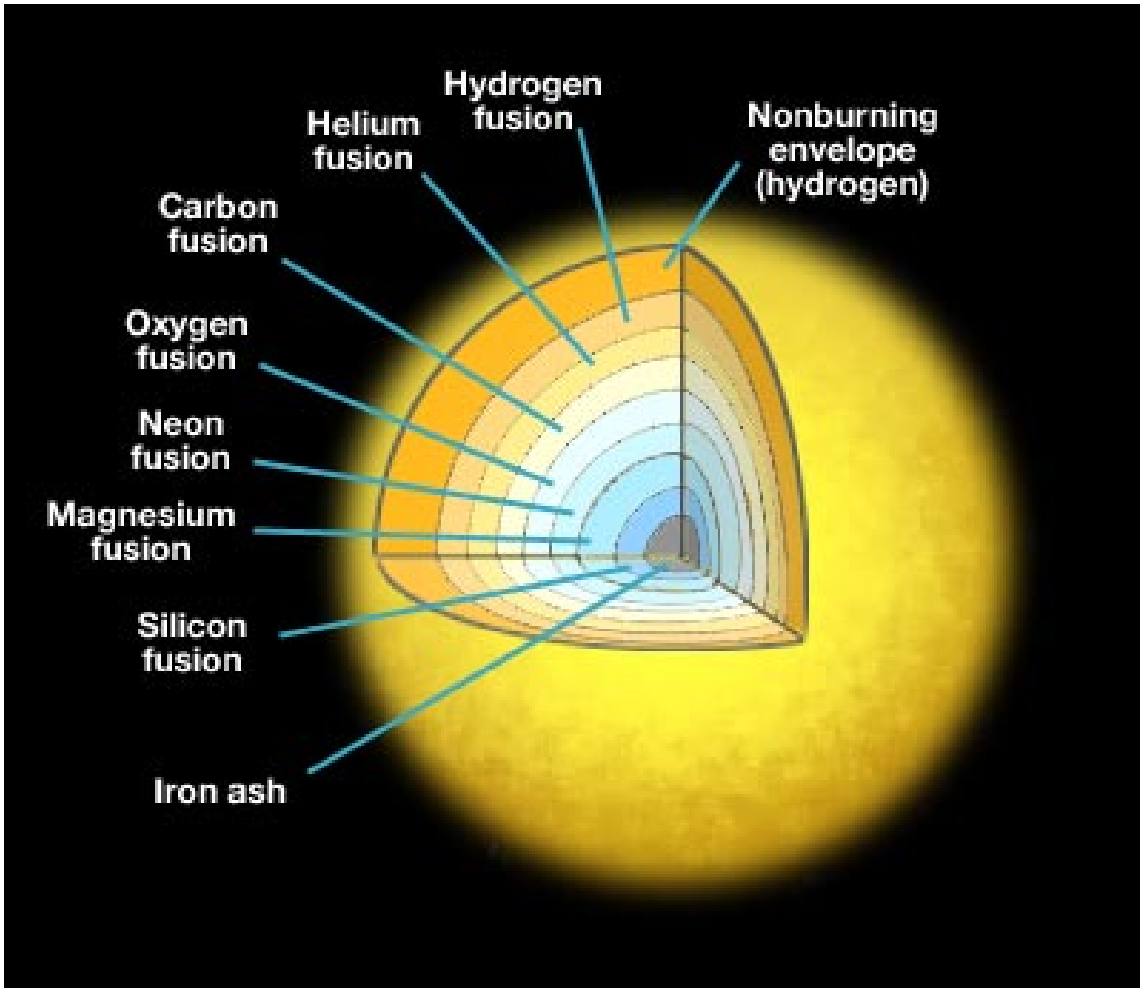

Figure 1.8: The onion skin structure of a massive star.
Credit : *https://www.e-education.psu.edu/astro801/book/export/html/1824*

white dwarf, or C-O white dwarf, or O-Ne-Mg white dwarf. The slow neutron capture happens in the quiscent stages of stellar evolution, mainly during the AGB phase. For build-up of heavier elements, neutrons are required. The required neutron flux is provided by the reactions $C^{13}(\alpha,n)O^{16}$ and $Ne^{22}(\alpha,n)Mg^{25}$. The elements formed (Li, He, C, N, O, and *s*-process elements such as Y, Zr, Ba etc) in this way are dredged up to the photosphere during the RGB and AGB phases. During the AGB phase, much of the enriched stellar material is thrown into the ISM due to heavy mass loss as a result of thermal pulses. AGB star contribution to ISM happens at much later epochs and hence one would expect stars formed in the earlier ephochs are less enriched with the *s*-process elements compared to stars in the later epochs.

Nucleosynthesis also occurs in SN Ia explosion which happens due to the mass accretion of white dwarf from its companion star (red giant star mostly). SN Ia events mainly produce iron peak elements (V, Cr, Mn, Fe, Co and Ni). The time scale of SN Ia is much more compared to that of SN II and AGB nucleosynthesis. Hence elemental abundances are good indicators of stellar enrichment history.

Chemical Tagging

One of the key goals of Galactic astronomy or the near field cosmology is to understand the structure and evolutionary history of the Galaxy. During the formation, different parts of the Galaxy have experienced dissipation and phase mixing to varying degrees. The stellar halo the least, the bulge partly and the disc the maximum (see the review Freeman & Bland-Hawthorn 2002). For halo stars, and some outer bulge stars, the phase space can provide valuable information regarding their formation history. However, the dissipative formation, and the subsequent dynamical evolution of the disc might have erased most of its dynamical information. Near-field cosmology aims in assembling the fossils from the epoch of last dissipation, or information which could survive the dissipative forces. To some extent this information can be retrieved by measuring elemental abundances.

In the absence of stellar mixing, the photospheric chemical composition of a star is basically the chemical composition of the cloud out of which it formed. Main sequence stars or dwarfs, with no convective mixing, are known to preserve original composition from their natal clouds. Thus, F and G type dwarfs are the best candidates for abundance studies to trace the chemical make up of the parental cloud. Also, it is understood that the chemical composition of stars varies from region to region within the Galaxy as well as epoch to epoch. A vast amount of fossil information is locked up in the detailed distribution of elemental abundances. Hence the concept of chemical tagging - to tag individual stars with elements of the protocloud.

Stars formed out of the same molecular cloud at around the same time, are expected to have the same chemical composition, as star forming clouds are expected to have well mixed. For example, member stars of open clusters or globular clusters which exhibit chemical homogeneity trace back to their common formation site and proves the viability of chemical tagging. The method of chemical tagging is proved to be very effective to reconstruct the stellar aggregates which are no longer clustered, but dispersed in the Galaxy as field stars.

1.11 Aim of Thesis

Our aim, in this thesis, is to study a few representative streams in the Galactic disc to find out clues for their presence as over densities in the velocity space. Idea of moving groups or streams has been around in the literature for a few decades. However, it is not very clear from the limited data, how they form and evolve. Understanding of their origin would help to address larger questions such as formation and evolution of the Galaxy, in general, and the disc in particular. There are three principal scenarios in the literature to explain stream formation : a) Open cluster disruption b) Satellite accretion and c) Dynamical perturbation. Our goal in this study is to chemically tag each of the individual member of the selected streams and compare the results with groups such as open clusters and dwarf spheroidal and study which one of the three scenarios best explains the results.

1.12 Thesis Overview

This thesis concerns mainly with chemical tagging of member stars of a few representative streams in the thin and thick disc components of the Galaxy. For this purpose, an appropriate sample is required for subjecting to high resolution spectroscopic studies, and hence the quantitative abundance analysis. A description of sample selection, observations and data reduction techniques are given in Chapter 2. Following this, in Chapter 3, we describe analysis techniques by applying to two standard reference stars: The Sun and Arcturus. The Sun spectra has been analysed as a reference to our main sequence sample in this study, and Arcturus as a reference to K giant sample. Analysis of reference spectra is to validate the procedure that is applied to the rest of the programme stars. In Chapter 4, we study two streams (AF06 and Arcturus) in the thick disc and discuss various origin scenarios. Abundance study of three streams in the thin disc component: Hyades-Pleiades, Sirius and Hercules are dealt in Chapter 5. Main results of the thesis and the future work to be done in this area are described in Chapter 6.

CHAPTER 2

DATA AND TECHNIQUES

In this chapter, we have given the description of the data used for the thesis study and the facilities/packages used to obtain and analyse the data. As spectroscopic data are used throughout, a brief introduction to astronomical spectoscopy is given below.

2.1 Astronomical Spectroscopy

2.1.1 Introduction

Wealth of information about stars can be gathered by studying their spectral features. From spectra, one can derive stars' composition, velocities, and magnetic field strengths which in turn provide crucial information about their origin and evolution. Hence, stellar spectroscopy became a powerful tool in astrophysics to understand various physical phenomenon of celestial objects. This led to the development of astronomical spectroscopy as a branch.

Radiation from stars can be approximated as black body described by Planck radiation formula, with spectral lines superimposed on it. Stellar spectrum has three basic components: a continuum emission described by the black body radiation function, and absorption and emission lines described by radiative transfer equation. Stars emit in the whole electromagnetic spectrum, but the surface temperature determines their flux distribution at different wavelengths and the wavelength at which the distribution peaks. Spectral line strengths vary with surface temperature and composition.

Based on the strengths of some prominent spectral features such as Balmer (hydrogen), helium and metallic lines, stars are classified into O, B, A, F, G, K and M types in the decreasing order of temperature. Stars at the hotter end (O, B, and A type) are referred

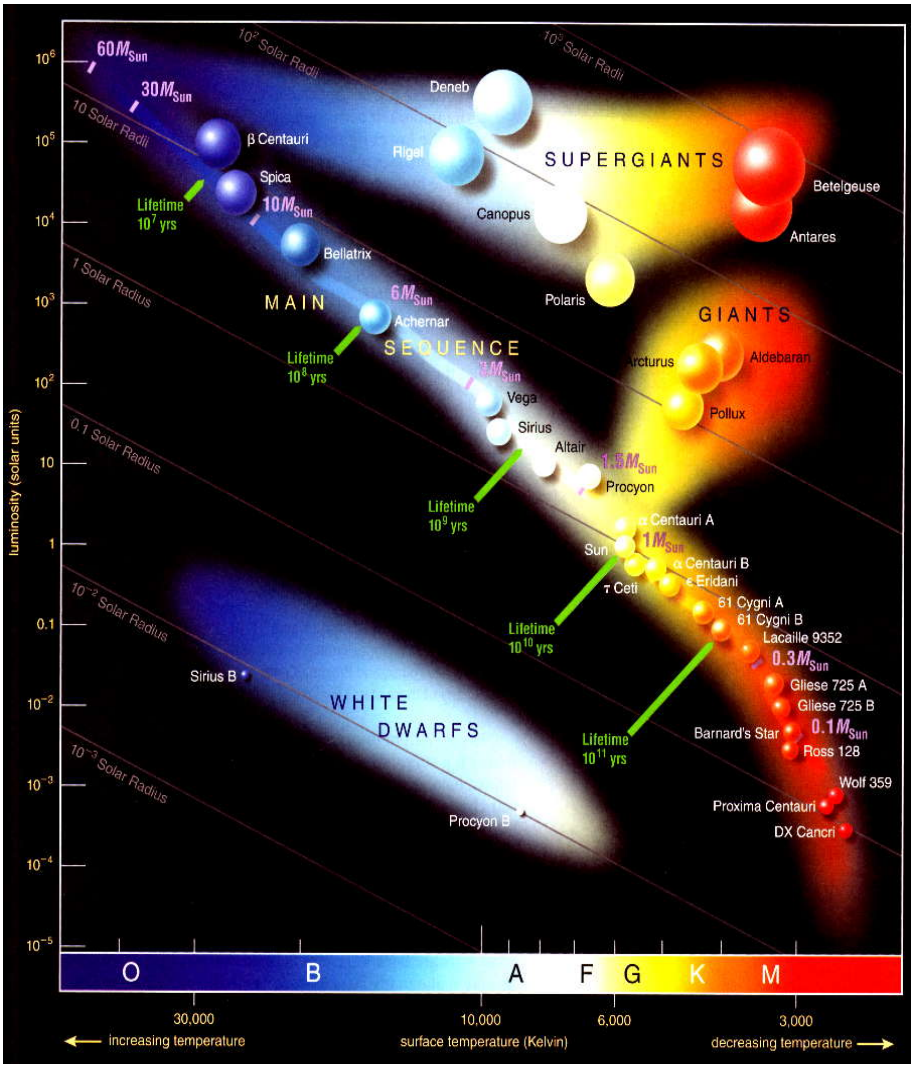

Figure 2.1: The Hertzsprung-Russel diagram.
Credit : *https://www.mtholyoke.edu/courses/mdyar/ast100/HW/hw3_JL.html*

to as early spectral types, while stars at the cooler end (F, G, K, and M) are referred as late type. Further, each spectral type is divided into 10 subdivisions depending on the sensitivities of spectral features to the surface temperature. In the atmosphere of cool stars (K, M type), molecules can survive without getting dissociated, giving rise to molecular absorption bands in the spectrum. Depending on the molecular line strengths, the original spectral classification scheme has been expanded by adding class W (Wolf-Rayet), class C (Carbon stars), class S, T, Y etc. Spectral lines are also found to be sensitive to intrinsic luminosity of stars apart from temperature. The width of spectral lines measures surface gravity of stars which is a function of luminosity. For example, spectral lines of stars of

main sequence (or dwarfs) are relatively broader compared to spectral lines of evolved stars like giants, super giants (brighter) etc. Based on luminosity, stars are classified as Luminosity class I (supergiants), II (bright giants), III (normal giants), IV (subgiants), V (dwarfs), VI (subdwarfs) and D (White dwarfs. The stellar spectral classifications based on temperature and luminosity are shown in Figure 2.1.

2.1.2 Astronomical Spectrograph

The basic principles of astronomical spectrograph which disperses stellar light into many distinct spectral feaures is shown in Figure 2.2. The image of a star is focussed onto the slit located in the focal plane of the telescope. In general, the slit width can be adjusted to suit spectral resolution requirement. A collimator is used to provide a parallel beam which upon focussed on the grating get dispersed into distinct wavelengths or colours. Collimator can be a mirror or lens or a combination of both. Disperser can be a Prism, Grating, or a Grism (e.g. a transmission grating onto the hypotenuse face of a right-angle prism). In modern spectrographs, diffraction grating is used as the disperser and the camera focusses the collimated dispersed light onto the detector. Photographic plates, films or the Charge Coupled Device (CCD) may serve as dectectors, but CCDs dominate the modern astronomy. CCD is a two dimensional array of finite number of pixels which perform discrete sampling of the dispersed light.

Any spectrograph has two important parameters: spectral dispersion and resolution. Dispersion is the spectral range per linear size, and the resolution defines the ability of the spectrograph to resolve two closest lines separated by wavelength $\Delta\lambda$. Thus, the linear dispersion of a spectrograph is given as,

$$\mathrm{d}\lambda/\mathrm{dx} = d \cos\theta \,/\, (\mathrm{n}\, \mathrm{F}_{Camera}) \tag{2.1}$$

where, x is the size of the detector, d is the space between the two adjacent grooves on a grating, θ is the blazing angle, F_{Camera} is the focal length of the camera, and n is the spectral order. Dispersion is usually measured in Å/mm or Å/pixel for a given CCD pixel size. Spectral resolution is defined as a dimensionless quantity,

$$R = (\lambda/\Delta\lambda) \tag{2.2}$$

known as resolving power of a spectrograph. For a given spectrograph of grating with N number of grooves the limiting resolution or the diffraction limited resolution is given

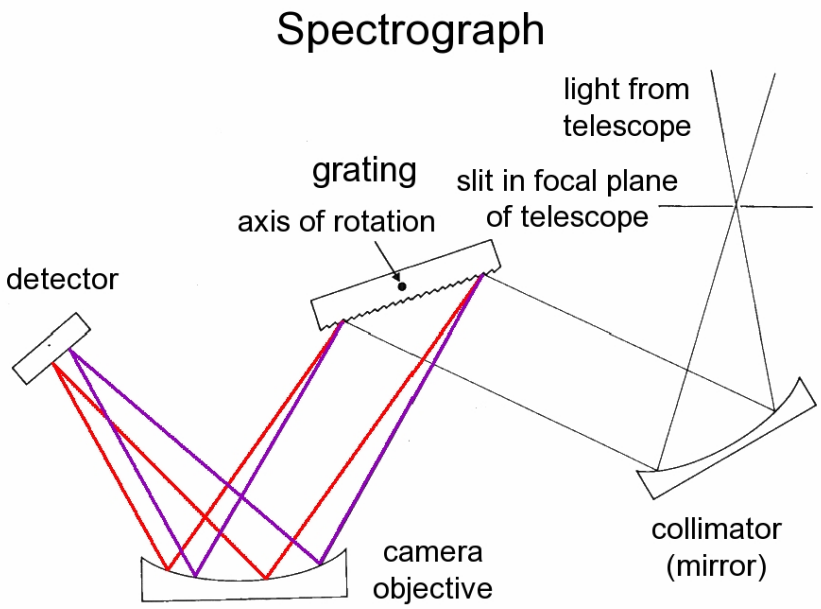

Figure 2.2: The schematic diagram of astronomical spectrograph.
Credit : *http://www.anst.uu.se/ulhei450/Spectroscopy.html*

as

$$R = \mathrm{Nn} = \mathrm{Wn/d} \tag{2.3}$$

where, n is the spectral order. Thus, better resolution could be achieved by choosing a grating with higher number of grooves and at higher order. In general, the grating is blazed to operate in the first order (n = 1) as the overlap between different orders is much severe in higher orders. An order-sorting filter is used to eliminate second order contamination.

2.1.3 Echelle Spectrograph

In Echelle spectrographs, the disperser is a specially designed diffraction grating to obtain very high resolution spectra. In Echelle diffraction grating, the spacing (d) between the grooves is much larger and also, the shape of grooves is such that they are optimized for high incidence angle, and hence high diffraction orders (n) (see the Eqn 2.3). However, each order with such high resolution covers a small range in wavelength. The required

coverage in wavelength is obtained by using many orders. Significant order overlapping in the red is overcome by placing a cross disperser in the light path following the Echelle Grating. Grating is blazed by appropriate amount so as to get maximum intensity in the desired higher orders.

2.2 Sample Selection

Here, we give a brief description of selection of the sample stars of five stellar streams : Arcturus, AF06 from thick disc, and Hercules, Hyades-Pleiades, and Sirius streams from the thin disc components of the Galaxy.

2.2.1 Streams in the Galactic Thick Disc

Arcturus and AF06

Sample stars for the two streams are taken from the study of Arifyanto & Fuchs (2006). They undertook a search for fine structures in the phase space populated by a large sample of 742 F and G subdwarfs. They derived space velocities using HIPPARCOS astrometry and radial velocities given in Carney et al. (1994). The entire sample is put in the velocity plane of V versus $\sqrt{U^2 + 2V^2}$, where $\sqrt{U^2 + 2V^2}$ represents orbital eccentricity. Data was analysed by dividing the sample into two metallicity regimes of [Fe/H] > -0.6 dex and [Fe/H] ≤ -0.6 dex.

The lower metallicity cut off would filter out stars from the dominant thin disc component. The lower cut off combined with upper limit on |W| < 100 km s^{-1} eliminates stars from the halo, and restricts to the disc. The remaining sample of 382 stars were subjected to a wavelet analysis using two dimensional Mexican hat wavelet. Their study resulted two distinct clumps (see Figure 2.3). The clump at $V = -125$ km s^{-1} and $\sqrt{U^2 + 2V^2} =$ 185 km s^{-1} was identified as Arcturus stream, and the more prominent second clump at V $= -80$ km s^{-1} and $\sqrt{U^2 + 2V^2} = 130$ km s^{-1} did not have a corresponding known star's motion. Later it was called as AF06 stream, after the suggestion by Klement et al. (2008). They catalogued 22 candidate stars for Arcturus stream and 44 stars for AF06. For the present study of chemical tagging of stellar stream members, we have taken 18 stars for Arcturus stream and 22 for AF06.

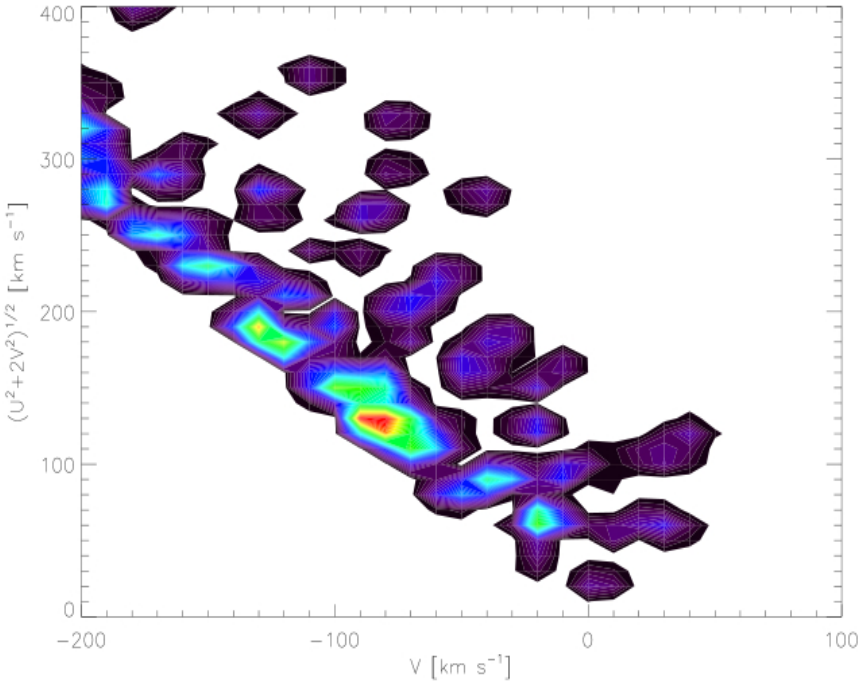

Figure 2.3: Moving groups detected in the V versus $\sqrt{U^2 + 2V^2}$ plane (Arifyanto & Fuchs 2006)

2.2.2 Streams in the Galactic Thin Disc

Hercules, Hyades-Pleiades and Sirius

Famaey et al. (2005) searched the Galactic disc for sub structures among a sample of about 8000 K and M giants. They employed a maximum likelihood method, based on Bayesian approach, to the kinematic data of the sample stars. The space motion (U, V, W) of stars is computed using HIPPARCOS astrometry. Radial velocities are adopted from CORAVEL (Baranne et al. 1979). From the analysis, they found clear overdensities over a smooth background of stars (see Figure 2.4) at U = -42.13 ± 1.95, V = -51.64 ± 1.07, W = -8.06 ± 1.30 and U = 6.53 ± 1.93, V = 3.96 ± 0.67, W = -5.80 ± 1.15. The two are identified as Hercules and Sirius streams, respectively. Another overdensity was seen at U = -30.34 ± 1.54, V = -20.62 ± 0.64, W = -4.82 ± 0.80 which is identified as Hyades and Pleiades stream as the kinematic definition of the clump is closer to Hyades and Pleiades kinematics. Using their technique, the two streams couldn't be resolved. Sample stars are shown in the U-V plane in Figure 2.4 (Famaey et al. 2005). Catalogue contains a list of

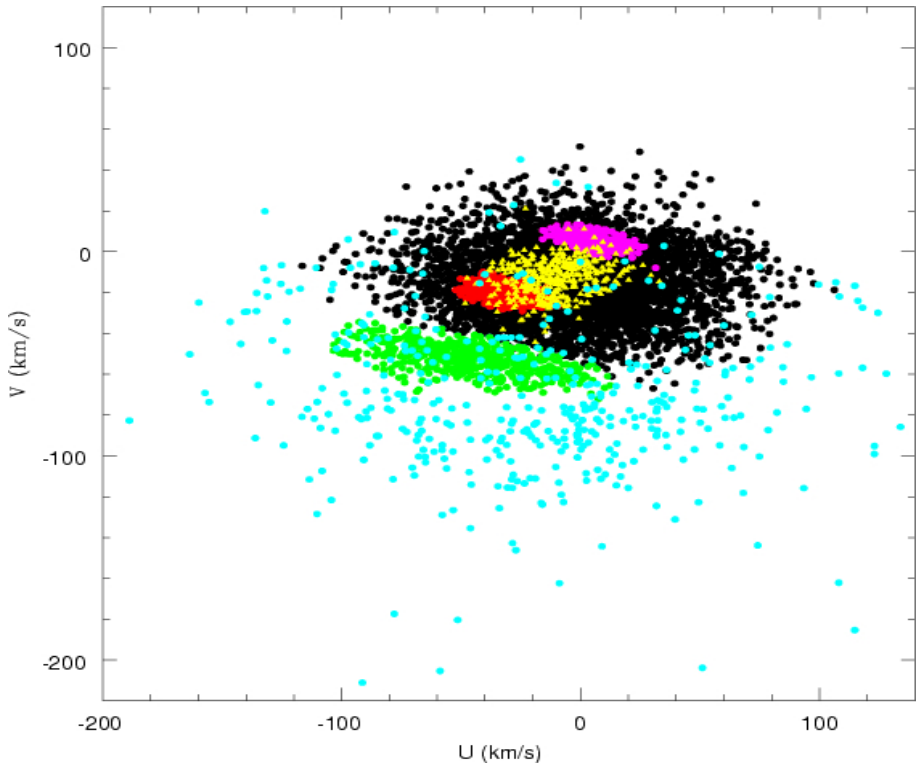

Figure 2.4: Moving groups detected in the $U - V$ plane (Famaey et al. 2005)

stars with kinematic motion, and the derived probability that a star belongs to one of the streams. Entire sample is shown in Figure 2.4, along with the identified streams. For the present study, we chose 58 stars for Hercules, 34 for Hyades-Pleiades, and 33 for Sirius stream with probabilities ranging from 60 % - 70 %. To avoid very cool stars as well as to restrict stars with atmospheric parameters similar to the bright star Arcturus, we imposed colour criterion of $V - I \leq 1.14$ for Hercules and Hyades-Pleiads samples and $V - I \leq 1.28$ for Sirius stream.

2.3 Data and Observations

High resolution spectroscopic observations of the selected sample stars were observed using the Echelle spectrograph equipped with two telescopes - Harlan J. Smith Telescope of McDonald Observatory and the Vainu Bappu Telescope (VBT) of Vainu Bappu Observatory. A brief description of both the telescopes and their instruments is given below.

2.3.1 Harlan J. Smith Telescope

Harlan J. Smith Telescope is a 2.72 m telescope at the W. J. McDonald Observatory located in the Davis Mountains, 450 miles west of Austin, Texas, USA (see Figure 2.5). Telescope is equipped with a high resolution cross-dispersed Echelle spectrograph (Tull et al. 1995) with a Tektronix 2048 x 2048 CCD (pixel size of 24 μm). Spectrograph operates at Coudé focus with an F-ratio (focal length/aperture) of 32.5. CCD has a negligible dark current, as it is cooled to a very low temperature using N2. Also, it has a very low read out noise of 2.59 electrons, and a gain of 0.584 e^{-}/ADU and has a two pixel resolution. With this instrument, spectra at a resolving power of R $\sim$ 60,000 were obtained with spectral coverage from about 3800 Å to 10,000 Å. Continous spectra is recorded with overlaps between orders upto about 5800 Å, beyond which spectral coverage is incomplete, with gaps between the orders. The gap increases as we go towards red side.

Figure 2.5: The 2.7 m Harlan J. Smith Telescope

Figure 2.6: The 2.3 m Vainu Bappu Telescope

2.3.2 Vainu Bappu Telescope

The 2.3 m Vainu Bappu Telescope is at the Vainu Bappu Observatory (VBO), at Javadi Hills, in Tamil Nadu, India (see Figure 2.6). This telescope is equipped with a high resolution fiber fed cross dispersed Echelle spectrometer (Rao et al. 2005) with a CCD of 4096 x 4096 pixel with a pixel size of 12 μm. CCD has a read out noise of 4.4 electrons, gain of about 0.85 e^{-}/ADU and is cooled to very low temperature using N2. Spectra of high resolution R $\sim$ 70,000 can be obtained with this instrument.

2.3.3 Observations

Each night, the images of stellar spectra of the programme stars and the calibration images: bias, dark, flat, and appropriate arc images were obtained. The detailed observations log of the member stars of streams in the thick disc are given in the Tables 2.1 and 2.2 and that of streams in the thin disc are given in the Tables 2.3-2.5. The role of each of the calibration images in obtaining final wavelength calibrated spectra is given below.

Table 2.1: Sample stars of Arcturus stream and observations log

No	Star	Right Ascension h m s	Declination d m s	V	Obs. date	Exp. time S
1	G 72−12	01 32 09.2	+34 33 20.8	10.77	13−11−2006	1800
2	G 4−2	02 11 20.0	+09 37 17.5	10.68	13−11−2006	1800
3	G 102−44	06 02 43.4	+13 04 37.1	10.69	19−11−2007	1800
4	G 103−53	06 43 46.5	+25 31 30.3	10.13	04−11−2007	1800
5	G 42−34	10 03 12.3	+19 50 27.0	10.70	19−11−2007	1800
6	G 139−49	17 36 48.0	+02 50 12.0	10.75	29−09−2005	1800
7	G 204−30	17 49 58.6	+37 31 18.6	10.28	25−09−2005	1800
8	G 241−7	22 25 42.7	+69 31 35.8	10.69	27−09−2005	1800
9	HIP 13111	02 48 37.4	+22 35 54.4	10.10	27−09−2005	1800
10	HIP 36491	07 30 29.0	+18 57 40.6	08.50	11−11−2006	1800
11	HIP 36710	07 33 04.4	+76 55 13.5	10.41	19−11−2007	1800
12	HIP 40613	08 17 29.3	−03 59 22.6	07.74	11−11−2006	1800
13	HIP 53070	10 51 28.1	+20 16 39.0	08.23	23−12−2007	1200
14	HIP 58253	11 56 50.4	+13 22 38.7	09.95	23−12−2007	1800
15	HIP 74033	15 07 46.5	+08 52 47.2	08.26	21−05−2006	1800
16	HIP 94931	19 19 00.5	+41 38 04.6	08.83	13−11−2006	1200
17	HIP 105888	21 26 42.9	+05 26 29.9	08.47	13−11−2006	1200
18	HIP 77637	15 50 58.9	+08 25 23.8	10.01	22−05−2006	1800

Table 2.2: Sample stars of AF06 stream and observations log

No	Star	Right Ascension h m s	Declination d m s	V	Obs. date	Exp. time S
1	HIP 9080	01 56 56.1	+11 39 48.7	10.56	13−11−2006	1800
2	HIP 10652	02 17 07.1	+21 34 00.5	09.04	11−11−2006	1800
3	HIP 11952	02 34 11.0	−12 23 03.5	09.78	27−09−2005	1800
4	HIP 16169	03 28 21.1	−06 31 51.3	08.23	11−11−2006	1800
5	HIP 17147	03 40 22.1	−03 13 01.1	06.67	12−11−2006	1200

Table 2.2 – continued from previous page

No	Star	Right Ascension h m s	Declination d m s	V	Obs. date	Exp. time S
6	HIP 22020	04 44 03.6	+52 58 53.8	09.11	13−11−2006	1200
7	HIP 24030	05 09 57.0	+05 33 26.7	09.72	13−11−2006	1800
8	HIP 26452	05 37 39.6	+68 44 06.6	09.55	13−11−2006	1800
9	HIP 29814	06 16 43.0	+47 03 37.2	09.20	13−11−2006	1800
10	HIP 31740	06 38 24.7	+48 47 55.0	10.06	04−11−2007	1800
11	HIP 34642	07 10 29.8	+53 15 06.4	08.80	12−11−2006	1500
12	HIP 102923	20 51 06.7	+07 01 37.2	09.83	05−11−2007	1800
13	HIP 104913	21 15 05.7	+62 50 28.0	09.52	13−11−2006	1800
14	HIP 115359	23 21 58.3	+16 37 57.1	08.98	01−11−2006	1200
15	G 30−46	00 08 13.4	+15 00 30.7	11.01	03−11−2007	1800
16	G 69−21	00 46 39.8	+33 49 32.7	10.33	10−11−2006	1800
17	G 5−44	03 34 17.9	+22 59 14.2	09.20	12−11−2006	1800
18	G 78−41	03 34 57.1	+38 18 24.1	10.22	13−11−2006	1800
19	G 99−40	05 52 55.4	−03 29 25.0	09.16	13−11−2006	1800
20	G 192−21	06 10 00.5	+50 09 05.5	08.52	11−11−2006	1800
21	G 146−76	10 59 57.5	+44 46 43.8	10.47	13−02−2006	1800
22	G 10−12	11 19 14.0	+05 40 46.0	09.30	12−02−2006	1800
23	G 197−45	12 09 28.9	+51 56 01.0	10.73	28−02−2008	1800
24	G 66−51	15 00 50.1	+02 07 37.5	10.63	12−02−2006	1800
25	G 25−5	20 49 20.6	+01 55 30.4	10.12	19−11−2007	1800
26	G 67−40	23 01 46.3	+11 49 17.2	10.66	12−11−2006	1800

Table 2.3: Sample stars of Hercules stream and observations log

No.	Star	Right Ascension h m s	Declination d m s	V	Obs. Date	Exp. Time S
1	HIP 114742	23 14 36.5	+24 06 10.4	6.34	2005−12−08	1500
2	HIP 19287	04 08 01.8	+43 10 45.3	7.05	2005−12−07	1500
3	HIP 20771	04 27 00.7	+02 04 45.9	6.23	2005−12−08	1800

Table 2.3 – continued from previous page

No.	Star	Right Ascension h m s	Declination d m s	V	Obs. date	Exp Time S
4	HIP 22765	04 53 50.5	+68 13 07.9	7.12	2005−12−07	1500
5	HIP 22176	04 46 16.8	+18 44 04.9	5.99	2005−12−08	1800
6	HIP 9517	02 02 25.0	+12 41 06.3	6.86	2005−12−08	1800
7	HIP 9307	01 59 35.7	+21 03 30.8	5.89	2005−12−08	1800
8	HIP 7119	01 31 44.5	+22 44 28.5	8.24	2005−12−07	1800
9	HIP 58654	12 01 39.5	+36 02 31.5	5.59	2005−12−08	900
10	HIP 52882	10 48 57.2	+29 24 57.8	6.16	2005−12−08	1200
11	HIP 51047	10 25 44.9	+35 25 31.5	6.48	2005−12−07	900
12	HIP 50526	10 19 12.0	+72 26 13.7	6.99	2005−12−08	1800
13	HIP 48140	09 48 50.0	+60 05 48.9	7.00	2005−12−08	1800
14	HIP 48417	09 52 14.6	+25 06 29.5	7.78	2005−12−07	1800
15	HIP 504	00 06 03.3	+24 54 59.8	7.48	2005−12−07	1800
16	HIP 3719	00 47 45.0	+26 17 30.0	6.94	2005−12−07	1500
17	HIP 37441	07 41 12.4	+48 07 53.5	5.60	2005−12−07	480
18	HIP 116348	23 34 34.4	+34 21 22.1	7.29	2005−12−07	1500
19	HIP 20540	04 24 04.5	+12 58 20.7	7.71	2005−12−07	1800
20	HIP 28168	05 57 07.7	+55 56 50.2	6.96	2005−12−07	1500
21	HIP 28677	06 03 18.0	+42 54 41.6	6.09	2005−12−08	1800
22	HIP 29949	06 18 16.9	+46 21 37.6	6.33	2005−12−07	900
23	HIP 31039	06 30 47.1	+58 09 45.5	5.88	2005−12−08	1800
24	HIP 32261	06 44 11.5	+53 17 45.4	6.27	2005−12−07	900
25	HIP 32844	06 50 45.9	+41 46 52.4	4.99	2005−12−08	1500
26	HIP 35146	07 15 54.9	+59 38 14.9	5.20	2005−12−08	1800
27	HIP 258	00 03 13.3	+17 33 08.2	6.57	2005−12−08	1800
28	HIP 96294	19 34 45.3	+16 38 30.0	7.34	2005−09−30	1800
29	HIP 87629	17 54 00.7	+49 47 42.5	8.35	2005−09−30	600
30	HIP 94576	19 14 50.2	+31 51 37.3	6.61	2005−09−30	600
31	HIP 95375	19 24 09.8	+60 20 56.1	7.67	2005−09−30	1200
32	HIP 96028	19 31 28.4	+55 15 53.2	6.85	2005−09−30	900
33	HIP 115899	23 28 52.0	+53 40 00.6	6.92	2005−09−30	900
34	HIP 116644	23 38 17.2	+17 03 47.8	8.06	2005−09−30	1800

Table 2.3 – continued from previous page

No.	Star	Right Ascension h m s	Declination d m s	V	Obs. date	Exp Time S
35	HIP 105502	21 22 05.2	+19 48 16.2	4.09	2005−09−29	240
36	HIP 106551	21 34 46.6	+38 32 02.6	4.88	2005−09−29	360
37	HIP 108914	22 03 43.3	+49 46 18.0	7.31	2005−09−29	900
38	HIP 109387	22 09 39.5	+22 14 31.9	7.47	2005−09−29	900
39	HIP 109585	22 11 56.9	+59 05 04.5	6.30	2005−09−29	600
40	HIP 113144	22 54 43.7	+35 59 01.1	7.48	2005−09−29	900
41	HIP 102010	20 40 17.7	+03 26 28.6	6.94	2005−09−28	900
42	HIP 104035	21 04 37.8	+12 01 29.0	7.72	2005−09−28	1200
43	HIP 22661	04 52 27.8	+39 17 02.8	7.87	2005−12−09	1800
44	HIP 28417	06 00 06.0	+27 16 19.9	6.62	2005−12−09	900
45	HIP 36647	07 32 12.9	+27 07 30.6	7.17	2005−12−09	1200
46	HIP 37049	07 36 48.5	+56 51 29.3	7.63	2005−12−09	1500
47	HIP 107502	21 46 24.0	+25 33 48.6	6.29	2005−11−06	900
48	HIP 108012	21 52 58.4	+15 55 55.7	6.88	2005−11−06	900
49	HIP 11117	02 23 00.6	+03 47 54.9	7.97	2005−11−06	1800
50	HIP 111728	22 37 55.8	+29 55 25.6	7.29	2005−11−06	1200
51	HIP 13786	02 57 28.7	+16 17 37.4	6.88	2005−11−06	900
52	HIP 3546	00 45 18.6	+27 57 48.7	8.11	2005−11−06	1800
53	HIP 6682	01 25 41.6	+44 47 11.5	7.25	2005−11−06	1200
54	HIP 8984	01 55 46.9	+51 41 17.3	7.25	2005−11−06	1200
55	HIP 4486	00 57 29.9	+21 29 10.3	7.00	2005−11−05	1200
56	HIP 7710	01 39 15.4	+14 17 08.0	6.75	2005−11−07	900
57	HIP 8926	01 54 55.8	+27 50 30.4	7.64	2005−11−07	1200
58	HIP 18865	04 02 39.8	+56 23 04.8	8.29	2006−02−10	1800

Table 2.4: Sample stars of Hyades-Pleiades stream and observations log

No	Star	Right Ascension h m s	Declination d m s	V	Obs. date	Exp. time S
1	HIP 113084	22 54 07.0	+40 22 36.9	5.82	07−12−2005	720
2	HIP 18565	03 58 29.2	+38 50 24.9	6.33	07−12−2005	900
3	HIP 19222	04 07 10.8	+74 00 01.3	6.49	08−12−2005	1800
4	HIP 34043	07 03 43.2	+33 53 36.2	7.46	07−12−2005	1800
5	HIP 36739	07 33 24.6	+15 38 20.9	6.63	08−12−2005	1800
6	HIP 24633	05 17 05.4	+12 33 55.8	7.06	09−12−2005	1500
7	HIP 93589	19 03 35.5	+02 32 44.7	6.90	25−04−2006	1200
8	HIP 35317	07 17 42.6	+38 52 34.6	6.49	25−04−2006	1200
9	HIP 41172	08 24 05.9	+31 18 03.5	7.34	25−04−2006	1500
10	HIP 49163	10 01 59.3	+74 45 32.7	6.89	25−04−2006	1200
11	HIP 51091	10 26 18.9	+67 41 06.8	7.54	25−04−2006	1500
12	HIP 51224	10 27 45.9	+59 35 50.1	6.85	25−04−2006	1200
13	HIP 56756	11 38 09.8	+08 53 01.6	6.19	25−04−2006	900
14	HIP 62405	12 47 19.9	+52 51 42.7	7.66	25−04−2006	1800
15	HIP 65366	13 23 46.7	+25 32 52.5	7.40	25−04−2006	1500
16	HIP 74080	15 08 18.4	+33 42 23.4	6.69	25−04−2006	1200
17	HIP 79164	16 09 26.0	+55 49 44.3	6.40	25−04−2006	960
18	HIP 79647	16 15 11.9	+47 02 24.3	7.86	25−04−2006	1800
19	HIP 79867	16 18 09.8	+68 33 16.4	6.36	25−04−2006	960
20	HIP 80656	16 28 01.2	+51 35 31.5	7.30	25−04−2006	1500
21	HIP 80839	16 30 29.7	+33 45 03.2	6.98	25−04−2006	1200
22	HIP 82219	16 47 47.5	+20 12 18.9	7.61	25−04−2006	1500
23	HIP 83289	17 01 16.9	+60 38 55.5	6.15	25−04−2006	1200
24	HIP 85160	17 24 11.1	+36 55 22.3	7.20	25−04−2006	1500
25	HIP 88204	18 00 44.0	+09 33 50.4	7.01	25−04−2006	1200
26	HIP 19641	04 12 31.4	+17 16 38.8	6.09	06−11−2005	540
27	HIP 17752	03 48 02.1	+07 07 46.7	7.88	06−11−2005	1800
28	HIP 113635	23 00 49.2	+21 22 53.4	7.44	07−11−2005	1200
29	HIP 114565	23 12 25.0	+36 58 04.1	6.91	07−11−2005	900
30	HIP 117954	23 55 32.6	+52 44 08.1	6.60	07−11−2005	600
31	HIP 2320	00 29 36.1	+62 03 50.9	7.01	07−11−2005	900

Table 2.4 – continued from previous page

No	Star	Right Ascension h m s	Declination d m s	V	Obs. date	Exp. time S
32	HIP 6939	01 29 23.5	+25 16 31.3	6.65	07−11−2005	600
33	HIP 1421	00 17 47.7	+01 41 19.4	6.19	07−11−2005	480
34	HIP 13887	02 58 49.4	+43 21 52.2	6.65	10−02−2006	900

Table 2.5: Sample stars of Sirius stream and observations log

No	Star	Right Ascension h m s	Declination d m s	V	Obs. date	Exp. time S
1	HIP 47719	09 43 42.8	+34 05 49.8	7.22	2011−05−13	1200
2	HIP 52926	10 49 26.8	+17 08 47.2	7.12	2011−05−13	1200
3	HIP 67364	13 48 24.6	+23 26 57.3	7.94	2011−05−13	1800
4	HIP 68737	14 04 12.7	+37 11 50.9	8.39	2011−05−13	1800
5	HIP 49103	10 01 18.3	+28 47 03.9	6.91	2011−05−14	900
6	HIP 53710	10 59 21.0	+15 32 25.6	7.99	2011−05−14	1800
7	HIP 66567	13 38 43.3	+09 58 51.0	7.85	2011−05−14	1800
8	HIP 68590	14 02 29.1	+43 59 21.3	8.72	2011−05−14	1800
9	HIP 68828	14 05 35.6	+44 20 25.4	8.05	2011−05−14	1800
10	HIP 80211	16 22 28.8	+53 32 30.6	8.64	2011−05−15	1800
11	HIP 51825	10 35 15.3	+04 49 22.1	7.93	2011−05−15	1800
12	HIP 53876	11 01 20.8	+46 33 49.1	7.00	2011−05−15	900
13	HIP 67021	13 44 06.2	+55 38 06.0	7.25	2011−05−15	1200
14	HIP 68935	14 06 41.6	+34 46 42.8	7.01	2011−05−15	1200
15	HIP 77401	15 48 05.8	+50 00 16.5	7.87	2011−05−15	1800
16	HIP 79326	16 11 23.1	+07 27 56.5	7.72	2011−05−15	1800
17	HIP 26711	05 40 35.8	+28 58 36.9	7.05	2011−11−13	1200
18	HIP 28556	06 01 39.7	+16 56 02.9	7.33	2011−11−13	1200
19	HIP 35431	07 18 52.5	+38 40 24.9	6.97	2011−11−13	1200
20	HIP 117938	23 55 22.7	+32 53 31.3	7.38	2011−11−13	1200
21	HIP 7668	01 38 42.8	+46 20 47.3	7.43	2011−11−13	1800

Table 2.5 – continued from previous page

No	Star	Right Ascension h m s	Declination d m s	V	Obs. date	Exp. time S
22	HIP 37030	07 36 34.2	+65 05 46.4	7.17	2011−11−15	1200
23	HIP 7906	01 41 39.2	+30 02 49.6	5.97	2011−09−22	2700
24	HIP 15554	03 20 22.4	+55 32 13.5	7.16	2011−09−22	3000
25	HIP 44946	09 09 21.5	+22 02 43.6	5.15	2011−05−15	1800
26	HIP 94156	19 09 56.4	+35 39 39.6	6.53	2011−05−13	1800
27	HIP 68418	14 00 23.4	+39 01 47.8	6.64	2011−05−14	1500
28	HIP 76366	15 35 49.2	+38 22 26.1	6.28	2011−05−13	1800
29	HIP 89065	18 10 40.3	+03 19 27.3	5.50	2011−05−13	1200
30	HIP 64179	13 09 12.4	+10 01 20.9	5.80	2011−05−14	1200
31	HIP 97282	19 46 17.5	+45 44 10.3	7.41	2011−05−15	2700
32	HIP 100116	20 18 35.1	+17 21 43.8	6.84	2011−05−16	2700
33	HIP 106771	21 37 38.8	+54 02 31.9	6.18	2011−09−22	2700

Bias Frames:

A bias frame is a zero duration exposure image which represents an offset of counts that vary from pixel-to-pixel, though not significantly. Since the offset varies slightly across the CCD and also from frame to frame, it is necessary to have a separate image to de-bias programme images pixel-by-pixel. In fact, in a given night a set of bias frames before and after the observations are taken. A master bias frame is created by averaging them. The master bias is used to correct bias level in other images.

Dark frames:

Pixels in every CCD generate thermal noise or dark current. Dark counts are a function of time and also temperature. At the facilities, where we made observations, CCDs are cooled to about −105 deg using liquid nitrogen which keeps dark current minimal. Dark frames are obtained with same exposure as those of programme images but with the CCD shutters closed. Similar to bias frames one obtains a set of dark images before and after the observations, and creates a master dark frame by averaging.

Flat Field Frames:

Quantum efficiency of pixels varies across the CCD. To make correction for this non-uniform illumination of CCD due to variation in pixel quantum efficiency, flat field images are obtained with bright uniform light source. Source can be twilight, diffuse dome light or a halogen lamp. In our case, it is a halogen lamp. Flat images are obtained with very good signal level so that all the pixels are well exposed. One should note that flat frames are neither under-exposed nor saturated. A master flat is constructed by averaging bias and dark corrected flat frames. Programme images are corrected by dividing with the master flat.

ThAr lamp spectrum:

An arc spectrum of known wavelengths is necessary to convert pixels positions into wavelengths. We have obatined ThAr lamp spectrum almost immediately after each programme image for this purpose.

2.4 Data Reduction

The unprocessed image or the raw image from the CCD is a two dimensional image as shown in the Figure 2.7. The horizontal and vertical axes are the dispersion axis and spatial axis (slit axis), respectively. The bright horizontal lines correspond to different orders of the spectrum.

The observed spectral images are reduced to one dimensional spectra (count versus wavelength) using the software, Image Reduction and Analysis Facility (IRAF). The data reduction procedure involves preprocessing of the CCD images, extraction of one dimensional spectrum from the images, and the subsequent wavelength calibration. Preprocessing involves bad-pixel correction, trimming, bias subtraction, dark subtraction, and flat-fielding.

There are few pixels on a CCD which are permanently damaged and are insensitive to light. These are called bad pixels. For every CCD, bad pixels are identified using flat frames or by some other means. The identified bad pixels are replaced by average counts of neighboring pixels. Images that are corrected for bad pixels will be trimmed to ensure to have only well exposed part of the CCD image. Further, the images are subjected to bias and dark corrections by subtracting master bias and dark frames, respectively. The combined correction of bias and dark can be replaced by overscan correction. A small

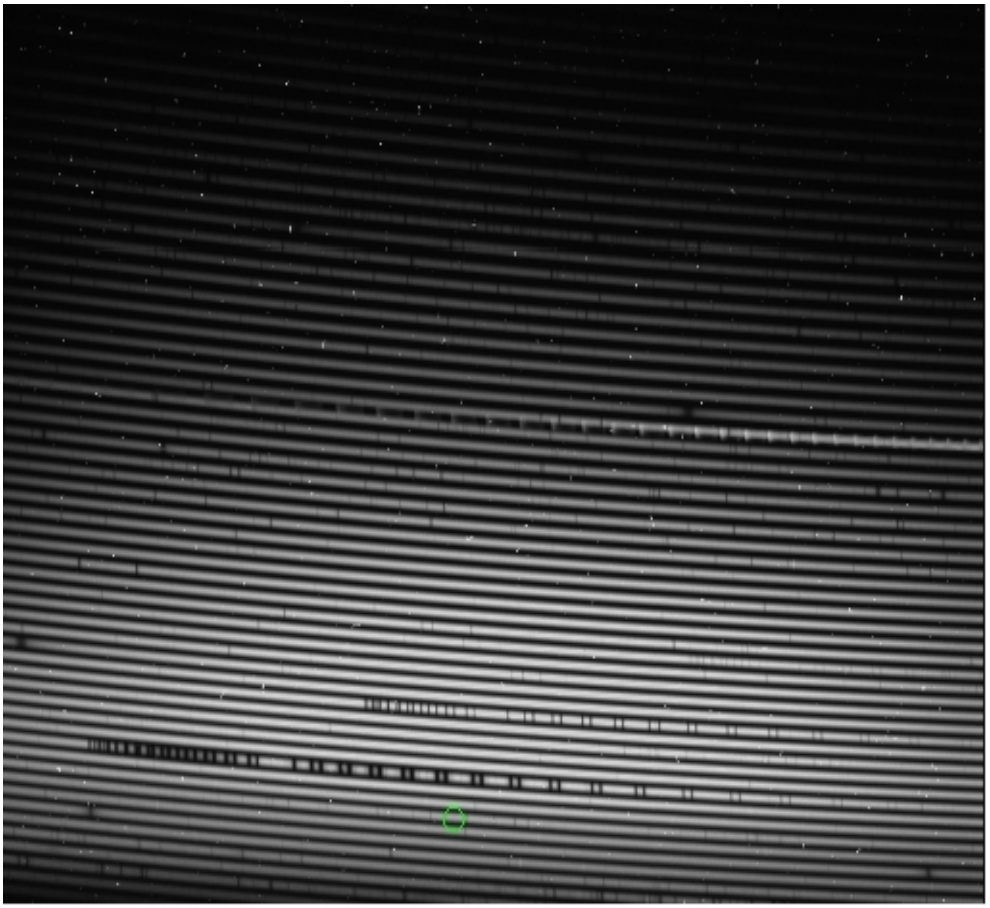

Figure 2.7: The raw CCD image

portion of the CCD frame is used for this purpose. The designated overscan region is not exposed to light during the exposure of frames. Since bias varies with pixels and the dark counts vary with time, overscan correction eliminates the two effects. Bias and dark counts of each pixel is estimated by fitting polynomial to the overscan region, and are subtracted from programme frames.

Flat Fielding and scattered light removal

The individual flat field images are median combined to generate one master flat. Next step is to remove the background counts due to scattered light from the master flat. Scattered light is due to the light diffusion and backward reflection on the optical elements of the spectrograph. Since the scattered light has a complex structure, it is removed by using smoothing polynomial in two dimensions. Next step is to normalize the scattered light corrected master flat.

Order Location and Tracing

Echelle spectrum has many orders in it, and it may not be easy to identify orders in the spectra of faint objects or in the spectra with very strong absorption features. For this purpose, a very well exposed frame of any bright object with less spectral features can be used. This can be used as a reference for defining the extraction window of different orders of programme frames, lamp as well as flat frames. The reference spectra is also used to trace the center of the spatial profile as a function of the dispersion axis.

Extraction and Wavelength Calibration of Spectra

The preprocessed images are extracted to one dimensional images of pixels versus counts. In extracting every object spectrum, a bright star spectrum is used for order tracing. The same is used for tracing the ThAr arc spectrum. Next step is to identify emission lines in the extracted arc spectrum by comparing with the ThAr spectrum obtained in the laboratory. Since wavelengths of these lines are known, one can construct a polynomial relation between the known wavelength of emission lines and the corresponding pixel positions. The solution is called the dispersion solution. This is applied to object spectra of pixel versus counts to convert it to wavelenghth versus counts. By checking known wavelengths of a few atmospheric or night sky emissions across the spectrum, it is made sure that the applied dispersion solution is correct.

Continuum Normalization:

For the purpose of measuring equivalent widths (W_λ) the continuum of object spectra are normalized to unity.

Doppler Correction

The radial velocities of stars are measured by cross-correlating a number of lines in the stars' spectra with those in the reference spectrum. The reference spectrum is generally of a radial velocity standard or of a star which does not show any variation in the radial velocity. A portion of wavelength calibrated and continuum fitted spectrum of one of the sample stars is shown in Figure 2.8.

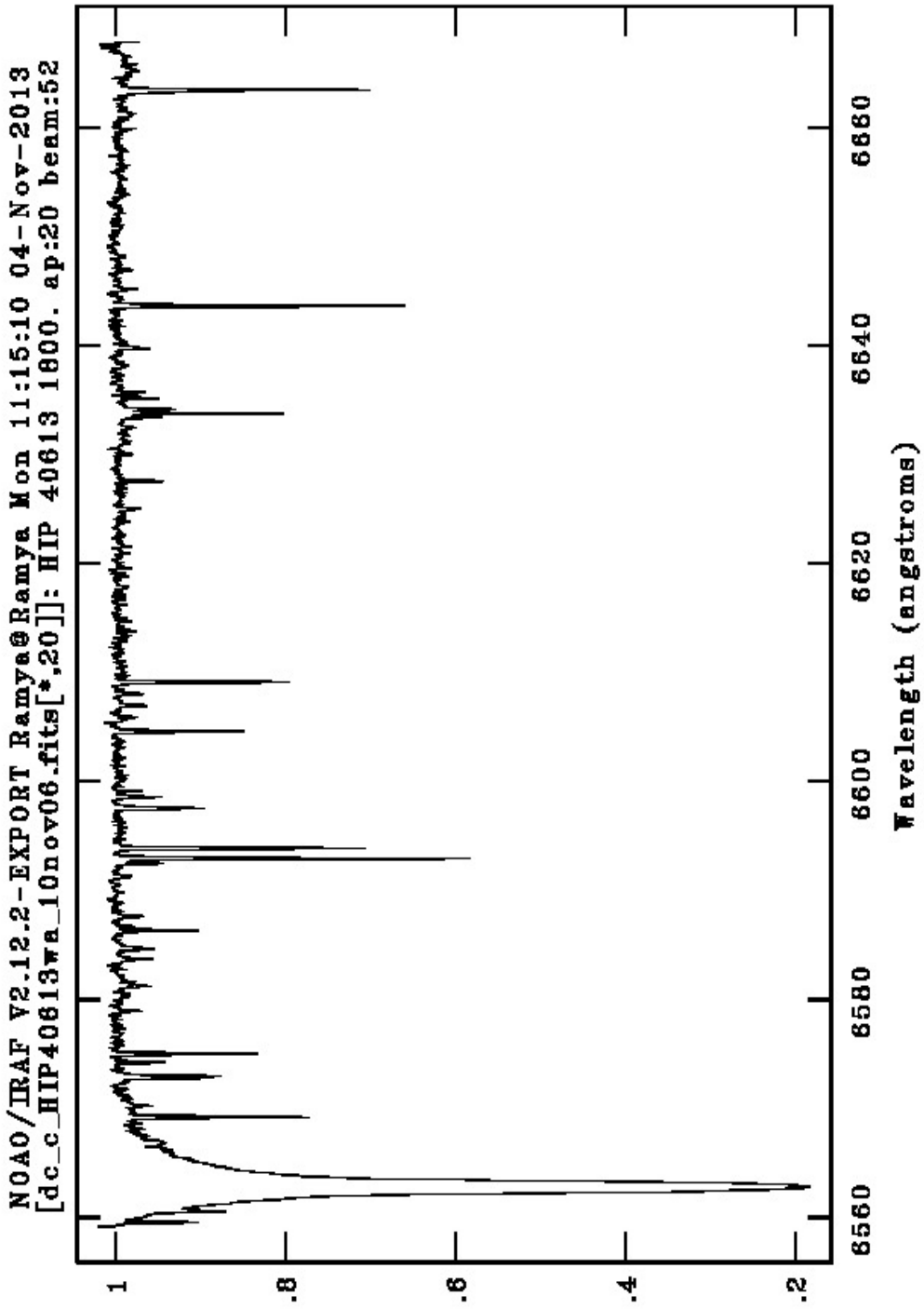

Figure 2.8: A part of wavelength calibrated continuum normalized spectrum of a sample star

2.5 Features in the Spectrum

Stellar spectrum is composed of radiation continuum, superimposed on it absorption or emission features. The features can be either from star itself or can be due to intervening interstellar medium or the earth's atmosphere.

2.5.1 Non-stellar features in the stellar spectrum

Earth's atmosphere blocks most of the UV radiation from the star making the continnum of the spectrum depressed. The electronic, rotational and vibrational transitions in the molecules absorb radiation at the corresponding wavelengths. The absorptions are collectively called telluric absorptions which can be lines or bands, mainly occur in the red and IR region. The major contributors of telluric absorptions are O_2, N_2 and water vapour (H_2O). The strength of telluric absorptions decreases with the altitude of the observatory, and also spectrum taken in winter (less water vapour) sessions show much weaker telluric bands compared to those taken in the summer (more humidity or water vapour in the atmosphere).

Also, stellar spectrum may have contributions from interstellar medium (ISM). ISM is composed of gas and dust (PAH molecules, long chain carbon molecules etc) which absorb star light. This results in many observed Diffused Interstellar Absorption Bands (DIB). The origin of DIBs is not well known. Also, one could notice night sky emissions or air glows in the spectrum. Strong atomic emission line of [O I] at 5577.35 Å is an example for the night sky emission in the spectrum.

2.5.2 Identification of Stellar Features

Stellar features in general are broadened compared to their counter parts from the earth's atmosphere and ISM. All the lines have got a natural width, as the energy levels are not infinitely sharp, and can be described by a Lorentzian profile. This is called natural broadening or radiation broadening, and is independent of the environment. This is common to all the lines. Apart from this, lines originated in stellar atmopsheres get broadened due to thermal and collisional broadening. The Doppler broadening or thermal broadening is due to the random motion of atoms giving rise to Doppler shifted wavelengths of the emitted or absorbed photons. Thermal line profile is Gaussian. The collisional broadening or pressure broadening happens when the energy levels of the atoms are perturbed due to collisional interactions or close encounters with the neighboring atoms or ions. This

broadens the spectral lines asymmetrically and gives rise to line shape which is again close to Lorentzian in nature. Apart from these, there are three major contributions to line broadening: stellar rotation, microturbulence and macroturbulence. The spectral features which are quite sharp compared to rest of the spectral features can be identified as either due to ISM or earth's atmosphere. One could use radial velocities to discriminate stellar features from that of ISM or the earth's atmosphere. A spectrum of very hot and high rotational velocity star is obtained to identify and remove spectral features that are due to ISM and earth's atmosphere.

2.5.3 Equivalent Width

The equivalent width (W_λ) of a spectral line is defined as the width of a rectangle of unit height whose area is same as that of the area enclosed by the spectral line. It is usually expressed in mÅ. The definition of equivalent width is illustrated in Figure 2.9. To measure equivalent width of a line, the continuum is identified properly, and a suitable profile is fit to the line (generally a Gaussian profile, but Voigt profile is preferred in cases where wings of profiles are too broad). Equivalent width is the single most important quantity directly measured from the observed spectrum. It is quite important to have this quantity measured very accurately. Error in W_λ can be due to improper continuum fitting, improper scattered light correction, and neglecting blendings.

2.6 Stellar Atmosphere

Stellar atmosphere represents outer layers of a star from where radiation escapes into space. The major portion of visible stellar spectrum originates from a region called photosphere which is defined as the layer with an optical depth of $\tau \approx 2/3$. Photosphere is a part of stellar atmosphere which is characterized by a set of parameters collectively known as stellar atmospheric parameters : effective surface temperature (T_{eff}), surface gravity ($\log g$), microturbulent velocity (ξ_t) and metallicity ([M/H]). The quantitative abundance measurements require the knowledge of stellar atmospheric parameters.

Effective Surface Temperature

T_{eff} of a star is defined as the temperature of a black body which gives the same total surface flux as the star as given in $L_\star = 4\pi R^2 \sigma T_{eff}^4$. It is expressed in units of Kelvin.

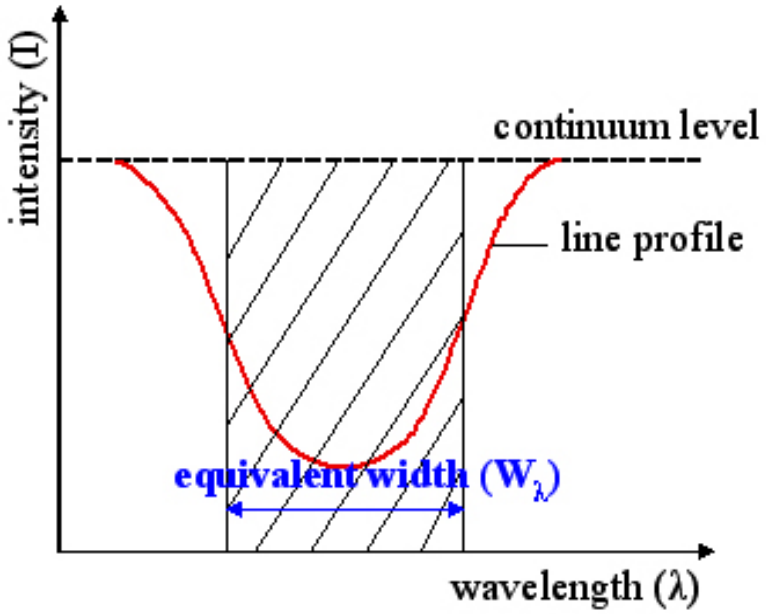

Figure 2.9: The equivalent width. Credit : *wikipedia.org*

Across spectral types, T_{eff} ranges from ~ 30,000 K for an O type star to ~ 3000 K for an M type star.

Surface Gravity

Stellar surface gravity is the gravitational acceleration experienced by particles on star's surface. In the abundance studies this is usually expressed as log g in units of cm s^{-2}. This is also a measure of pressure in the photosphere as given by P = h, where ρ is the density and h is the height. Surface gravity decreases along the luminosity class : with the least value for supergiants, and maximum for white dwarfs. High surface gravity (hence the high pressure) increases the collision rate in the photosphere and broadens spectral lines.

Microturbulent Velocity

Microturbulent velocity denoted as ξ_t is expressed in units of km s^{-2}. It is the non-thermal component of the particle velocity in the photosphere. It is due to the small scale photospheric turbulent motion, with the turbulent element being smaller as compared to the

mean free path of photons. Microturbulence broadens spectral lines. Strong lines are greatly affected by microturbulence compared to weaker lines. Microturbulent velocity is measured by comparing strong broadened lines with weak lines.

Metallicity

Metallicity (Z) of a star can be defined as the relative abundance of elements other than H and He in its photosphere. In astrophysics, all the elements other than hydrogen and helium are considered to be metals. The value of solar metallicity is $Z_{\odot} = 0.02$. In general, metallicities inferred from photometry such as colours are denoted by [M/H].

In the spectroscopic abundance analysis, one normally measures metallicity in terms of Fe abundance with respect to solar value as given below,

$$[\text{Fe/H}] = \log\,(N_{Fe}\,/\,N_H)_{star} - \log(\,N_{Fe}\,/N_H)_{\odot} \tag{2.4}$$

where, N_A is the abundance of the species A by number or the number density of the species A. Solar metallcity $[\text{Fe/H}]_{\odot} = 0$, by definition. Thus, [Fe/H] = +1 implies that the star is metal rich by a factor of 10 compared to the Sun. Similarly, [Fe/H] = −1 means star is metal poor by a factor of 10 compared to the Sun. Abundances are expressed in logarithmic units, dex (decimal exponent).

2.7 Local Thermodynamic Equilibrium (LTE)

In the highly dense, highly opaque and hot stellar interiors, the collision rates are very high and the radiation field can be described as Planck function of one particular temperature. Hence, stellar interiors can be safely assumed to be in thermodynamic equilibrium. But at the stellar suface, from where the radiation escapes into space, the radiation field departs from thermodynamic equilibrium. Also, the colllision rates of particles (atoms, ions etc) in the less dense stellar atmospheres are much less than that in the interior. But as their mean free path is short compared to that of the photons, collision is still considered random. As a result of this, most of the collisions between photons and the gas particles could be viewed as occuring between particles in thermodynamic equilibrium. Therefore, although the radiation field departs from that of a black body, the interactions determining the state of the gas continue to lead to the establishment of an energy distribution for the gas particles characteristic of thermodynamic equilibrium. This allows the complex properties of the gas to be determined by the local temperature alone and

is known as Local Thermodynamic Equilibrium (LTE). In LTE environment, the Boltzmann distribution, Saha's Ionization equation, Maxwellian distribution and Planck radiation formula describe the level populations, ionization states, velocity distribution and the radiation field and hence making the calculations much simpler. However, as we go to the uppermost layers of the atmosphere, where the collision rate almost goes to zero, LTE approximation breaks down. Resonance scattering, overionization, Photon pumping and photon suction are some of the non-LTE effects (Asplund et al. 2009) which contribute significantly.

2.8 Abundance Analysis

Apart from the observed spectrum, it requires a set of tools for deriving elemental abundances. Each one of them is described briefly in this section.

2.8.1 Required data/tools

Theoretical Stellar Model Atmosphere

Model atmospheres are theoretical representation of stellar atmospheres which predict the emergent spectrum for a given set of stellar parameters. The models are constructed using numerical solution of the radiative transfer equation at a predetermined set of optical depths. The models are constructed under LTE conditions like radiative equilibrium, hydrostatic equilibrium, time independence, and homogeneous plane parallel layers in the atmposphere. The two widely used model atmospher grids in the literature are KURUCZ (Kurucz 1998) and MARCS (Gustafsson et al. 2008). In our study, we have extensively used Kurucz models. The model atmosphere grids characterized by specific values of the parameters are taken from the website (http://kurucz.harvard.edu/grids.html), and for all other intermediate values, model atmospheres are generated by interpolating the existing grids.

Spectral Line Data

Choosing suitable lines of various elements with accurate atomic data is important in abundance analysis. One needs to take care that the chosen lines are not highly asymmetric, not blended with other transitions and are reasonably away from atmospheric lines. For the set of identified lines, one needs to gather reliable and accurate atomic data which

includes precise wavelength (λ), Lower Excitation Potential (LEP) of the transition, dissociation energies (in case of molecular lines), oscillator strength or transition probabilities ($\log gf$). For this study we made use of the well reserached compiled list of lines and their atomic data from Reddy et al. (2003) and Ramírez & Allende Prieto (2011), and references therein.

Spectrum Analysis and Synthesis Code

Radiative transfer code MOOG developed on LTE techniques by Chris Sneden (Sneden 1973) is used to calculate abundances for a given model atmophere and input line list which includes equivalent width. MOOG is periodically revised by incorporating latest atomic data and opacity tables. In this study we used the version released in 2009. MOOG is a very versatile programme and has a number of drivers to suit the user. In our study we made use of two drivers *abfind* and *blends*. *abfind* force-fit the abundances to match single line equivalent widths while *blends* takes into account contributions from lines that are blending with a given line for which equivalent width is given. MOOG computes the abundances from each line, by computing the theoretical curve of growth and comparing with the equivalent widths from the observed spectrum.

2.8.2 Curve of Growth Analysis Method

Curve of Growth (COG) analysis is the widely used technique in high resolution spectroscopy to determine the number of absorbers (N_a) or the abundance of elements. Curve of growth is a plot of equivalent width versus the abundance or the number of absorbers of an element (see Figure 2.10).

COG can be split into three regimes depending on strength or equivalent widths of the lines, which essentially categorize the lines into three groups, namely weak, saturated and strong. As depicted in the figure, for weak lines $W_\lambda \propto N_a$, for saturated lines, $W_\lambda \propto \sqrt{logN_a}$ and for strong lines $W_\lambda \propto \sqrt{N_a}$. By comparing measured equivalent width with the theoretical curve of growth, abundance can be determined. The weak lines are the best for abundance estimations.

2.8.3 Derivation of Stellar Atmospheric Parameters

Finding right set of stellar atmospheric parameters for a given set of input line list is an iterative process. The first step towards this process is to choose an element such that it has numerous lines in the spectra with good range in line strengths (say W_λ in the range

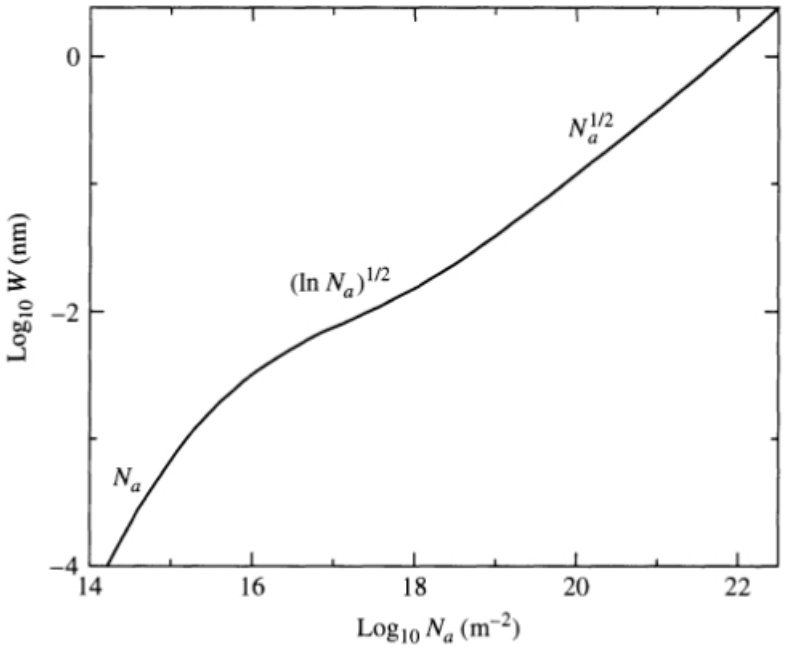

Figure 2.10: The Curve of Growth
Credit : Aller, The Atmospheres of the Sun and Stars, Ronald Press, New York, 1963

3 − 150 mÅ) and LEP (say 0 − 5 eV). It is important to have adequate number of both neutral and ionized lines of this particular element in the spectra. Element iron (Fe) which satisfies these conditions, is used for finding out the atmospheric parameters.

The effective temperature was set by the requirement that the Fe abundance provided by Fe I lines be independent of the lower excitation potential (LEP) of the selected lines (refer Boltzmann equation). While deriving T_{eff}, caution was taken to minimize the effect of microturbulence by choosing, initially, very weak lines with a sufficient range in LEP. Later, microturbulence (ξ_t) was derived by adding moderately strong ($W_\lambda \leq 120$ mÅ) Fe I lines so that the abundance trend becomes sensitive to changes in ξ_t. The lines of different strengths are affected differently by the microturbulence in the stellar atmosphere. The weak lines are unaffected by microturbulence while the strong lines are highly affected. Hence, the chosen value of ξ_t is that, for which the abundance is independent of equivalent width. The surface gravity log g was obtained by requiring that, for the given T_{eff} and ξ_t, Fe I and Fe II lines give the same Fe abundance (refer Saha's ionization equation). The process of deriving atmospheric parameters of the Sun and Arcturus is explained in detail in Chapter 3. The metallicity of the star can be obtained from the estimated Fe abundance.

It is possible to photometrically estimate stellar parameters except the microturbulent

velocity ξ_t. Various colour-temperature empirical calibration relations are available for the photometric estimation of the temperature. Similarly, surface gravity can be determined by fitting isochrones or evolutionary tracks to the stars on colour-magnitude or temperature-magnitude diagram.

2.8.4 Derivation of Chemical Abundances

Once, the stellar atmospheric parameters are determined, the model atmosphere corresponding to these parameters is constructed. Using the model atmosphere that well represents the physical conditions of stellar atmosphere, abundances of various elements are estimated using the *abfind* driver of MOOG. Inputs to the MOOG are the model atmosphere and the line list with atomic data and equivalent widths of transitions of a given star. The differential abundance analysis is performed by using solar photospheric abundances as reference.

The abundance of any element A in the star is expressed in logarithmic unit as follows,

$$\log \varepsilon_A = \log(\ N_A\ /N_H) + 12 \qquad (2.5)$$

where, N_A is the abundance of the species A by number. N_H is the abundance of hydrogen by number. In differential abundance analysis, with the Sun as a reference, the abundance of the element A with respect to any other element B is stated by comparing their ratio with that of the Sun, as given below,

$$[\mathrm{A/B}] = \log(N_A/N_B)_* - \log(N_A\ /N_B)_\odot \qquad (2.6)$$

Hyperfine Structure

Hyperfine fine structure and isotopic shift are two mechanisms which broaden the spectral lines. Hyperfine structure of the energy levels of an atom happens because of the interaction of the nucleus with the electrons around it. Nuclei with even number of protons and even number of neutrons have zero spin. Nuclei with odd number of protons and odd number of neutrons have integral spin, while the rest have half integral spin. When the spin angular momentum of the nucleus interacts with the total angular momentum of the electrons, the hyperfine splitting of the energy levels occurs. As a result of the transition between different hyperfine levels, the overall line width is increased and the

peak intensity of the line is lowered. The resultant line profile may be asymmetric, and significantly vary from the normal profile. This will lead to the wrong measurement of the equivalent width and hence the erroneous elemental abundance estimation. In general, this effect is more relevant in strong lines, where the line gets desaturated and leads to the over-estimation of the equivalent width, and hence the abundance. But, in the case of weak unsaturated lines, the equivalent width will be preserved, even though it may get broadened. Sc, V, Mn, Co, Cu are examples of odd-Z elements while Ba, La and Eu are examples of even-Z elements with hyperfine splitting. In our study, we have considered hyperfine splitting of absorption lines of these elements whenever needed. We adopted the hyperfine components and their relative strengths from Kurucz database, but with the probabilities scaled to the total log gfs used in our study. We made use of the *blends* driver in MOOG to apply hyperfine correction using the HFS data. The *blend* driver re-estimates the elemental abundance by matching the equivalent width measured from the spectrum, and the one synthsized from the HFS data. The correction was taken into account only when the re-estimated abundance was significantly different (compared to the standard deviation) from the abundance without hyperfine structure considered.

The methods described in this chapter are applied for all the sample stars and the calibrated spectra obtained are used for the further analysis.

CHAPTER 3

ANALYSIS OF REFERENCE STARS : SUN AND ARCTURUS

3.1 Introduction

Abundances of stars are not the direct observables but are derived quantities whose reliability is subject to assumptions in the input parameters. For example, stellar model atmospheres are built on the assumption of Local Thermodynamic Equilibrium (LTE) and 1D atmopsheres, in which radiation energy at each plane parallel layer is constant, and temperature is depth independent. However, the real situation is different from the LTE. Any deviations from LTE are treated in Non-LTE and/or 3D calculations (see Asplund et al. 2009) which are yet to become matured to be applied to a large sample of stars with large range in stellar atmospheric parameters. Another input in deriving abundances is the atomic data. Oscillator strengths or gf-values for many transitions are yet to be measured accurately in the laboratory. Some of these would introduce systematic errors in the results and are difficult to quantify. One way to understand the reliability of the analysis and the results is to analyse reference stars for which many of the input parameters are well known, and whose abundances are well established.

In this study we chose to analyse spectrum of the Sun as a reference to our main sequence (dwarfs) sample of thick disc streams, and Arcturus spectrum as a reference to red giant sample of thin disc streams. Arcturus is a bright K giant whose abundances are well measured. We analyse the reference spectra in the same way as that of the programme stars i.e the same atomic data, same line list and the same set of model atmospheres.

3.2 The Sun : Representative Dwarf

Sun is a G type main sequence star or a G dwarf. Chemical composition of the Sun is well established compared to any star in the Galaxy. Because of its proximity, the Sun was studied in detail using very high quality and ultra resolution spectra (see Asplund et al. 2009 for references). The derived abundances and stellar parameters were obtained using some independent methods which established the current solar photospheric abundances. Abundances of the Sun have been measured directly in the laboratory using mass spectroscopy of meteorites. Chondrite type of meteorites are pristine, and are known to have retained the original composition of the Sun barring a few volatile elements such as H, He, C, N, O, and Ne. Solar photospheric abundances and the abundances measured from meteorites taken from Asplund et al. (2009) are given in Table 3.1. As given in the table, there are few elements whose solar photospheric abundances are still not known but many of them have been measured in the chondrites. The abundances, in large majority, obtained from both solar spectrum and meteorites match well. This suggests that the composition of the Sun is not altered since the formation of the solar system 4.5 Gyr ago, except in the case of Li, a light and fragile element, which is depleted in the Sun by a factor of 100 from the meteorite value (log ϵ = 3.26 dex) due to diffusion and mixing.

Table 3.1: Elemental abundances of solar photosphere and meteorites taken from Asplund et al. (2009)

Z	Element	Photosphere	Meteorites	Z	Element	Photosphere	Meteorites
1	H	12.00	8.22 ± 0.04	44	Ru	1.75 ± 0.08	1.76 ± 0.03
2	He	[10.93 ± 0.01]	1.29	45	Rh	0.91 ± 0.10	1.06 ± 0.04
3	Li	1.05 ± 0.10	3.26 ± 0.05	46	Pd	1.57 ± 0.10	1.65 ± 0.02
4	Be	1.38 ± 0.09	1.30 ± 0.03	47	Ag	0.94 ± 0.10	1.20 ± 0.02
5	B	2.70 ± 0.20	2.79 ± 0.04	48	Cd	...	1.71 ± 0.03
6	C	8.43 ± 0.05	7.39 ± 0.04	49	In	0.80 ± 0.20	0.76 ± 0.03
7	N	7.83 ± 0.05	6.26 ± 0.06	50	Sn	2.04 ± 0.10	2.07 ± 0.06
8	O	8.69 ± 0.05	8.40 ± 0.04	51	Sb	...	1.01 ± 0.06
9	F	4.56 ± 0.30	4.42 ± 0.06	52	Te	...	2.18 ± 0.03
10	Ne	[7.93 ± 0.10]	-1.12	53	I	...	1.55 ± 0.08
11	Na	6.24 ± 0.04	6.27 ± 0.02	54	Xe	[2.24 ± 0.06]	-1.95
12	Mg	7.60 ± 0.04	7.53 ± 0.01	55	Cs	...	1.08 ± 0.02

Table 3.1 – continued from previous page

Z	Element	Photosphere	Meteorites	Z	Element	Photosphere	Meteorites
13	Al	6.45 ± 0.03	6.43 ± 0.01	56	Ba	2.18 ± 0.09	2.18 ± 0.03
14	Si	7.51 ± 0.03	7.51 ± 0.01	57	La	1.10 ± 0.04	1.17 ± 0.02
15	P	5.41 ± 0.03	5.43 ± 0.04	58	Ce	1.58 ± 0.04	1.58 ± 0.02
16	S	7.12 ± 0.03	7.15 ± 0.02	59	Pr	0.72 ± 0.04	0.76 ± 0.03
17	Cl	5.50 ± 0.30	5.23 ± 0.06	60	Nd	1.42 ± 0.04	1.45 ± 0.02
18	Ar	[6.40 ± 0.13]	-0.50	62	Sm	0.96 ± 0.04	0.94 ± 0.02
19	K	5.03 ± 0.09	5.08 ± 0.02	63	Eu	0.52 ± 0.04	0.51 ± 0.02
20	Ca	6.34 ± 0.04	6.29 ± 0.02	64	Gd	1.07 ± 0.04	1.05 ± 0.02
21	Sc	3.15 ± 0.04	3.05 ± 0.02	65	Tb	0.30 ± 0.10	0.32 ± 0.03
22	Ti	4.95 ± 0.05	4.91 ± 0.03	66	Dy	1.10 ± 0.04	1.13 ± 0.02
23	V	3.93 ± 0.08	3.96 ± 0.02	67	Ho	0.48 ± 0.11	0.47 ± 0.03
24	Cr	5.64 ± 0.04	5.64 ± 0.01	68	Er	0.92 ± 0.05	0.92 ± 0.02
25	Mn	5.43 ± 0.04	5.48 ± 0.01	69	Tm	0.10 ± 0.04	0.12 ± 0.03
26	Fe	7.50 ± 0.04	7.45 ± 0.01	70	Yb	0.84 ± 0.11	0.92 ± 0.02
27	Co	4.99 ± 0.07	4.87 ± 0.01	71	Lu	0.10 ± 0.09	0.09 ± 0.02
28	Ni	6.22 ± 0.04	6.20 ± 0.01	72	Hf	0.85 ± 0.04	0.71 ± 0.02
29	Cu	4.19 ± 0.04	4.25 ± 0.04	73	Ta	...	-0.12 ± 0.04
30	Zn	4.56 ± 0.05	4.63 ± 0.04	74	W	0.85 ±0.12	0.65 ± 0.04
31	Ga	3.04 ± 0.09	3.08 ± 0.02	75	Re	...	0.26 ± 0.04
32	Ge	3.65 ± 0.10	3.58 ± 0.04	76	Os	1.40 ± 0.08	1.35 ± 0.03
33	As	...	2.30 ± 0.04	77	Ir	1.38 ± 0.07	1.32 ± 0.02
34	Se	...	3.34 ± 0.03	78	Pt	...	1.62 ± 0.03
35	Br	...	2.54 ± 0.06	79	Au	0.92 ± 0.10	0.80 ± 0.04
36	Kr	[3.25 ± 0.06]	-2.27	80	Hg	...	1.17 ± 0.08
37	Rb	2.52 ± 0.10	2.36 ± 0.03	81	Tl	0.90 ± 0.20	0.77 ± 0.03
38	Sr	2.87 ± 0.07	2.88 ± 0.03	82	Pb	1.75 ± 0.10	2.04 ± 0.03
39	Y	2.21 ± 0.05	2.17 ± 0.04	83	Bi	...	0.65 ± 0.04
40	Zr	2.58 ± 0.04	2.53 ± 0.04	90	Th	0.02 ± 0.10	0.06 ± 0.03
41	Nb	1.46 ± 0.04	1.41 ± 0.04	92	U	...	-0.54 ± 0.03
42	Mo	1.88 ± 0.08	1.94 ± 0.04				

The good matching of the composition derived from two independent methods made the Sun as a reference star to compare with any other abundances in the universe. In this study we used solar spectrum taken from Hinkle et al. (2000) which has spectral resolution of R $\approx$ 70,000. Most of the lines used in this study come from the careful study by Reddy et al. (2003) who picked lines from the solar spectrum that are symmetric, unblended, and weak to medium strong lines. Many of the lines have laboratory oscillator strengths. In cases where gf values were not available they inverted solar and stellar spectra to get best possible gf values (see Reddy et al. 2003). Data for few other lines which are not included in Reddy et al. (2003) study come from Ramírez & Allende Prieto (2011). A total of 151 lines for 16 elemental species were measured, of which 60 were Fe I and 10 were Fe II lines. The entire line list with measured equivalent widths and the logarithmic abundances from each line are given in Tables 3.2 and 3.3.

Table 3.2: Adopted iron line data for the giant sample (thin disc streams)

Wavelength (λ) Å	LEP eV	log gf	$W_{\lambda_\odot}$ mÅ	log $\varepsilon_\odot$ dex	$W_{\lambda_{Arcturus}}$ mÅ	log $\varepsilon_{Arcturus}$ dex
			Fe I			
5295.31	4.420	-1.590	29.1	7.53	46.5	6.99
5379.57	3.690	-1.510	60.5	7.39	94.9	6.92
5386.33	4.150	-1.670	32.1	7.43	54.8	6.87
5441.34	4.310	-1.630	30.3	7.49	52.3	6.99
5638.26	4.220	-0.770	75.8	7.41	100.9	6.97
5679.02	4.652	-0.750	58.2	7.45	71.4	6.91
5705.46	4.301	-1.355	37.7	7.36	59.8	6.83
5731.76	4.260	-1.200	56.5	7.52	80.5	7.02
5778.45	2.588	-3.440	22.2	7.45	73.2	6.89
5793.91	4.220	-1.619	33.2	7.45	55.5	6.90
5855.08	4.608	-1.478	20.9	7.38	35.5	6.88
5905.67	4.650	-0.690	56.8	7.36	71.9	6.84
5927.79	4.650	-0.990	41.5	7.38	54.9	6.82
5929.68	4.550	-1.310	39.5	7.57	55.8	7.02
6003.01	3.880	-1.060	81.7	7.48	109.6	6.95

Table 3.2 – continued from previous page

Wavelength (λ) Å	LEP eV	log gf	$W_{\lambda_\odot}$ mÅ	log $\varepsilon_\odot$ dex	$W_{\lambda_{Arcturus}}$ mÅ	log $\varepsilon_{Arcturus}$ dex
6027.05	4.076	-1.090	63.2	7.35	91.1	6.86
6056.00	4.730	-0.400	70.6	7.37	83.6	6.88
6079.01	4.650	-1.020	44.9	7.47	59.3	6.93
6093.64	4.607	-1.300	30.2	7.42	44.2	6.86
6096.66	3.984	-1.810	36.9	7.48	63.3	6.91
6151.62	2.176	-3.282	48.7	7.42	117.8	6.97
6165.36	4.143	-1.460	43.9	7.42	69.6	6.89
6187.99	3.940	-1.620	46.1	7.43	76.8	6.91
6240.65	2.223	-3.287	47.8	7.45	116.0	6.99
6270.23	2.858	-2.540	51.6	7.40	104.0	6.89
6703.57	2.759	-3.023	36.1	7.46	90.3	6.92
6705.10	4.607	-0.980	45.4	7.38	63.1	6.87
6713.75	4.795	-1.400	20.8	7.44	29.6	6.89
6726.67	4.607	-1.030	46.0	7.43	60.8	6.87
6793.26	4.076	-2.326	12.4	7.41	30.0	6.90
6810.26	4.607	-0.986	48.6	7.44	65.6	6.92
6828.59	4.640	-0.820	54.6	7.41	71.3	6.90
6842.69	4.640	-1.220	39.1	7.52	54.4	6.99
6843.66	4.550	-0.830	59.5	7.42	77.6	6.90
6999.88	4.100	-1.460	53.8	7.52	80.4	6.98
7022.95	4.190	-1.150	63.6	7.47	87.6	6.92
7132.99	4.080	-1.650	42.1	7.47	67.2	6.90
5358.12	3.300	-3.162	9.5	7.43	35.6	6.91
5661.35	4.280	-1.756	21.7	7.38	43.6	6.90
5849.69	3.695	-2.930	6.6	7.38	24.4	6.92
5856.10	4.294	-1.558	32.5	7.44	56.4	6.95
5858.79	4.220	-2.180	12.5	7.44	28.8	6.95
5859.60	4.550	-0.608	69.3	7.41	88.7	6.97
6159.38	4.610	-1.830	12.6	7.45	25.3	7.00
6271.28	3.330	-2.703	23.8	7.45	59.3	6.87

Table 3.2 – continued from previous page

Wavelength (λ) Å	LEP eV	log gf	$W_{\lambda_\odot}$ mÅ	log $\varepsilon_\odot$ dex	$W_{\lambda_{Arcturus}}$ mÅ	log $\varepsilon_{Arcturus}$ dex
6436.41	4.186	-2.360	10.0	7.46	24.1	6.95
6518.37	2.830	-2.450	56.2	7.36	111.7	6.87
6581.21	1.480	-4.680	20.8	7.51	99.2	6.97
6591.33	4.593	-1.950	10.4	7.44	21.5	6.99
6608.04	2.279	-3.914	17.2	7.43	75.2	6.90
6699.14	4.590	-2.100	7.9	7.45	18.1	7.04
6725.36	4.103	-2.167	17.0	7.44	36.0	6.90
6733.15	4.638	-1.400	25.9	7.43	38.7	6.87
6739.52	1.560	-4.794	11.5	7.39	76.4	6.80
6837.01	4.590	-1.687	17.6	7.44	29.9	6.92
6857.25	4.076	-2.038	22.3	7.43	41.2	6.83
6971.94	3.020	-3.340	12.6	7.41	49.1	6.87
7751.12	4.990	-0.730	45.3	7.43	57.9	6.97
7802.51	5.080	-1.310	15.4	7.41	18.5	6.84
7807.92	4.990	-0.509	58.8	7.44	68.2	6.93
			Fe II			
5234.62	3.221	-2.180	83.3	7.36	89.1	6.94
5425.26	3.200	-3.220	41.3	7.44	43.9	6.91
6149.25	3.889	-2.630	35.7	7.36	32.5	6.91
6247.56	3.892	-2.271	52.8	7.39	42.4	6.82
6456.39	3.903	-2.065	62.3	7.39	52.7	6.88
5264.80	3.230	-3.130	47.9	7.53	46.6	6.92
5414.07	3.221	-3.580	27.5	7.50	28.7	6.90
6369.46	2.891	-4.110	19.4	7.48	23.7	6.93
6432.68	2.891	-3.570	40.9	7.46	44.8	6.93
6516.08	2.891	-3.310	52.6	7.45	57.9	6.96

Table 3.3: Adopted line list for elements other than iron, for the giant sample (thin disc streams)

Species	Wavelength (λ) Å	LEP eV	loggf	$W_{\lambda_\odot}$ mÅ	log $\varepsilon_\odot$ dex	$W_{\lambda_{Arcturus}}$ mÅ	log $\varepsilon_{Arcturus}$ dex
[O I]	6363.78	0.020	-10.19	2.0	8.99	29.6	8.78
	6300.31	0.000	-9.75	5.4	8.98	66.0	8.84
Na I	6154.23	2.10	-1.55	36.6	6.28	70.6	5.89
	6160.75	2.10	-1.25	56.5	6.29	92.7	5.91
Mg I	5711.09	4.34	-1.73	104.1	7.54	151.6	7.57
	6318.72	5.11	-1.95	44.5	7.58	74.8	7.46
	6319.24	5.11	-2.32	27.4	7.65	59.1	7.59
	7657.61	5.11	-1.28	98.5	7.59	127.1	7.51
Al I	6696.02	3.14	-1.48	36.9	6.40	91.5	6.39
	6698.67	3.14	-1.78	20.8	6.36	60.3	6.22
	7835.31	4.02	-0.69	41.1	6.41	64.9	6.30
	7836.13	4.02	-0.45	55.0	6.36	80.8	6.29
Si I	5690.42	4.93	-1.77	48.1	7.47	59.5	7.23
	5701.10	4.93	-1.95	37.9	7.47	50.1	7.23
	5772.15	5.08	-1.65	52.3	7.55	62.2	7.34
	6142.49	5.62	-1.540	33.3	7.58	33.0	7.33
	6145.02	5.61	-1.479	37.6	7.59	38.6	7.38
Ca I	5260.39	2.52	-1.72	32.1	6.27	75.6	5.89
	5867.56	2.93	-1.57	22.6	6.27	58.6	5.95
	6166.44	2.52	-1.14	69.1	6.31	120.6	6.01
	6169.04	2.52	-0.80	90.3	6.32	142.8	6.06
	6169.56	2.53	-0.48	108.7	6.28	157.5	5.99
	6455.60	2.52	-1.34	55.9	6.28	110.6	5.99
	6471.66	2.53	-0.69	90.6	6.20	148.7	5.99
	6499.65	2.52	-0.82	84.7	6.23	140.9	5.98
Sc II	5357.20	1.51	-2.11	4.8	3.19	27.4	2.82
	5552.23	1.46	-2.28	4.6	3.28	25.0	2.87
	5684.21	1.51	-1.07	37.1	3.24	87.5	2.88
	6245.64	1.51	-1.04	35.2	3.14	89.5	2.84

Table 3.3 – continued from previous page

Species	Wavelength (λ) Å	LEP eV	loggf	$W_{\lambda_\odot}$ mÅ	log $\varepsilon_\odot$ dex	$W_{\lambda_{Arcturus}}$ mÅ	log $\varepsilon_{Arcturus}$ dex
	6300.75	1.51	-1.95	8.2	3.24	33.6	2.77
	6320.84	1.50	-1.92	8.9	3.24	40.9	2.86
Ti I	5295.77	1.07	-1.58	13.2	4.95	103.1	4.67
	5490.15	1.46	-0.88	22.0	4.89	108.2	4.58
	5702.66	2.29	-0.59	7.3	4.83	59.8	4.58
	5716.44	2.30	-0.72	5.9	4.87	53.2	4.61
	6092.79	1.89	-1.32	4.1	4.89	54.4	4.64
	6303.75	1.44	-1.51	8.8	4.99	90.0	4.72
	6312.23	1.46	-1.50	8.1	4.95	88.7	4.72
	6599.10	0.90	-2.03	9.3	4.98	113.9	4.78
	7357.73	1.44	-1.07	22.2	4.97	131.8	4.77
Ti II	4583.41	1.17	-2.87	33.0	5.06	86.1	4.76
	4708.66	1.24	-2.37	53.3	5.04	103.6	4.72
	5336.78	1.58	-1.63	71.7	4.96	125.6	4.78
	5418.77	1.58	-2.11	48.5	4.97	99.0	4.69
V I	6039.73	1.06	-0.65	12.3	3.93	95.6	3.45
	6081.44	1.05	-0.58	13.0	3.87	112.6	3.49
	6090.21	1.08	-0.06	32.3	3.89	136.9	3.50
	6119.53	1.06	-0.32	21.0	3.88	118.8	3.49
	6135.36	1.05	-0.75	10.2	3.91	107.5	3.52
	6274.65	0.27	-1.67	6.9	3.87	122.5	3.51
Cr I	5287.20	3.44	-0.89	11.3	5.65	32.6	5.18
	5300.74	0.98	-2.08	59.3	5.60	142.9	5.14
	5304.18	3.46	-0.68	16.0	5.63	37.3	5.09
	5628.62	3.42	-0.76	14.7	5.62	35.8	5.07
	5781.16	3.01	-1.00	16.7	5.54	46.8	4.96
	6882.48	3.44	-0.38	32.4	5.67	65.0	5.15
	6883.00	3.44	-0.42	30.5	5.67	64.1	5.17
Mn I	4671.69	2.89	-1.66	14.8	5.47	42.7	4.70
	4739.11	2.94	-0.60	60.7	5.39	102.1	4.73

Table 3.3 – continued from previous page

Species	Wavelength (λ) Å	LEP eV	loggf	$W_{\lambda_\odot}$ mÅ	log $\varepsilon_\odot$ dex	$W_{\lambda_{Arcturus}}$ mÅ	log $\varepsilon_{Arcturus}$ dex
	5004.89	2.92	-1.64	14.0	5.45	41.1	4.73
Co I	5280.63	3.63	-0.03	20.3	4.90	59.6	4.62
	5352.04	3.58	0.06	25.1	4.88	67.5	4.62
	5647.23	2.28	-1.56	13.9	4.90	78.9	4.70
	6455.00	3.63	-0.25	14.8	4.89	54.0	4.68
Ni I	6176.80	4.09	-0.26	62.0	6.22	82.6	5.80
	5088.96	3.678	-1.240	28.2	6.19	58.6	5.83
	5094.42	3.833	-1.074	30.4	6.22	54.7	5.78
	5115.40	3.834	-0.281	75.2	6.29	93.8	5.81
	6111.08	4.088	-0.808	33.6	6.22	51.5	5.74
	6130.14	4.266	-0.938	21.6	6.24	32.0	5.71
	6175.37	4.089	-0.550	47.7	6.24	64.3	5.73
	6177.25	1.826	-3.508	14.1	6.22	68.6	5.76
	6772.32	3.658	-0.972	48.0	6.24	75.2	5.76
	7797.59	3.900	-0.348	75.3	6.27	100.8	5.85
	7826.77	3.700	-1.840	12.5	6.23	30.2	5.78
Zn I	4810.54	4.080	-0.170	71.6	4.45	82.1	4.10
	6362.35	5.790	0.140	21.2	4.53	20.8	4.39
Ba II	5853.68	0.604	-1.000	60.3	2.15	118.7	1.61
	6141.73	0.704	-0.032	109.1	2.23	177.9	1.75
	6496.91	0.604	-0.377	94.6	2.18	176.7	1.85

Regarding representative model atmospheres, there are two widely used model grids: ATLAS9 model atmospheres (Kurucz 1998) and MARCS models originally developed by Gustafsson et al. (1975). Both are LTE, 1D, line blanketted and convective models. Following the detailed discussion in Reddy et al. (2003), we adopt Kurucz models throughout. Kurucz models come in two flavours: with convective overshoot and without convective overshoot. Again, following the rational described in Reddy et al. (2003), and also with the intention of comparing our results with the thin and thick disc results from them we adopted convective overshoot models for the main sequence sample of thick

disc streams, and for the giant sample of thin disc streams, we used models without convective overshoot. The radiative transfer code MOOG originally developed by Sneden (1973) was used for abundance derivation. Since its original use in 1973, MOOG has been revised several times incorporating latest line data and opacities. We used in this study the MOOG version updated in 2009.

With the recipe described above, using the Kurucz model atmospheres without overshoot option, and the line list given in Table 3.2, we derived solar atmopsheric parameters: T_{eff}, log g, ξ_t and [Fe/H]. This has been an iterative process as described in previous chapters. (see Chapter 2, Section 2.6, for method description). Final results plots: Abundance versus LEP, abundance versus reduced equivalent width (W_λ/λ) and abundance versus wavelength (λ) obtained for Fe I lines, are shown in Figure 3.1. The analysis yields the following solar parameters : T_{eff} = 5835 K, log g = 4.55 cm s^{-2}, ξ_t = 1.25 km s^{-1}, for [M/H] = 0. Abundance of Fe I is taken as the metallicity ([Fe/H]) as it is based on a large number of lines which have accurate atomic data. Uncertainties in the parameters are estimated by analysing sensitivities of the fittings to the abundance trends. For example, noticeable change in the abundance trends is seen for changes in T_{eff} by ± 50 K. Similarily, we found ± 0.20 cm s^{-2} for log g, ± 0.20 km s^{-1} for ξ_t and ± 0.1 dex for [Fe/H]. Within the uncertainties, the parameters derived in this study for the Sun are well matched with the values derived in the literature.

Derived abundances of 16 elements using convective models without overshoot option and the line list in Table 3.3, are given in Table 3.4. For lines of Mn and V hyperfine structure is taken into account. Our results are compared with the values taken from the recent study by Asplund et al. (2009). As shown in the Table 3.4, solar abundances derived agree well with those from the literature. However, for oxygen the difference is significant which is about 0.28 dex higher in our study. For oxygen we used two forbidden [O I] lines: at 6300.31 Å (W_λ = 5.4 mÅ) and 6363.78 Å (W_λ = 2 mÅ). The forbidden [O I] line at 6300.31 Å is known to have a Ni I blend (Lambert 1978, Allende Prieto et al. 2001), and the other forbidden [O I] line at 6363.78 Å is affected by CN feature (Asplund et al. 2009).

For comparison, we have derived solar photospheric abundances using model atmospheres with overshoot option. These are tabulated in Table 3.4 and denoted as *over*. The comparison between the two sets of abundances (with and without overshoot options, as $\triangle$(Abundance) = without overshoot - with overshoot) is illustrated in Figure 3.2. Results from models without overshoot for the Sun are systematically lower compared to the results from models with overshoot option. With the intention of comparing our results

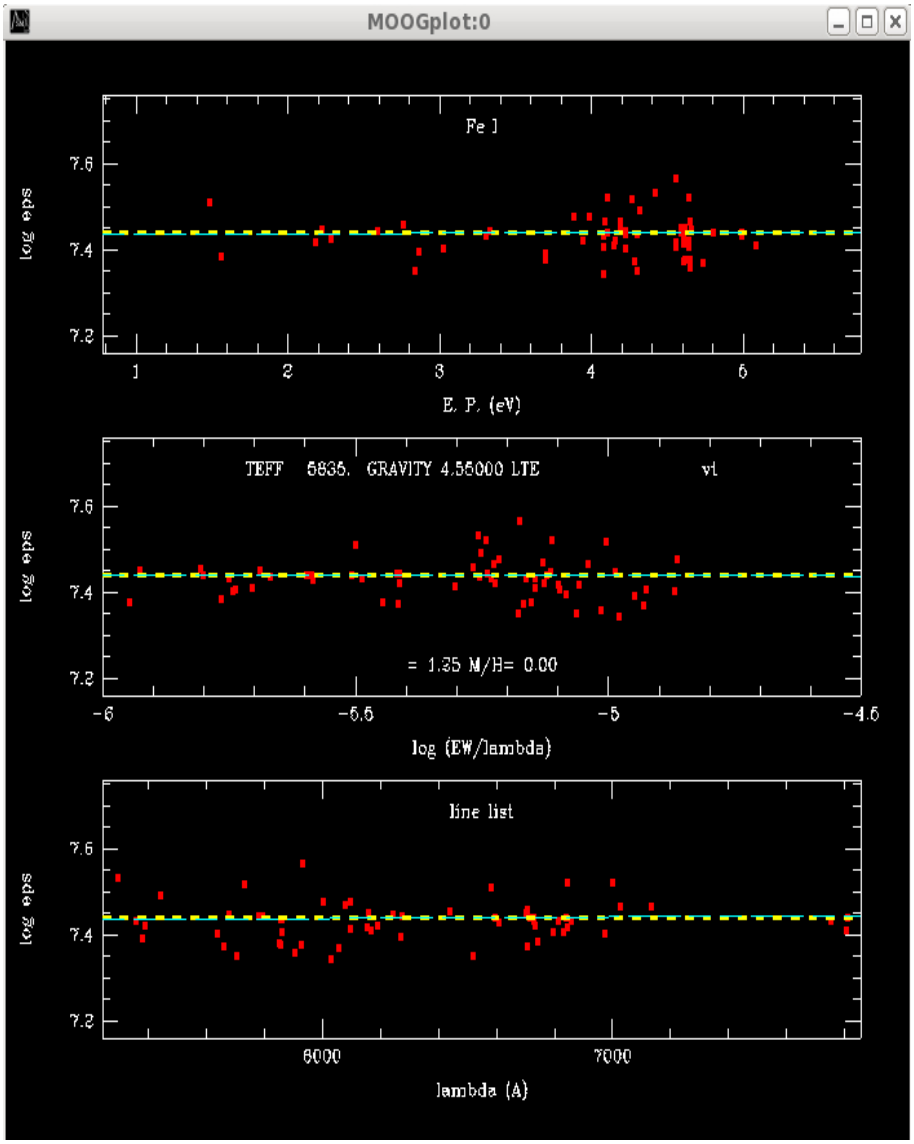

Figure 3.1: The MOOG output window for Fe I lines

with those of thin and thick disc populations (Reddy et al. 2003, Reddy et al. 2006) whose abundances have been derived using models with overshoot option, we adopted models with convective overshoot for the dwarf sample of thick disc streams. Also, it is observed that the solar model constructed by ATLAS9 with overshoot option best matches many of the Sun's observables such as center-to-limb darkening and Fe I and Fe II abundances (see Castelli et al. 1997, Reddy et al. 2003).

Table 3.4: Solar abundances derived using *over* and *nover* models. Abundances from Asplund et al. (2009) are given for comparison

Species	Current Study			Literature	Difference	
	$(\log\varepsilon \pm \sigma)_{nover}$	$(\log\varepsilon \pm \sigma)_{over}$	N	$\log\varepsilon \pm \sigma$	*nover*	*over*
	dex	dex		dex	dex	dex
[O I](λ 6363.78 Å)	8.99 ± ...	9.00 ± ...	1	8.69 ± 0.05	+0.30	+0.31
[O I](λ 6300.31 Å)	8.98 ± ...	8.99 ± ...	1	8.69 ± 0.05	+0.29	+0.30
Na I	6.29 ± 0.01	6.32 ± 0.01	2	6.24 ± 0.04	0.05	+0.08
Mg I	7.59 ± 0.04	7.62 ± 0.04	4	7.60 ± 0.04	-0.01	+0.02
Al I	6.38 ± 0.03	6.40 ± 0.03	4	6.45 ± 0.03	-0.07	-0.05
Si I	7.53 ± 0.06	7.56 ± 0.06	5	7.51 ± 0.03	0.02	+0.05
Ca I	6.27 ± 0.04	6.30 ± 0.04	8	6.34 ± 0.04	-0.07	-0.04
Sc II	3.22 ± 0.05	3.24 ± 0.05	6	3.15 ± 0.04	0.07	+0.09
Ti I	4.93 ± 0.06	4.95 ± 0.05	9	4.95 ± 0.05	-0.02	0.00
Ti II	5.01 ± 0.05	5.04 ± 0.05	4	4.95 ± 0.05	0.06	+0.09
V I	3.89 ± 0.03	3.91 ± 0.03	6	3.93 ± 0.08	-0.04	-0.02
Cr I	5.63 ± 0.05	5.65 ± 0.05	7	5.64 ± 0.04	-0.01	0.01
Mn I	5.44 ± 0.04	5.47 ± 0.04	3	5.43 ± 0.04	0.01	+0.04
Fe I	7.44 ± 0.05	7.46 ± 0.05	60	7.50 ± 0.04	-0.06	-0.04
Fe II	7.44 ± 0.06	7.46 ± 0.06	10	7.50 ± 0.04	-0.06	-0.04
Co I	4.89 ± 0.01	4.92 ± 0.01	4	4.99 ± 0.07	-0.1	-0.07
Ni I	6.23 ± 0.03	6.26 ± 0.03	11	6.22 ± 0.04	0.01	+0.04
Zn I	4.49 ± 0.05	4.53 ± 0.05	1	4.56 ± 0.05	-0.06	-0.03
Ba II	2.19 ± 0.05	2.21 ± 0.04	2	2.18 ± 0.09	0.01	+0.03

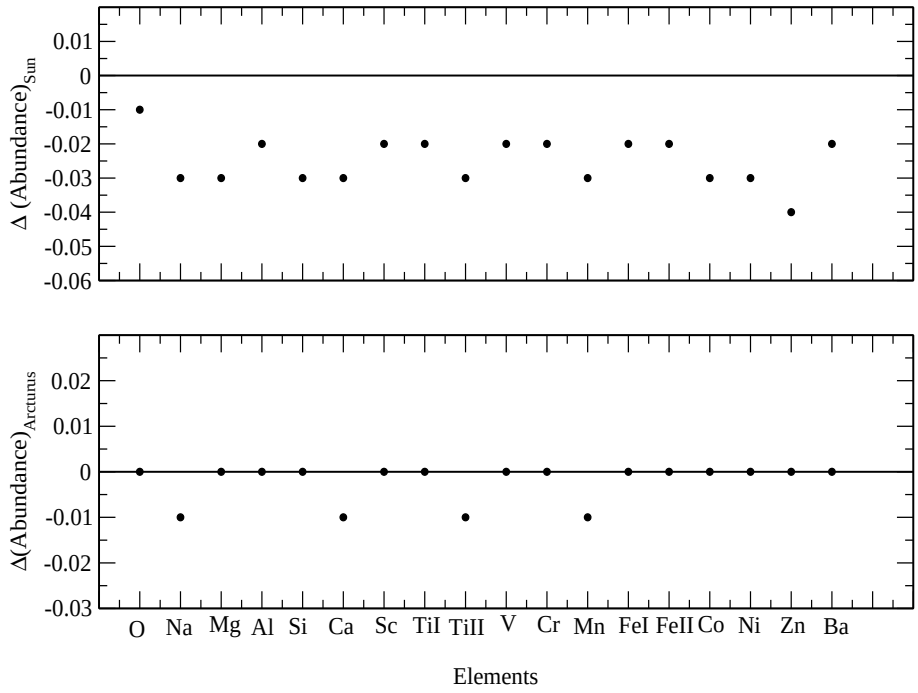

Figure 3.2: Comaprison between elemental abundances derived using model atmospheres with and without convective overshoot, for the Sun (top) and for Arcturus (bottom)

3.3 Arcturus : Representative Giant

The sample for thin disc streams is K giants. We chose Arcturus as a reference star. Arcturus has been studied well and many studies recorded it's chemical composition. Among them study of Peterson et al. (1993) is one of the well known for Arcturus. Recently, Ramírez & Allende Prieto (2011) made a very detailed abundance study of Arcturus based on high quality spectrum. For the analysis, we used Arcturus spectrum of resultion R $\approx$ 70,000 obtained by Hinkle et al. (2000) from Kitt Peak National Observatory (KPNO). The adopted line list is given in Tables 3.2 and 3.3. For giants we used Kurucz convective models but without overshoot option. It is pointed out that overshoot model for stars of too hot and too cold compared to the Sun are not in agreement with many observables.

Using the adopted input line list, stellar model grids with no overshoot option combined with MOOG code and the measured equivalent widths, we derived Arcturus atmospheric parameters: T_{eff} = 4350 K, log g = 1.70 cm s^{-2}, ξ_t = 1.59 km s^{-1} and [M/H] = – 0.52 dex. Fe abundances from neutral and ionized lines were found to be log $\varepsilon_{\rm FeI}$ = 6.92 dex and log $\varepsilon_{\rm FeII}$ = 6.91 dex, respectively. The derived parameters are in good agreement

with those by Ramírez & Allende Prieto (2011) whose values are: T_{eff} = 4286 K, log g = 1.66 cm s^{-2}, and ξ_t = 1.74 km s^{-1}, [Fe I/H] = −0.52 ± 0.02, and [Fe II/H] = − 0.40 ± 0.03. Abundance results of 16 elements along with the results obtained in Ramírez & Allende Prieto (2011), are given in Table 3.5.

Table 3.5: Abundances of Arcturus derived using *over* and *nover* models. For comparison, abundances derived by Ramírez & Allende Prieto (2011) are also given. Literature value of Ba abundance is from Peterson et al. (1993). $(\log\varepsilon_{\rm FeI})_\odot = (\log\varepsilon_{\rm FeII})_\odot = 7.44$ is adopted to calculate the [Fe I/H] and [Fe II/H].

	Current Study			Literature		Difference	
Species	$(\log\varepsilon \pm \sigma)_{nover}$ dex	$(\log\varepsilon \pm \sigma)_{over}$ dex	N	$\log\varepsilon \pm \sigma$ dex	N	*nover* dex	*over* dex
[O I] (λ 6363.78)	8.78 ± ...	8.78 ±...	1	8.67 ± +0.01	3	+0.11	0.11
[O I] (λ 6300.31)	8.84 ± ...	8.84 ±...	1	8.67 ± +0.01	3	+0.17	0.17
Na I	5.90 ± 0.02	5.91 ± 0.02	2	5.82 ± 0.03	4	+0.08	+0.09
Mg I	7.53 ± 0.06	7.53 ± 0.06	4	7.47 ± 0.10	5	+0.06	+0.06
Al I	6.30 ± 0.07	6.30 ± 0.07	4	6.26 ± 0.06	4	+0.04	+0.04
Si I	7.30 ± 0.07	7.30 ± 0.07	5	7.30 ± 0.06	5	+0.00	+0.00
Ca I	5.98 ± 0.05	5.99 ± 0.05	8	5.94 ± 0.07	10	+0.04	+0.05
Sc II	2.84 ± 0.04	2.84 ± 0.04	6	2.86 ± 0.04	7	-0.02	-0.02
Ti I	4.67 ± 0.08	4.68 ± 0.08	9	4.66 ± 0.07	13	+0.01	+0.02
Ti II	4.74 ± 0.04	4.75 ± 0.04	4	4.66 ± 0.05	4	+0.08	+0.09
V I	3.50 ± 0.02	3.50 ± 0.02	6	3.58 ± 0.05	8	-0.08	-0.08
Cr I	5.11 ± 0.08	5.11 ± 0.08	7	4.99 ± 0.09	11	+0.12	+0.12
Mn I	4.72 ± 0.02	4.73 ± 0.02	3	4.74 ± 0.10	5	-0.02	-0.01
Co I	4.65 ± 0.04	4.65 ± 0.04	4	4.71 ± 0.13	7	-0.06	-0.06
Ni I	5.78 ± 0.04	5.78 ± 0.04	11	5.73 ± 0.07	6	+0.05	+0.05
Zn I	4.25 ± 0.20	4.25 ± 0.19	2	4.21 ± 0.08	2	+0.04	+0.04
Ba II	1.74 ± 0.12	1.74 ± 0.12	3	1.63 ± ...	...	+0.11	+0.11
[Fe I/H]	-0.58 ± 0.05	-0.58 ± 0.06	60	-0.52 ± 0.02	37	-0.06	-0.06
[Fe II/H]	-0.59 ± 0.04	-0.59 ± 0.04	10	-0.40 ± 0.03	9	-0.19	-0.19

Table 3.5 shows that results derived by us for Arcturus agree very well with those derived by Ramírez & Allende Prieto (2011), within the uncertainties. For a comparison we obtained results for Arcturus using models with overshoot option as well, which are also tabulated in Table 3.5. Figure 3.2 shows that, both the results agree well with each other. As we use model without convective overshoot to the giant star members, their derived abundances were referenced to the solar abundances derived using the same models with no overshoot option.

The study of the Sun and Arcturus yields results compatible with the literature values, validating our analysis techniques. Hence, the same techniques are applied to the programme stars of various streams studied in this thesis, in the following chapters.

CHAPTER 4

STREAMS IN THE GALACTIC THICK DISC

4.1 Introduction

In this chapter, we study chemical tagging of a sample of stars of two identifed streams that are known to belong to the Galactic thick disc. The two streams are: Arcturus and a new stream known as AF06. A brief description of each of the streams is followed by kinematic and abundance study, discussion on the origin scenarios of the two streams and concluding remarks.

4.2 Arcturus Stream and AF06 Stream

The stream Arcturus is named after a bright K type red giant, Arcturus (HIP 69673). Arcturus is one of the brightest stars in the night sky with a visual magnitude of V = −0.04. It is a nearby star with high proper motion: $\mu_\alpha \cos\delta$ = -1094 mas/yr and μ_δ = -2000 mas/yr. It was O. J. Eggen, who first detected that a significant fraction of high proper motion stars in the solar neighborhood moves with Arcturus, or shares its kinematics. He named this group of stars as Arcturus stream (Eggen 1971c). Arcturus stream is a classical high velocity stream, present in the Galactic disc, lagging LSR by ∼ 100−125 km s^{-1}. Later, Arcturus stream was detected independently by various studies (Helmi et al. 2006, Arifyanto & Fuchs 2006, Bovy et al. 2009, Williams et al. 2009, Minchev et al. 2009, Antoja et al. 2009, Klement et al. 2008), using different kinematic parameters such as $U - V - W$ space, V - $\sqrt{U^2 + 2V^2}$ space, $A - P - J_z$ space etc.

The second stream in this study comes from the study of Arifyanto & Fuchs (2006)

who identified this as a new stream as it did not have any known kinemtic relation with any other bright star or open cluster. This is one of the streams that have been detected using modern statistical techniques and improved astrometry. The stream was identified as a clear overdensity in the kinemtic plane of V versus $\sqrt{U^2 + 2V^2}$. The new stream later coined as AF06 by Klement et al. 2009 after the authors of the original study. Members of AF06 lag LSR by ~ 90 km s^{-1}. The overdensity at the same kinematic coordinates was independently confirmed in other studies (Helmi et al. 2006, Klement et al. 2008, and Klement et al. 2009).

4.3 Analysis of the Programme Stars

A sample of total 40 main sequence stars for the two thick disc streams has been chosen for chemical tagging study : 18 for Arcturus stream and 22 for AF06 stream. A full description of the sample is given in Chapter-2 (see Tables 2.1 and 2.2)

4.3.1 Stellar Atmospheric Parameters

Atmospheric parameters – effective temperature (T_{eff}), surface gravity (log g) and metallicity ([M/H]) have been derived from both photometric and spectroscopic data. In the former case, we relied on published catalogues of photometry and parallaxes, empirical calibrations and the theoretical stellar evolutionary models. And, in the latter case, high resolution spectra were used to derive atmospheric parameters including microturbulence (ξ_t). Below, both the procedures are described in brief.

Photometry

The T_{eff} is derived using $V - K_s$ colour and Strömgren photometry (*uvby*) calibrations. The K_s magnitude is taken from 2MASS catalogue* (Cutri et al. 2003). The subscript 's' stands for the bandpass of the K filter in the 2MASS survey, i.e., the K_s filter is narrower than the Johnson K filter. The K_s magnitudes are converted to standard 'K' magnitudes using relations given in Ramírez & Meléndez (2005). The mean difference between the two magnitudes is very small K_s - $K_{tcs} = -0.001 \pm 0.005$, and will have no effect when K_s is used in place of K magnitudes in the calibration between $V - K$ and T_{eff}. The V

*This publication makes use of data products from the 2MASS, which is a joint project of the University of Massachusetts and the Infrared Processing and Analysis Centre/California Institute of Technology, funded by the National Aeronautics and Space Administration (NASA) and the National Science Foundation

magnitudes for all the stars were adopted from Kharchenko (2001). The $V-K$ colour and the empirical relations provided in Alonso et al. (1996) are used in deriving T_{eff} (with [Fe/H]= 0).

Strömgren colours and indices ($b-y$, m_1, c_1) are available for 26 out of 44 stars in the sample (Hauck & Mermilliod 1998). Values of metallicity and T_{eff} were obtained using empirical calibrations of Strömgren colours and indices given in Schuster & Nissen (1989) and Alonso et al. (1996), respectively. Values of metallicity are quite sensitive to reddening as it makes observed ($b-y$) more positive and m_1 values more negative than their intrinsic colours. However, we expect no significant reddening as the stars are nearby (d < 130 pc from the Sun). Using the methods given in Schuster & Nissen (1989), reddening values $E(b-y)$ have been estimated and, indeed, all reddening estimates are vanishingly small: $E(b-y) \leq 0.001 \pm 0.006$. Temperatures derived using $V-K_s$ and Strömgren colours are given in Appendix B.1 and B.2 as $(T_{eff})_{V-K}$ and $(T_{eff})_{b-y}$, respectively. The mean difference between the two temperatures, $(T_{eff})_{V-K} - (T_{eff})_{b-y}$ = 18 ± 90 K, excluding the outliers HIP 24030, HIP 53070, HIP 11952 and G 192−21, for which the difference is large 245 ± 24 K, i.e., T_{eff} derived from $V-K_s$ colour are hotter than those from ($b-y$). The ($b-y$) temperature of HIP 24030 and $V-K_s$ temperature of G 192−21 are much closer to the values obtained using spectroscopy. In the case of the other two, we suspect errors in one of the their colours.

The log g values derived from the trigonometrical parallax, the $B-V$ colour, and theoretical isochrones (Demarque et al. 2004) are given in Appendix B.1 and B.2. Errors in the parallax and $B-V$ colour are taken into account in estimating the uncertainty in the log g value.

Spectroscopy

A full set of atmospheric parameters (T_{eff}, log g, ξ_t, [M/H]) has been derived from spectral line analysis by standard LTE techniques and are given in Appendix B.1 and B.2. In this exercise, the LTE Kurucz grid of ATLAS9 model atmospheres with the convective overshoot option was adopted (Kurucz 1998). Rational for choosing overshoot models is described in Chapter 3. We intend to compare our results with the results from the thin and thick disc studies of Reddy et al., and hence, we followed their analysis techniques. The LTE line analysis code MOOG (Sneden 1973) in its 2009 version was used throughout.

We used 54 Fe I lines and 9 Fe II lines of equivalent width $W_\lambda \leq 120$ mÅ adopted from Reddy et al. (2003) for the spectrsocopic estimation of the atmospheric parameters,

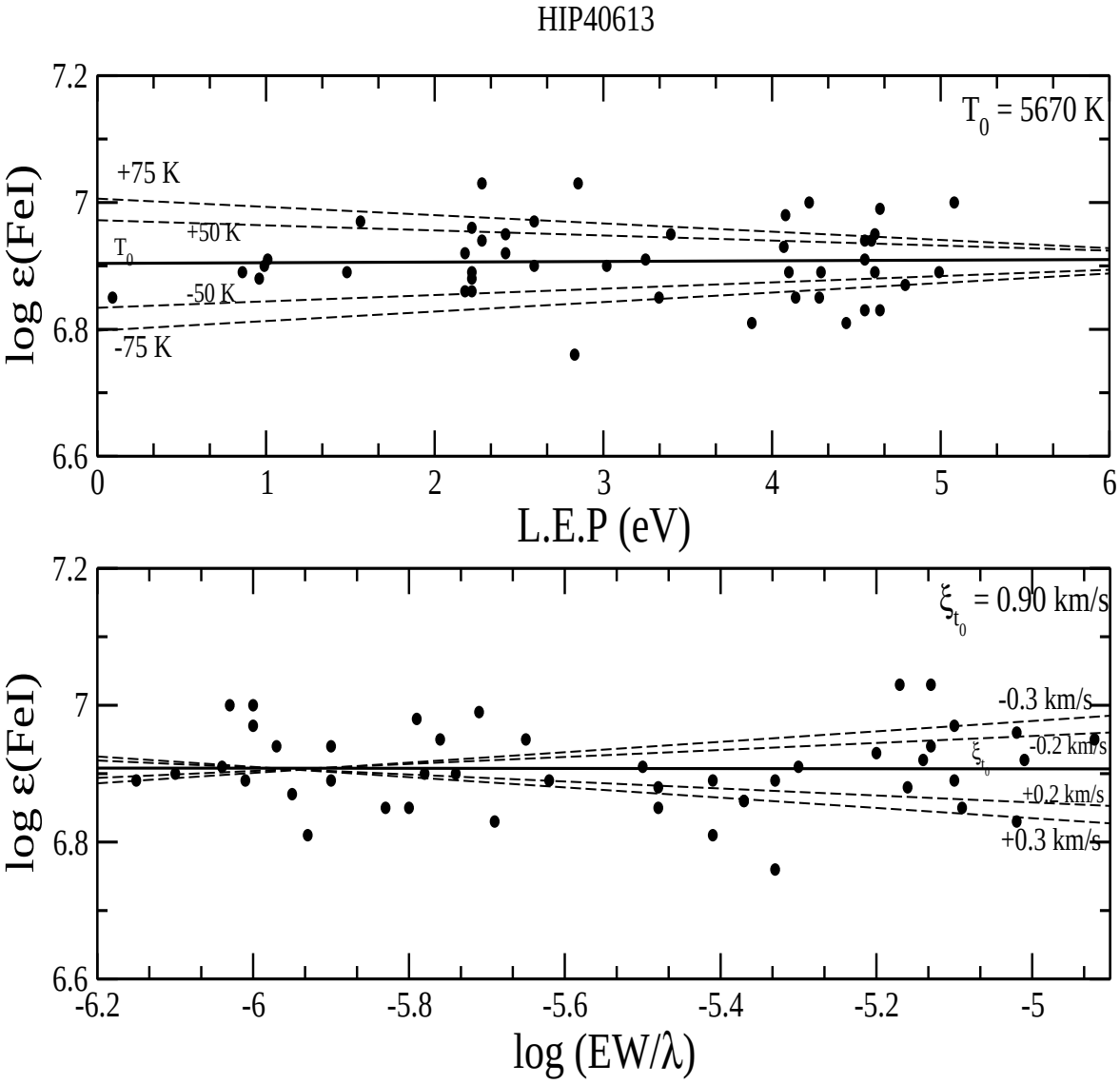

Figure 4.1: Estimation of uncertainties in the T_{eff} (top) and ξ_t (bottom). The solid center line is for the best representative model parameter. Broken lines represent models with increasing or decreasing T_{eff} and ξ_t in steps of 25 K and 0.1 km s^{-1}, respectively.

the procedure of which is already explained in Chapter 2. The uncertainties in the derived parameters have been estimated by inspection of dependencies for combinations of models of different sets of parameters. In the case of T_{eff}, we varied the best representative T_{eff} in steps of 25 K for given log g, ξ_t and [M/H]. For steps of 25 K changes, we found no significant changes in the slope as well as in abundances, however, we see (See Figure 4.1) noticeble changes in abundance trends by increasing or decreasing 50 K from its

mean model T_{eff}. Thus, we estimate ± 50 K as an uncertainty in the best fit model atmosphere. Similarly, we found model uncertainties in log g and ξ_t. In Figure 4.1, estimation of uncertainties is illustrated for T_{eff} and ξ_t. In this way, we found model uncertainties in T_{eff}, log g, and ξ_t: ± 50 K, ± 0.20 cm s^{-2}, ± 0.20 km s^{-1}, respectively. These individual uncertainties translate to an effective error of ± 0.05 dex in metallicity [Fe/H].

Next, photometric and spectroscopic estimates of model atmosphere parameters are compared. Temperature, log g and metallicity comparisons are given in Figure 4.2. The mean difference between $(T_{eff})_{V-K}$ and spectroscopic T_{eff} is just −9 ± 87 K. There are a few outliers HIP 24030 and HIP 94931 (for which $(T_{eff})_{b-y}$ values are closer to spectroscopic T_{eff}), G 10−12 and HIP 9080 (for which $(T_{eff})_{b-y}$ not available) with a difference of −77 ± 174 K. Excluding the outliers the mean difference becomes -2 ± 73 K. The log g values obtained from photometry are in good agreement with the spectroscopic values : the difference between the two methods is only 0.002 ± 0.18 cm s^{-2} for 23 stars for which photometric gravities could be obtained, a difference within the combined uncertainties. The mean difference between the photometric metallicity from Strömgren photometry and the spectroscopic metallicity is −0.03 ± 0.11 dex for 25 stars for which Strömgren photometry is available. Star G 192−21 is an outliers whose spectroscopic metallicity is about 0.7 dex metal rich compared to the corresponding photometric value. Difference is probably due to erroneous Strömgren photometry. For the two metal poor stars HIP 53070 and HIP 11952, too few lines are available for a spectroscopic determination of parameters and, therefore, we have adopted photometric $(T_{eff})_{b-y}$ and log g values. The microturbulent velocity ξ_t calculated using the relation given in Reddy et al. (2003) between ξ_t, T_{eff}, and log g was adopted for both stars. In the final calculations of abundances we adopt parameters derived from spectroscopy but no conclusions would change were the photometric parameters adopted.

4.3.2 Abundances

Elemental abundances have been derived using measured equivalent widths and synthetic spectra with LTE model atmospheres for the adopted stellar parameters taken from Kurucz grid (Kurucz 1998) and the 2009 version of LTE line analysis code MOOG. The line list compiled by Reddy et al. (2006) was adopted. Solar abundances derived by Reddy et al. (2003) have been used as reference values, except for Eu abundance. The solar Eu abundance (log ε(Eu) = 0.55) has been derived, for this study, using the Atlas solar spectrum (Hinkle et al. 2000) and two Eu II lines (6645.13 Å, 4129.72 Å). For transitions with significant hyperfine structure (HFS) data were taken from Kurucz HFS data base

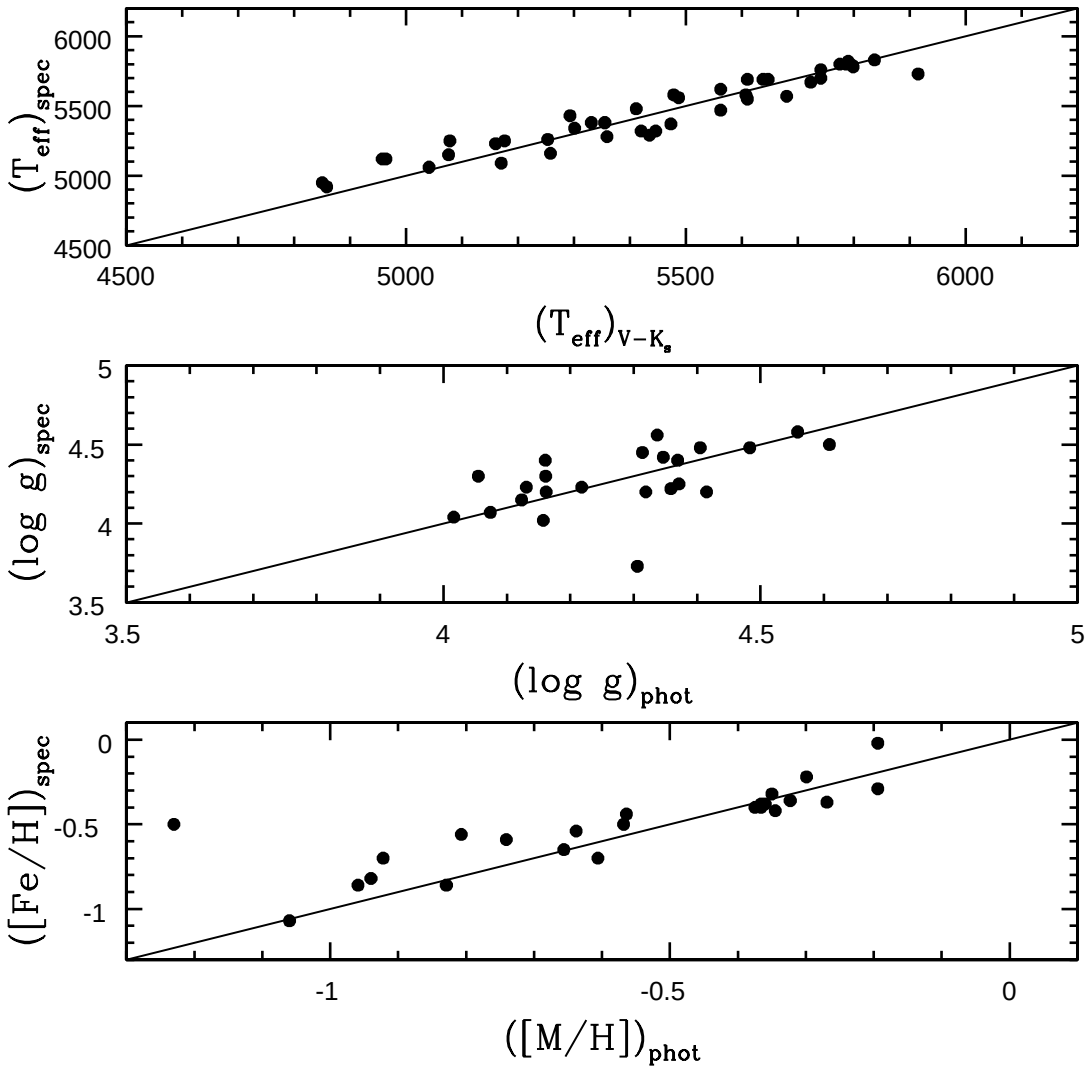

Figure 4.2: Comparison of atmospheric parameters derived using spectroscopy and photometry.

(Kurucz 1998). The lines of Mn, V, Cu, and Eu with HFS were analyzed by computing synthetic spectra. In the case of vanadium, the line at 6216.36 Å, one of the six lines used previously, is now judged to be blended in the cooler stars and is omitted from the analysis of such stars. Elemental abundances are summarized in Appendix B.6-B.9.

Uncertainties in the derived abundances arise primarily from uncertainties in the derived atmospheric parameters, the equivalent widths (W_λ) and oscillator strengths (log gf). The latter two quantities affect primarily the line-to-line scatter. Of course, the line-

to-line scatter is to some extent also influenced by uncertain model parameters. Uncertainty in the log gf values is minimized as our analysis is a differential one with respect to solar spectrum analysis. Error in the measured W_λ is estimated following the recipe given in (Cayrel 1988). For the quality of our data, uncertainty in the measured W_λ varies from 1 mÅ to about 2.5 mÅ. We have taken on average 2 mÅ as the uncertainty in the measured W_λ. In Table 4.1, we have provided for one representative star (HIP 40613), estimated uncertainties for each element in the form of Δ[X/Fe] due to δT_{eff}, δlog g, $\delta\xi_t$, δ[M/H], and δW_λ. Assuming all five sources of error discussed above are independent, the combined error is obtained by adding them in quadrature. This we call our measured uncertainty or σ_{model}.

Uncertainties in abundances can also be gauged by comparing results for stars that are common in this and other studies. For seven stars that are common with thick disc sample study by Reddy et al. (2006), differences in the derived abundance ratios [X/Fe] between the studies are given in Table 4.2. The differences are quite small and less than measured uncertaintity (σ_{model}). The good agreement between the two studies implies that the results of the two streams in this study can be compared directly with the results of thick disc sample study from Reddy et al. (2006). This is akin to a differential analysis with respect to thick disc.

Table 4.1: Error estimates for a typical sample star (HIP 40613)

Quantity	N	ΔT_{eff} ± 50 K	$\Delta \log g$ ± 0.2 dex	$\Delta \xi_t$ ± 0.2 km s^{-1}	Δ[M/H] ± 0.1 dex	ΔW_λ ± 2 mÅ	σ_{model}
Δ [O I/Fe]	3	± 0.05	± 0.04	± 0.01	± 0.01	± 0.02	± 0.07
Δ [Na I/Fe]	2	± 0.03	± 0.01	± 0.00	± 0.00	± 0.03	± 0.04
Δ [Mg I/Fe]	2	± 0.03	± 0.03	± 0.02	± 0.00	± 0.02	± 0.05
Δ [Al I/Fe]	5	± 0.02	± 0.03	± 0.01	± 0.00	± 0.01	± 0.04
Δ [Si I/Fe]	7	± 0.01	± 0.01	± 0.01	± 0.00	± 0.01	± 0.02
Δ [Ca I/Fe]	5	± 0.04	± 0.03	± 0.03	± 0.00	± 0.01	± 0.06
Δ [Sc II/Fe]	3	± 0.01	± 0.08	± 0.02	± 0.02	± 0.03	± 0.09
Δ [Ti I/Fe]	7	± 0.05	± 0.02	± 0.02	± 0.00	± 0.01	± 0.06
Δ [V I/Fe]	5	± 0.06	± 0.01	± 0.00	± 0.00	± 0.03	± 0.07
Δ [Cr I/Fe]	4	± 0.05	± 0.01	± 0.01	± 0.00	± 0.02	± 0.06
Δ [Cr II/Fe]	1	± 0.02	± 0.08	± 0.02	± 0.02	± 0.08	± 0.12
Δ [Mn I/Fe]	3	± 0.06	± 0.01	± 0.01	± 0.00	± 0.01	± 0.06
Δ [Fe I/H]	45	± 0.04	± 0.01	± 0.03	± 0.01	± 0.00	± 0.05
Δ [Fe II/H]	6	± 0.02	± 0.08	± 0.04	± 0.02	± 0.01	± 0.09
Δ [Co I/Fe]	3	± 0.04	± 0.00	± 0.01	± 0.00	± 0.02	± 0.05
Δ [Ni I/Fe]	16	± 0.03	± 0.01	± 0.02	± 0.00	± 0.01	± 0.04
Δ [Cu I/Fe]	3	± 0.04	± 0.02	± 0.04	± 0.01	± 0.04	± 0.07
Δ [Zn I/Fe]	2	± 0.01	± 0.02	± 0.05	± 0.02	± 0.03	± 0.07
Δ [Y II/Fe]	4	± 0.01	± 0.08	± 0.04	± 0.02	± 0.02	± 0.09
Δ [Ba II/Fe]	3	± 0.02	± 0.03	± 0.12	± 0.03	± 0.01	± 0.13
Δ [Ce II/Fe]	1	± 0.01	± 0.08	± 0.01	± 0.03	± 0.13	± 0.16
Δ [Nd II/Fe]	1	± 0.02	± 0.09	± 0.01	± 0.03	± 0.16	± 0.19
Δ [Eu II/Fe]	2	± 0.01	± 0.09	± 0.01	± 0.03	± 0.07	± 0.12

Table 4.2: Comparison of current study with the Reddy et al. (2006) sample for common stars

Quantity	HIP 40613	HIP 74033	HIP 9080	HIP 10652	HIP 22020	HIP 24030	HIP 34642	Mean (dex)
ΔT_{eff}	0.00	116.00	88.00	81.00	86.00	−8.00	53.00	59 ± 47
Δ log g	−0.14	0.09	−0.20	−0.16	−0.12	−0.44	−0.07	−0.15 ± 0.16
Δ [Fe I/H]	0.08	0.15	0.20	0.08	0.13	−0.07	0.02	0.08 ± 0.09
Δ [O/Fe]	−0.08	−0.20	−0.33	−0.15	−0.15	0.04	−0.06	−0.13 ± 0.12
Δ [Na/Fe]	−0.06	−0.07	−0.02	0.02	−0.09	−0.07	−0.01	−0.04 ± 0.04
Δ [Mg/Fe]	−0.02	−0.06	−0.06	0.05	−0.03	0.07	0.15	0.01 ± 0.08
Δ [Al/Fe]	−0.01	...	−0.09	0.05	−0.04	0.08	−0.01	0.00 ± 0.06
Δ [Si/Fe]	−0.05	−0.11	−0.12	0.06	−0.05	0.00	0.00	−0.04 ± 0.06
Δ [Ca/Fe]	0.02	−0.12	...	0.09	−0.01	0.12	0.06	0.03 ± 0.09
Δ [Sc/Fe]	−0.13	−0.02	−0.21	−0.15	−0.03	−0.15	0.12	−0.08 ± 0.11
Δ [Ti/Fe]	0.04	−0.05	0.08	0.12	0.05	0.07	0.11	0.06 ± 0.06
Δ [V/Fe]	0.00	−0.14	0.08	0.07	−0.01	...	0.11	0.02 ± 0.09
Δ [Cr/Fe]	−0.15	...	−0.02	−0.06	0.00	0.03	−0.06	−0.04 ± 0.06
Δ [Mn/Fe]	−0.01	0.05	−0.14	0.03	0.00	0.12	0.08	0.02 ± 0.08
Δ [Co/Fe]	−0.03	−0.10	−0.07	0.02	0.03	0.10	0.14	0.01 ± 0.09
Δ [Ni/Fe]	0.00	−0.06	−0.13	0.05	0.04	−0.04	0.07	−0.01 ± 0.07
Δ [Zn/Fe]	0.18	0.14	0.06	0.02	0.10	0.15	0.20	0.12 ± 0.07
Δ [Y/Fe]	−0.02	−0.06	0.35	0.08	0.08	−0.20	0.12	0.05 ± 0.17
Δ [Ba/Fe]	0.04	0.03	0.01	−0.11	−0.01	−0.04	...	−0.01 ± 0.06
Δ [Ce/Fe]	−0.11	−0.06	0.08	0.10	0.02	...	0.14	0.03 ± 0.10
Δ [Nd/Fe]	−0.04	−0.03	...	...	...	...	0.20	0.04 ± 0.14
Δ [Cu/Fe]	0.03	0.07	0.20	0.07	0.12	0.07	0.17	0.10 ± 0.06
Δ [Eu/Fe]	0.00	−0.01	−0.20	−0.17	−0.07	...	0.07	−0.06 ± 0.10

4.3.3 Kinematics

Both the streams were identified by Arifyanto & Fuchs (2006) as over-densities of stars in phase space. To represent stars in phase space, one requires information such as co-ordinates, radial velocities, distance (parallaxes), and proper motions. In the calculation of Galactic motions Arifyanto & Fuchs (2006) used HIPPARCOS data (Perryman et al. 1997) and radial velocities from Carney et al. (1994). Recently, HIPPARCOS observations were re-reduced by van Leeuwen (2007). Consequently, we have rederived the Galactic velocities (U, V, W) for stream members using the revised HIPPARCOS parallaxes and proper motions and including the radial velocities derived from our high resolution spectra of the sample stars. Radial velocities obtained in this study are in very good agreement with the velocities given in Arifyanto & Fuchs (2006). The mean difference between the two studies is 0.15 ± 0.50 km s^{-1}.

The U, V and W velocities with respect to the Sun are calculated using the method given in Johnson & Soderblom (1987). A right-handed coordinate system is used throughout where U is positive towards the Galactic center, V is positive in the direction of Galactic rotation and W is positive towards the North Galactic Pole (NGP). Velocities (U, V, W) are in good agreement with values given by Arifyanto & Fuchs (2006); differences between the two studies are mainly due to the updated parallaxes. None of the stars identified as members by Arifyanto & Fuchs (2006) lost their membership in either stream. Derived radial velocities (V_r) and Galactic velocities (U_{LSR}, V_{LSR}, W_{LSR}) relative to Local Standard of Rest (LSR) are given in Appendix A.1 and A.2, for Arcturus and AF06 streams respectively. In conversion to the LSR frame, the solar motion of ($U_\odot$, $V_\odot$, $W_\odot$) = (+10.0, +5.3, +7.2) km s^{-1}) is used (Dehnen & Binney 1998).

The mean motion (U_{LSR}, V_{LSR}, W_{LSR}) of the Arcturus stream based on 18 member stars observed by us is (-6.48 ± 49.29, -124.79 ± 8.92, -11.5 ± 49.59) and for AF06 stream the mean motion is (-41.55 ± 47.45, -87.35 ± 7.83, 3.82 ± 54.34). These values are in good agreement with the streams' central values given in Arifyanto & Fuchs (2006).

To compute orbital parameters, the (U, V, W) of each star is integrated over the Galactic potential provided by D. Lin (private communication). Orbital parameters: mean of apogalactic and perigalactic distance (R_m), eccentricity (e), maximum distance star away from the Galactic plane (Z_{max}) have been derived and given in Appendix A.1 and A.2. A distance of 8.5 kpc beween the Sun and the Galactic center is used in the calculation.

Probabilities:

The (U, V, W) of both the streams, as Arifyanto & Fuchs (2006) appreciated, suggest that the streams are part of the thick disc. Probabilities that a particular star belongs to the halo, the thick or the thin disc are calculated using the definitions and recipes given in Reddy et al. (2006), who had adopted the method employed in Bensby et al. (2003), Bensby et al. (2004) and Mishenina et al. (2004). The method described in Reddy et al. (2006) is given below.

The sample is assumed to be a mixture of the three populations - the thick disc, the thin disc and the halo. Each of these populations is represented by Gaussian distribution functions of the velocity components U_{LSR}, V_{LSR} and W_{LSR} with given mean values and dispersions. The relative number of thin disc, thick disc and halo stars are taken from literature. The equations establishing the probability that a star belongs to the thin disc (P_{thin}), the thick disc (P_{thick}) or the halo (P_{halo}) are,

$$P_{thin} = \mathrm{f}_1\ \mathrm{P}_1/P\ ;\ P_{thick} = \mathrm{f}_2\ \mathrm{P}_2/P\ ;\ P_{halo} = \mathrm{f}_3\ \mathrm{P}_3/P \tag{4.1}$$

where $P = \Sigma\ \mathrm{f}_i\ P_i$

$$P_i = \mathrm{K}_i\ \exp\ [\ -\frac{U_{LSR}^2}{2\sigma_{U_i}^2}\ -\frac{(V_{LSR}-V_{ad})^2}{2\sigma_{V_i}^2}\ -\frac{W_{LSR}^2}{2\sigma_{W_i}^2}] \tag{4.2}$$

$$\text{with } \mathrm{K}_i = \frac{1}{(2\pi)^{2/3}\sigma_{U_i}\sigma_{V_i}\sigma_{W_i}}\ (\mathrm{i} = 1, 2, 3) \tag{4.3}$$

The asymmetric drift V_a is explained in Chapter 1. The values of U_{LSR}, V_{LSR} and W_{LSR} are given in Appendix A.1 and A.2. The values of σ and the population fractions f_i are given in Table 1.1, which are taken from the studies of Robin et al. (2003), Ojha et al. (1996), Ojha et al. (1999) and Soubiran et al. (2003). The asymmetric drifts V_a given by Robin et al. (2003) are referred to the Sun and, therefore, we have corrected them for the solar motion relative to the LSR ($V_\odot$ = +5.3 km s^{-1}).

The percentage probability (P_{thick}) that a star belongs to the thick disc is given in Appendix A.1 and A.2. All the Arcturus stream members in our sample are thick disc stars with a probability $P_{thick} \geq 80$ %, while 15 out of the 26 AF06 stream members have a probability that would qualify them as thick disc members with the remaining 11 stars having probabilities placing them in either the thin or thick discs.

Angular Momemtum

In Figure 4.3, sample stars of the two streams along with the representative members of the thick disc, the thin disc and the halo are shown in the space of angular momentum per unit mass components J_z, and $J_\perp = \sqrt{J_x^2 + J_y^2}$ the azimuthal and perpendicular components, respectively.

The components angular momentum per unit mass - J_x, J_y and J_z are calculated as given below,

$$J_x = (yv_z) - (v_y z) \tag{4.4}$$

$$J_y = (zv_x) - (v_z x) \tag{4.5}$$

$$J_z = (xv_y) - (v_x y) \tag{4.6}$$

$$J_\perp = \sqrt{J_x^2 + J_y^2} \tag{4.7}$$

where,

$$v_x = U_{LSR} \tag{4.8}$$

$$v_y = V_{LSR} + V_0 \tag{4.9}$$

$$v_z = W_{LSR} \tag{4.10}$$

All these values are calculated in the right-handed coordinate system and the LSR velocity is assumed to be $V_0 = 220$ km s^{-1}.

In angular momentum space, stars are clustered in a small region compared to their distribution in the velocity space (see Helmi & de Zeeuw 2000). The high value of J_z implies high velocity in the direction of the Galactic rotation. The $J_\perp$ represents extent of tilt of star's orbit with respect to the Galactic plane. Obviously, for the thin disc it is quite small. Arcturus stream and AF06 stream have a mean J_z of -811 ± 77 kpc km s^{-1} and -1130 ± 63 kpc km, s^{-1}, respectively.

The presence of the Arcturus stream was detected by Navarro et al. (2004) in catalogues of metal-poor stars by Beers et al. (2000) and Gratton et al. (2003). They found the Arcturus stream lagging the LSR by 120 km s^{-1} but with a large dispersion of $\sigma_V \sim$ 50 km s^{-1}. Their detected structure has angular momentum (J_z) in the range of (700 − 1100) km s^{-1} kpc. It appears to us that this structure detected by Navarro et al. (2004) is

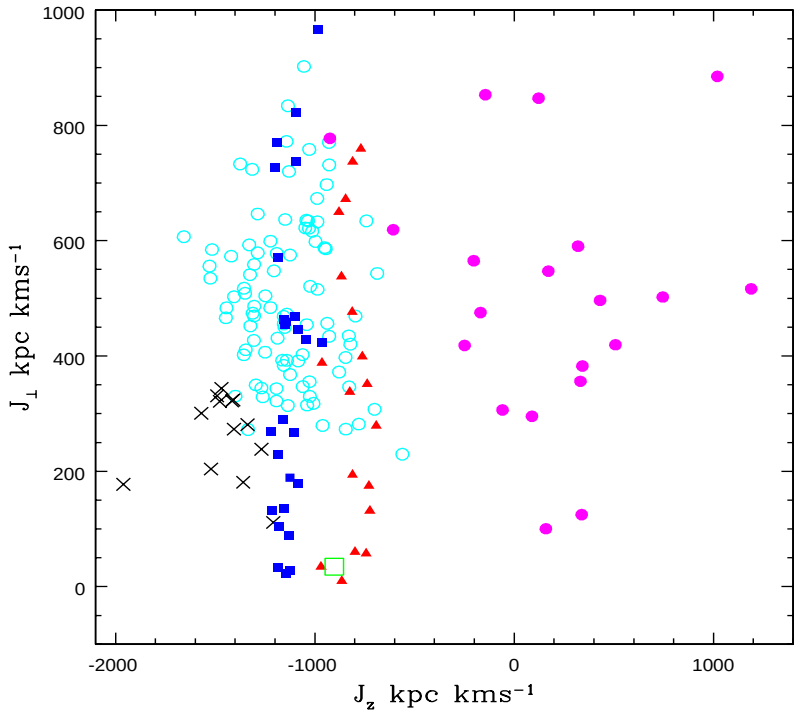

Figure 4.3: Stream stars are shown with members of halo, thick disc and thin disc stars taken from Reddy et al. (2006) in the angular momentum space: $J_{\perp}$ versus J_z. Red triangles: Arcturus stream, Blue filled squares: AF06 stream, Cyan open circle: Thick disc, Black crosses: Thin disc, Magenta filled circles: Halo, Green open square: Giant Arcturus.

the combined structure of the Arcturus and the AF06 stream but this structure was separated into two different streams by Arifyanto & Fuchs (2006) using the wavelet transform technique. By combining our samples of both streams, we get mean values V_{LSR} and J_z (-102.67 ± 20.34, -1000 ± 173) very similar to what Navarro et al. (2004) found for the structure that they thought to be the single structure labelled the Arcturus stream. The Arcturus stream has been identified in recent studies (Klement et al. 2008) as a significant over density in phase space. Klement et al. (2008)'s study is based on more than 7000 stars within a distance of 500 pc taken from RAVE survey. They have identified stars with high orbital eccentricities having over-densities at about V= -120 km s^{-1} and the second one at V=-95 km s^{-1} which coincide with phase space coordinates of the Arcturus and AF06 streams as given in Arifyanto & Fuchs (2006). Williams et al. (2009) examined a data set of 16,000 giants from the RAVE survey and showed pronounced over-density of stars at velocities overlapping with the Arcturus stream in the solar circle.

4.3.4 Ages

Determination of stellar ages from location of a star in a colour-magnitude diagram is an uncertain procedure because the majority of the stars in both streams fall very close to the zero age main sequence. Ages were estimated for few stars that appear relatively evolved off the main sequence. Mean ages with upper and lower limits are given in Appendix A.1 and A.2. Errors in $B - V$ and parallaxes are used to estimate the limits. In Figure 4.4, the stars are shown in the HR diagram of M_v versus $B - V$ colour along with isochrones of ages 10 Gyr, 12 Gyr and 16 Gyr for the metallicities [Fe/H] =−0.70 dex and [Fe/H] = −0.51 dex, for Arcturus stream and AF06 stream respectively. Ages of the stream members range from 10 to 14 Gyr. The stellar ages, therefore, are very similar to the ages of thick disc field stars which are all older than about 10−11 Gyr (Reddy et al. 2006). The derived ages are in good agreement with previous studies of Arcturus group (cf. Williams et al. 2009, Helmi et al. 2006, Navarro et al. 2004) based on different selections of stream members.

4.4 Discussion

4.4.1 Chemical Signatures

Since their discovery (cf. Eggen 1957), various theories have been put forward to explain the substructures in phase space known variously as moving groups or stellar streams. The most prominent theories identify a stellar stream as either a) a dissolved open cluster, b) debris from an accreted satellite galaxy, or c) the result of dynamical perturbations within the Galaxy.

In establishing the correct explanation for a particular stream, the importance of the chemical signatures or chemical tagging of stream members has been recognized (Freeman & Bland-Hawthorn 2002, Bensby et al. 2007, Williams et al. 2009, De Silva et al. 2007) not only to pinpoint their origin but also to understand the formation and evolution of the disc.

Quantitative abundances of twenty elements has been extracted here for members of the two streams. There are three main groups of elements: iron peak (V, Cr, Mn, Fe, Ni, Co), α-elements (O, Mg, Si, Ca, Ti), and heavy elements such as s-process (Ba, Nd) and r-process (Eu) elements. For the present (thin) disc, iron peak elements mostly come from Type Ia supernovae explosions (SN Ia) and the α-elements are primarily produced in Type II supernovae (SN II). The s-process elements are known to be produced mainly

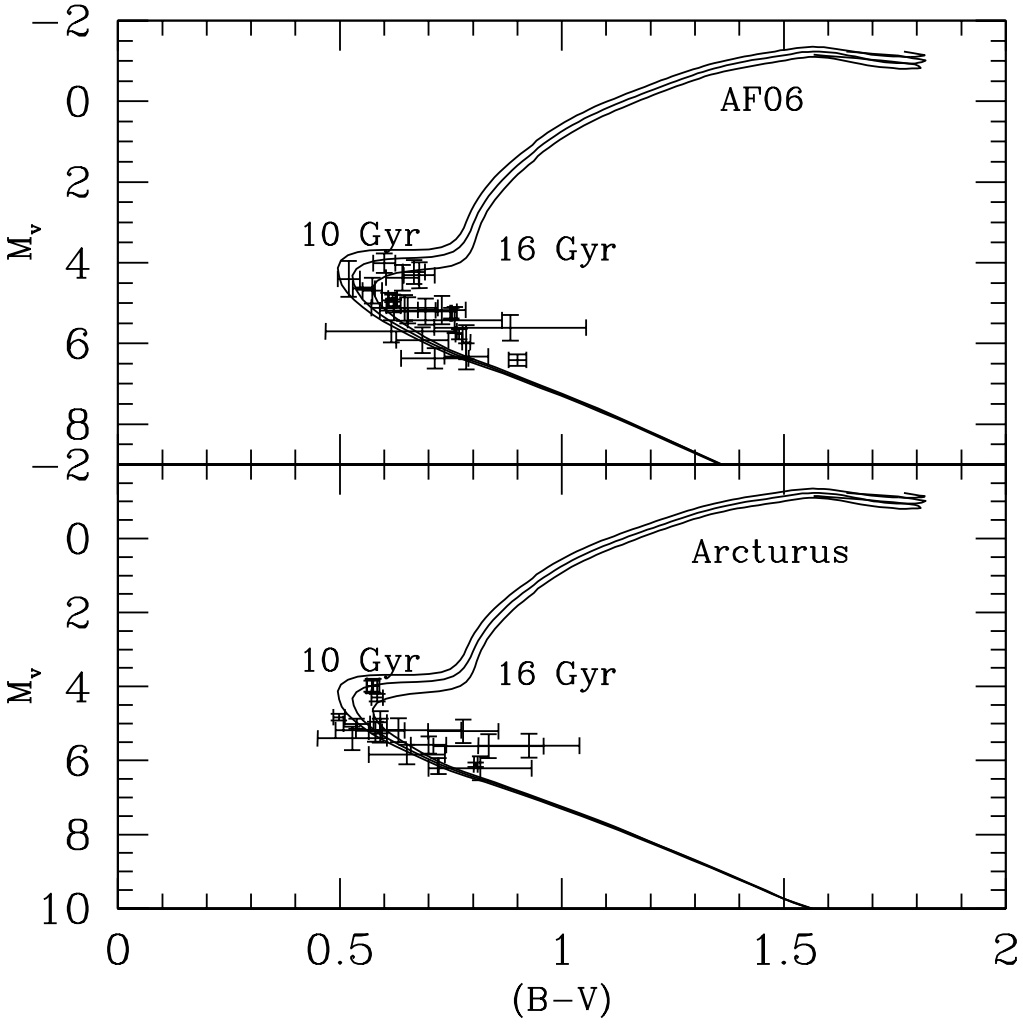

Figure 4.4: The colour-magnitude diagram for Arcturus and AF06 streams

in evolved stars of low and intermediate mass (1 − 8 $M_{\odot}$) with the lighter *s*-process elements also contributed by SN II. Eu, an *r*-process element, is most probably produced in SN II. Therefore, an abundance ratio of products of SN Ia and SN II helps to track the chemical history of a stellar system. Abundances of elements from O to Eu in the form of [X/Fe] ratios, where X is any element, are given in Appendix B.6-B.9 and shown in Figures 4.5, 4.6, and 4.7 as the run of [X/Fe] against [Fe/H]. The metallicity distribution of the streams is shown in Figure 4.8 for the Arcturus and AF06 streams. Next, we discuss these abundances for the Arcturus and AF06 streams in the light of the proposed scenarios for the origin of stellar streams.

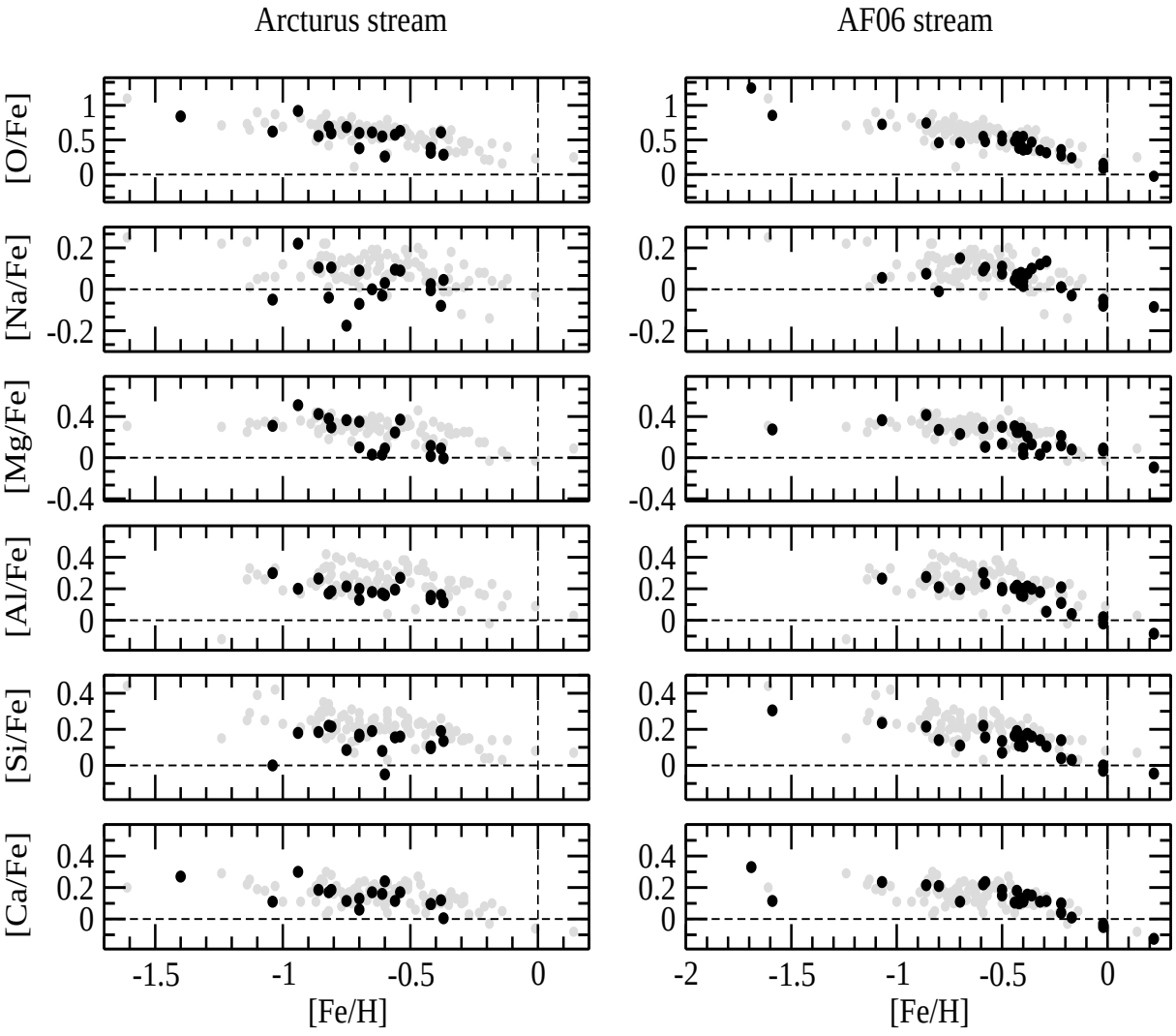

Figure 4.5: Abundance plots of elements O, Na, Mg, Al, Si and Ca for Arcturus stream (left column) and AF06 stream (right column). Grey symbols represent the field thick disc members from Reddy et al. (2006)

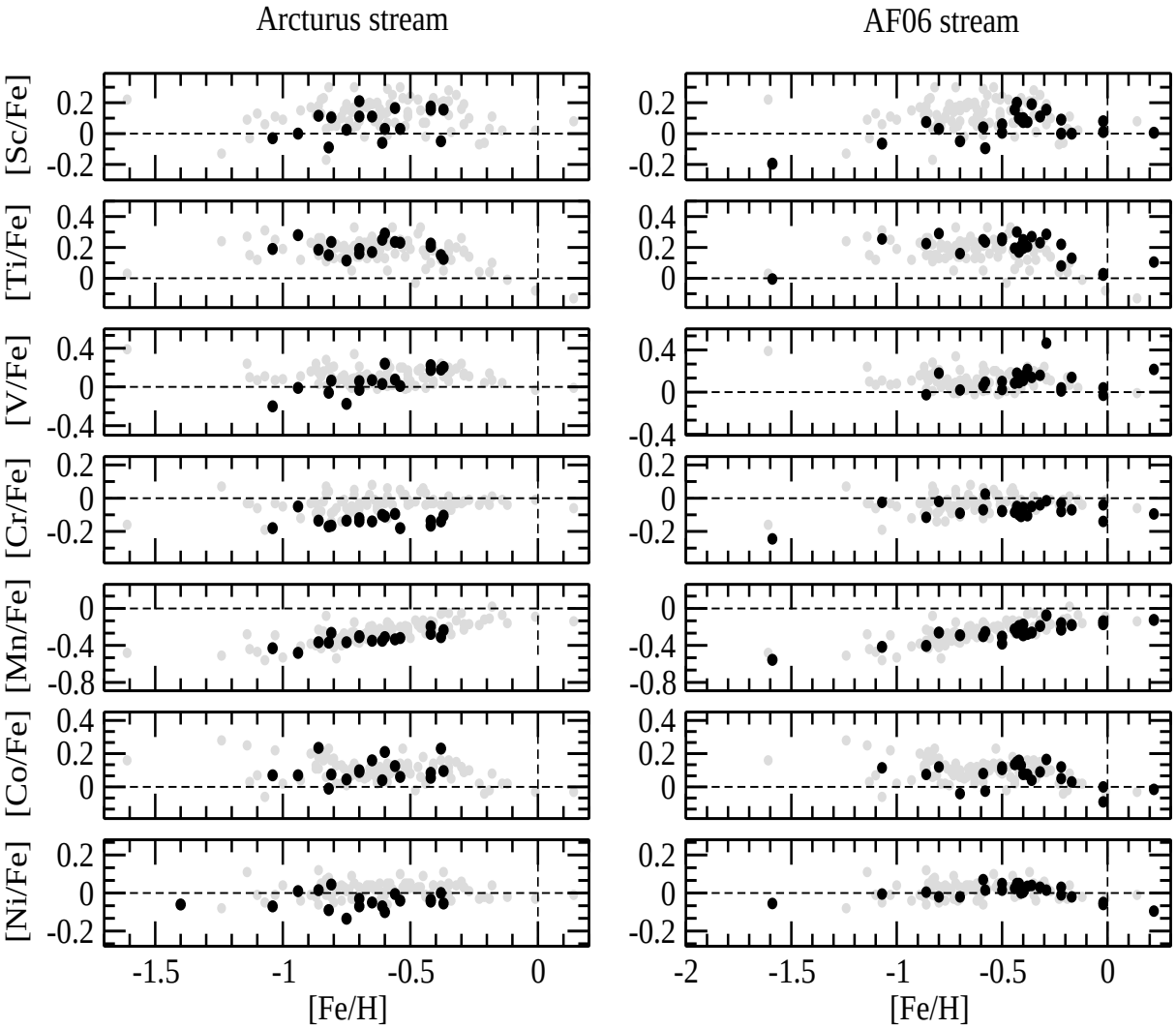

Figure 4.6: Same as Figure 4, but for elements Sc, Ti, V, Cr, Mn, Co and Ni

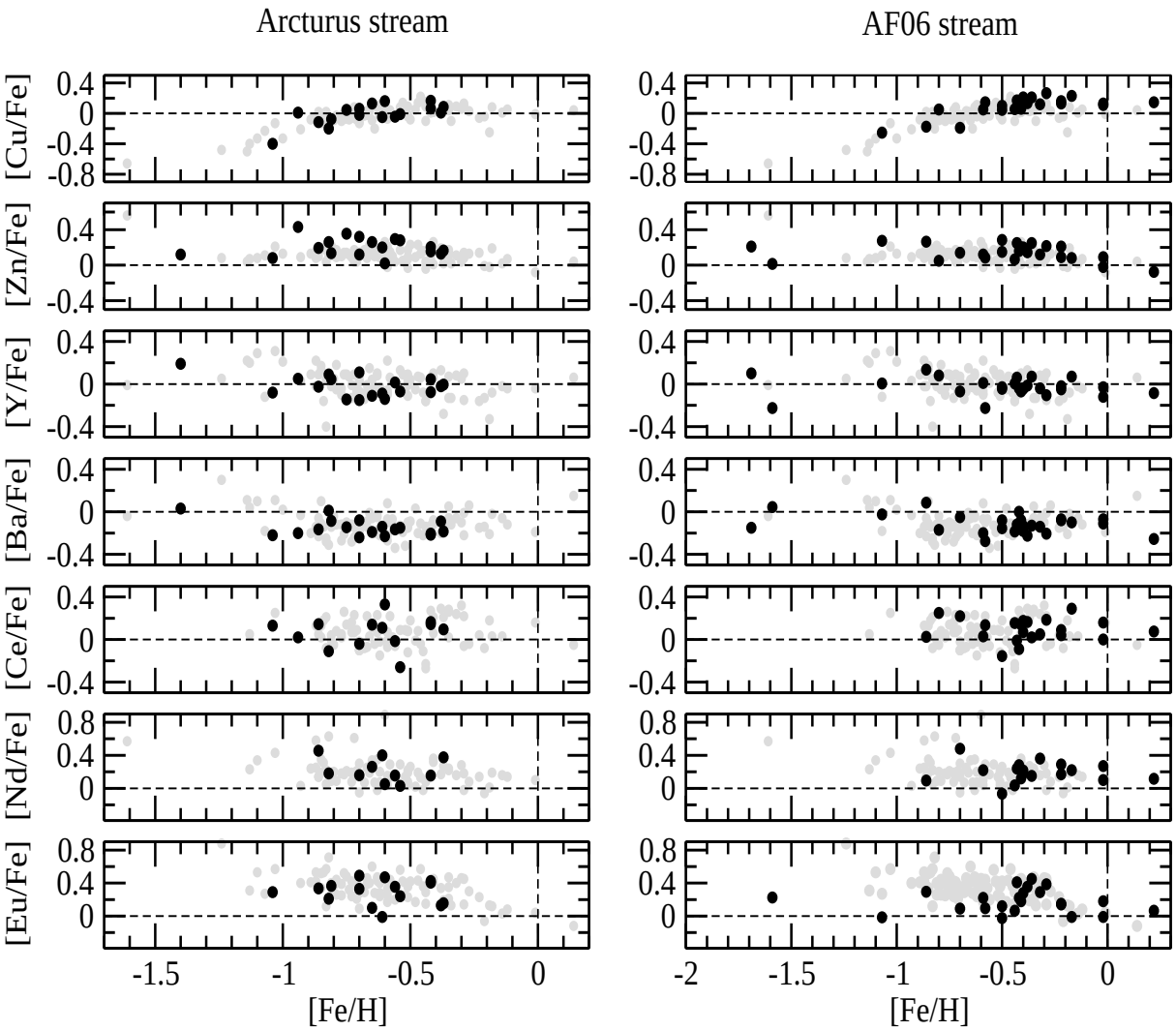

Figure 4.7: Same as Figure 4, but for elements Cu, Zn, Y, Ba, Ce, Nd and Eu

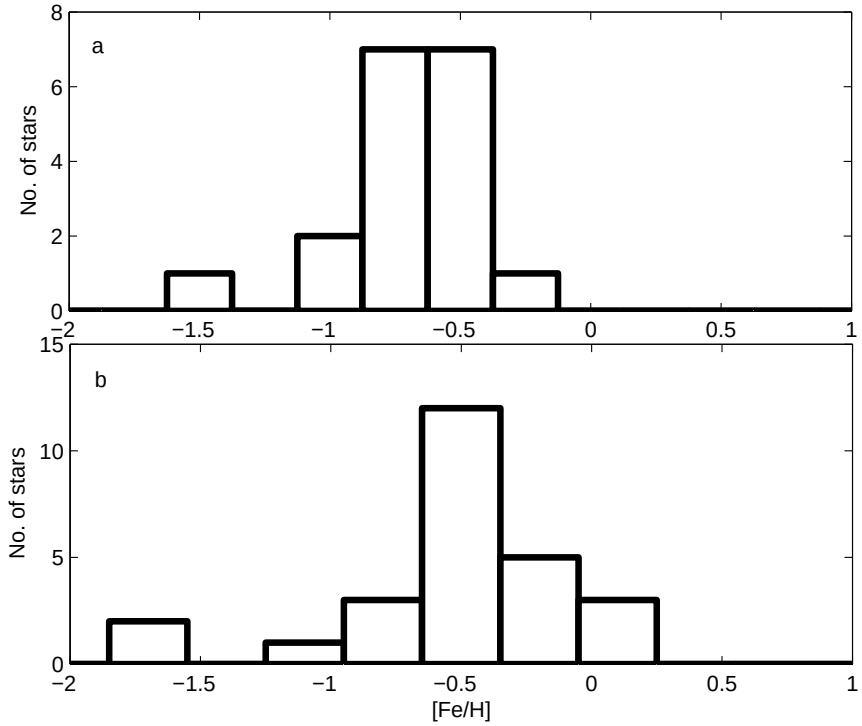

Figure 4.8: Metallicity distribution of the two streams. Arcturus (top, bin size = 0.25 dex) and AF06 (bottom, bin size = 0.30 dex)

4.4.2 Dissolved Stellar Clusters

Dispersal of an open cluster as the origin of a stellar stream is one explanation from the suite of potential explanations that is directly testable from photometric and spectroscopic determinations of stellar compositions. Given that open clusters exhibit chemical homogeneity, if a stream represents a dissolved cluster, one expects chemical homogeneity among the stream members.

Chemical homogeneity is not a characteristic of the two streams. Results shown in Figure 4.8 show that stellar metallicities span a wide range. For the Arcturus stream, [Fe/H] runs from −1.40 to −0.37. For AF06 stream, the range is from −1.69 to +0.22 but the range is −1.69 to −0.17 for those 15 members with a high probability of belonging to the thick disc. For a strictly homogenous populations such as open and globular clusters the degree of chemical homogeneity is quite high, which is about 0.05 dex (De Silva et al. 2006, Pancino et al. 2010) for more elements. In the case of [Fe/H] dispersions are found to be in the range of 0.02 − 0.1 and in some extreme cases dispersions are of the order of 0.2 dex (Paunzen et al. 2010). The wide range in metallicity clearly shows that the

systems from which the stream members originated had a relatively long history with a multiple episodes of star formation.

We have also inspected the sample for an evidence of a sub-group with chemical homogeneity. Results shown in Figures 4.5, 4.6 and 4.7 indicate existence of no such group among Arcturus stream sample, however, for the stream AF06, we find a hint of clustering of stars at [Fe/H] = −0.4. About 8 stars (out of total 26) show metallicity [Fe/H] = −0.4 within the dispersion of 0.04 dex. Does it mean that part of the sample stars originated from the disrupted cluster? Probably not, this may be a manifestation of thick disc metallicity distribution which peaks at about −0.6 dex, and to some extent due to a smaller sample size. Thus, neither the Arcturus nor the AF06 stream, as shown by metallicity distribution of member stars of the two streams (see Figure 4.8), is a dissolved open cluster. Similar conclusion about the Arcturus stream was reached also by Williams et al. (2009) who selected 134 stream members by selection criteria different from those used by Arifyanto & Fuchs (2006). Their analysis of high-resolution spectra led to a [Fe/H] range similar to that quoted above (see also Navarro et al. 2004).

4.4.3 Are the Streams Chemically identical to Thick Disc Field Stars?

Among thick disc field stars in the solar neighborhood, there is a strikingly very small dispersion in elemental abundance ratios, i.e., [X/Fe] at a given [Fe/H]. Indeed, Reddy et al. (2006) found the [X/Fe] to be Gaussian-like with a dispersion σ of less than 0.10 dex for the most of the elements except for V, Y, and Zr for which σ is slightly more than 0.1 dex. Furthermore, such dispersions were uncorrected for measurement uncertainties so that the intrinsic or 'cosmic' dispersion must be very small.

In sharp contrast to the very similar [X/Fe] ratios at a given [Fe/H] for local field stars, element ratios reflecting different contributions from major processes of stellar nucleosynthesis do vary from stellar system to stellar system. For example, ratios in the Galactic bulge are not uniformly identical at a given [Fe/H] to those among local thick or thin disc field stars. Similarly, ratios of α-elements ([α/Fe]) at a given [Fe/H] among stars of dwarf spheroidal galaxies differ appreciably from those of local stars and from galaxy to galaxy (Venn et al. 2004, Tolstoy et al. 2009, Kirby et al. 2010).

Therefore, the chemical signatures or tags in the form of [X/Fe] for those key elements from the major processes of nucleosynthesis may test some proposed origins for the streams. To address the question, 'Are these two streams chemically identical to thick disc field stars ?′, we show plots of [X/Fe] versus [Fe/H] in Figures 4.5 - 4.7 with field stars from Reddy et al. (2006) shown as by grey symbols, and Arcturus and AF06 stream

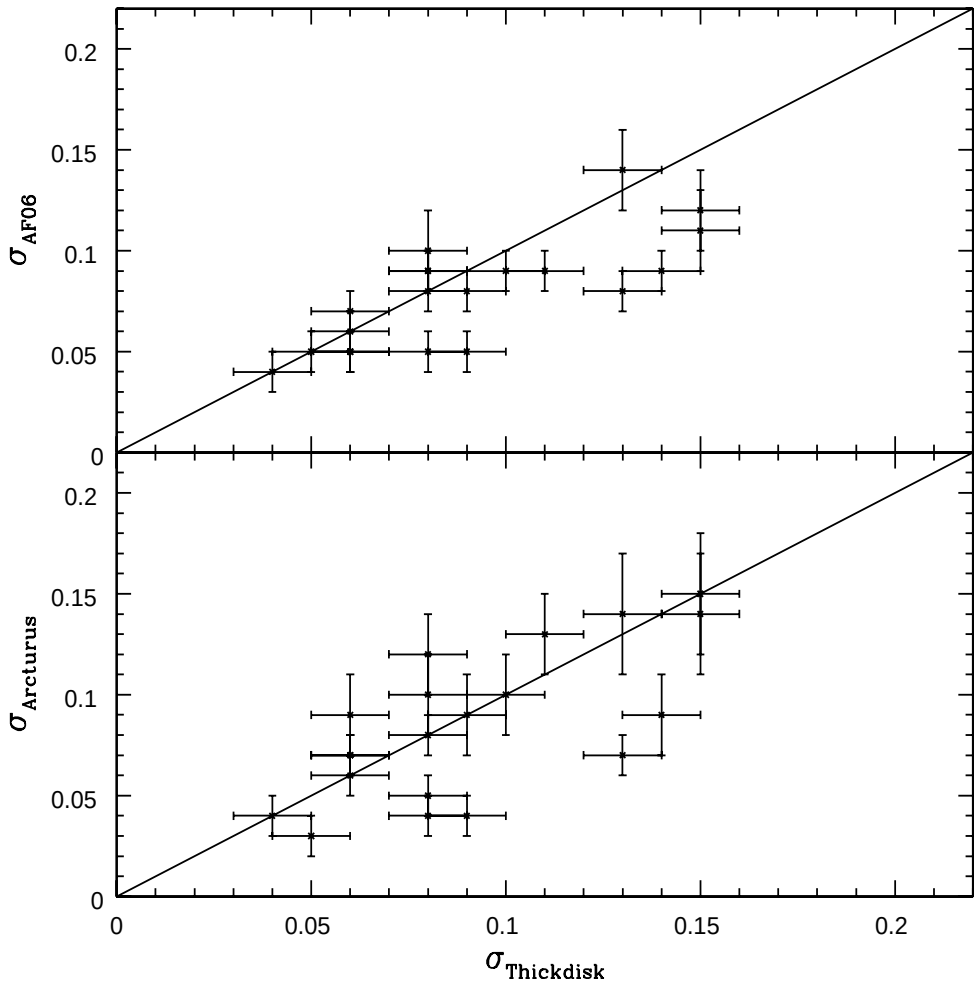

Figure 4.9: The dispersions in [X/Fe] of members of the Arcturus stream, the AF06 stream and the field thick disc sample.

members shown as black filled circles. To quantify possible systematic offsets between the field thick disc and stream members, we compute mean values and dispersions for streams over [Fe/H] interval −0.30 to −1.0. Dispersions about the trends is a combination of both the cosmic scatter as well as errors associated with the model parameters. The values (σ_{AF06}, $\sigma_{Arcturus}$) are computed as the standard deviation of the residuals from straight line fits to abundance trends of [X/Fe] against [Fe/H]. Similarly, $\sigma_{Thickdisc}$ for the thick disc abundance trends of Reddy et al. (2006) are computed over the same interval. Results are given in Table 4.3. In Figure 4.9, we made comparison of $\sigma_{Thickdisc}$ with those of Arcturus and AF06 streams. Dispersion values about the abundance trends of Arcturus

stream show very good agreement with that of the thick disc within about 0.02. However, for AF06 stream, in most cases, dispersions are lower by 0.01 − 0.03 compared to thick disc dispersions. With the current limited sample it would be far fetching to attribute this to the different chemical evolution for the AF06 stream and hence external origin to it. Mean abundances of Arcturus and AF06 streams are quite similar and the differences are within 0.05 dex except three elements (O, Cu, Eu) for which difference is 0.06 − 0.07 dex. Dispersions about the trends for all the elements are comparable to the estimated scatter (σ_{model}) due to uncertainties in model parameters. Differences between dispersions and σ_{model} are within 0.05 dex. Thus, we conclude that the streams are chemically identical to within high precision with the field thick disc stars. Given that external galaxies of the Local Group have different element ratios across the [Fe/H] range sampled by these two streams, especially for α-elements (see, for example, Tolstoy et al. 2009, Figure 11), it seems most unlikely that either stream represents debris from an accreted satellite galaxy.

Table 4.3: Mean elemental abundance ratios and dispersions

Element	Arcturus		AF06		Thick disc		σ_{model}
	Mean	σ	Mean	σ	Mean	σ	
[O/Fe]	0.54	0.13	0.48	0.08	0.60	0.12	0.07
[Na/Fe]	0.03	0.09	0.07	0.04	0.10	0.06	0.04
[Mg/Fe]	0.21	0.11	0.21	0.09	0.30	0.07	0.05
[Al/Fe]	0.18	0.04	0.21	0.03	0.26	0.08	0.04
[Si/Fe]	0.14	0.06	0.15	0.04	0.22	0.06	0.02
[Ca/Fe]	0.14	0.05	0.16	0.04	0.16	0.06	0.06
[Sc/Fe]	0.07	0.09	0.07	0.07	0.14	0.09	0.09
[TiI/Fe]	0.20	0.05	0.23	0.04	0.19	0.07	0.06
[V/Fe]	0.07	0.08	0.11	0.06	0.11	0.08	0.07
[CrI/Fe]	−0.13	0.03	−0.07	0.04	−0.03	0.04	0.06
[CrII/Fe]	−0.01	0.05	−0.03	0.08	...	...	0.12
[Mn/Fe]	−0.32	0.05	−0.27	0.05	−0.26	0.07	0.06
[Co/Fe]	0.10	0.07	0.09	0.05	0.10	0.05	0.05
[Ni/Fe]	−0.04	0.05	0.02	0.02	0.02	0.04	0.04
[Cu/Fe]	0.01	0.08	0.08	0.08	−0.02	0.07	0.07

Table 4.3 – continued from previous page

Element	Arcturus		AF06		Thick disc		σ_{model}
	Mean	σ	Mean	σ	Mean	σ	
[Zn/Fe]	0.22	0.09	0.17	0.07	0.12	0.06	0.07
[Y/Fe]	−0.03	0.08	−0.02	0.08	0.00	0.11	0.09
[Ba/Fe]	−0.15	0.06	−0.13	0.08	−0.14	0.09	0.13
[Ce/Fe]	0.06	0.15	0.08	0.11	0.06	0.13	0.16
[Nd/Fe]	0.22	0.14	0.19	0.14	0.20	0.16	0.19
[Eu/Fe]	0.29	0.15	0.22	0.13	0.36	0.12	0.12

4.5 Satellite Accretion versus Dynamical Origin

Navarro et al. (2004) suggested Arcturus stream to be a peculiar grouping of metal poor stars with similar apocentric radius, common angular momentum, and distinct metal abundance patterns. Lack of net radial motion as seen in the U-component of velocity, large velocity dispersion of ~ 50 kms^{-1}, in V-component, high rotational lag which dynamical perturbations can not introduce, unique slope in the [α/Fe]-[Fe/H] space- all these properties were consistent with those expected for a group of stars originating from the debris of a disrupted satellite. Hence, an extra-galactic origin was assigned to the Arcturus stream that they originated from a single satellite system that was dragged and shredded into the disc of the Galaxy early during its assembly, 5 to 8 Gyr ago.

As a result of disruption of a satellite galaxy falling into its parent galaxy, the satellite debris can end up in several cold star streams with roughly the same characteristic eccentricities of their orbit (Helmi et al. 2006). Arifyanto & Fuchs (2006) searched for such overdensities in the space of V versus $\sqrt{U^2 + 2V^2}$, and detected Arcturus and a new stream namely AF06 stream reinforcing their extra-Galactic origin. Similarly Helmi et al. (2006), in the $A - P - J_z$ space of the Nordström et al. (2004) sample, found three coherent groups, which were proposed to be the remnants of past accretion events in the Milky Way, out of which two had the characteristics (kinematics and metallicities) of

Arcturus and AF06 stream giving further support to the extra-Galactic origin of Arcturus, and AF06 stream too. Klement et al. (2008) also could detect the presence of Arcturus and AF06 streams in the data of first RAVE public data release. Although extra-Galactic origin was proposed for these two streams, nothing was known about the progenitor for Arcturus stream, if it is a merger remnant.

Later, Bovy et al. (2009) independently detected the Arcturus stream by reconstructing the velocity distribution of nearby stars ($\lesssim$ 100 pc) from HIPPARCOS data. The detected structure had a small dispersion (2-3 km s^{-1}) contrary to the previous results. Similarly, Williams et al. (2009) confirmed the presence of Arcturus overdensity, with very small velocity dispersion, possibly favouring negative U-velocities, and concluded it as solar circle phenomenon, rather than merger remnant. It was widely believed that the dynamical perturbations introduced by the Galactic bar and the spiral arms will not be able to introduce a high rotational lag similar to that of Arcturus and AF06 streams, and it is highly improbable that such non-axisymmetries perturbing the Galactic thick disc.

In this context, Minchev et al. (2009) proposed one model explaining the high velocity streams, such as Arcturus seen in the solar neighborhood. As per this model, the dynamical perturbations induced by the merging satellites can perturb the Galactic disc, especially the thick disc, giving rise to high velocity streams. Again, using varous simulations, Antoja et al. (2009), Gardner & Flynn (2010) and Monari et al. (2013) have shown that, it is possible to have an internal origin to high velocity streams such as Arcturus, favouring the dynamical origin to it.

In Figure 4.10 where ratio of [α-process/Fe] (mean of α-process elements Mg, Si, Ca and Ti) is compared with that of thick disc (Reddy et al. 2006) and a number of dwarf spheroidal galaxies for which data was taken from (Venn et al. 2004, Monaco et al. 2005). The chemical evolution of dwarf galaxies is different from that of giant galaxies like Milky Way. From the figure, it is clear that, almost all the dwarf galaxies plotted (Draco, Sculptor, Sextans, Ursa Minor, Carina, Fornax, Leo I, from Venn et al. 2004), are metal poor, not even reaching the Milky Way disc metallicity. The Sagittarius dwarf galaxy (Monaco et al. 2005) has a metallicity similar to thick disc, but has an α abundance pattern entirely different from the thick disc. Our abundance analysis of the stream members show that the stream chemistry is entirely different from that of the currently surviving dwarf spheroidals in the Local Group. If there existed dwarf galaxies massive enough to reach the same elemental abundance pattern as that of Milky Way, which merged with Milky Way, then it would have been called a major merger. The presence of thin disc, clearly rule out the possibility of a major merger atleast in the past

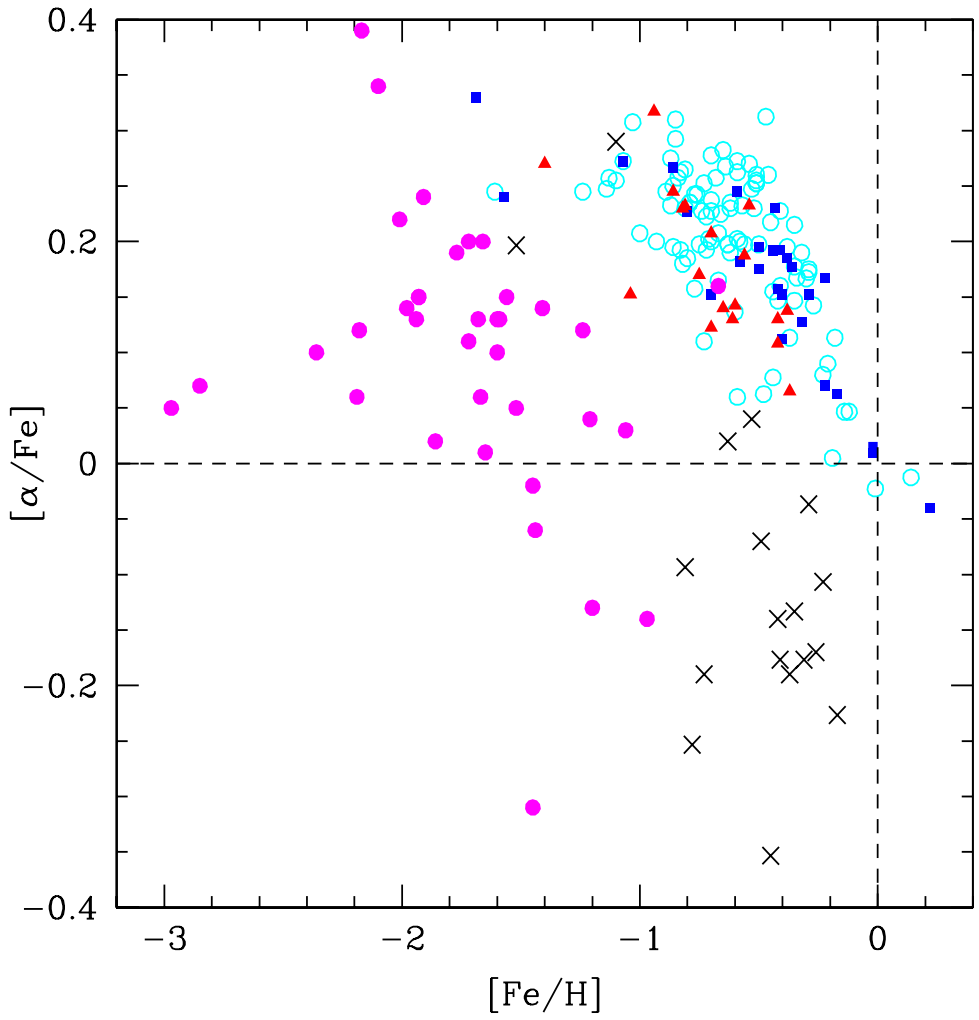

Figure 4.10: The [α/Fe] versus [Fe/H] plot. Red triangles: Arcturus stream, Blue squares: AF06 stream, Cyan open circles: Thick disc, Magenta filled circles: dSph satellite galaxies (Draco, Sculptor, Sextans, Ursa Minor, Carina, Fornax, Leo I) from Venn et al. (2004), Black crosses: Sgr dSph from Monaco et al. (2005) with [α/Fe] = ([Mg/Fe]+[Ca/Fe]+[Ti/Fe])/3.

10 Gyr. Hence, with these observational evidence, we can state that the members of Arcturus and AF06 streams are not from outside of the Galaxy, but formed within the Galaxy itself.

4.6 Conclusions

The outstanding results of our abundance analyses are that the subdwarfs comprising the Arcturus stream and AF06 stream identified as overdensities in phase space by Arifyanto & Fuchs (2006) have (i) a considerable spread in metallicity and (ii) relative abundance [X/Fe] identical to those of the Galactic thick disc. The metallicity spread excludes the hypothesis that either stream represents a dissolved open cluster. The high degree of similarity between [X/Fe] at a given [Fe/H] for these streams and the field stars of the thick disc greatly strains a proposal that these streams represent the tidal debris of an accreted satellite galaxy. By exclusion, the likely origin of these streams is that they are the product of dynamical interactions.

However, chemical identiy with the thick disc and the non-similarity of their chemistry with the satellite galaxies within local group alone may not suffice to rule out the possibility of these streams being a result of disrupted satellites. It is still a matter of debate how perturbation can create streams with such a very high velocity drag and exhibit very tight abundance trends. It would be important to know from the models the extent of regions that get affected due to bar/spiral perturbations and their effect on the abundance trends of clumped stars in phase space. Astrometry from GAIA will provide unprecedented sample size as well as accuracy to map the Galaxy precisely which would decipher the Galaxy formation and evolution.

CHAPTER 5

STREAMS IN THE GALACTIC THIN DISC

5.1 Introduction

The moving groups chosen for study in this chapter have been known in the literature for more than 50 years or so. Many of these studies are concerned with the kinematic distributions of stars and segregating them as groups with similar velocities. Efforts in this direction have been intensified with the advent of HIPPARCOS mission which helped to determine accurate astrometry for a large number of stars. A number of studies (Dehnen & Binney 1998, Famaey et al. 2005, Zhao et al. 2009, Antoja et al. 2010) employed sophisticated statistical techniques to unravel the complex velocity distribution of stars. They found a number of substructures as overdensities.

Sample stars for the three moving groups come from the study of Famaey et al. (2005). Their study involved a detailed statistical analysis of a sample of about 6000 K and M giants, mostly K giants, taken from HIPPARCOS catalogue with accurate astrometry and radial velocities from CORAVEL. Using the maximum-likelihood method based on a Bayesian approach, they have identified a number of overdensity regions in the $U - V$ velocity space. The overdensities are identified as moving groups whose kinematic positions match with the groups that were known earlier as moving groups. Importantly, their approach makes no prior assumptions about kinematic characteristics of the moving groups. Thus, the study re-affirmed the reality of their existence with refined velocity definitions in the velocity space.

In this chapter, we report the findings of our analysis of chemical tagging of 125 K giants belonging to the three kinematically identified moving groups: Hercules, Hyades-Pleiades and Sirius. With the derived abundance and age results, we test various origin and evolution hypotheses of the three moving groups. Are the member stars coeval and

associated with open clusters ? Or, are they due to inhomogeneous star formation events? Or, are they manifestations of dynamical perturbations within the Galaxy ? These are some of the questions which we would like to address for the three moving groups.

5.2 Hercules stream

5.2.1 Introduction

Hercules stream or Hercules moving group is one of the prominent group of stars sharing well defined kinematic motion. Eggen (1958b) based on a set of 700 high velocity stars with the available astrometric data and computed group parallax values identified a group of stars with shared kinematic motion which are similar to ζ Herculis, a bright star in the Hercules constellation. Hence the group is called the Hercules moving group. He found the mean motion (U, V, W) = -54, -45, -26 km s^{-1} with respect to the Sun. In many later studies Hercules moving group was found to be significantly offset from the bulk of the observed velocity distribution of stars in the disc but coinciding with earlier velocity definitions. A summary of mean kinematic motion (U, V, W) of the Hercules group as identified using different techniques is given in Table 5.1. Irrespective of the technique, all the studies confirm the existence of this moving group with its kinematic motion within a few km s^{-1}, in particular, U and V velocities. In all the studies Hercules group found to be significantly lagging the LSR by $\sim$ 50 km s^{-1}. The group is also called as an U-anomaly (Raboud et al. 1998) for its large outward velocity from the Galactic center.

Here, we report our results of elemental abundances of 58 red giant members of Hercules moving group. For details of sample selection we refer the reader to Chapter 2, Section 2.2.2. The observation details of the Hercules stream members are given the Table 2.3.

5.2.2 Atmospheric Parameters

The study involves deriving quantitative elemental abundances which requires accurate determination of stellar atmospheric parameters : T_{eff}, log g, ξ_t and [M/H] for choosing best representative model atmospheres. As in the case of earlier chapter we derived atmopsheric parameters through both spectroscopic and photometric data. In the case of spectroscopy, apart from observed line strengths, we used atomic data, theoretical stellar models and radiative transfer code. Details of which are given in the previous chapters.

Table 5.1: Kinematic definitions of Hercules stream. UVW components are heliocentric, except for Klement et al. (2008) which are with respect to Local Standard of Rest

U (σ_U) km s^{-1}	V (σ_V) km s^{-1}	W (σ_W) km s^{-1}	Reference
-42.13 (28.3)	-51.64 (9.31)	-8.06 (17.1)	Famaey et al. (2005)
-30	-50		Famaey et al. (2007)
-32 (5)	-48 (5)	-15 (12)	Zhao et al. (2009) (dwarf sample)
-35 (5)	-51 (5)	-11 (15)	Zhao et al. (2009) (giant sample)
-35	-45		Fux (2001)
-20	-33		Bovy et al. (2009)
-20	-50		Klement et al. (2008) (U-V space)
	-65		Klement et al. (2008) (U- $\sqrt{U^2 + 2V^2}$ space)

Temperature : For derivation of T_{eff} we made use of optical and infrared photometry combined with empirical calibrations. Two colours $J - K$ and $V - K$ and the colour- temperature relations derived in Alonso et al. (1999) have been used. The $(J-K)$-temperature relation does not depend on metallicity. The J and K magnitudes are taken from 2MASS sky survey. The 2MASS magnitudes are transformed to the standard TCS system using the calibration of Ramírez & Meléndez (2005). For $V - K$ colour, the V magnitude is adopted from Tycho2 catalogue where this is given as V_T. Values of V_T have been converted to Johnson broad band magnitude V using the relation provided in Tycho2 catalogue. The K_s magnitudes in 2MASS have been converted to K magnitudes of Johnson systems using the relation in Bessell (2005). Note, for relations involving $V - K$ colour we assumed [Fe/H] = 0. Since our sample of stars are nearby, extinction is expected to be very less or nil. Neverthless we have estimated extinctions using the following relations given (Ramírez & Meléndez 2005):

$A_{J_{TCS}} = 0.84\ E(B-V)$ and $A_{K_{TCS}} = 0.36\ E(B-V)$

$(V-K)_0 = (V-K) - 2.72\ E(B-V)$ (Ramírez & Meléndez 2005)

Also, values of T_{eff} for all the stars have been derived using spectral line analysis combined with model atmospheres as described in earlier Chapters. Derived T_{eff} values from $J-K$, $V-K$ and spectroscopy ($(T_{eff})_{spec}$) are tabulated in Appendix B.3 and are compared with each other in Figure 5.1 (red symbol). T_{eff} values derived from $V-K$ colour match very well with those of values derived from spectroscopy. However, number of values (10 stars) derived from $J-K$ are found to be 300-400 K cooler than values from spectroscopy. This is attributed to somewhat large errors in J magnitudes and unaccountable error in extinction. We adopt spectroscopic temperature throughout this study.

Surface Gravity : Surface gravity or simply log g values have been derived using both the photometry and spectroscopy. Photometric estimation involves $B-V$ color and absolute magnitude M_v combined with theoretical stellar evolutionary tracks. We have used isochrones computed by Demarque et al. (2004) which are known as Y^2 tracks. Tracks contain information such as mass, age along with values such as log g, luminosity and colour. The observed position of stars in the $(B-V)$-M_v plane provides corresponding log g values which are read from the Y^2 data. Errors in log g are estimated using the quoted errors in parallax and colours. Also, log g values have been obtained using Fe I and Fe II abundances such that both the abundances are equal for a given T_{eff} and log g. The derived values are tabulated in Appendix B.3 and the photometric-spectroscopic values are compared in Figure 5.1 as well. As seen in the plot log g values from photometry are systematically lower by of about 0.2 dex compared to values from spectroscopy. However, in two cases (HIP 96294 and HIP 116644) the difference is quite large of about 0.4 dex. Given the errors in the parallaxes, colours and also in isochrones, the agreement between the two methods is quite comforting. We have adopted log g values derived from spectroscopy.

Microturbulent velocity, metallicity : Choosing a best representative model atmosphere requires microturbulent velocity ξ_t and metallicity [M/H]. The former can't be obtained from photometry. Since ξ_t causes spectral line broadening and also increasing of equivalent widths (W_λ), its value has been determined using a number of spectral lines with a range of line strengths. The right ξ_t is such for which both the weak and strong lines would give same abundance. More details on this parameter and its derivation are

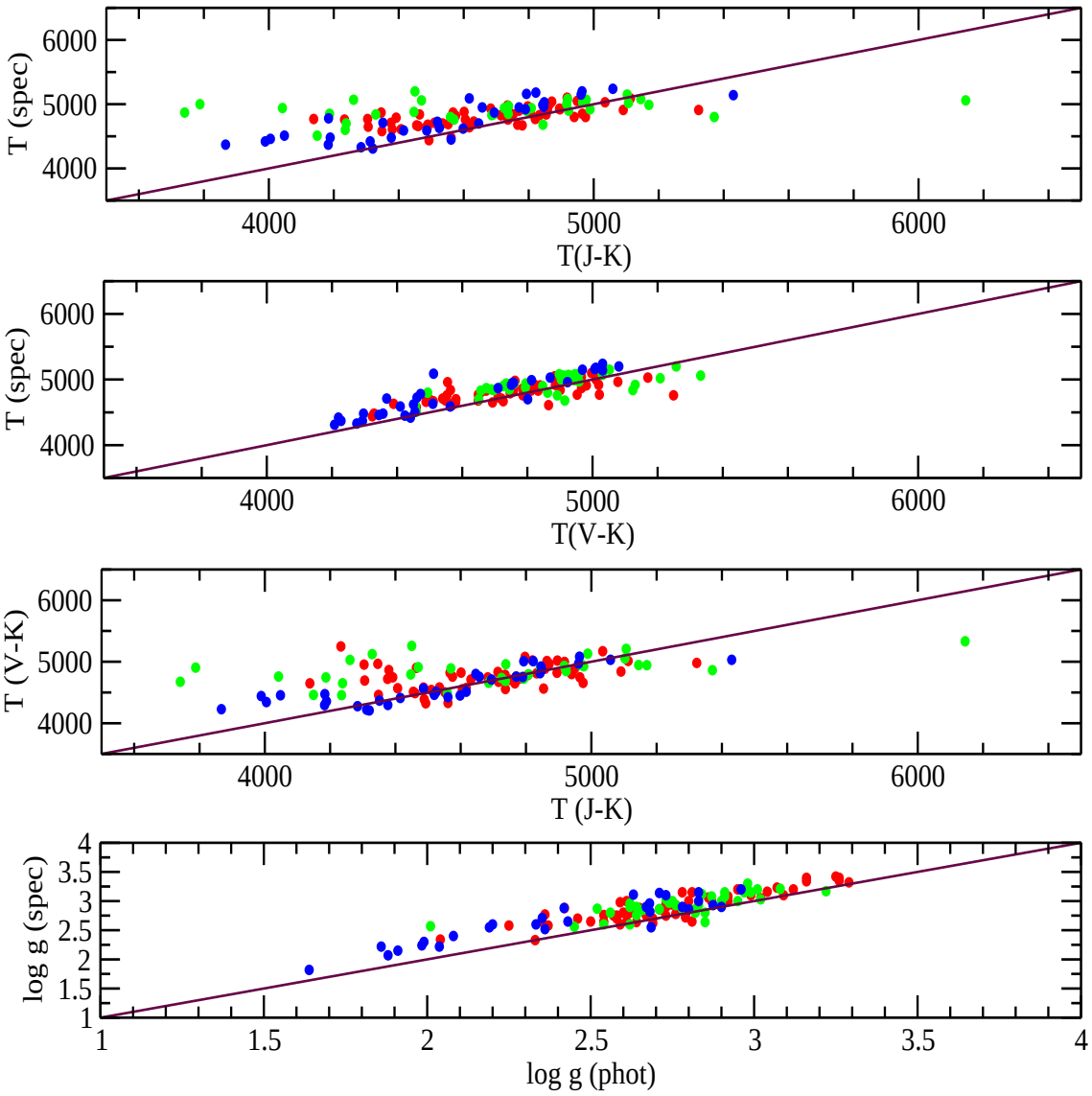

Figure 5.1: Comparison of photometric and spectroscopic parameters. Red : Hercules stream, Green : Hyades-Pleiades stream, Blue : Sirius stream

given in earlier chapters.

Metallicity, [M/H] can be obtained either from Strömgren photometry or from spectroscopy. Since many of the sample stars lack Strömgren photometry we used spectroscopically derived [Fe/H] values as metallicity. The [M/H] values used in the opted model atmosphere for each star are given in Appendix B.3, as $([M/H])_{model}$.

5.2.3 Elemental Abundances

We have derived abundances of 16 elements of 58 giants of Hercules stream. The measured line strengths (W_λ), adopted atomic data such as log gf values and the appropriate model atmospheres are the input data to radiative transfer code *MOOG*. The line list with measured W_λ values, and atomic data are given in earlier chapters (see Tables 3.2 and 3.3).

Abundances of 58 giants with respect to stellar Fe abundance ([X/Fe] = [X/H] − [Fe/H]) are given in Appendix B.10-B.12. Transitions of Mn and V are affected by hyperfine structure (HFS) which have been accounted using HFS data taken from Kurucz data base. Two forbidden oxygen lines at λ 6300 Å and λ 6363 Å are used to derive oxygen abundance. We have not used permitted oxygen triplet lines at 777 nm as these are prone to non-LTE effects. Zn abundance is based on two transitions at λ 4810.54 Å and λ 6362.35 Å. However, measurement of W_λ of transition at λ 4810.54 Å is found to be unreliable as one wing of it overlaps with FeII/CrI lines (Hinkle et al. 2000). Thus, we listed Zn abundance when only both the lines are measured. In the case of Ba, we adopted average abundance of two Ba II lines at at λ 5853.68 Å and λ 6141.73 Å. The transition at λ 6496.91 Å is quite strong and gives systematically higher Ba abundance. This was not considered in the analysis, and is listed as a separate column for the reference. Ba II transitions suffer from HFS. But the lines considered here are least affected by HFS, and hence, has been neglected (Sneden et al. 1996).

Results have been shown in Figures 5.2-5.5 as [Fe/H] versus [X/Fe]. Abundance results of thin and thick disc taken from Bensby et al. (2005) are superposed with the results of Hercules sample from this study. In general, [X/Fe] trends follow the background thin disc results with a few exemptions. There are not many thick disc stars which are as metal rich as Hercules and hence it is difficult to compare with thick disc results.

Uncertainties and Comparisons

Uncertainties in abundance results have been estimated by estimating uncertainties in the derived atmospheric parameters and in the measured line strengths. The basic procedure has been described in Chapter 3 and Chapter 4. For continuity, a brief description of error estimation is given here.

Uncertainties in the atmospheric parameters have been gauged by performing abundance trend sensitivity to incremental changes in the respective parameters. Uncertainty in a particular parameter is the change in the parameter above which abundance trends become sensitive to changes. The procedure has been employed to a typical member

(HIP 8926) of Hercules stream and found the following uncertainties in the atmospheric parameters: ± 50 K for T_{eff}, ± 0.20 dex for log g, ± 0.20 km s^{-1} for ξ_t, and ± 0.1 dex for [Fe/H]. Uncertainty in the measurement of lines strengths (W_λ) is estimated as $\Delta W_\lambda / \sqrt{N}$, where N is the number of lines used in the analysis. Changes in abundance ratios due to the quoted uncertainties in the parameters are tabulated in Table 5.2, for the representative star HIP 8926. With the assumption that the uncertainties in the parameters are unrelated to each other and are independent, the net uncertainty in the abundance ratio is calculated as a quadratic sum. This has been given in the last coloumn of the Table 5.2 as σ_{model}. Abundance ratios of singly ionized species Ti II, Fe II and Ba II are found to have large net uncertainties due to their higher sensitivity to uncertainties in log g and ξ_t.

Results obtained in this study have been subjected to a detailed comparison with the recent study by Pakhomov et al. (2011). There are 11 stars which are common in the two studies. Differences in abundance ratios Δ [X/H] between the two studies have been calculated for common elements and are given in Table 5.3. Agreement between the two results is, in general, satisfactory except in few cases where the differences are quite significant. The exemption being HIP 107502 whose abundances (most of them) are systematically higher in our study. Probably this is due to our higher value of T_{eff} by 290 K and log g by 1.1 dex compared to Pakhomov et al. (2011). Also, one notices significantly higher values of Mn and Co for most of the stars in our study. It is not clear whether the difference could be due to different treatment of HFS in the two studies. Also, seen are the large difference in elements such as Ba II and Fe II. This is probably due to their lines sensitivity to changes in atmospheric parameters in particular to T_{eff} and ξ_t (see Table 5.2).

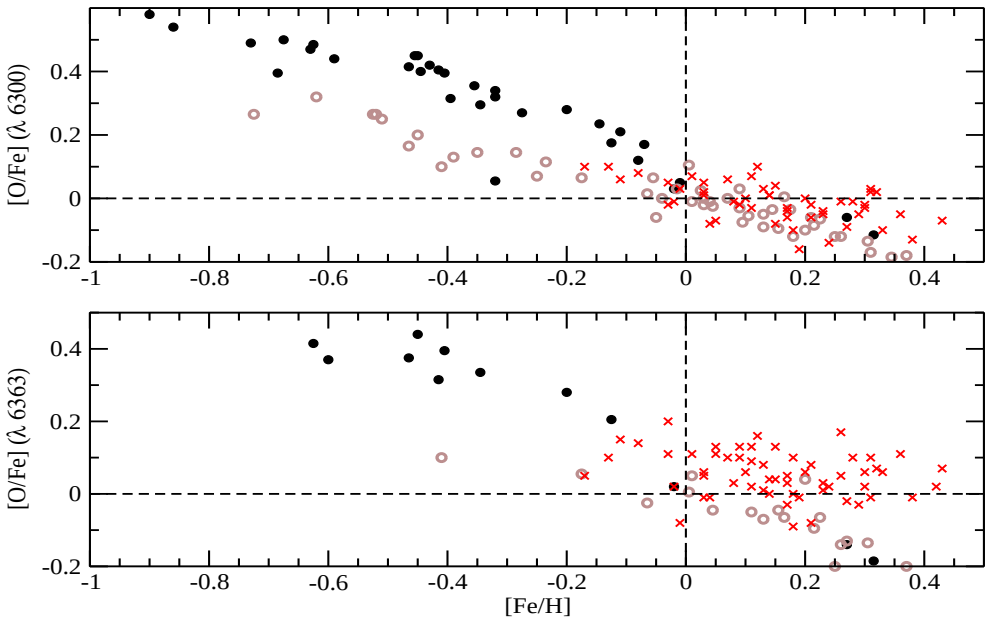

Figure 5.2: Oxygen abundance plots for Hercules stream (red cross). Black and Brown circles represent thick and thin disc stars respectively from Bensby et al. (2005)

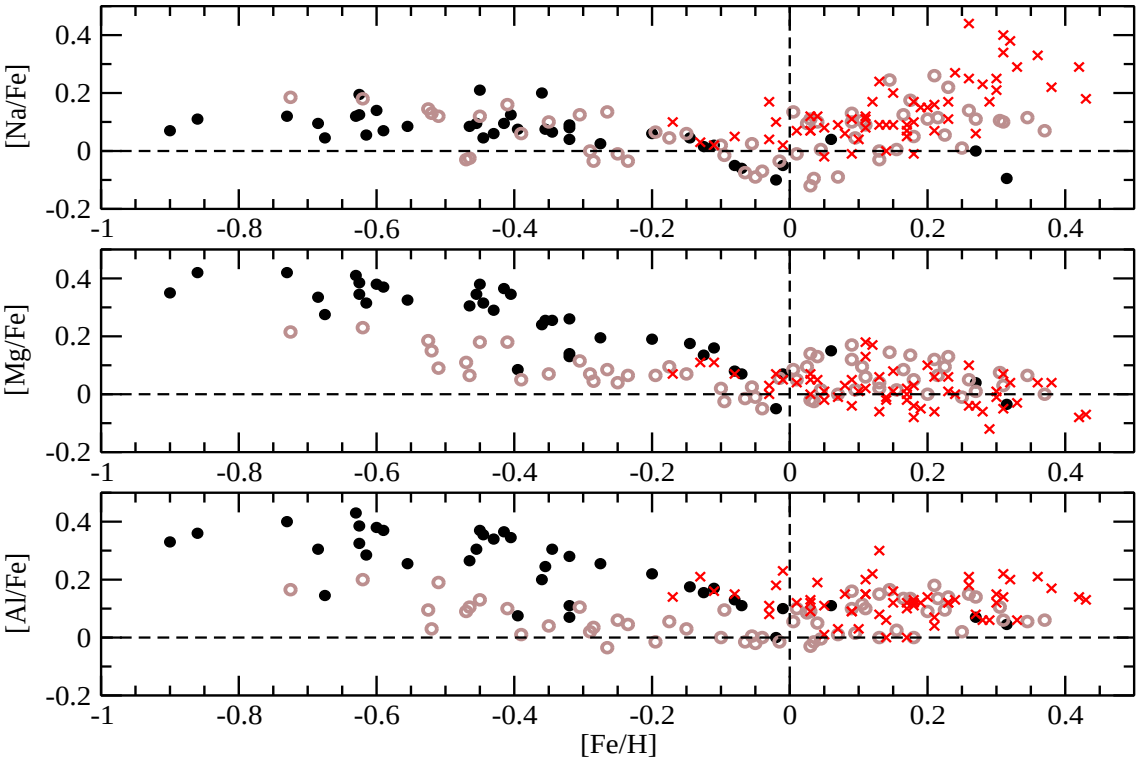

Figure 5.3: Same as the previous plot, but for elements Na, Mg and Al

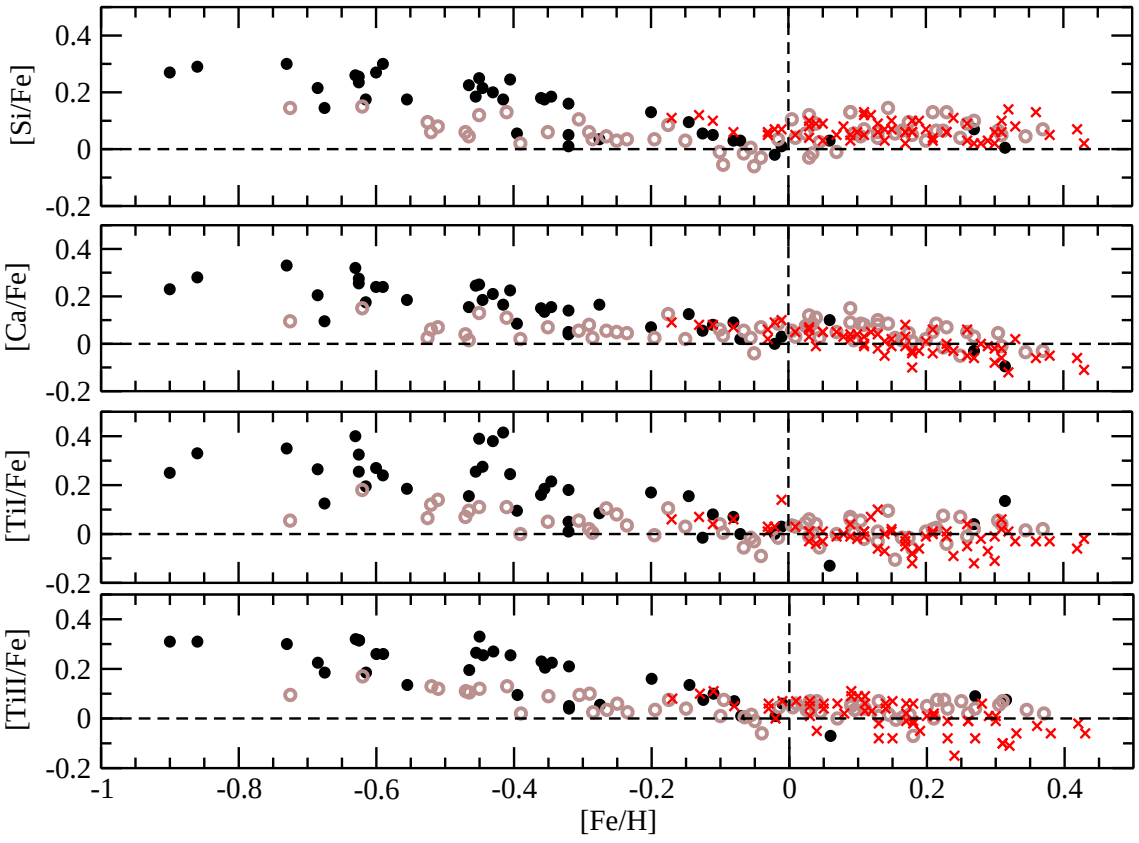

Figure 5.4: Same as the previous plot, but for elements Si, Ca and Ti

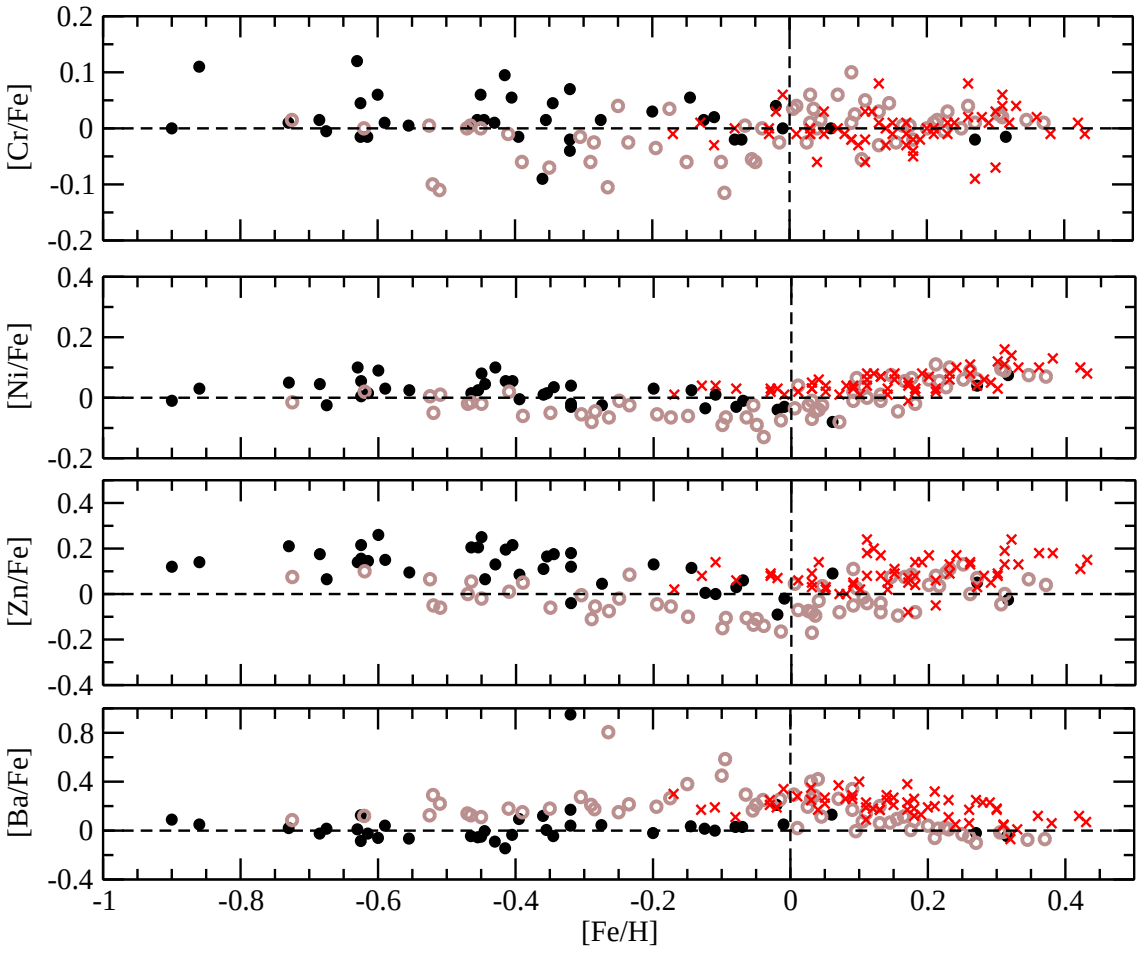

Figure 5.5: Same as the previous plot, but for elements Cr, Ni, Zn and Ba

Table 5.2: Abundance sensitivities to various parameters for a typical sample stars (HIP 8926)

Quantity	N	ΔT_{eff} ±50 K	$\Delta \log g$ ±0.2 cm s^{-2}	$\Delta \xi_t$ ±0.2 km s^{-1}	Δ[M/H] ±0.10 dex	$\Delta W_\lambda / \sqrt{N}$ ± 2 mÅ	σ_{model}
Δ[O I] (λ 6363.78 Å)	1	± 0.02	± 0.11	± 0.00	± 0.04	± 0.11	± 0.16
Δ[OI] (λ6300.31 Å)	1	± 0.01	± 0.11	± 0.01	± 0.03	± 0.05	± 0.13
Δ[Na I/Fe]	2	± 0.04	± 0.01	± 0.06	± 0.01	± 0.02	± 0.08
Δ[Mg I/Fe]	4	± 0.03	± 0.01	± 0.05	± 0.00	± 0.02	± 0.06
Δ[Al I/Fe]	4	± 0.04	± 0.01	± 0.03	± 0.01	± 0.02	± 0.06
Δ[Si I/Fe]	5	± 0.03	± 0.06	± 0.05	± 0.02	± 0.02	± 0.09
Δ[Ca I/Fe]	8	± 0.05	± 0.02	± 0.10	± 0.01	± 0.01	± 0.11
Δ[Sc II/Fe]	6	± 0.02	± 0.10	± 0.05	± 0.05	± 0.02	± 0.13
Δ[Ti I/Fe]	8	± 0.07	± 0.01	± 0.05	± 0.01	± 0.01	± 0.09
Δ[Ti II/Fe]	4	± 0.02	± 0.11	± 0.12	± 0.04	± 0.03	± 0.17
Δ[V I/Fe]	5	± 0.08	± 0.01	± 0.04	± 0.01	± 0.02	± 0.10
Δ[Cr I/Fe]	6	± 0.05	± 0.00	± 0.08	± 0.02	± 0.02	± 0.10
Δ[Mn I/Fe]	3	± 0.05	± 0.01	± 0.05	± 0.01	± 0.02	± 0.07
Δ[Fe I/H]	57	± 0.03	± 0.03	± 0.08	± 0.02	± 0.01	± 0.10
Δ[Fe II/H]	8	± 0.06	± 0.13	± 0.09	± 0.04	± 0.02	± 0.17
Δ[Co I/Fe]	4	± 0.03	± 0.04	± 0.06	± 0.02	± 0.02	± 0.08
Δ[Ni I/Fe]	11	± 0.02	± 0.04	± 0.09	± 0.02	± 0.02	± 0.10
Δ[Zn I/Fe]	2	± 0.04	± 0.07	± 0.10	± 0.03	± 0.04	± 0.14
Δ[Ba II/Fe]	2	± 0.03	± 0.07	± 0.16	± 0.05	± 0.03	± 0.19
Δ[Ba II/Fe] (λ6496.91 Å)	1	± 0.02	± 0.05	± 0.15	± 0.05	± 0.02	± 0.17

Table 5.3: Comparison with Pakhomov et al. (2011) for common stars. The star HIP107502 is neglected while calculating the mean age difference

Quantity	HIP 105502	HIP 106551	HIP 107502	HIP 108012	HIP 109585	HIP 116348	HIP 32844	HIP 35146	HIP 9307	HIP 94576	HIP 96028	Mean±σ
Δ[Na I/H]	0.13	0.04	0.19	−0.04	0.00	0.08	−0.11	0.08	0.06	0.19	0.07	0.06 ± 0.09
Δ[Mg I/H]	0.10	0.00	0.07	0.05	0.07	0.01	−0.21	−0.04	−0.01	0.02	0.05	0.01 ± 0.08
Δ[Al I/H]	0.04	0.06	0.21	−0.07	−0.01	0.11	−0.1	0.07	−0.04	0.06	−0.05	0.03 ± 0.09
Δ[Si I/H]	0.04	0.03	−0.02	0.07	−0.11	0.00	−0.08	−0.16	−0.07	−0.19	0.08	−0.04 ± 0.09
Δ[Ca I/H]	−0.03	0.03	−0.07	−0.32	−0.14	−0.23	−0.34	−0.17	−0.30	0.04	−0.08	−0.15 ± 0.14
Δ[Sc II/H]	0.20	0.03	0.40	−0.03	−0.08	−0.01	−0.08	0.01	0.03	0.10	−0.04	0.05 ± 0.14
Δ[Ti I/H]	0.14	−0.02	0.37	0.01	−0.01	0.10	−0.18	−0.01	0.10	0.10	0.01	0.06 ± 0.14
Δ[V I/H]	0.10	−0.11	0.26	−0.17	−0.02	0.04	−0.16	−0.04	0.12	0.17	−0.17	0.01 ± 0.15
Δ[Cr I/H]	0.10	−0.04	0.20	−0.06	−0.09	0.01	−0.07	−0.06	0.00	0.06	−0.03	0.01 ± 0.09
Δ[Mn I/H]	0.24	0.16	0.34	0.14	0.15	0.00	−0.01	0.22	0.11	0.36	0.09	0.16 ± 0.12
Δ[Fe I/H]	0.14	0.02	0.19	−0.01	−0.07	0.01	−0.08	0.03	0.01	0.05	0.04	0.03 ± 0.08
Δ[Fe II/H]	0.17	0.04	0.21	−0.01	−0.07	0.06	−0.07	0.05	0.05	0.06	0.03	0.05 ± 0.09
Δ[Co I/H]	0.24	0.20	0.54	0.24	0.31	0.24	0.17	0.25	0.18	0.37	0.31	0.28 ± 0.11
Δ[Ni I/H]	0.19	0.07	0.26	0.04	−0.03	0.06	−0.09	0.07	0.05	0.07	0.06	0.07 ± 0.09
Δ[Ba II/H]	0.39	−0.02	0.62	0.18	0.08	0.56	0.33	0.30	0.25	0.28	0.20	0.29 ± 0.19
ΔT_{eff}	160	50	290	20	80	140	−23	115	168	250	20	115 ± 98
Δlog g	0.66	0.13	1.10	0.18	0.00	0.32	0.05	0.34	0.48	0.50	0.08	0.35 ± 0.33
$\Delta\xi_t$	0.14	0.3	0.01	0.14	0.18	0.14	0.15	0.00	0.06	0.14	0.03	0.12 ± 0.08
ΔAge	−0.75	0.26	−11.38	0.44	−0.28	−0.51	0.295	−0.26	−0.38	−0.212	0.40	−0.10 ± 0.42

Ages

Age information is very crucial for deducing information about stars, such as their evolution, origin and distribution in the Galaxy. Ages are estimated mainly by using computed stellar evolutionary tracks or isochrones. We have used theoretical isochrones computed by Demarque et al. (2004) knwon as Y^2 tracks. As the isochrones are predicted for a set of $B-V$ colour and absolute magnitude M_v it is necessary to have accurate observerd values of colour and M_v for the sample stars. We took magnitudes B_T and V_T from Tycho2 catalogue and transformed them to standard Johnson values of V magnitude and $B-V$ colour using the relations given in the Tycho2 Catalogue.

Sample stars are nearby (d < 500 pc). Interstellar extinction is expected to be very low, nevertheless we estimated extinction to each of the stars using extinction maps surveyed by Schlegel et al. (1998). It was noted that the $E(B-V)$ values derived from the maps are erroneous when the extinction exceeds $E(B-V) = 0.1$ (Arce & Goodman 1999, Bonifacio et al. 2000). We adopted Schlegel et al. (1998) map's value as it is, if the $E(B-V)$ values are less than 0.1. In case of higher extinction values (> 0.1), we used a recipe provided by Bonifacio et al. (2000) to get corrected $E(B-V)$ values. Observed magnitudes V and colour $B-V$ of the Hercules sample stars have been corrected for extinction using the derived $E(B-V)$ values and $A_v = 3.12\ E(B-V)$. The absolute magnitude M_v is calculated using the relation M_v = V - (5 log $(1/\pi)$)+ 5, where π, in arc second, is the parallax from new HIPPARCOS catalogue (van Leeuwen 2007). Ages are estimated star-by-star by best matching the theoretical isochrones with the observed values. Isochrones have been generated for each star's metallicity, [Fe/H] and [α/Fe] by interpolation provided along with the tracks. Age estimation has been illustrated in Figure 5.6 (bottom one) for isochrones of [Fe/H] = 0.15 dex and [α/Fe] = 0.02 for three different ages : 0.1 Gyr, 0.5 Gyr, 1 Gyr and 3 Gyr. The age distribution of Hercules stream members is given in the Figure 5.6 (top one), which shows that Hercules stream members have considerable range in the ages, starting from 170 Myr to 4.2 Gyr in general, with the exception of the star HIP 48417 having an age of $\sim$ 12 Gyr with large error bars in the value.

Errors are estimated by accounting errors in the parallax and in the colours, though the errors due to parallax dominate error in the ages. Estimated ages, and the upper and lower limits to errors are given in Appendix A.3. As shown in Figure 5.6, isochrones get converged towards RGB clump region where most of our sample stars lie. The narrow region through which isochrones pass warrants significant errors in the estimated ages. One would be cautious with the interpretation of ages. We have compared our age estimates with Pakhomov et al. (2011) for the common stars. Our values are in general

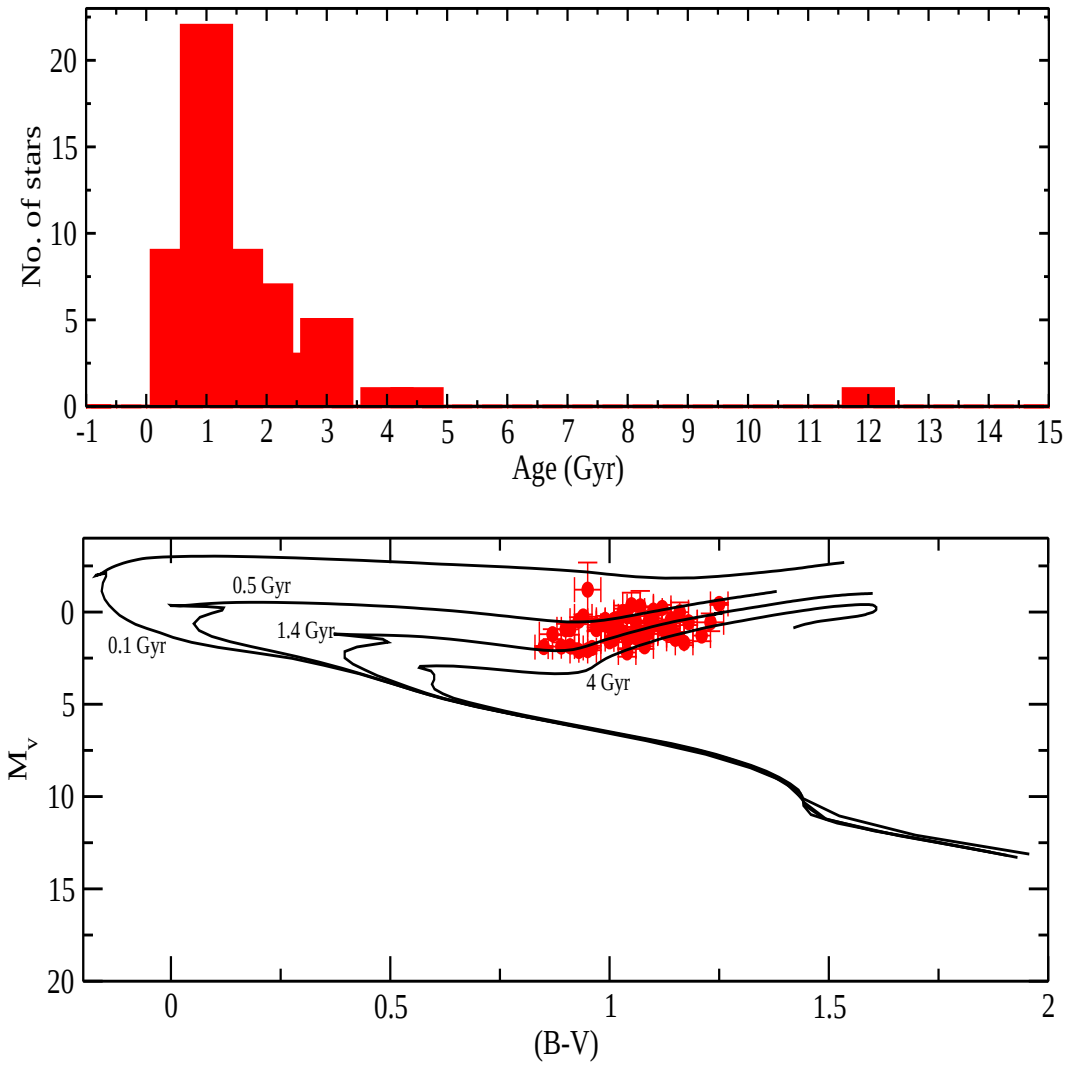

Figure 5.6: *Top* : The age distribution of Hercules stream members (bin size = 0.5 Gyr), *bottom* : Hercules stream members in $B - V$ versus M_v plane.

lower than their values by 200 Myr to 750 Myr. For HIP 107502, the difference is quite large. Pakhomov et al. (2011) estimated a value of 12.6 Gyr, which is quite different from our estimation of 1.2 Gyr. Note, this is the same star for which log g determined by Pakhomov et al. (2011) puts it as an evolved star compared to ours. Excluding the outlier HIP 107502, the mean difference in age is about 100 Myr between the two studies which indeed shows the maturity of both the analysis.

Kinematics

Kinematic motion (U, V, W) of the sample stars is re-calculated in the light of updated version of HIPPARCOS catalogue (van Leeuwen 2007). Radial velocities (V_r) are determined afresh using the high resolution spectra in this study. Radial velocities are estimated by cross-correlation with a template spectrum. The typical error in radial velocity is ± 1 km s^{-1}. The measured radial velocities in this study match well with those from Famaey et al. (2005). The mean difference is just +0.47 ± 1.25 km s^{-1}. Using the updated astrometry, derived radial velocities combined with the formulas for calculating Galactic space velocities given in Johnson & Soderblom (1987), velocities U, V and W were computed.

Throughout the study we used right handed coordinate system, with U pointing towards the Galactic center, V in the direction of Galactic rotation and W towards the North Galactic Pole. Solar motion $(U_\odot, V_\odot, W_\odot)$ = (+10.0, +5.3, +7.2) km s^{-1} (Dehnen & Binney 1998) is used to convert stars' kinematic motion to with respect to the LSR. The derived values relative to LSR (U_{LSR}, V_{LSR} and W_{LSR}) are tabulated in Appendix A.3. Errors in the velocities are due to the quoted errors in radial velocities and astrometry : parallaxes and proper motions. The mean differences between the values derived in this study and that are given in Famaey et al. (2005) are -1 ± 8, 0.3 ± 7 and 0.2 ± 3 km s^{-1} respectively for U, V and W. Both the values agree well in general though the dispersion is quite large. This is very likely due to updated astrometry and differences in radial velocities as well.

The space velocities, U, V and W of each star are integrated over the Galactic potential using the Galactic potential algorithm developed by D. Lin (private communication) to compute orbital parameters such as the apogalactic (R_{max}) and perigalactic distances (R_{min}), eccentricity of stellar orbits (e) and maximum distance of stars away from the Galactic plane (Z_{max}). The radial distance of the Sun from the Galactic center was taken as 8.5 kpc in the calculations. The calculated orbital parameters are given Appendix A.4. Using the derived space velocities, percentage probability (P_{thin}) of belonging to thin disc component for each member of the Hercules stream sample is assigned and tabulated in Appendix A.4. Probabilities are computed as described in Chapter 4. As given in Appendix A.4, except HIP 7719, rest of the sample stars are overwhelmingly thin disc stars. Note, HIP 7719 has very large uncertainty in parallax (68%).

Angular momentum components per unit mass, J_x, J_y and J_z are calculated in a right handed coordinate system as explained in Chapter 4. Derived values of J_z and $J_\perp = \sqrt{J_x^2 + J_y^2}$ are given in Appendix A.4. The mean J_z of the Hercules stream is -1475.74

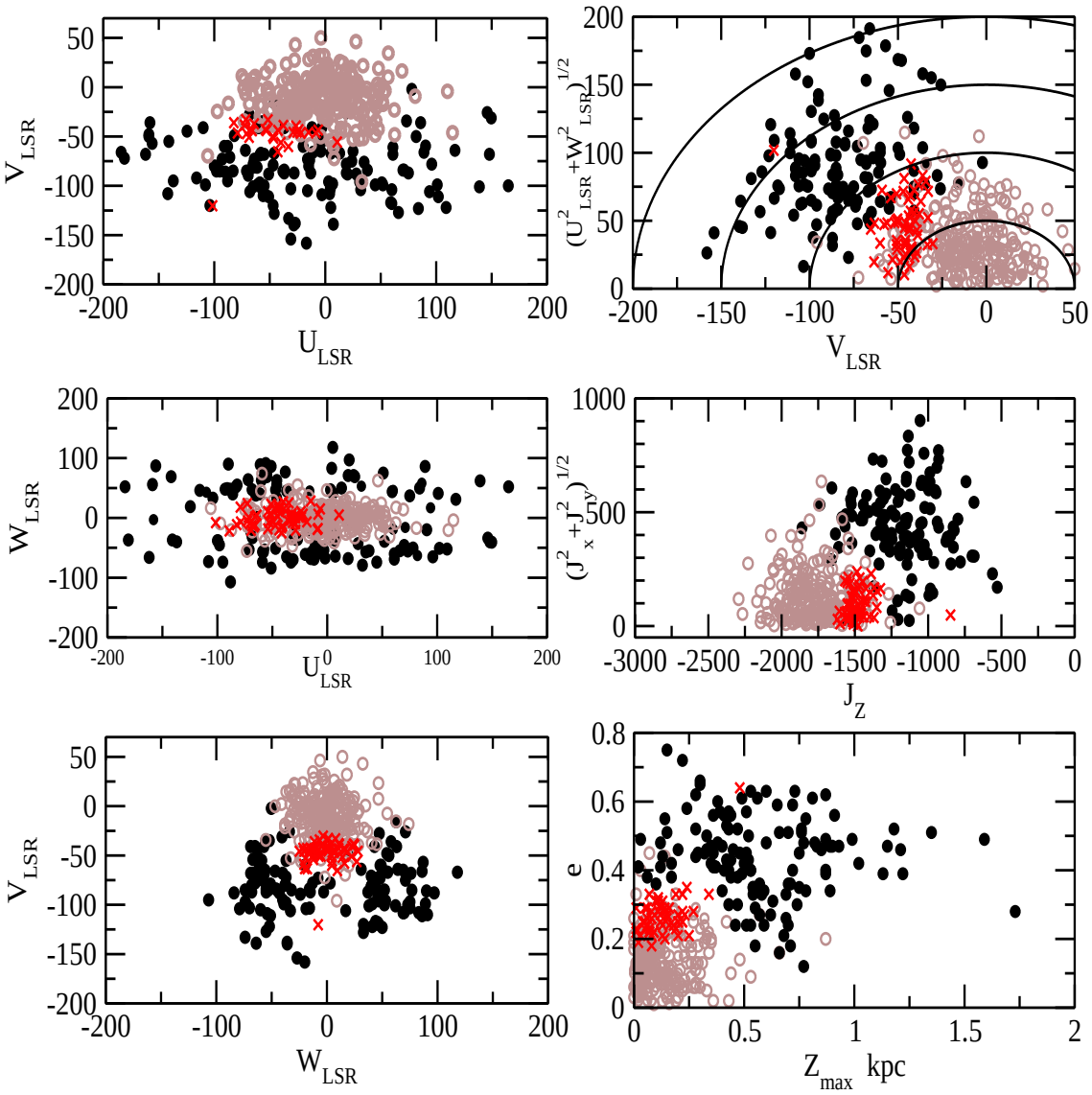

Figure 5.7: Kinematical parameters of the Hercules stream (red cross) are compared with that of thick disc (black) and thin disc (brown) stars

± 106.82. Kinematical properties of the stream members are compared with the Galactic thick and thin disc kinematics in Figure 5.7.

5.2.4 Discussion

Is Hercules Stream a Heterogeneous Population?

Establishing the membership composition of the moving groups is an important objective to understand their origin scenarios. The Hercules stream is suggested to have contained stars from both thin and thick disc components (Bensby et al. 2007, Pakhomov et al. 2011). Based on the results in this study, we attempted to investigate how uniform the members stars of Hercules stream in terms of both their kinematical and chemical properties.

It is known that the Hercules stream has been identified as a group significantly off set in its azimuthal velocity from the bulk of the distribution in the solar neighborhood (Dehnen & Binney 1998, Bovy et al. 2009). In fact, Hercules stream stars lag the local group by $V_{LSR} \simeq -50$ km s^{-1} which is typical of thick disc velocity lag with respect to the LSR. However, the other two velocity components - U and W are very typical of thin disc population. In Fig 5.7, different kinematical properties of Hercules group stars have been shown along with their counter parts in the thin and thick disc taken from Reddy et al. (2003), Reddy et al. (2006), Bensby et al. (2003) and Bensby et al. (2005). Kinematics of Hercules group seems to be more aligned with the thin disc population rather than thick disc population. In particular, in the planes of Z_{max} versus e, and J_z versus $J_\perp$ Hercules stream stars are well separated from the thick disc population and overlapped with the thin disc population. HIP 7119 is the only candidate out of 58 sample stars of Hercules, which has thick disc kinematics. However, we discard the anomaly as being due to large error in the parallax, and hence in the space velocities. The probabilities computed for the group members suggest that all the 57 members belong to thin disc population with $P_{thin} \geq 80$ %. In Table 5.4, mean values of kinematic and orbital parameter of Hercules stream stars are compared with the three major components of the Galaxy (thin disc, thick disc and halo). Hercules group mean values are very similar to thin disc values suggesting group's origin within the thin disc.

Conclusion drawn from kinematic properties is also supported by two other properties : age and metallicity. Though, the group shows large range in metallicity (−0.17 dex to +0.43 dex) it peaks at metallicity, [Fe/H] = + 0.15 ± 0.14 dex very typical of thin disc population groups. Sample stars show metallicity distribution (Figure 5.8) which is close to Gaussian. The mean metallicity obtained in this study is in good agreement with the value [Fe/H] = + 0.11 ± 0.12 dex, obtained by Pakhomov et al. (2011) for their sample of 17 Hercules stream members. However, Zhao et al. (2009)'s study of Hercules stars based on two sets of samples - dwarfs from Nordström et al. (2004) and giants from Famaey

et al. (2005) found mean metallicity to be [Fe/H] = −0.16 dex with a dispersion of 0.20 dex which is close to the values in this study. It is to be noted that thick disc population is more metal poor with mean [Fe/H] = −0.65 dex and dominated by metal poor stars.

Further, except a single member, rest of the group members are found to be younger with ages spanning from 0.17 Gyr to 4.2 Gyr. Exemption being the star HIP 48417 for which age has been estimated as 12^{+7}_{-5} Gyr. However, its metallicity [Fe/H] = 0.04 and its high probability to belong to thin disc (P_{thin} = 89 %) suggest it is a thin disc star. Of course it has large errors in age. We treat it as an outlier. Excluding the outlier, we find group mean age as 1.4 ± 1.7 Gyr. This is very similar to thin disc populations whose ages range from a few Myrs to 10 Gyr. On the other hand, thick disc stars are known to have a small age range (3-4 Gyr) with mean age of about 10.7 ± 2.2 Gyr, estimated from Reddy et al. (2006). We also see that Hercules stream members have an age-[Fe/H] trend similar to thin disc stars (see Figure 5.9).

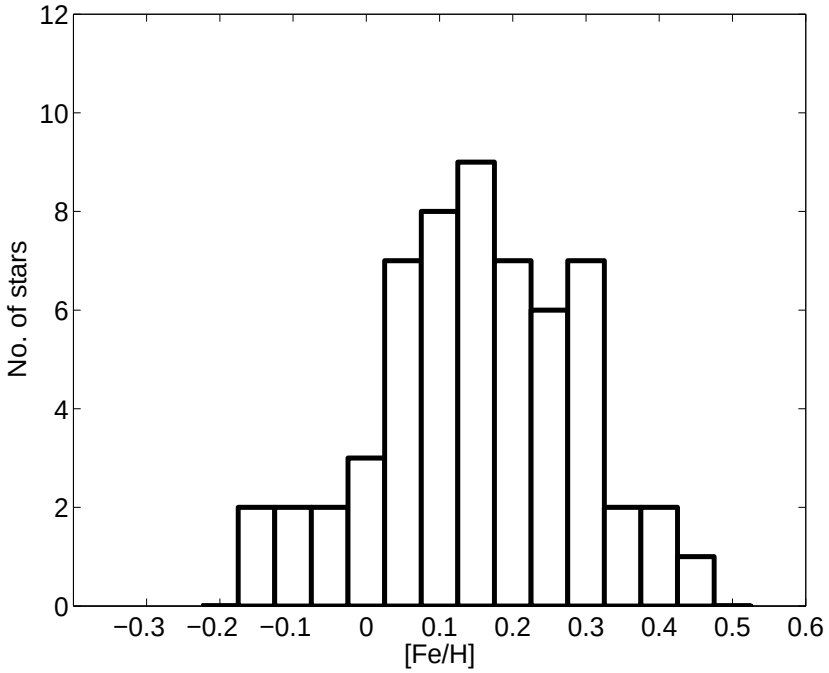

Figure 5.8: The metallicity distribution of Hercules stream members (bin size = 0.05 dex)

Table 5.4: Mean values of derived parameters of three streams compared with the thick, thin and halo components in the Galaxy. The mean thick disc parameters are calculated from Reddy et al. (2006). The thin disc parameters are calculated from the thin disc stars of Reddy et al. 2003 and Reddy et al. 2006. Halo parameters are calculated from the Halo stars listed in Reddy et al. (2006). Other references are mentioned wherever necessary. The Hercules stream member HIP 48417 of age 12^{+7}_{-5} Gyr is excluded due to large error bar, while calculating mean age. 'a′ denotes the mean [Fe/H] value from Allende Prieto et al. (2004) and 'b′ denotes the mean ages from Bensby et al. (2005)

Stream	[Fe/H] dex	Age Gyr	e	[α/Fe]	R_{min} kpc	R_{max} kpc	R_m kpc
Hercules	+0.15 ± 0.14	1.41 ± 1.67	0.27 ± 0.06	0.02 ±0.04	5.27± 0.54	9.09± 0.44	7.18±0.29
HyPl	+0.16 ± 0.12	0.98 ± 0.90	0.11 ± 0.02	0.02 ±0.03	7.10± 0.27	8.89± 0.19	7.99±0.14
Sirius	+0.12 ± 0.11	0.90 ± 0.758	0.06 ± 0.02	-0.01±0.04	8.33± 0.20	9.43± 0.43	8.88±0.27
Thick disc	−0.62 ± 0.28	10.67± 2.26	0.45 ± 0.12	0.21±0.07	...	...	6.49±0.75
	−0.37 ± 0.28[b]	9.7 ± 3.1[b]					
Thin disc	−0.30 ± 0.16	0.85 ± 1.28	0.15 ± 0.09	0.05± 0.04	...	...	8.08±0.82
	−0.05 ± 0.27[b]	4.3 ± 2.6[b]					
	−0.10 ± 0.20[a]						
Halo	−1.11 ± 0.36	12.94± 1.88	0.86 ± 0.16	0.20± 0.08	...	...	45.71±90.33

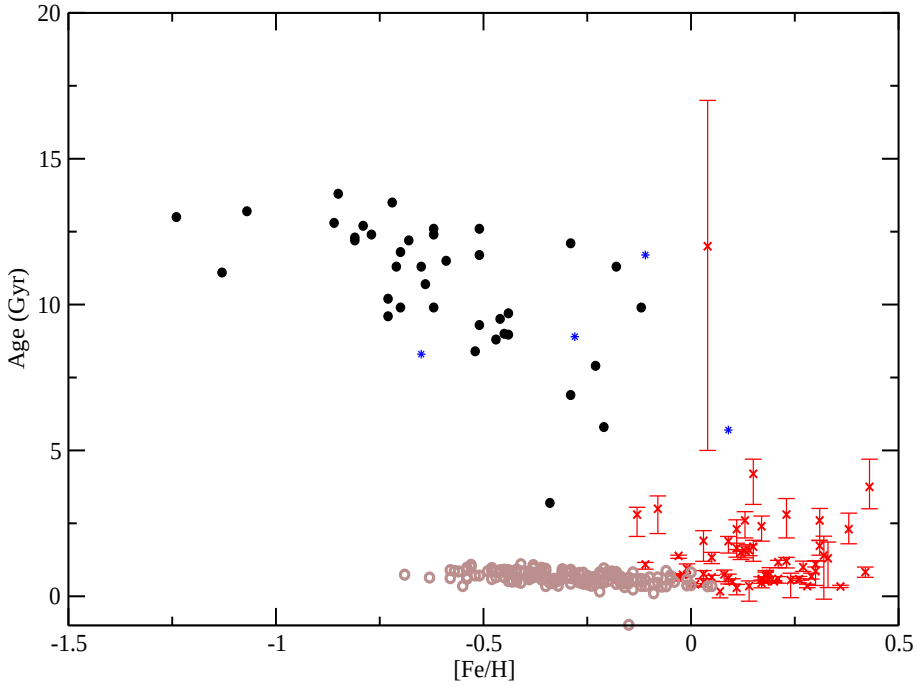

Figure 5.9: Age-metallicity plot. Hercules stream : Red cross, thick disc from (Reddy et al. 2006) : black circle, thin disc (Reddy et al. 2003) : Brown circle, thin disc (Reddy et al. 2006) : Blue star

Thus, contrary to Bensby et al. (2007) results which show Hercules stream containing a wide range of metallicities (-1.0 dex to 0.4 dex) and ages (a few Myrs to 15 Gyr) and interpret Hercules as a mixture of different populations, our results suggest that the Hercules stream is a subset of thin disc population and unlikely it is a mixture of different populations (thick disc, Halo). Pakhomov et al. (2011) also claims that their Hercules stream sample is a mixture of both thin and thick discs based on abundance ratio [Na/Fe] (see their Figure 4). In their plot of [Na/Fe] versus log g, they showed a significant fraction of stars follow thick disc [Na/Fe] ratios. Unfortunately, we can't test this claim as we do not have access to thin and thick disc giants abundances in this metallicity regime. However, we note that Na abundances are prone to severe non-LTE effects and results obtained with LTE need to be taken with caution. The study of (Klement et al. 2009) based on SDSS data hints that Hercules stream may consists of wide range of metallicities. They binned their sample into four metallicity groups (-1 < [Fe/H] ≤ -0.5 ; -1.5 < [Fe/H] ≤ -1.0 ; -2.0 < [Fe/H] ≤ -1.5 ; [Fe/H] ≤ -2.0) and analysed the data for detecting moving groups. At azimuthal velocity of about 169 km s−1 (V_{LSR} = −51 km s^{-1}), the characteristic velocity of Hercules stream, they found overdensity in at least

three metallicity groups : (-1 < [Fe/H] ≤ -0.5 ; -2.0 < [Fe/H] ≤ -1.5 ; [Fe/H] ≤ -2.0). As parallaxes for the sample come from photometry, and radial velocities from low resolution spectra one may need exercise great caution to interpret such overdensities to Hercules merely based on the coincidence of one velocity parameter.

This warrants to check whether the chosen sample is biased towards more metal rich thin disc population. As per our understanding the original data, from which Famaey et al. (2005) identified Hercules stream, is unbiased sample of K and M giants. It is very unlikely, we introduced bias in the sample by choosing stream stars with probability to belong to Hercules stream > 70% as given in the catalogue. In fact, we did estimate probabilities for the entire sample of 529 Hercules stars in the catalogue, and found them overwhelmingly of thin disc stars with $P_{thin} \geq 70\%$, excluding the stars with large errors in the parameters.

Another selection criterion was $V - I$ colour cut off. We have taken only stars with $V - I \leq 1.15$ to avoid cooler stars in the sample as their spectra is complex for accurate abundances. To test whether this has introduced bias towards more metal rich and younger stars, we have plotted our sample of Hercules stars in a plot of colour $B - V$ versus [Fe/H] (Figure 5.10 ; bottom one) to see any trend of colour with [Fe/H]. Figure shows a weak trend of increasing [Fe/H] with colour. Figure suggests that, by having $V - I$ cut off at 1.15, we might have missed more metal rich, and probably younger candidates but not the metal poor stars. We arrive at a similar conclusion from the Figure 5.10 (top one) where we plotted all the 529 Hercules stars from Famaey et al. (2005) in the colour-luminosity diagram superposed with 10 Gyr isochrones wth four different metallicities. Only a small fraction of stars go through 10 Gyr isochrone with [Fe/H] = −0.15, and the fraction gets reduced significantly towards metal rich isochrones.

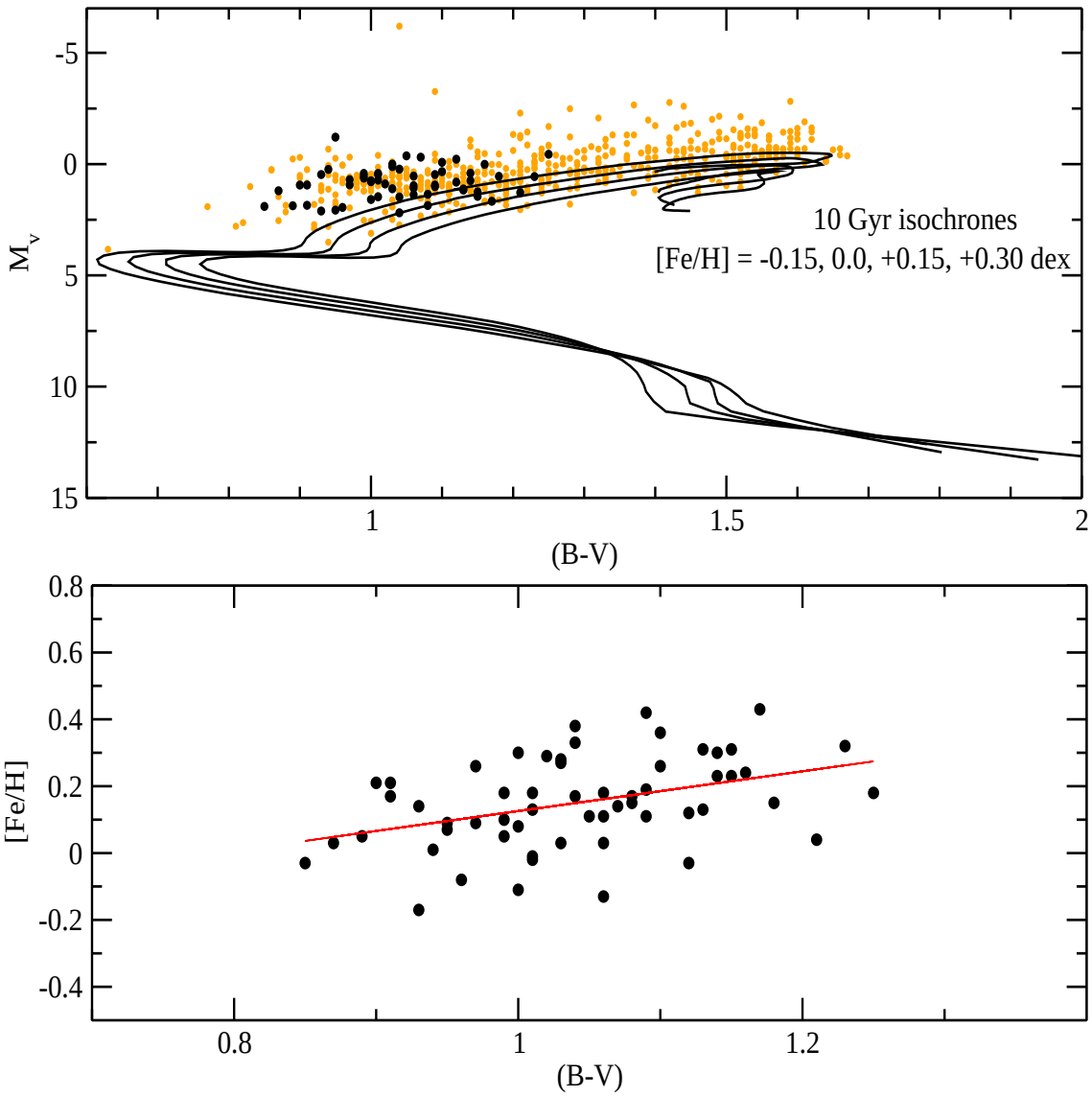

Figure 5.10: The Hercules stream members (Orange circle : Total sample of Hercules stream from Famaey et al. (2005), Black circle : the 58 members studied by us) in the $(B-V)$ - M_v plane (top). The 58 Hercules stream members studied by us in the [Fe/H]-$(B-V)$ plane (bottom)

5.2.5 Origin of Hercules stream

Until recently, the discussion on the origin of moving groups has been centered around the kinematic properties of the member stars of the moving groups. Now, this has been shifted to chemical properties of the member stars as well. In this study we derived elemental abundances, ages and kinematical properties of 58 member stars of Hercules stream. These results have been discussed in the context of three main origin hypotheses for the Hercules stream : cluster dispersion, satellite accretion and in-situ formation caused by dynamical perturbations either by Galactic bar/spiral or/and by merging satellites.

Cluster Dispersion

This is one of the earliest suggestions advocated by Eggen (see for example Eggen 1996) in many of his studies of moving groups. Suggestion being the member stars which share space velocities can be traced back to their spacially coherent groups or open clusters. Open clusters are known to disperse over time scales of a few Million to a couple of Giga years depending on their location in the Galaxy. For example, open clusters of high Galactic latitudes (say in thick disc) may suffer interactions with gas or spirals relatively less and survive longer as spatially coherent groups compared to their counter parts at low Galactic latitudes. If the member stars are in fact as a result of dispersed open cluster, one would expect not only similarity in their kinematic motion, but also homogeneity in their chemistry, and coevality.

As shown in Figure 5.8, member stars of Hercules stream show large range in metallicity (about 0.6 dex) which is relatively much higher compared to any typical surviving open clusters. In Table 5.5, we compared mean and standard deviations of Hercules stream with two open clusters : Berkeley 32 and Hyades (Carrera & Pancino 2011). The surviving open clusters show very little star-to-star dispersion. The large star-to-star dispersion for Hercules stream stars is also evident in other elements. We have considered only abundances which are based on three or more than three transitions e.g. Ni, Ca, Ti etc. The large range in abundances is incompatible with the idea that the member stars of the Hercules stream were once part of an open cluster. This conclusion is supported by a wide range (about 5 Gyr) of ages which member stars exhibit. However, both the ranges in abundances and ages fit well within the thin disc population. Also, abundance ratios shown in Figures 5.2-5.5 along with thick and thin disc results indicate that stream abundances are very similar to thin disc though it is difficult to disentangle the thick disc abundance trends from the thin disc, in the super solar metallicity regions. The conclu-

sions arrived in this study in the context of Hercules stream, are different from the earlier studies by Bensby et al. (2007) and Pakhomov et al. (2011) which suggested Hercules stream is a mixture of different populations with wide range of metallicity (about 1.5 dex) and ages (about 16 Gyrs). Thus, from the results in this study we conclude that members of the Hercules stream are a group of stars which share space velocities but not chemistry or coevality and unambiguously belong to the thin disc population.

Table 5.5: Mean abundances of Hercules stream are compared with the abundances of two open clusters. For clusters, the mean [Fe/H] =([FeI/H] + [FeII/H])/2, [X/H] = [X/Fe] + [Fe/H]

Entity	Hercules (58 stars)	Berkeley 32 (2 stars)	Hyades (3 stars)
[Fe/H]	0.15 ± 0.14	-0.30 ± 0.02	0.11 ± 0.01
[O/H] (λ6300 Å)	0.14 ± 0.12	(-0.30 ± 0.24)	(-0.16 ± 0.06)
[O/H] (λ6363 Å)	0.21 ± 0.14	(-0.30 ± 0.24)	(-0.16 ± 0.06)
[Na/H]	0.29 ± 0.22	-0.41 ± 0.07	0.30 ± 0.02
[Mg/H]	0.17 ± 0.12	0.01 ± 0.07	0.25 ± 0.07
[Al/H]	0.28 ± 0.15	-0.18 ± 0.02	0.12 ± 0.01
[Si/H]	0.22 ± 0.13	-0.15 ± 0.02	0.21 ± 0.01
[Ca/H]	0.16 ± 0.10	-0.35 ± 0.03	0.05 ± 0.01
[Sc/H]	0.20 ± 0.15	-0.30 ± 0.01	0.09 ± 0.02
[TiI/H]	0.14 ± 0.12	-0.37 ± 0.07	0.02 ± 0.02
[TiII/H]	0.16 ± 0.11	-0.38 ± 0.15	0.10 ± 0.02
[V/H]	0.17 ± 0.13	-0.40 ± 0.07	0.15 ± 0.04
[Cr/H]	0.15 ± 0.14	-0.40 ± 0.23	0.16 ± 0.02
[Mn/H]	0.09 ± 0.15	...	
[Co/H]	0.38 ± 0.22	-0.24 ± 0.07	0.14 ± 0.02
[Ni/H]	0.21 ± 0.16	-0.32 ± 0.05	0.14 ± 0.01
[Zn/H]	0.24 ± 0.17	...	...
[Ba/H]	0.35 ± 0.12	0.14 ± 0.10	0.47 ± 0.05
[Ba/H](λ6496 Å)	0.49 ± 0.14	(0.14 ± 0.10)	(0.47 ± 0.05)

External Origin: Accretion of Satellite galaxies

There are studies which suggests that the Galaxy accretes satellites and due to the strong pull of Galaxy's potential, satellites can be disintegrated. Depending on the inclination of their orbits during the accretion, the debris may even enter the Galactic disc (Abadi et al. 2003a, Abadi et al. 2003b, Helmi et al. 2006). In this scenario, it is predicted that the member stars of the accreted satellite galaxies will have much higher rotational lag relative to Local Standard of Rest and rotate in the Galaxy with very high eccentricity. However, results of space velocities and orbital motions tabulated in Appendix A.3 and A.4 shows that the Hercules moving group is of low velocity, and rotates around the Galactic center with near circularity ($e \sim 0.27$). Another important property of the Hercules group is that the net radial outflow ($U_{LSR} \simeq -50$ km s^{-1}) which is not typical in the case of stars originated from an accreted satellite (Navarro et al. 2004). Combined with net outflow and lack of significant vertical motion (Seabroke et al. 2008) of member stars of Hercules stream may suggest that its origin may not lie in the satellite galaxies.

Further, one may deduce clues from the abundance and age results. Hercules stream abundances are quite different from those of dwarf spheroidals. None of the surviving dwarf spheroidals in the Local Group is as metal rich and young as these streams (See Figure 4.10). If the Hercules origin had to be due to merger of satellite, then the satellite would have been a massive galaxy. So that multiple star formation episodes would give rise range of metallicity and age as the Hercules stream members exhibit. The presence of thin disc gives evidence that, no major merger has happend with Milky Way, atleast in the past 10 Gyr (The upper age of thin disc). Thus, both the kinematics and chemistry suggest it is unlikely the member stars originated from the satellite galaxy.

Effects of Dynamical Perturbation

Third option is an in-situ formation due to dynamical perturbation of stellar orbits. The suggestion has been one of the most favoured for many of the moving groups that are identified within the disc (Kalnajs 1991, Famaey et al. 2005, Antoja et al. 2010). In particular, the large radial outflow velocity (u) of stars in the solar neighborhood prompted studies like Raboud et al. (1998) and Fux (2001) to simulate dynamical effects due to the Galactic bar on the stellar orbits. In the case of ideal scenario in which the Galaxy is axisymmetric with bulge, disc and halo, one would expect stars in the disc rotate in circular orbits but with no net radial outflow. However, the presence of bar in the center of the Galaxy and its resonance with stars' orbits affects stars to move large spacial distances within the Galaxy (Raboud et al. 1998). In fact simulations by a number of studies

(Dehnen 2000, Gardner & Flynn 2010; Mincheve et al. 2007) show that the Hercules stream space velocities can be recovered at bar's Outer Lindblad resonance (OLR) with local orbits. Of course the position of Hercules stream in the simulated $U - V$ plane depends on various parameters such as bar's mass, rotation rate of the bar (pattern speed), and its angle with respect to the line-of-sight to the Sun.

Results obtained in this study provide important clues that members of Hercules stream most probably an effect of bar on orbits for the following reasons: a) as argued in earlier sections, member stars of the stream are a subset of the thin disc population, b) they exhibit a range of metallicities and ages with significant portion of them are metal rich, indicating migration of stars from inner disc, where the interstellar medium is more metal rich c) net radial flow and lack of large vertical velocity suggest dynamical origin (Navarro et al. 2004).

5.3 Hyades stream and Pleiades stream

5.3.1 Introduction

Early identification of the two moving groups along with some others has been credited to Mädler (1846) and Proctor (1869) (see Antoja et al. 2010, for historical developments). The modern definitions of the moving groups based on velocities were studied by O J Eggen (see Eggen 1996 and the references there in). Various recent studies confirm that Hyades stream and Pleiades stream are two prominent overdensities in the velocity space, with very similar rotational lag of $\sim$ 10-20 km s^{-1} with respect to LSR. But they differ in the amount of radial motion they possess in the disc of the Galaxy. See Table 5.6, for a few examples of the detections of these two streams in the $U - V$ plane.

The defining clusters :

Hyades and Pleiades superclusters or moving groups owe their names to the Hyades and Pleiades open clusters, respectively. Also, Hyades group shares the motion of Praesepe cluster, along with that of Hyades cluster. Hyades cluster and Praesepe cluster have heliocentric velocities, U = -44.4 ± 0.8, V = -17.0 ± 1.0, W = -5.0 ± 1.3 and U = -37.1 ± 1.6, V=-23.5 ± 2.4 , W = -7.0 ± 1.7 (Gomez et al. 1990) respectively. Hyades cluster (Mellotte 25) is at a distance of 46.5 pc from the Sun (van Leeuwen 2009) located in the Taurus constellation. The mean age of it is 625 ± 50 Myr (Perryman et al. 1998). Similarly, Pleiades stream (Local Association) shares the motion of Pleiades open cluster (heliocentric U = -5.8 ± 1.3 , V = -24.0 ± 2.0, W = -12.4 ± 2.0 ; Gomez et al. 1990) along with a few other clusters namely M 34, NGC 2516, IC 2602, Melotte 20, Stephenson 1 etc and Scorpio-Centaurus OB association.

Hyades supercluster was a subject of recent abundance studies. (de Silva et al. 2011 ; Pompéia et al. 2011 ; Tabernero et al. 2012). These studies concluded that the Hyades moving group is a mixture of stars originated from Hyades cluster and from inner regions of the Galactic disc as a result of dynamical perturbations. Our study of moving groups based on elemental abundances of a sample od stars was conceived independently almost five years ago. In this chapter, we studied 34 member stars of Hyades-Pleiades supercluster by analysing their chemical properties. We compare and contrast our results with that of the recent studies.

Table 5.6: Kinematic definitions of Hyades and Pleiades streams in the literature. UVW components are heliocentric

Hyades stream			Pleiades stream			
U (σ_U) km s^{-1}	V (σ_V) km s^{-1}	W (σ_W) km s^{-1}	U (σ_U) km s^{-1}	V (σ_V) km s^{-1}	W (σ_W) km s^{-1}	Reference
-40.4	-18.3	-1.9	-11.6	-20.7	-10.4	Eggen (1992a)
-44.4 (5.3)	-17.8 (3)	-1.5 (9.7)	-10.0 (7.9)	-19.0 (8.6)	-8.1 (5.8)	Chen et al. (1997) (4D space)
-45.5 (7.7)	-25.4 (13)	0.0 (10.3)	-5.9 (6.2)	-26.5 (4.3)	-6.1 (4.8)	Chen et al. (1997) (3D space)
-38 (6)	-18 (6)	-10 (10)	-12 (6)	-23 (6)	-10 (10)	Zhao et al. (2009) (dwarf sample)
-38 (6)	-17 (6)	-11 (12)	-15 (6)	-23 (6)	-10 (12)	Zhao et al. (2009) (giant sample)
-40	-20	0	-12	-22	-7	Dehnen 1998
-37	-17	...	-15	-25	...	Famaey et al. (2007)
-42	-18	...	-13	-19	...	Fux 2001
-40	-20	...	-15	-20	..	Bovy et al. (2009)
-39.7	-17.7	-2.4	-11.6	-21.0	-11.4	Montes et al. (2001)

5.3.2 Sample stars and Observations

As noted, Hyades moving group has been studied using abundances (de Silva et al. 2011 ; Pompéia et al. 2011 ; Tabernero et al. 2012). However, our adopted sample is different from tthe earlier studies. de Silva et al. (2011) chose their sample from the observations of Wilson (1990) and Eggen (1998c) with stars having velocities closer to $U = -40$ km s^{-1} and $V = -17$ km s^{-1}. In the case of Pompéia et al. (2011), sample stars are randomly selected from Geneva-Copenhagen survey with velocities in the range of -23 km s^{-1} $\leq$ V $\leq$ -12 km s^{-1} and -50 km s^{-1} $\leq$ U $\leq$ -25 km s^{-1}. Tabernero et al. (2012) chose the Hyades supercluster sample using the kinematical criteria based on the UVW Galactic velocities of a chosen target being within approximately 10 km s^{-1} of the mean velocity of the group as given in Montes et al. (2001).

In our case, sample stars were chosen from the study of Famaey et al. (2005) who assembled a large number of stars from HIPPARCOS catalogue with accurate astrometry from which they deduced the substructures. For details of sample selection, refer Chapter 2, Section 2.2.2. They identified Hyades-Pleiades (HyPl) as a single clump with mean motion of $U = -40$ km s^{-1}, $V = -20.3$ km s^{-1} and $W = -4.8$ km s^{-1}, as the methods used by them could not resolve the closely spaced (in the velocity space) Hyades and Pleiades as two different groups. We chose stars from their catalogue which are the most likely members (Probability to belong to the group is $\geq$ 70 %) of the HyPl moving group. A total of 34 K giants were chosen with $V - I \geq 1.15$. High resolution Echelle spectra with $R \approx$ 60,000 and with a very good S/N ratio ($>$ 100) were obtained using 2.7 m Harlan J. Smith Telescope, McDonald Observatory, USA. The observation details of the sample is given in Table 2.4 of Chapter 2. Data reduction was done as described in the earlier chapters.

5.3.3 Kinematics and Ages

Kinematic motions of the sample stars are recomputed using the radial velocities obtained in this study and the recalibrated HIPPARCOS astrometry (van Leeuwen 2007). The derived radial velocities and the computed kinematic motions in this study are in good agreement with the values given in the Famaey et al. (2005) catalogue. We derived Galactic space velocity components and the orbital parameters such as R_{min}, R_{max}, R_m, Z_{max}, e, J_z, $J_\perp$ etc for all the 34 giants, in the same fashion as in earlier sections, and are are tabulated in Appendix A.5 and A.6. Also, we calculated the kinematical probability with which these 34 members belong to Galactic thin, thick and halo components

of the Galaxy. we find all the members belong to the Galactic thin disc with very high probability (P_{thin} = 99 %). The various kinematical properties of the 34 HyPl members are compared with those of the Galactic thick and thin disc stars in the Figure 5.11. The figure clearly indicates that, HyPl members are definitely the thin disc stars kinematically, with no exceptions found in the sample.

Ages have been derived using HR diagram (($B - V$) - M_v plane) and Y^2 isochrones. In Figure 5.12 (bottom one), age determination of the HyPl sample stars is illustrated in which isochrones of ages 200 Myr, 1 Gyr and 4 Gyr of metallicity [Fe/H] = +0.16 dex (note that [Fe/H] = +0.16 dex is the mean metallicity of the 34 HyPl stars) are superposed. Derived ages are given in Appendix A.5. The age distribution of 34 members is shown in Figure 5.12 (top one). It is clear that, our sample is dominated by young stars of age $\lesssim$ 1 Gyr. All the sample stars are having an age which is less than 10 Gyr. Note that this is essentially the Galactic thin disc trend.

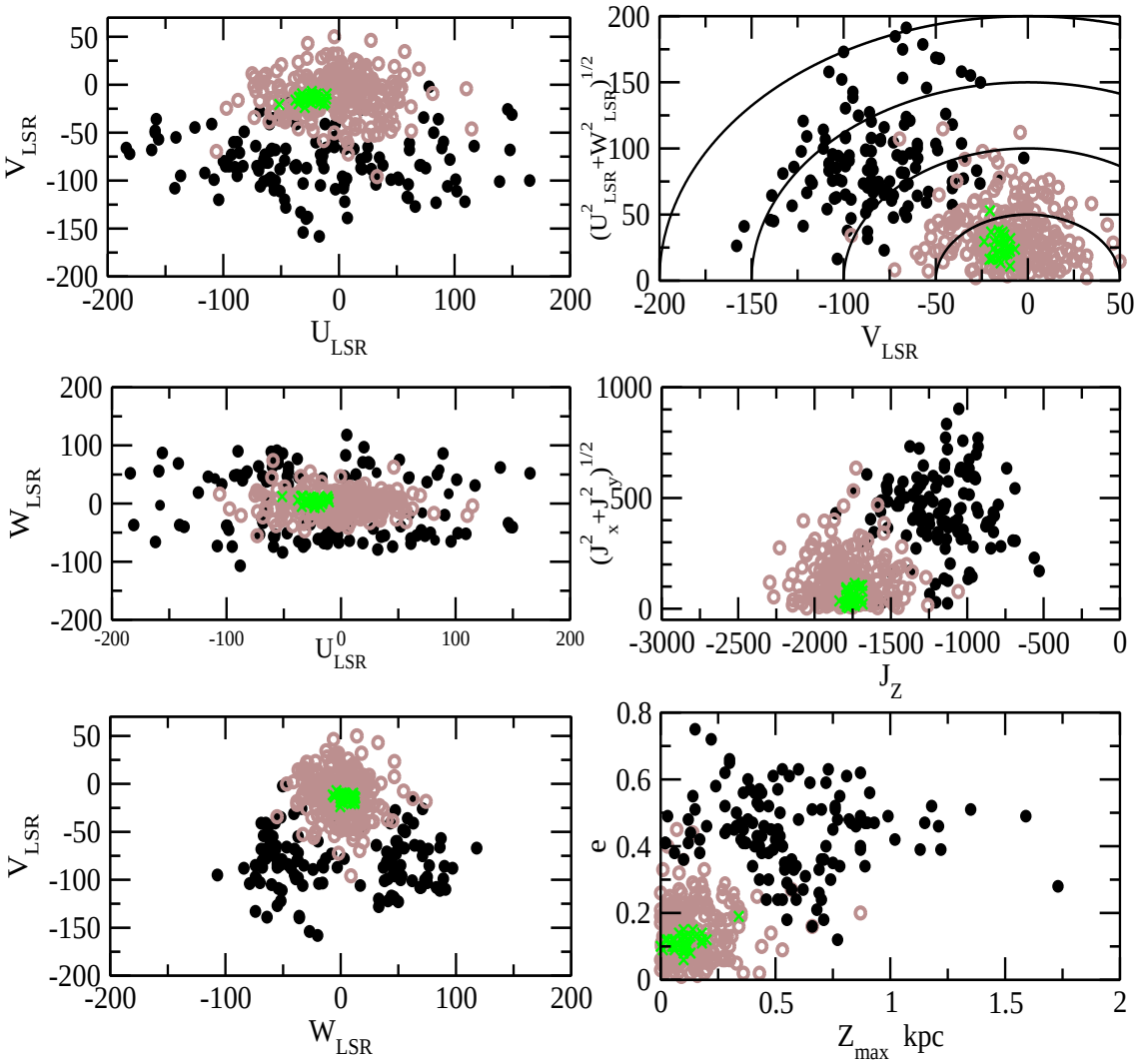

Figure 5.11: The kinematical properties of HyPl stream members (Green cross) are compared with those of thick disc (black circle) and thin disc (brown circles) field stars

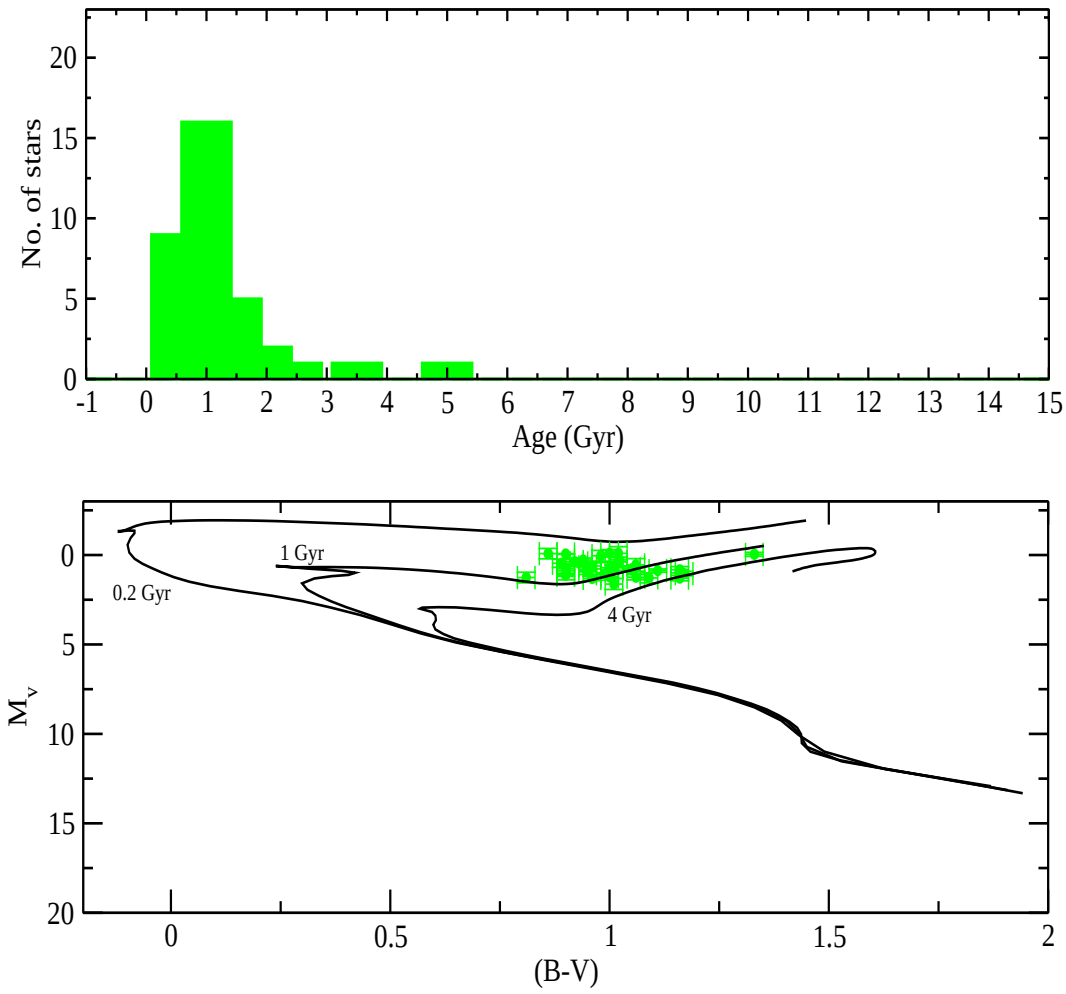

Figure 5.12: The age distribution (top), and the $(B-V)$ - M_v plane (bottom) of the HyPl stream members

5.3.4 Separating the sample into Hyades and Pleiades moving groups

Since our HyPl sample stars came from Famaey et al. (2005) study, the sample may contain members of the two moving groups. They could not separate Pleiades as a separate group as it has very similar azimuthal velocity as that of Hyades. But, later Famaey et al. (2008) applying wavelet transform technique on the same set of data attempted to distinguish them as two separate clumps. They could resolve Hyades and Pleiades with the following velocity boxes, in which they got nonzero wavelet coefficients,

Hyades : $U \simeq$ [-41, -23] and $V \simeq$ [-24, -12]

Pleiades : $U \simeq$ [-23, -9] and $V \simeq$ [-28, -18]

Simlarly, in the study of Hyades supecluster, Famaey et al. (2007) had defined the Hyades velocity box as, -21 km s^{-1} $\leq V \leq$ -12 km s^{-1} and -50 km s^{-1} $\leq U \leq$ -25 km s^{-1}. On the other hand the kinematic motion of Hyades stream members in Tabernero et al. (2012) study ranges from -55.59 km s^{-1} to -25.48 km s^{-1} in U and -27.25 km s^{-1} to -10.61 km s^{-1} in V, excluding the star HIP 14838 with U = -60.17 ± 5.44 km s^{-1} and V = -48.96 ± 7.19 km s^{-1}. Note that in definitions given above, UVW values are heliocentric. We used solar motion ($U_\odot$, $V_\odot$, $W_\odot$) = (+10.0, +5.3, +7.2) km s^{-1} (Dehnen & Binney 1998) to convert heliocentric velocities to velocities with reference to LSR.

It is clear that the radial velocity U is the only differentiator between the two moving groups (see Table 5.6 also). Assuming that the chosen sample is a sole mixture of Hyades and Pleiades moving groups, we made a simple demarcation based on U velocity. Our sample of 34 HyPl stars ranges from -51.5 km s^{-1} to -10.6 km s^{-1} in U_{LSR}, while the V_{LSR} ranges from -23.7 km s^{-1} to -7.0 km s^{-1}. Since, our sample is from Famaey et al. (2005), we used the velocity definitions given by Famaey et al. (2008), for separating Hyades and Pleiades stars. The Famaey et al. (2008) velocity definitions of Hyades group gives the U_{LSR} range as U_{LSR} [-31, -13]. Based on this new definition, stars have been separated into two groups - stars as most likely members of the Hyades moving group and as most likely members of the Pleiades moving group. We have taken stars with $U \leq -13$ km s^{-1} as sure members of the Hyades moving group and stars with $U > -13$ km s^{-1} as Pleiades moving group. Though, we placed the dividing line between Hyades and Pleiades groups at U_{LSR} = -13 km s^{-1}, one should note that, probability of stars belonging to the Hyades or Pleiades overdensity will be very similar at the dividing line. We found 31 stars with $U_{LSR} \leq$ -13 km s^{-1}. 8 stars out of this set of 31 stars have $U_{LSR} <$ -31 km s^{-1}, which is

outside the definition of Famaey et al. (2008), but we note that 7 out of 8, qualify to be Hyades group members as per Famaey et al. (2007) velocity definition of Hyades group (-40 km s^{-1} $\leq$ U_{LSR} $\leq$ -15 km s^{-1}, correcting the original definition for solar motion). The outlier is HIP 65366, with U_{LSR} = -51.5 ± 10.34 km s^{-1}. It has large error associated with the value. Hence, we consider the set of 31 stars described above, as Hyades stream members and the remaining 3 stars with U_{LSR} > -13 km s^{-1} as Pleiades stream members. We wont be discussing further about Pleiades as the sample stars are very few in number. We also note that the three Pleiades stream members (HIP 83289, HIP 79164 and HIP 74080) are indistinguishable from the 31 Hyades group members in all other kinematical properties and ages. The ages of these three stars are 680 Myr, 1.04 Gyr and 1.05 Gyr respectively.

5.3.5 Atmospheric Parameters

Atmospheric parameters : T_{eff}, log g, ξ_t and [M/H] are derived the same way as described in the earlier sections. The derived T_{eff} and log g values using photometry and spectroscopy are tabulated in Appendix B.4. In many cases, the T_{eff} values from $J-K$ colour are significantly cooler compared to values from spectroscopy and $V-K$ colour. This is similar to what has been seen for the Hercules stream in the previous section suggesting probably a larger error in J magnitdues. The log g values from the two methods match well within ± 0.16 (σ = 0.15). Values of metallicity are based on Fe I abundances. Sample stars show solar or supersolar metallicity. The atmospheric parameters derived both spectroscopically and photometrically are compared in the Figure 5.1 (green symbol).

5.3.6 Chemical Abundances

Abundance results [X/Fe] for 16 elements of the 34 sample stars are presented in Appendix B.13-B.15 and also plotted as a run of [Fe/H] versus [X/Fe] in the Figures 5.13-5.15. Abundances of Galactic thin and thick disc field stars taken from Bensby et al. (2005) are also plotted for comparison. In general, the sample stars show solar to supersolar metallicity. Three stars in the sample have subsolar metallicity - [Fe/H] ~ -0.10 dex for two stars, and [Fe/H] = -0.03 dex for the third one. Metallicity of the sample spans from −0.12 dex to +0.34 dex. The three Pleiades stream members - HIP 83289, HIP 79164 and HIP 74080 have metallicity values of [Fe/H] = +0.24 dex, +0.12 dex and +0.11 dex respectively and are indistinguishable from the rest of the 31 stars (classified

Hyades group members) in the elemental abundance plane. Hence, we wont be discussing about these three stars specifically now onwards. The [X/Fe] values are normal for any typical stars in that metallicity range. In general, they fit into the Galactic thin disc abundance trends.

The α-elements (Mg, Si, Ca, Ti) seem to follow the Galactic field star trend in general, although Mg abundances seem to lie below the Galactic trend. The Iron-peak elements Cr and Ni very tightly follow the Galactic trend, with a very small scatter, as shown in the Figure. The abundances of odd-Z elements are consistent with the Galactic trend except Na, which shows large scatter and abundances are higher than the Galactic trend. This is more prominently visible in the metal rich regimes of the sample. We see that similar kind of Na enhancement in giants is reported by other studies as well. de Silva et al. (2011) has reported Na enhancement in the Hyades supercluster sample of giant stars as compared to the dwarf stars of the Galactic disc, and attributed this enhancement to the internal mixing in some of the giant stars. In the recent study by Smiljanic (2012), the issue of Na enhancement in giants, especially in the open clusers is dealt with. Although, various suggestions such as the NLTE effects, deep internal mixing, different atomic data, put forward to explain the issue, Na enhancement in giants still remains a mystery. Smiljanic (2012) also, found a high Na abundance ([Na/Fe] = +0.30) in Hyades cluster giants. Similarly, Tabernero et al. (2012) has reported that, the abundance of odd-Z elements Al, Na and V, except for Sc, of the giant stars in their sample deviate from the Galactic trend. Similarly, in the case of Zn, Tabernero et al. (2012) has reported a slight deviation of Zn abundance from the Galactic trend, for the giant stars in their sample, while we observe Zn abundance follow Galactic trend in general.

Exemption to the generality is the Ba abundance. As shown in Appendix B.15, values of [Ba/Fe] for most of the stars show significant enhancement. Similar enhancement is seen in the case of Hyades cluster stars. (see Table 5.10, to be discussed later). It is not clear why we see such a significant overabundance of Ba in otherwise normal stars. Similar Ba abundances were reported for the Hyades moving groups stars by de Silva et al. (2011) and Hyades cluster stars by Carrera & Pancino (2011). Tabernero et al. (2012) also has reported enhancement in Ba. Given the young age of the stars in the moving group enhancement cant be attributed to nucleosynthesis. Also, it would be difficult to interpret this as due to chemical composition of their natal clouds which are enhanced in the *s*-process elements. Most likely, in our view, the apparent enhancement may be due to insufficient corrections to HFS and errors associated with stronger lines such as blending. Note that, although slight Ba enhancement is observed in the case of Hercules stream

members also (see Figure 5.5), it is not as high as observed for Hyades sample, especially in the metal rich regime.

Typical errors in the abundances arising due to uncertainties in the atmospheric parameters and other measurements are given in Table 5.2 for representative star HIP 8926. To estimate uncertainties, we made a comparison of our results with three common stars found in Tabernero et al. (2012) study of Hyades group, which is given in Table 5.7. Out of the three common stars, one star named HIP 20889 (ϵ Tau / Melotte 25 MMU 70) is a known giant member of Hyades open cluster listed in WEBDA open cluster database. It appears to us that, Tabernero et al. (2012) did not remove Hyades cluster members effectively while chosing the moving group members. We also note the presence of this particular member (HIP 20889) in the HyPl sample of Famaey et al. (2005). We have observed and analysed this star, so as to enable a differential study of Hyades stream with Hyades cluster, and is discussed in the Section 5.3.7. The mean difference ([X/Fe]$_{ours}$ - [X/Fe]$_{Tabernero}$ between the two studies for most of the elements (Na, Ca, Sc, Cr, Co, Ni, Zn) is less than 0.08 dex, which is quite good. However, for a few elements (Fe, Al, Ti) two studies match within ± 0.13 dex which is within the unceratinties (see Table 5.2). However, Tabernero et al. (2012) values of Mg, Si, V and Mn for the three common stars are quite high compared to ours, and the Ba abundance is significantly lower than ours. In their sample there are only 9 K giants and rest of them are mainly dwarfs and a few subgiants. We note that, the Mn enhancement is confined to only K giants of their sample. We attribute these differences to lack of large number of lines and adopting different atomic data rather than having any physical significance.

In Table 5.8, the mean elemental abundances of 31 Hyades stream members derived in this study is compared with the study of Tabernero et al. 2012.

Table 5.7: Comparison study with Tabernero et al. (2012), for 3 common stars. Δ[X/Fe] = [X/Fe]$_{current}$ - [X/Fe]$_{Tabernero}$

Quantity	HIP 20889	HIP 49163	HIP 56756	Mean $\pm\sigma$
Δ[Fe/H]	0.08	0.103	0.138	0.11 ± 0.03
Δ[Na I/Fe]	-0.055	0.02	-0.07	-0.04 ± 0.05
Δ[Mg I/Fe]	-0.125	-0.23	-0.12	-0.16 ± 0.06
Δ[Al I/Fe]	-0.205	-0.07	-0.10	-0.13 ± 0.07
Δ[Si I/Fe]	-0.215	-0.16	-0.18	-0.19 ± 0.03
Δ[Ca I/Fe]	-0.045	0.00	-0.08	-0.04 ± 0.04
Δ[Sc II/Fe]	-0.055	0.08	-0.04	-0.01 ± 0.07
Δ[Ti I/Fe]	-0.15	-0.14	-0.10	-0.13 ± 0.03
Δ[V I/Fe]	-0.125	-0.16	-0.32	-0.20 ± 0.10
Δ[Cr I/Fe]	-0.065	-0.04	-0.01	-0.04 ± 0.03
Δ[Mn I/Fe]	-0.445	-0.28	-0.42	-0.38 ± 0.09
Δ[Co I/Fe]	-0.105	-0.03	-0.01	-0.05 ± 0.05
Δ[Ni I/Fe]	0.005	-0.04	-0.02	-0.02 ± 0.02
Δ[Zn I/Fe]	-0.005	-0.10	-0.12	-0.08 ± 0.06
Δ[Ba II/Fe]	0.375	0.40	0.34	0.37 ± 0.03

Table 5.8: Mean elemental abundances of Hyades stream

Quantity	Current study 31 stars	Tabernero et al. (2012) 61 stars
[Fe/H]	0.16 ± 0.12	0.05 ± 0.14
[Na/Fe]	0.18 ± 0.09	0.05 ± 0.10
[Mg/Fe]	−0.02 ± 0.06	0.01 ± 0.07
[Al/Fe]	0.08 ± 0.05	0.08 ± 0.08
[Si/Fe]	0.06 ± 0.04	0.10 ± 0.05
[Ca/Fe]	0.04 ± 0.05	0.09 ± 0.04
[Sc/Fe]	0.02 ± 0.04	0.05 ± 0.10
[TiI/Fe]	−0.01 ± 0.05	0.13 ± 0.07
[V/Fe]	0.01 ± 0.05	0.25 ± 0.15
[Cr/Fe]	0.02 ± 0.03	0.10 ± 0.03
[Mn/Fe]	−0.06 ± 0.04	0.11 ± 0.11
[Co/Fe]	0.16 ± 0.10	0.08 ± 0.07
[Ni/Fe]	0.04 ± 0.04	0.05 ± 0.03
[Zn/Fe]	0.04 ± 0.08	0.02 ± 0.09
[Ba/Fe]	0.29 ± 0.10	0.09 ± 0.10

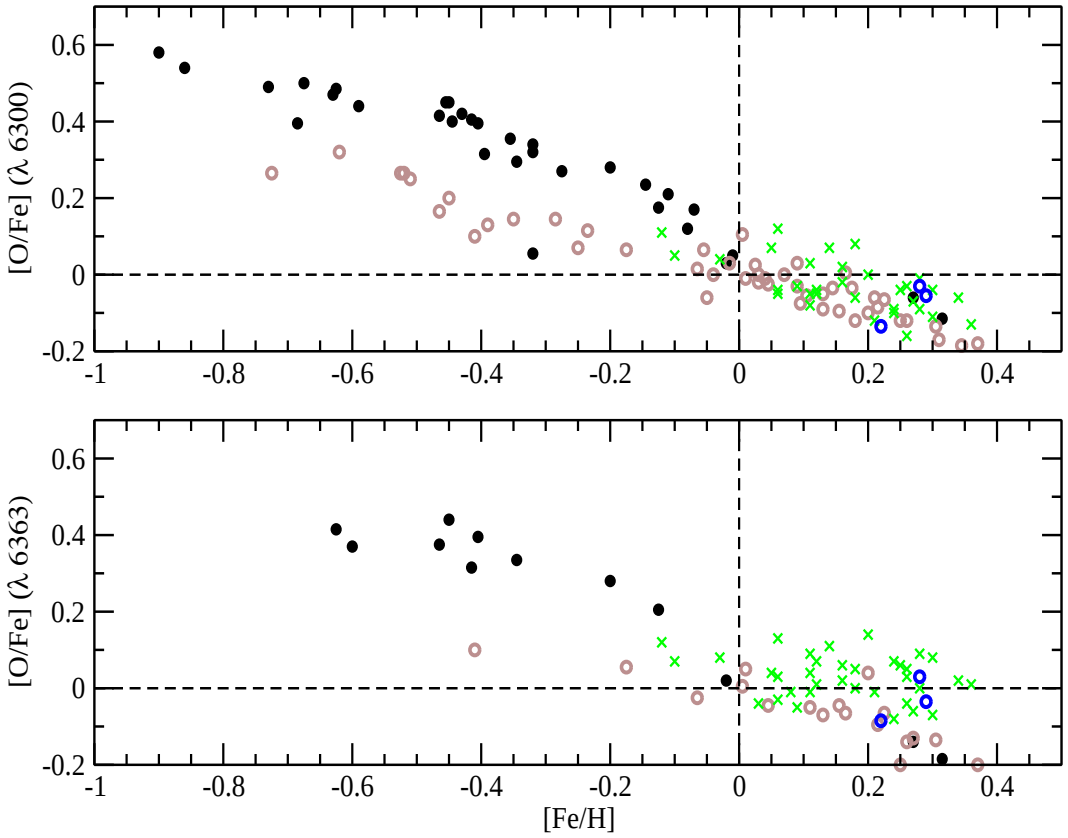

Figure 5.13: Oxygen abundance plot of HyPl stream (green cross). Black and Brown circles represent thick and thin disc stars from Bensby et al. (2005). Blue open circles represent the Hyades open cluster members (ε Tau, γ Tau, δ Tau) derived by us

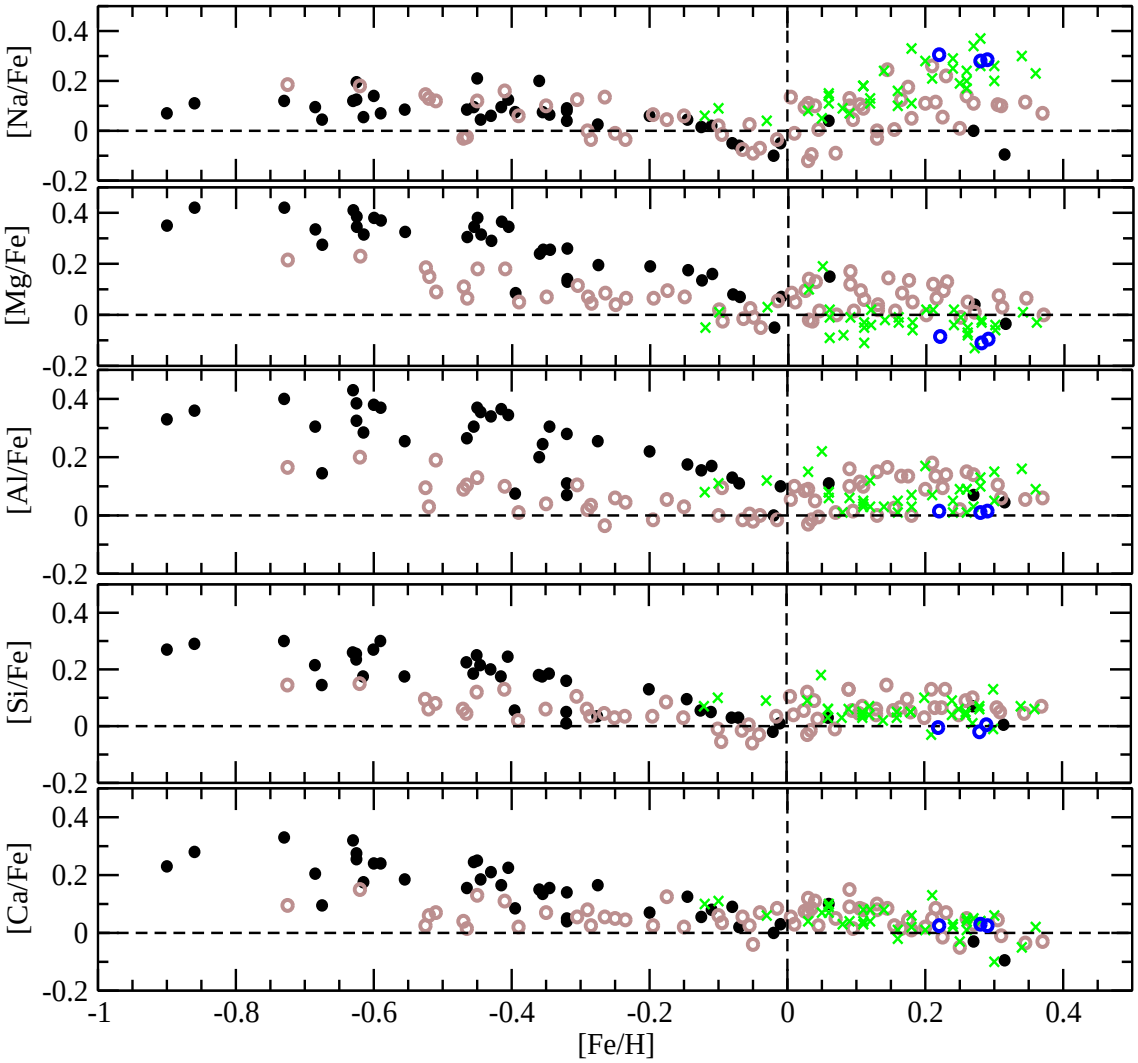

Figure 5.14: Same as the previous plot, but for elements Na, Mg, Al, Si and Ca

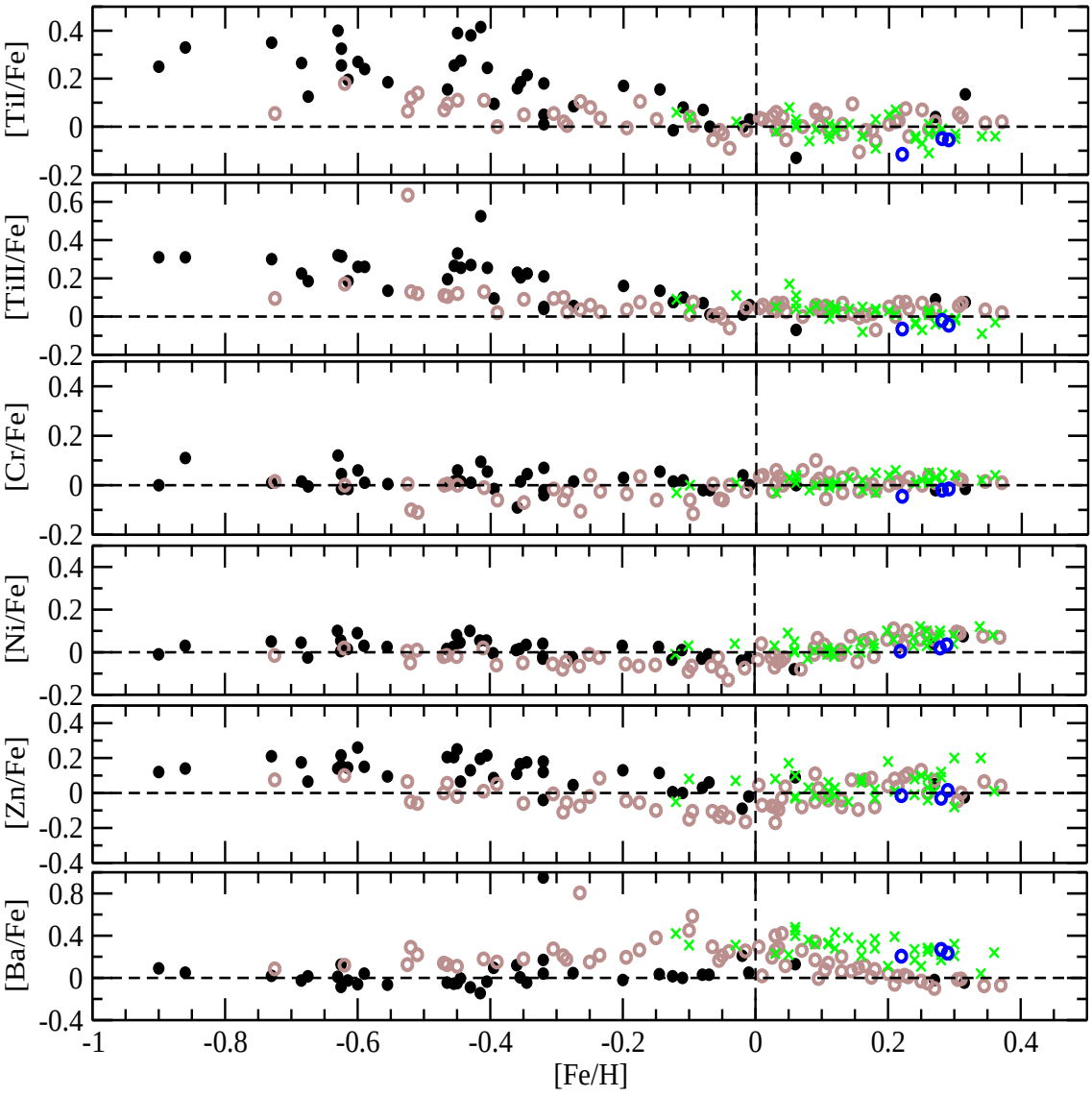

Figure 5.15: Same as the previous plot, but for elements Ti, Cr, Ni, Zn and Ba

5.3.7 Discussion

Does Hyades stream contain dissociated Hyades cluster members ?

To understand Hyades moving group's likely association to the surviving Hyades open cluster, we intent to compare the elemental abundances of stream members derived by us with those of Hyades open cluster. Hyades is a well studied open cluster and the elemental abundances of Hyades cluster members are available in literature (see Carrera & Pancino 2011). But, it wont be a good idea to use the Hyades abundances given in literature for comparisons demanding high level of accuracy, as different studies adopt different lines, atomic data and above all different methods to derive various elemental abundances which may introduce systematic offsets in the values even for common stars, with other studies.

Hence, to make the comparisons more efficient, we observed three members of Hyades open cluster and analysed them in the same way as that of the moving group members, which essentially puts all the measurements on the same scale. Also, we observed three members (HD 73598, HD 73665 and HD 73710) of Praesepe cluster too, which has similar kinematical properties as the Hyades cluster. The three Hyades cluster members being γ Tau (HIP 20205), δ Tau (HIP 20455) and ϵ Tau (HIP 20889). The kinematical motion, ages and the spectroscopically derived atmospheric parameters of cluster members are given in Table 5.9. All the chosen cluster members are giants, to enable a more effective abundance comparison with our sample stars. The elemental abundances of these cluster members, derived in a similar fashion as our stream members, are given in the Table 5.10.

We note that both the clusters exhibit high degree of chemical homogeneity, with star-to-star dispersion in the mean abundances in each cluster less than 0.05 in most of the cases. Also note that both these clusters are chemically homogeneous with each other too. In Table 5.10, the Hyades cluster and Praesepe cluster abundances derived in the current study are compared with the literature value taken from Carrera & Pancino (2011). We can see that, the [Fe/H] value derived by us $\sim$ +0.15 dex higher than Carrera et al value for both the clusters. While most of the elements, such as Al, Si, Sc, V, Cr, Co and Ni derived in both the studies, agree well with each other ($<$ 0.10 dex), Mg abundance in the current study is much lower than that by Carrera et al. While Ca and Na derived by us are more by $\sim$ 0.10 dex, Ba derived by us is less by $\sim$ 0.10 dex, than the literature value given in the table.

Table 5.9: Derived properties of Hyades and Praesepe open cluster members

	Hyades cluster			Praesepe cluster		
star	δ Tau (HIP 20455)	ϵ Tau (HIP 20889)	γ Tau (HIP 20205)	212 (HD 73598)	253 (HD 73665)	283 (HD 73710)
d (pc)	47.7	45.0	50.0	276.2	186.6	218.3
V_r (km s^{-1})	42.85	39.00	38.96	36.24	34.58	35.29
$U_{LSR} \pm \sigma$ (km s^{-1})	-35.6±1.01	-31.6±1.01	-32.8±0.99	-40.3±6.79	-33.2±1.81	-36.1±2.60
$V_{LSR} \pm \sigma$ (km s^{-1})	-14.0±0.85	-13.9±0.67	-15.9±0.71	-20.1±3.60	-13.8±0.98	-16.9±1.41
$W_{LSR} \pm \sigma$ (km s^{-1})	4.8±0.66	5.9±0.53	7.7±0.61	-13.3±11.71	-2.0±2.68	-6.8±4.22
$(T_{eff})_{spec}$ (K)	5030	5050	5120	5120	5120	5020
log g (cm s^{-2})	2.83	2.95	3.10	3.05	3.00	2.83
[M/H]$_{model}$ (dex)	+0.22	+0.30	+0.27	+0.27	+0.32	+0.27
ξ_t (km s^{-1})	1.56	1.58	1.53	1.50	1.58	1.62

It may be true that the current observational results are not compatible with the ideas that the entire moving group may be the result of an evaporated primordial Hyades cluster, but one can't rule out the possibility of mixing of evaporated members of Hyades cluster in the moving group.

As already explained, to test the possibility that whether our Hyades stream sample contains members evaporated from the Hyades cluster or not, we scrutinized and compared elemental abundances of the moving group with the observed members of Hyades open cluster. We can see from Table 5.10, that, the open cluster abundances are highly homogeneous, with very small value of star-to-star scatter of << 0.05 dex, except for Ti II and Mn for Praesepe, which are not used in the discusiion. In addition, O (single lines) and Zn (two line with high line to line scatter) abundancses are are avoided. Interestingly, we find three stream members, namely HIP 34043, HIP 114565 and HIP 80839 having the same elemental abundance pattern as the Hyades cluster agreeing within 0.05 dex (see the Table 5.11). The three stars belong to the group of 'sure Hyades stream members', as per kinematical definitions (see Section 5.3.4). If we relax the rigorous conditions, by not considering Na, and Ba, which have only two lines each, we may accommodate more members to this category. Are three stars, the former members of the Hyades open cluster? Is it just a coincidence, 3 out of 31 stars in the moving group happend to have similar abundances as those open cluster? Apart from abundances, these three stars have very similar ages (530 ± 27 Myr) which is very close to the age of the parent Hyades cluster (~ 600 Myr).

Table 5.10: The abundance ratios of the open cluster members

Star	Hyades cluster					Praesepe cluster				
	δ Tau	ϵ Tau	γ Tau	Mean $\pm\sigma$ Current	Mean $\pm\sigma$ Carrera 2011	212	253	283	Mean $\pm\sigma$ Current	Mean $\pm\sigma$ Carrera 2011
[Fe/H]	0.22	0.29	0.28	0.26 ± 0.04	+0.11	0.28	0.31	0.27	0.29 ± 0.02	+0.16
[O/Fe]	-0.135	-0.055	-0.030	-0.07 ± 0.05	(-0.27)	-0.070	-0.080	-0.095	-0.08 ± 0.01	(-0.11)
(λ 6300 Å)										
[O/Fe]	-0.085	-0.035	0.030	-0.03 ± 0.06	(-0.27)	0.060	0.020	-0.005	0.03 ± 0.03	(-0.11)
(λ 6363 Å)										
[Na/Fe]	0.305	0.285	0.280	0.29 ± 0.01	+0.18	0.290	0.360	0.345	0.33 ± 0.04	+0.25
[Mg/Fe]	-0.085	-0.095	-0.110	-0.10 ± 0.01	+0.10	-0.120	-0.100	-0.115	-0.11 ± 0.01	+0.27
[Al/Fe]	0.015	0.015	0.010	0.01 ± 0.01	+0.00	0.000	-0.010	0.025	0.01 ± 0.02	+0.00
[Si/Fe]	-0.005	0.005	-0.020	-0.01 ± 0.01	+0.09	0.000	0.010	0.015	0.01 ± 0.01	+0.06
[Ca/Fe]	0.025	0.025	0.030	0.03 ± 0.01	-0.07	0.030	0.030	0.015	0.03 ± 0.01	-0.08
[Sc/Fe]	-0.055	-0.025	-0.030	-0.04 ± 0.02	-0.02	-0.030	-0.020	-0.015	-0.02 ± 0.01	-0.04
[Ti I/Fe]	-0.115	-0.055	-0.050	-0.07 ± 0.04	0.09	-0.040	-0.090	-0.075	-0.07 ± 0.03	-0.07
[Ti II/Fe]	-0.065	-0.045	-0.020	-0.04 ± 0.02	...	-0.020	0.000	-0.155	-0.06 ± 0.08	...
[V/Fe]	-0.065	-0.005	0.020	-0.02 ± 0.04	+0.04	0.020	-0.010	-0.015	0.00 ± 0.02	+0.06
[Cr/Fe]	-0.045	-0.015	-0.020	-0.03 ± 0.02	+0.04	0.000	0.000	-0.025	-0.01 ± 0.01	+0.05
[Mn/Fe]	-0.165	-0.145	-0.170	-0.16 ± 0.01	...	-0.120	-0.050	-0.185	-0.12 ± 0.07	...
[Co/Fe]	0.055	0.135	0.090	0.09 ± 0.04	+0.03	0.090	0.080	0.085	0.09 ± 0.01	+0.04
[Ni/Fe]	0.005	0.035	0.020	0.02 ± 0.02	+0.03	0.020	0.030	0.035	0.03 ± 0.01	+0.02
[Zn/Fe]	-0.015	0.015	-0.030	-0.01 ± 0.02	...	0.020	0.000	0.065	0.03 ± 0.03	...
[Ba/Fe]	0.205	0.235	0.270	0.24 ± 0.03	+0.36	0.250	0.250	0.235	0.25 ± 0.01	+0.33
[Ba/Fe]	0.445	0.495	0.520	0.49 ± 0.04	...	0.470	0.440	0.445	0.45 ± 0.02	...
(λ 6496 Å)										

Table 5.11: Abundance similarity of three stream members with Hyades open cluster

Quantity	HIP 34043	HIP 114565	HIP 80839	Mean $\pm\sigma$	Hyades OC (current study)
$(T_{eff})_{spec}$ (K)	4970	5080	5070	5040 ± 60	5066 ± 47
log g (cm s^{-2})	2.80	3.15	3.08	3.01 ± 0.19	2.96 ± 0.14
ξ_t (km s^{-1})	1.65	1.42	1.44	1.50 ± 0.13	1.56 ± 0.03
Age (Myr)	560	518	510	529 ± 27	~ 600
[Fe/H]	0.24	0.30	0.26	0.27 ± 0.03	0.26 ± 0.04
[O/Fe](6300Å)	-0.09	-0.11	...	-0.10 ± 0.01	-0.07 ± 0.05
[O/Fe](6363Å)	-0.08	-0.07	-0.04	-0.06 ± 0.02	-0.03 ± 0.06
[Na/Fe]	0.29	0.20	0.24	0.24 ± 0.05	0.29 ± 0.01
[Mg/Fe]	-0.04	-0.04	-0.07	-0.05 ± 0.02	-0.10 ± 0.01
[Al/Fe]	0.01	0.05	0.01	0.02 ± 0.02	0.01 ± 0.01
[Si/Fe]	0.04	-0.01	0.05	0.03 ± 0.03	-0.01 ± 0.01
[Ca/Fe]	0.03	0.06	0.01	0.03 ± 0.03	0.03 ± 0.01
[Sc/Fe]	-0.04	-0.05	-0.02	-0.04 ± 0.02	-0.04 ± 0.02
[TiI/Fe]	-0.04	-0.05	-0.11	-0.07 ± 0.04	-0.07 ± 0.04
[TiII/Fe]	-0.03	-0.02	0.02	-0.01 ± 0.03	-0.04 ± 0.02
[V/Fe]	-0.04	-0.04	-0.02	-0.03 ± 0.01	-0.02 ± 0.04
[Cr/Fe]	0.01	0.04	0.01	0.02 ± 0.02	-0.03 ± 0.02
[Mn/Fe]	-0.10	-0.11	-0.01	-0.07 ± 0.06	-0.16 ± 0.01
[Co/Fe]	0.07	0.08	0.13	0.09 ± 0.03	0.09 ± 0.04
[Ni/Fe]	0.03	0.04	0.03	0.03 ± 0.01	0.02 ± 0.02
[Zn/Fe]	-0.01	-0.08	0.03	-0.02 ± 0.06	-0.01 ± 0.02
[Ba/Fe]	0.27	0.32	0.28	0.29 ± 0.03	0.24 ± 0.03
[Ba/Fe](6496Å)	0.44	0.41	....	0.43 ± 0.02	0.49 ± 0.04

5.3.8 Origin of the Hyades stream

First scenario to be checked is, whether the Hyades stream members (31 stars) are all remnant of disrupted open cluster or not. If the members of the Hyades moving group are indeed originated from an open cluster, one would expect high level of chemical homogeneity. The metallcity distribution of Hyades stream is shown in Figure 5.16. The distribution ranges from -0.12 dex to +0.36 dex, with a mean of 0.16 ± 0.12 dex. In the Table 5.12, the mean values and star-to-star dispersions of various elements in Hyades stream (31 stars), Hyades cluster (both current study and literature) and Berkeley 32 cluster are given.

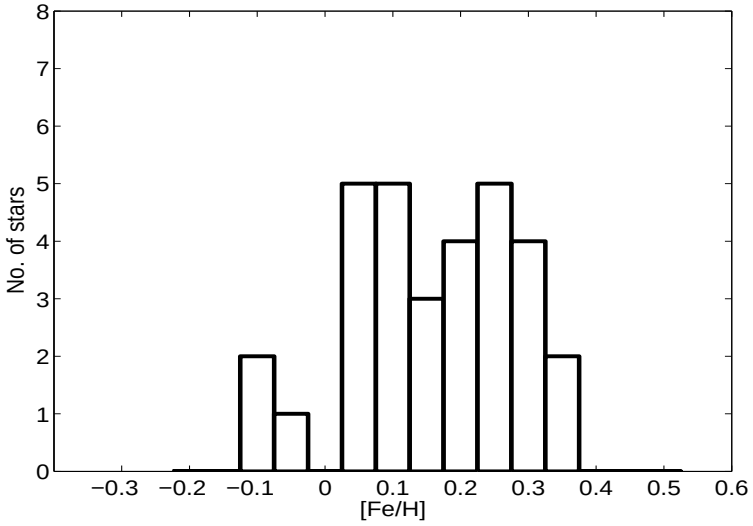

Figure 5.16: The metallicity distribution of 31 Hyades stream members (bin size = 0.05 dex)

It is clear from this table that the mean values ([X/H]) for most of the moving group members significantly differ from the mean values of the open cluster, resulting in large star-to-star scatter in the mean values. Most importantly, star-to-star dispersion (σ) for the moving group is much larger than the expected scatter for any cluster. For example, σs of two clusters (Hyades and Berkeley 32) given in the Table 5.12 are $\sim$ 0.05 for most of the elements. Also, the coevality characteristic of open clusters is not compatible with the results as members of the moving group show large range in ages (355 Myr - 4.8 Gyr). Thus, the abundances and ages suggest that the Hyades moving group can't be entirely due to disperserd members of the primordial Hyades cluster or any other open cluster that is evaporated.

Table 5.12: Mean abundances of Hyades stream are compared with the abundances of two open clusters. For clusters, the mean [Fe/H] =([FeI/H] + [FeII/H])/2, [X/H] = [X/Fe] + [Fe/H]

Entity	Hyades stream (31 stars)	Hyades cluster (3 stars) current study	Berkeley 32 Carrera 2011	Hyades Carrera 2011
[Fe/H]	0.16 ± 0.12	0.26 ± 0.04	-0.30 ± 0.02	0.11 ± 0.01
[O/H] (λ 6300 Å)	0.14 ± 0.09	0.19 ± 0.09	(-0.30 ± 0.24)	(-0.16 ± 0.06)
[O/H] (λ 6363 Å)	0.19 ± 0.12	0.24 ± 0.09	(-0.30 ± 0.24)	(-0.16 ± 0.06)
[Na/H]	0.33 ± 0.20	0.56 ± 0.03	-0.41 ± 0.07	0.30 ± 0.02
[Mg/H]	0.14 ± 0.12	0.17 ± 0.03	0.01 ± 0.07	0.25 ± 0.07
[Al/H]	0.24 ± 0.13	0.28 ± 0.04	-0.18 ± 0.02	0.12 ± 0.01
[Si/H]	0.21 ± 0.12	0.26 ± 0.04	-0.15 ± 0.02	0.21 ± 0.01
[Ca/H]	0.20 ± 0.10	0.29 ± 0.04	-0.35 ± 0.03	0.05 ± 0.01
[Sc/H]	0.18 ± 0.12	0.23 ± 0.05	-0.30 ± 0.01	0.09 ± 0.02
[TiI/H]	0.15 ± 0.11	0.19 ± 0.07	-0.37 ± 0.07	0.02 ± 0.02
[TiII/H]	0.18 ± 0.10	0.22 ± 0.06	-0.38 ± 0.15	0.10 ± 0.02
[V/H]	0.18 ± 0.13	0.25 ± 0.08	-0.40 ± 0.07	0.15 ± 0.04
[Cr/H]	0.17 ± 0.14	0.24 ± 0.05	-0.40 ± 0.23	0.16 ± 0.02
[Mn/H]	0.10 ± 0.14	0.11 ± 0.05	...	
[Co/H]	0.32 ± 0.19	0.36 ± 0.08	-0.24 ± 0.07	0.14 ± 0.02
[Ni/H]	0.20 ± 0.15	0.29 ± 0.05	-0.32 ± 0.05	0.14 ± 0.01
[Zn/H]	0.20 ± 0.16	0.26 ± 0.05	...	...
[Ba/H]	0.45 ± 0.11	0.50 ± 0.06	0.14 ± 0.10	0.47 ± 0.05
[Ba/H](λ 6496 Å)	0.58 ± 0.12	0.75 ± 0.07	(0.14 ± 0.10)	(0.47 ± 0.05)

Hyades moving group may not be solely originated from disrupted Hyades cluster or any other open cluster, but a fraction of stars possibly originated from the Hyades cluster. We could find three stars out of 31 Hyades group members (which is 10 % of the sample), exhibiting chemical homegeneity and having similar ages as Hyades open cluster. From this result, one may argue that part of Hyades stream is originated from the Hyades cluster.

One argument to be dicussed in this context is that the overdensities in the velocity space can have contamination from the field star - the stars happend to be there with the particular kinematics. Hence, we can expect the contribution from field stars in any sample of stream candidates selected randomly based on kinematics. Famaey et al. (2007) had shown that 75 % of stars in the Hyades velocity box can be Hyades stream members. Our sample consists of 31 stars, 75 % of the sample is 23 stars, considering the sample to be random. If Hyades stream solely originated from Hyades cluster, atleast 23 stars in our sample should have shown the chemical and age coherence with Hyades cluster to support the cluster origin of Hyades stream. But the results obtained here do not support this and in fact favour the argument that Hyades stream is not from Hyades cluster alone. In their study, Pompéia et al. (2011), Tabernero et al. (2012) and de Silva et al. (2011) also reached at a conclusion similar to this. Pompéia et al. (2011) found 2 out of 21 Hyades stream members (ie., ~ 10 % of the sample), having abundances compatible with an origin in the cluster, similar to our study, while Tabernero et al. (2012) found 46 % of their total sample as disrupted Hyades cluster member. de Silva et al. (2011) found 4 out of 26 stars (~ 15 %) with Hyades open cluster metallicity and similar abundance patterns.

If cluster disruption is not solely responsble for the formation of Hyades stream, how to explain its formation ? The metallicity and age distribution of the Hyades stream members (31 stars) unambiguosly suggest that the member stars of the moving group are drawn from the background thin disc. In fact, kinematic probabilities with which the member stars belong to the Galactic thin disc (P_{thin}) is 99 % for all the member stars. Now the question is how spatially disconnected stars could share the same kinematics. The answer seems to lie in the dynamics of the disc.

The dynamical perturbations make the stars, born in different epochs and in different locations within the disc, appear as a group with shared kinematic motion. This could happen when the bar or the spirals interact resonantly with local stellar orbits. Also, from the metallicity distribution (see Figure 5.16) we can see that Hyades stream is dominated by super solar metallicity members, or in other words the mean metallicity of the Hyades stream is more than that of the solar neighborhood thin disc stars which is slightly subsolar

(see Table 5.4). This favours the argument that Hyades has a origin from the inner Galactic radii, where interstellar medium is more metal rich than at the solar Galactocentric radius. Famaey et al. (2007) proposed a resonant origin for Hyades stream by comparing the mass distribution and metallicity of the stream to those of field disc stars. While the mass distribution was similar to the Present-day-mass- distribution of the field, rather than like that of cluster, the metallcity distribution favoured origin from inner Galactic radii. Famaey et al. (2008) also reached at similar conclusion by independently performing the isochrone analysis in the parallax space for Hyades stream members. They found that, the fraction of stars making up the velocity-space overdensity superimposed on the background is higher than the fraction of stars compatible with the isochrone of the associated cluster, favouring a dynamical origin for Hyades group.

What are the sources of dynamical perturbation, if they are the ones responsible for the formation of Hyades stream ? Pompéia et al. (2011) interpreted Hyades stream as an inner 4:1 resonance of the spiral pattern, and placed the origin of the Hyades stream up to 1 kpc inwards from the solar radius, which might explain the observed metallicity excess of the stream population. Similarly Quillen & Minchev (2005) found that a two-armed spiral density wave with pattern speed placing the Sun near the 4:1 inner Lindblad resonance can explain the formation of Hyades/Pleiades streams in the solar neighborhood. While Minchev & Famaey (2010) has favoured the idea that Hyades stream can be due to spiral arms, and can not be explained as due to the Galactic bar.

Thus, we conclude that Hyades moving group is most probably a mixure of stars from the parent cluster and from the background thin disc.

5.4 Sirius stream

5.4.1 Introduction

Sirius stream is a low velocity stream which leads the LSR by a small velocity of about ~ 10-15 km s^{-1}. It revolves the Galactic center in a highly circular orbit. In the literature it is also known as Ursa Major moving group or Sirius supercluster (Eggen 1994) or Ursa Major association (Fuhrmann 2004) as the stream shares kinematics of Ursa Major star cluster. The Ursa Major star cluster has kinematic motion (U, V, W) : U = +14.5 ± 0.8 , V = 2.5 ± 0.6 , W = -8.5 ± 0.9 (Gomez et al. 1990), which is similar to that of the Sirius stream or Ursa Major moving group (see Table 5.13).

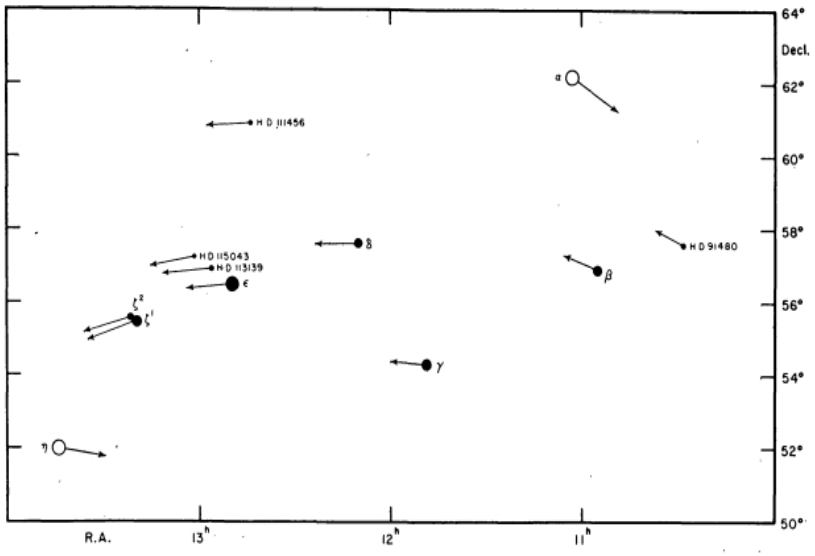

FIG. 1—The Stars of the Ursa Major Cluster. The arrows represent the apparent motion in 50,000 years. Note the prominent stars, α and η, whose motions show that they are not members of the cluster.

Figure 5.17: The stars in the Ursa Major star cluster (Petrie 1953)

Ursa Major (UMa) open cluster is located in the Big Dipper, which is part of UMa constellation at a distance of 25 pc from the Sun. It was proposed to be the remains of an almost evaporated, initially much richer open star cluster (Wielen 1978). The five stars - β, γ, δ, ϵ and ζ of the UMa constellation (see Figure 5.17) were noted to have approximately equal proper motion converging to one common point in the sky (towards the solar apex, α = 307.5 degree, δ = -39.3 degree) (Smart 1939). In 1909, Hertzsprung demonstrated that many widely separated bright stars including Sirius (α Canis Majoris − the brightest star

in the night sky) shared the motion of the five co-moving Big Dipper stars (Hertzsprung 1909). With this, UMa cluster came to be known also as Sirius supercluster. Many studies were undertaken to search for dispersed members of the UMa cluster to understand the evaporation process of open clusters (Eggen 1958a, Eggen 1960).

Table 5.13: Kinematic definitions of Sirius stream in literature. UVW components are heliocentric, except for Klement et al. (2008) which are with respect to Local Standard of Rest

U (σ_U) km s^{-1}	V (σ_V) km s^{-1}	W (σ_W) km s^{-1}	Reference
15	1	-11	Eggen (1992b)
13.0 (8.4)	3.2 (6.5)	-7.5 (6.5)	Chen et al. (1997) (U, V, W, Age) space
10.8 (7.9)	2.3 (5.9)	-8.1 (6.4)	Chen et al. (1997) (U, V, W) space
10 (6)	3 (6)	-11 (10)	Zhao et al. (2009) (dwarf sample)
10 (6)	3 (6)	-14 (13)	Zhao et al. (2009) (giant sample)
15	1	-11	Eggen (1992b)
9	3	...	Dehnen (1998)
10	-5	...	Famaey et al. (2007)
6.53 (14.37)	3.96 (4.63)	-5.8 (9.66)	Famaey et al. (2005)
9	3		Fux (2001)
9	4		Bovy et al. (2009)
14.9	1	-10.7	Montes et al. (2001)
14.9	1.3	-11.2	Figueras et al. (1997)
6	4		Klement et al. (2008) $U - V$ space
	4		Klement et al. (2008) V - $\sqrt{U^2 + 2V^2}$ space

In the pre HIPPARCOS era, UMa was considered to have composed of two subgroups - a moderately compact cluster of stars sharing accurately the same space motion, and an extended stream of stars possessing approximately the same space motion (Roman 1949, Soderblom & Mayor 1993). The five central stars in the Big Dipper and a few more fainter stars in the same region moving with equal velocities within the errors of observation were found in a volume of space less than 10 pc across. On the other hand, stars of the extended UMa group seemed to fill a volume of space which was limited only by the effects of observational selection (Roman 1949). With an estimated small age of $\sim$ 300 Myr (Levato & Abt 1978), which is of the order of the dissolution age of classical open clusters in the Galactic disc, UMa cluster is an interesting group to understand cluster disruption process. However, many of the earlier studies were handicapped by lack of accurate astrometry. As a result, membership of many stars to UMa group remained somewhat controversial. This stems from the fact that many authors priori assumed that the members of the UMa moving group or Sirius moving group should have similar properties as that of UMa star cluster. With the launch of HIPPARCOS and its accurate astrometry (Perryman et al. 1997), many studies independently confirmed the existence of Sirius moving group in the solar neighborhood (see Table 5.13).

5.4.2 Sample and Observations

Selected sample stars and observations log are given in Table 2.5. Sample stars are chosen from the catalogue of Famaey et al. (2005), who independently detected a number of streams and Sirius stream is one of them. For further details of detecting the moving group and the sample stars, reader is referred to Chapter 2 and Section 2.2.2. Each star in the catalogue is assigned propbabilities to belong to various streams. We chose 33 stars that are most likely candidates of Sirius stream with probabilities, $P \geq 60\%$. While selecting, we also applied colour criteria of $V - I \leqslant 1.28$ to ensure not to have very cool stars in the sample. Sample consists of giants of both K and M spectral types. High resolution (R$\sim$ 60,000) spectra have been obtained using 2.7 m Harlan J. Smith telescope and the 2.3 m Vainu Bappu Telescope.

5.4.3 Kinematics and age

Stellar space velocity components (U_{LSR}, V_{LSR}, W_{LSR}) are re-calculated using the updated HIPPARCOS astrometry (van Leeuwen 2007) and the radial velocities determined from high resolution spectra obtained in this study. Calculated velocity components are tabu-

lated in the Appendix A.7. The mean kinematic motion as determined from the 33 sample stars of the Sirius stream is U_{LSR} = 17.9 ± 5.8, V_{LSR} = 10.3 ± 3.8, W_{LSR} = 3.7 ± 4.5 km s^{-1}. This is in good agreement with the velocities given in the catalogue. Another parameter is the ages. Ages of the samples stars are derived using the $(B - V)$ - M_v plane and by fitting the Y^2 isochrones taken from Demarque et al. (2004). The derived ages are given in Appendix A.7. In Figure 5.18 (bottom), we showed 33 Sirius stream stars in the $(B - V)$ - M_v plane which are superposed by three isochrones of age 100 Myr, 1 Gyr and 4 Gyr. The three isochrones are generated for a mean [Fe/H] = +0.12 dex, [α/Fe] = 0.0. Note that [Fe/H] = +0.12 dex is the mean metallcity of the stream stars. The age distribution of the sample stars is shown in Figure 5.18 (top). Ages of the Sirius stream members range from 190 Myr to 3.28 Gyr with a mean age of 0.90 ± 0.758 Gyr. These values are in agreement with the literature values which are in the range of 200 - 600 Myrs (König et al. 2002, King & Schuler 2005). Distances of the Sirius stream members suggest that they are all in the solar neighborhood within a distance of < 500 pc. HIP 53710 is an exception with high error in parallax (σ_π/π = 133.3 %, see Appendix A.8), leading to large distance yielding erroneous values for other parameters.

The orbital parameters, such as the minimum and maximum Galactocentric distances (R_{min} and R_{max}), eccentricity (e), the maximum perpendicular distance of the stars (Z_{max}) are calculated as explained in the previous sections and are tabulated in the Appendix A.8, along with the angular momentum components per unit mass expressed as J_z and $J \perp$ and the relative percentage error in the opted parallax (π) values. Stream members show a mean J_z of -1972.5 ± 53 kpc km s^{-1}. The mean kinematical parameters of the sample are compared with those of the Galactic thin and thick disc stars (Figure 5.19). Kinematic results as shown in Figure 5.19 suggest that the stream members belong to the thin disc and they are indistinguishable from the kinematic properties of the Galactic thin disc.

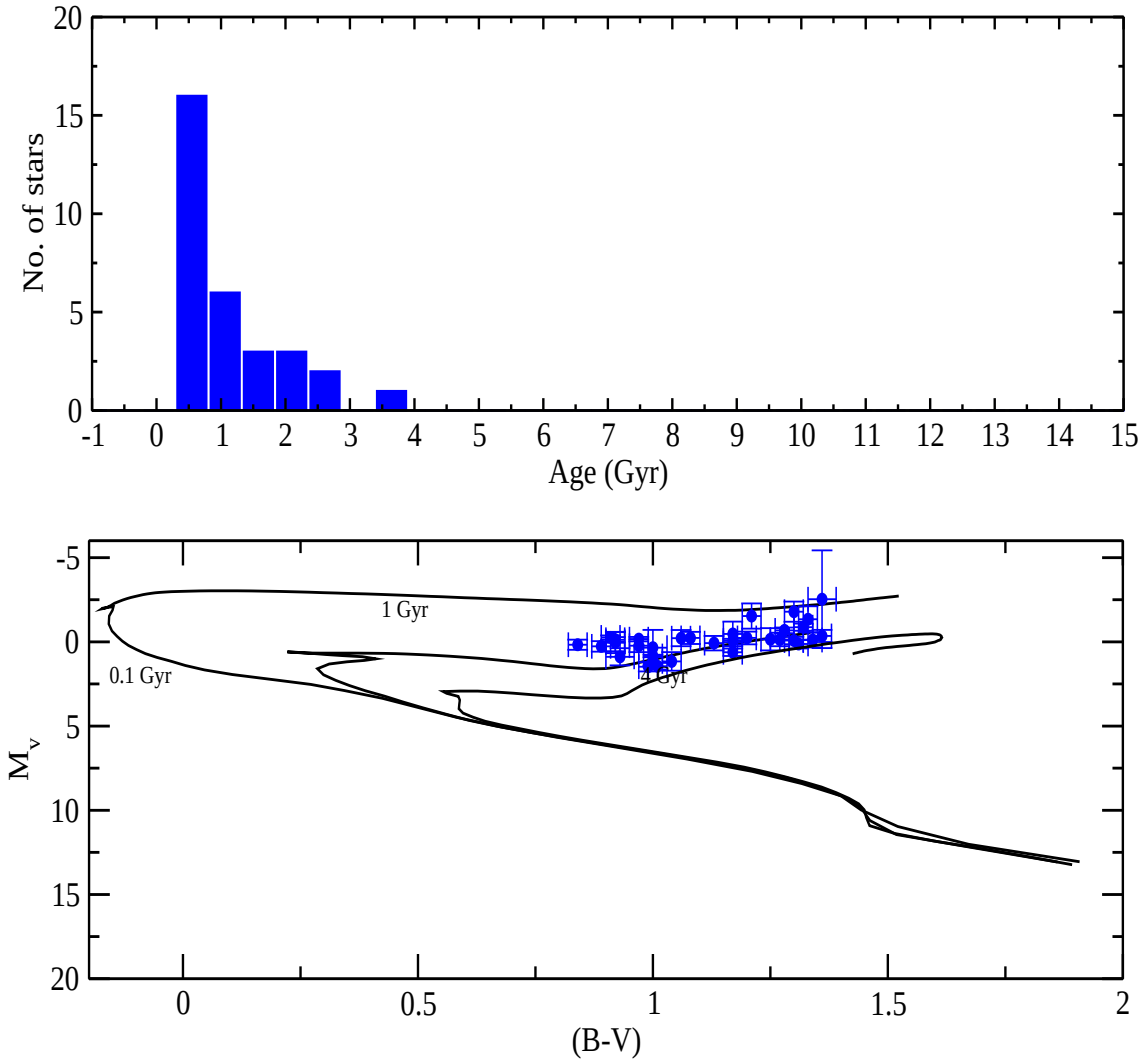

Figure 5.18: The age distribution (top) of Sirius stream with a bin size = 0.5 Gyr, and the $(B-V)$-M_v plane (bottom) of the Sirius stream members

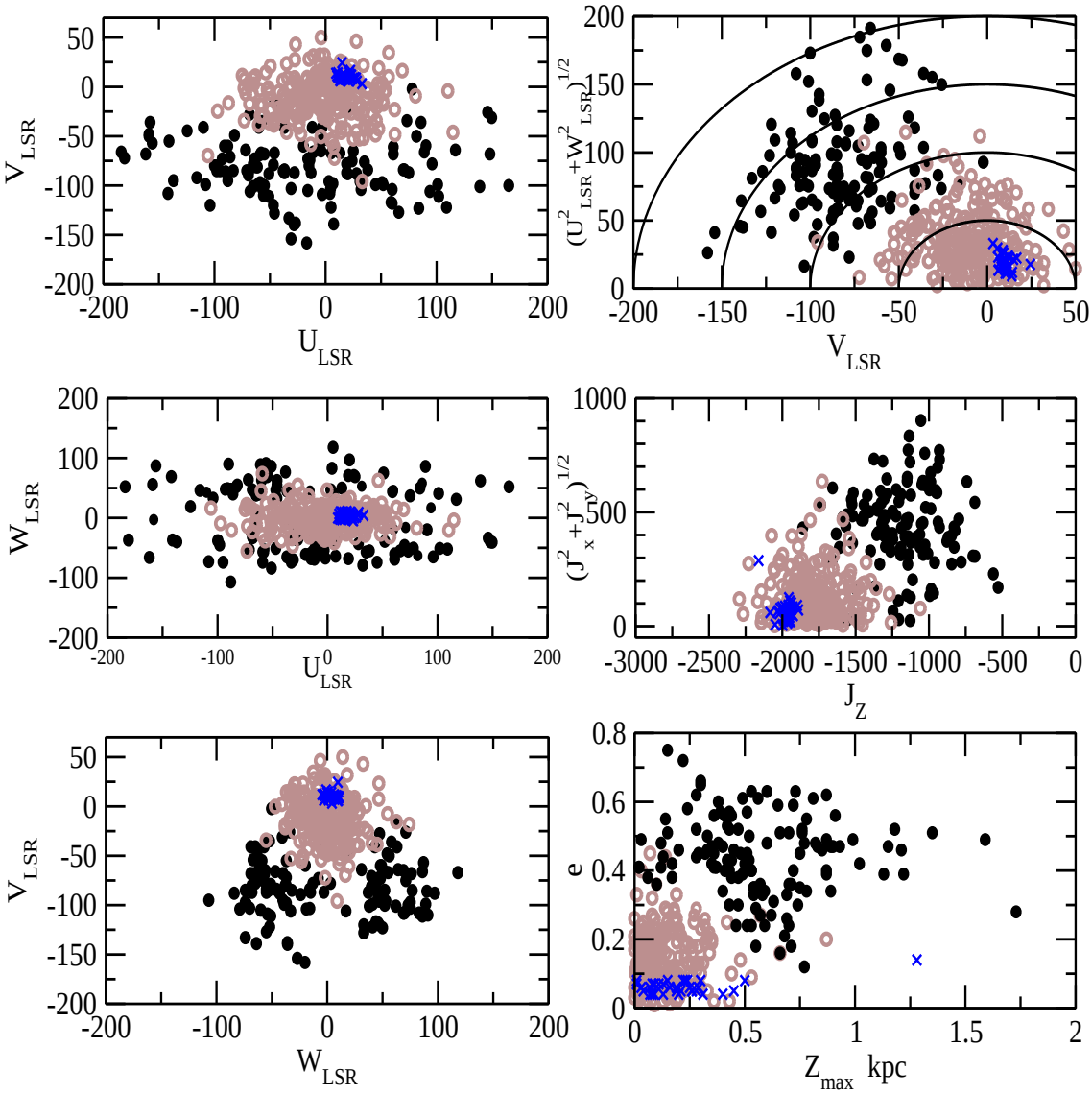

Figure 5.19: The kinematical properties of Sirius stream (blue cross) is compared with those of thin disc (brown circle) and thick disc (black circle) stars taken from Bensby et al. (2005)

5.4.4 Atmospheric parameters and elemental abundances

The atmospheric parameters of the sample stars derived using photometry and spetroscopy are given in Appendix B.5. The photometric $(T_{eff})_{V-K}$ is in good agreement with the values derived from spectroscopy, $(T_{eff})_{spec}$. As noted earlier, values of $(T_{eff})_{J-K}$ are in general cooler than the other two values which we attributed to larger uncertainty in the J magnitude. Values of log g are also derived using both spectroscopy and photometry. Values from the photometry are significantly smaller compared to the values from spectroscopy ((log $g)_{phot}$ - (log $g)_{spec}$ = -0.24 ± 0.14). Comparison of values is shown in Figure 5.1 (blue symbol).

The derived abundances of 16 elements are given in Appendix B.16-B.18. Results are given as ratios, [X/Fe]. Abundance results show that stream stars are of solar metallicity ranging from −0.12 dex to +0.28 dex. Most of the sample stars (28 out of 33) are in fact super-solar, and 5 of them are of sub-solar metallicity. Abundance results of Sirius stream stars are compared with the background field stars of thin and thick discs. These are shown in Figures 5.20-5.22 as [X/Fe] versus [Fe/H]. In general, Sirius abundances follow the Galactic thin disc abundance trends. However, for many elements (Al, Mg, Ca, Ti I, Ti II, Cr and Ni) Sirius abundances are lower than the Galactic trend. At the same time results show that Ba abundances of Sirius stream are quite enhanced compared to the field stars. It is not clear whether the subtle differences are due to difference in the analysis of field stars and the stream stars. Otherwise there is no reason for young metal rich stars such as Sirius stream members having lower abundances compared to the Galactic chemical evolution trends.

To quantify the differences, we divided the sample into two groups: stars with [Fe/H] < +0.1 and stars with [Fe/H] > +0.1 dex and computed mean [X/Fe] values for each of the elements. In Table 5.14 the mean [X/Fe] values are compared with thin disc mean values in the same metallicity ranges. In the sub solar regime mean [X/Fe] values of the stream and the thin disc stars agree very well. Only in the super solar regime, we found slight underabundances (0.02 - 0.1 dex) compared to the background stars.

For 22 stars we obtained results using 2.7-m Harlan J. Smith telescope and for 11 stars we used 2.3-m VBT spectra. In Table 5.15 we compared abundance values derived from the spectra obtained from VBT and Harlan J. Smith Telescope, for three common stars. Both the results are in good agreement within the estimated uncertainties.

Table 5.14: Mean abundances and dispersions of various elements of Sirius stream are compared with those of thin disc

Species	Sirius stream		Thin disc	
	[Fe/H] < 0.10 mean $\pm\sigma$	[Fe/H] > 0.10 mean $\pm\sigma$	[Fe/H] < 0.10 mean $\pm\sigma$	[Fe/H] > 0.10 mean $\pm\sigma$
[Al/Fe]	0.04 ± 0.06	0.03 ± 0.06	0.04 ± 0.06	0.10 ± 0.06
[Ba/Fe]	0.41 ± 0.14	0.39 ± 0.08	0.26 ± 0.14	0.04 ± 0.08
[Ca/Fe]	0.03 ± 0.06	-0.03 ± 0.06	0.06 ± 0.04	0.05 ± 0.04
[Na/Fe]	0.11 ± 0.08	0.12 ± 0.08	0.01 ± 0.08	0.11 ± 0.09
[Mg/Fe]	0.00 ± 0.07	-0.02 ± 0.05	0.04 ± 0.06	0.07 ± 0.05
[Si/Fe]	0.06 ± 0.05	0.05 ± 0.05	0.03 ± 0.06	0.08 ± 0.03
[TiI/Fe]	-0.01 ± 0.05	-0.08 ± 0.04	0.01 ± 0.04	0.01 ± 0.05
[TiII/Fe]	0.02 ± 0.03	-0.03 ± 0.04	0.03 ± 0.03	0.03 ± 0.04
[Cr/Fe]	-0.00 ± 0.03	-0.02 ± 0.03	0.00 ± 0.05	0.01 ± 0.03
[Ni/Fe]	-0.03 ± 0.04	-0.03 ± 0.05	-0.04 ± 0.05	0.04 ± 0.04
[Zn/Fe]	-0.00 ± 0.08	0.00 ± 0.10	-0.07 ± 0.08	0.03 ± 0.07

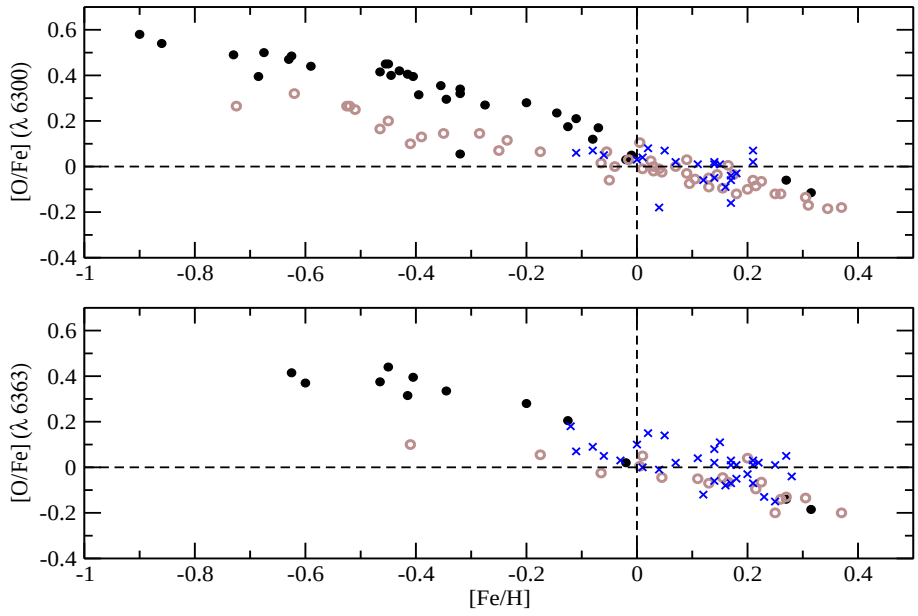

Figure 5.20: The abundance plots for Sirius stream (blue cross) for oxygen from the lines λ 6300 Å and λ 6363 Å. Black and Brown circles represent thick and thin disc stars from Bensby et al. (2005)

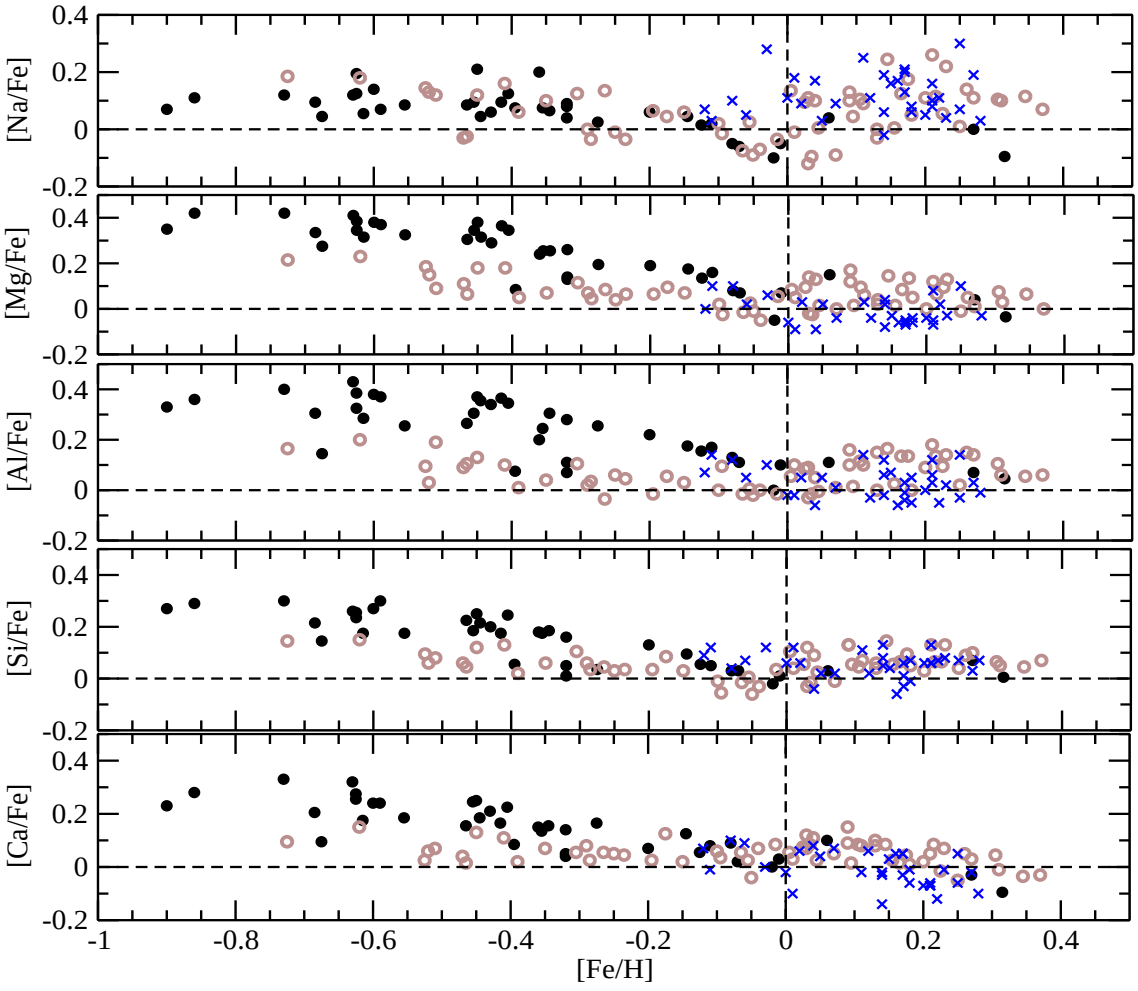

Figure 5.21: Same as the previous plot, but for the elements Na, Mg, Al, Si and Ca

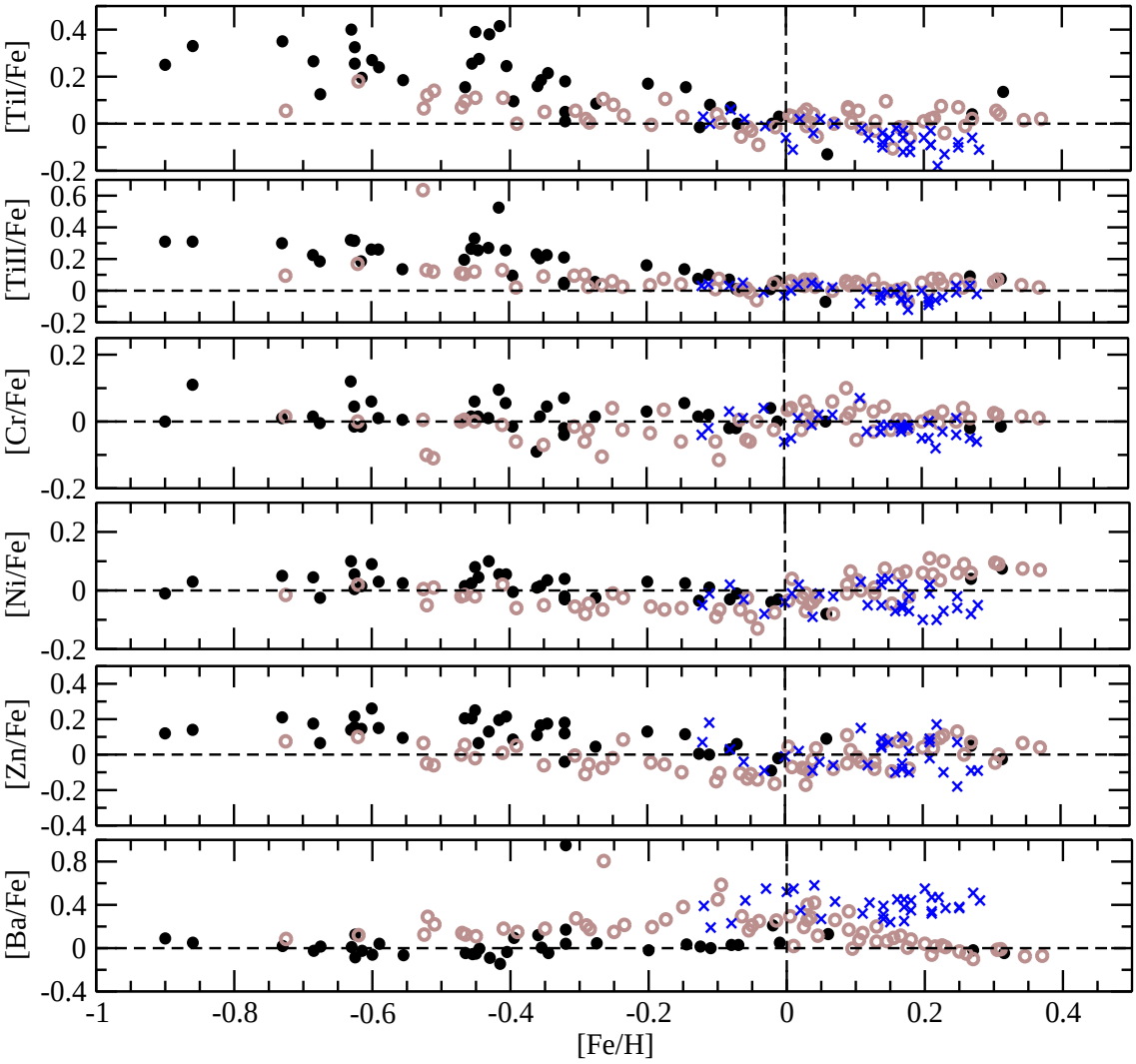

Figure 5.22: Same as the previous plot, but for the elements Ti, Cr, Ni, Zn and Ba

Table 5.15: Comparison between McD and VBT observations for common stars

Quantity	HIP 67364				HIP 47719				HIP 52926				(McD-VBT)±σ
	McD			VBT			McD			VBT			
T_{eff}	4630			4700			4620			4660			-40± 30
log g	2.60			2.73			2.55			2.63			-0.06±0.08
ξ_t	1.45			1.47			1.49			1.41			0.04±0.05
[M/H]	+0.16			+0.26			+0.21			+0.22			-0.06±0.05
	logε	σ	N	logε	σ	N	logε	σ	N	logε	σ	N	(Δ logε)±σ
Na I	6.59	0.01	2	6.61	0.04	2	6.53	0.01	2	6.56	0.02	2	-0.01±0.03
Mg I	7.71	0.06	4	7.74	0.08	2	7.72	0.05	4	7.70	0.13	2	-0.03±0.05
Al I	6.58	0.02	4	6.61	0.03	2	6.52	0.06	4	6.59	0.08	2	-0.05±0.02
Si I	7.76	0.07	5	7.82	0.02	3	7.71	0.05	5	7.79	0.05	3	-0.08±0.03
Ca I	6.41	0.07	8	6.48	0.08	8	6.40	0.06	8	6.44	0.08	6	-0.04±0.04
Sc II	3.38	0.05	6	3.46	0.05	2	3.37	0.04	6	3.47	0.03	3	-0.07±0.03
TiI	4.98	0.06	6	5.04	0.05	3	5.03	0.07	8	5.13	0.11	4	-0.04±0.07
TiII	5.12	0.05	4	5.25	0.09	2	5.14	0.06	4	5.22	0.08	4	-0.06±0.08
V I	3.97	0.04	5	4.06	0.06	4	4.00	0.05	5	4.09	0.06	4	-0.07±0.04
Cr I	5.79	0.05	6	5.88	0.07	6	5.80	0.05	5	5.83	0.06	6	-0.05±0.03
Mn I	5.52	0.03	3	5.61	0.06	3	5.52	0.03	3	5.61	0.02	3	-0.07±0.03
FeI	7.60	0.07	57	7.71	0.09	42	7.63	0.06	56	7.66	0.07	42	-0.06±0.04
FeII	7.62	0.05	9	7.70	0.05	5	7.62	0.05	8	7.65	0.09	7	-0.06±0.03
Co I	5.26	0.03	4	5.41	0.05	2	5.20	0.05	4	5.34	0.01	2	-0.12±0.05
Ni I	6.42	0.06	11	6.47	0.07	4	6.40	0.07	11	6.37	0.08	5	0.01 ±0.05
Zn I	4.76	0.21	2	4.80	0.22	2	4.69	0.21	2	4.67	0.19	2	-0.01±0.03
Ba II	2.61	0.01	2	2.67	0.05	2	2.72	0.02	2	2.75	0.02	2	-0.04±0.02
Ba II (λ 6496.91 Å)	2.73	...	1	2.90	...	1	2.84	...	1	3.12	...	1	-0.14±0.15
[O I] (λ 6300.31 Å)	9.09	...	1	...			9.14	...	1	...			...
[O I] (λ 6363.78 Å)	9.19	...	1	9.21	...	1	9.18	...	1	9.21	...	1	-0.03 ± 0.01

5.4.5 Discussion

Age and abundance results suggest that the Sirius moving group may not have been formed from the dispersed cluster. Large range in metallicity (0.4 dex) and ages (4 Gyr) imply chemical inhomogeneity and noncoeval nature of the member stars. In Table 5.16, mean abundances and star-to-star scatter of Sirius stream are compared with a few representative open cluster results. Stream members exhibit significant scatter in abundances compared to their counter parts in the open cluster. Results suggest that the cluster disruption may not be the sole cause for the Sirius stream.

Table 5.16: Mean abundances of Sirius stream are compared with the abundances of two open clusters. For clusters, the mean [Fe/H] =([FeI/H] + [FeII/H])/2, [X/H] = [X/Fe] + [Fe/H]

Entity	Sirius (33 stars)	Berkeley 32 (2 stars)	Hyades (3 stars)
[Fe/H]	0.12 ± 0.11	-0.30 ± 0.02	0.11 ± 0.01
[O/H] (λ6300 Å)	0.09 ± 0.09	(-0.30 ± 0.24)	(-0.16 ± 0.06)
[O/H] (λ6363 Å)	0.13 ± 0.09	(-0.30 ± 0.24)	(-0.16 ± 0.06)
[Na/H]	0.24 ± 0.14	-0.41 ± 0.07	0.30 ± 0.02
[Mg/H]	0.10 ± 0.11	0.01 ± 0.07	0.25 ± 0.07
[Al/H]	0.15 ± 0.11	-0.18 ± 0.02	0.12 ± 0.01
[Si/H]	0.17 ± 0.11	-0.15 ± 0.02	0.21 ± 0.01
[Ca/H]	0.12 ± 0.10	-0.35 ± 0.03	0.05 ± 0.01
[Sc/H]	0.13 ± 0.12	-0.30 ± 0.01	0.09 ± 0.02
[TiI/H]	0.07 ± 0.09	-0.37 ± 0.07	0.02 ± 0.02
[TiII/H]	0.11 ± 0.10	-0.38 ± 0.15	0.10 ± 0.02
[V/H]	0.10 ± 0.11	-0.40 ± 0.07	0.15 ± 0.04
[Cr/H]	0.11 ± 0.11	-0.40 ± 0.23	0.16 ± 0.02
[Mn/H]	0.02 ± 0.13	...	
[Co/H]	0.26 ± 0.15	-0.24 ± 0.07	0.14 ± 0.02
[Ni/H]	0.09 ± 0.12	-0.32 ± 0.05	0.14 ± 0.01
[Zn/H]	0.12 ± 0.13	...	...
[Ba/H]	0.51 ± 0.16	0.14 ± 0.10	0.47 ± 0.05
[Ba/H](λ 6496 Å)	0.63 ± 0.17	(0.14 ± 0.10)	(0.47 ± 0.05)

In the literature it is widely suggested that Sirius stream members might have come from the UMa cluster. There are a number of stars in the stream, whose metallicity and ages are quite compatible with the stars of UMa cluster. The mean metallicity of UMa cluster is close to solar value : +0.06 ± 0.11 dex (Paulson & Yelda 2006) and 0.01 ± 0.01 dex (Biazzo et al. 2012). These values are within the range of Sirius stream metallicity, [Fe/H] = -0.12 dex to +0.28 dex with a mean metallicity of +0.12 ± 0.11 dex. The metallicity distribution is given in the Figure 5.23. Also, the age distribution of Sirius stream peaks at about 400 Myr which is close to the accepted value (300 Myr) of UMa cluster. Distribution also shows there are 21 young stars with ages less than 1 Gyr and and 10 stars with ages higher than 1 Gyr. Clumping of few stars at the metallicity and age of the UMa cluster (see Figure 5.24) may suggest that the Sirius stream possibly contains the dispersed members of the UMa super cluster.

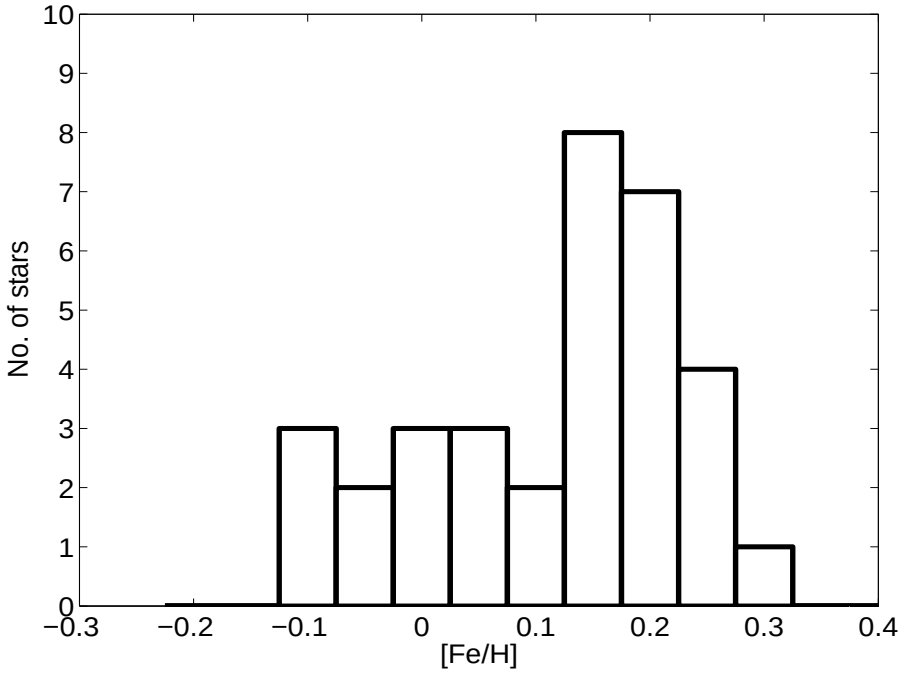

Figure 5.23: The metallicity distribution of Sirius stream members (bin size = 0.05 dex)

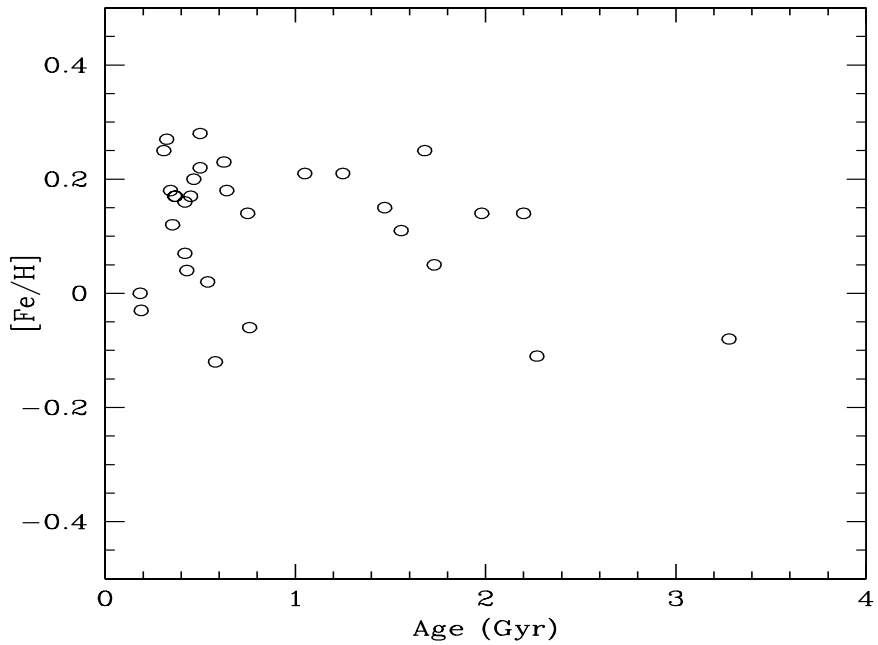

Figure 5.24: The age-metallicity plot for the members of Sirius stream

However, Sirius stream stars have a wide range in ages and metallcities. Different ages and metallicities indicate that the stars formed at different epochs at the same place or at different Galactocentric radii moved to the same orbit due to dynamical perturbations. Famaey et al. (2005) found the metallicity of 12 Sirius stream giants is very similar to the bulk of giants in the solar neighborhood. Also, they found large spread in the ages of their Sirius stream members. From which they inferred that the Sirius moving group could be a feature recently formed by the passage of a transient spiral. In their later study Famaey et al. (2008) found that the fraction of stars making up this velocity-space overdensity superimposed on the background is higher than the fraction of stars compatible with the isochrone of the embedded cluster. This supports dynamical nature of Sirius moving group. Studies such as Sellwood & Binney (2002) and Quillen & Minchev (2005) linked the origin of Sirius moving group with the spiral structure of the Galaxy. They suggested that Sirius group could be related to a higher m Lindblad resonance, or perhaps there is a spiral density wave moving at a slower pattern speed at larger Galactocentric radius. From the results, we conclude that probably Sirius moving group is a mixture of stars affected by dynamical perturbation and the stars from its parent cluter, UMa cluster.

5.5 Conclusion

In this chapter we performed chemical tagging of three stellar streams - Hercules, Hyades-Pleiades and Sirius all of them belong to the thin disc component of the Galaxy. We found members of the three streams are subsets of the thin disc unlike in some earlier studies which suggested mixture of both the thin and thick disc components. Kinematics, ages and abundance results strongly suggest that the three streams are results of transient phenomenon caused by dynamical perturbations in the Galaxy. One can't rule the possibility that some members of the moving group might have originated in the dispersed open cluster.

CHAPTER 6

CONCLUSION

6.1 Summary and Conclusion

In this thesis, we have undertaken a systematic study of small scale kinematical structures called stellar streams or moving groups in the Galactic disc. We studied elemental abundances of individual stars of a few representative streams to find clues of the streams existence in the velocity space as overdensities. Though the moving groups have been known for long time, their origin and evolution is not fully understood. There are three principal suggestions for their presence in the velocity space: a) cluster disruption, b) vestiges of merging satellite galaxies, c) in-situ formation due to dynamical interactions of bar/spirals with stellar orbits. The principal goal of the thesis is to verify which one of the three hypothesis best represents the chemical abundance data. For this purpose, two streams in the Galactic thick disc (Arcturus, AF06) and three streams in the Galactic thin disc (Hercules, Hyades and Sirius) have been subjected to quantitative abundance analysis based on high quality and high resolution Echelle spectroscopy.

Sample stars for thick disc streams are taken from the study of Arifyanto & Fuchs (2006) having high probability of belonging to the respective streams. Similarly, sample stars of thin disc streams are taken from the study of Famaey et al. (2005) who identified a number of streams using a large sample of red gaints. For uniformity, we have recomputed kinematic motion of each of the sample stars using the updated Hipparcos astrometry and the derived radial velocities in this study. It is quite satisfactory that the new space velocities did not change stars' original classification into various streams though their probabilities marginally changed.

High resolution ($R \sim 60{,}000$) spectra of the entire sample (169 stars) were obtained using 2.7-m Harlan J. Smith Telescope, McDonald Observatory, USA and 2.3-m Vainu

Bappu Telescope, India. Entire data were analysed and studied in detail. For every individual star of the stream we derived abundances of 16 elemental species, ages and kinematic motions. Results of each of the five streams are compared with the results from previous studies, if any, and compared stream results with those of a few representative open clusters, dwarf spheroidals, and the three main components of the Galaxy : the thin disc, the thic disc and the halo. Below a brief summary of our findings for each of the streams is given.

Arcturus stream : Arcturus stream is a high velocity stream (V_{LSR} $\sim$ -125 km s^{-1}) within the Galactic thick disc. The kinematic motion (U, V, W) of the stream indicates it is a subset of the main thick disc component. In fact, assuming that the solar neighborhood contains stars of the thick disc, the thin disc, and the halo components, our computed probabilities based on their space velocities suggest member stars of Arcturus belong to the thick disc component ($P_{thick} \geq 80$ %). Arcturus stream members revolve around the Galactic center on orbits with a mean eccentricity of $\sim$ 0.60 and are found to be very old ($\sim$ 12 Gyr). Stream stars are metal-poor with range in metallicity starting from [Fe/H] = -1.40 to -0.37 dex. Stream abundance ratios ([X/Fe]) trends with [Fe/H] are very similar to the thick disc abundance trends. Kinematics, age, metallicity and abundance trends establish that the Arcturus stream is a subset of the thick disc. Further, the computed mean values and dispersions of Arcturus stream in the metallicity, [Fe/H] interval -0.30 dex to -1.0 dex shows very good agreement with those of the background thick disc stars within about 0.02 dex. Thus, the abundance distribution of the Arcturus stream shows no distinct or unique behaviour, and are indistinguishable from the background thick disc field stars.

As per its origin scenarios, large range in age and metallicity of the Arcturus stream members suggest its member stars might not have come from the dispersed open cluster or any other spacially coherent group of stars. Comparion with chemical composition of dwarf spheroidals and their dissimilarity in the abundance trends indicate that the stream's origin may not be due to the merged satellite galaxies. Results point towards in-situ formation of Arcturus stream due to dynamical interactions between non-axisymmetric components of the Galaxy such as bar and spirals with stellar orbits. However, we note current data does not provide clear answer how the stars from the merged satellites can't form such clumps in the Galaxy.

AF06 stream : This is a high velocity stream (V_{LSR} $\sim$ -90 km s^{-1}) within the thick disc component. This has been recently identified as an overdensity in the velocity space of high velocity stars and came to known as a new stream and later AF06 stream after

their discoverers (Arifyanto & Fuchs 2006). A sample of 26 stars of AF06 were studied. Kinematics and probability results show that only 15 of them belong to the thick disc with high probabilities and the rest 11 are in the undecided zone of thick or thin disc components. Note that the 11 members have relatively large errors in the astrometry and hence also in their kinematic motion and the final probabilities.

However, AF06 abundance trends, like Arcturus stream are very similar to the background thick disc stars. The mean and dispersion of various elements of member stars of AF06 stream the interval [Fe/H] = -0.30 dex to -1.0 dex are comparable with those of the Galactic thick disc. In most cases, for AF06 members, we find star-to-star scatter (dispersion) is lower lower by 0.01-0.03 compared to thick-disc stars. Does it mean that AF06 stream members originated from a well mixed region in the Galaxy or the members of stream are the former members of an open cluster ? With the limited data available and the uncertainties involved it would be far fetching to interpret in the direction of cosmic scatter. Stream members are old ($\sim$ 12 Gyr) and the ages are comparable with their thick disc counter parts. Though some of the member stars kinematics do not have thick disc kinematics, abundance trends of the entire sample do suggest they are part of the thick disc component.

Stream members show range in metallicity starting from the metal poor value of [Fe/H] = -1.69 dex to metal rich value [Fe/H] = +0.22 dex. Metallicity distribution does indicate an hint of clustering of stars at [Fe/H] = -0.40 dex (about 8 stars out of total of 26). Does this mean AF06 is a mixture of stars, some from dispersed cluster and some from the thick disc ? Also, we note that thick disc metallicity peaks at about [Fe/H] $\sim$ -0.6 dex. So the clustering may be the manifestation of the thick disc metallicity distribution. Abundance results in partcular range in metallicity rules out the hypothesis of cluster disruption. Abundance trends of AF06 are significantly different from those of the present dwarf spheroidals which may argue that the stream stars may not have been the members of such merging satellites. The argument against external origin is also supported by the fact that AF06 has total net outward radial motion (U_{LSR} = -41.55 $\pm$ 47.45). Similar to Arcturus stream, we conlude that disc dynamics are the cause for the AF06 moving group.

Hercules stream : Hercules stream is a very prominent overdensity in the Galactic disc, sharing the kinematics of a star ζ Herculis. It has been found to have a rotational velocity characteistic of the Galactic thick disc (V_{LSR} = $\sim$ -50 km s^{-1}), but the kinematic motion suggest member stars belong to the thin disc component. In fact, stars have Z_{max} $\sim$ 0.10 kpc and very less vertical velocity (W_{LSR} $\sim$ 0 km s^{-1}). The computed kinematic probabilities show that the member stars belong to the thin disc with probablity (P_{thin} >

89 %). Other kinematical properties of Hercules stream, such as angular momentum (J_z = -1475.74 ± 106.82 kpc km s^{-1}), orbital eccentricity ($e \sim 0.27$) are very similar to the thin disc component.

Hercules members are very young (∼ 1.4 Myr) with ages ranging from 170 Myr to 4.2 Gyr. Except a lone member HIP 48417 which we found very old with an age of 12 Gyr. However, we found its astrometry is quite uncertain. The metallicity of the stream sample ranges from [Fe/H] = -0.17 dex to +0.43 dex with a mean value of [Fe/H] = 0.15 ± 0.14 dex which is very typical of thin disc population stars. Unlike in some earlier studies which show that the Hercules members are a mixture of thin and thick disc stars, we find them mostly of thin disc stars. Again, from the age and metallicities we rule out the cluster disruption scenario. Results show the sample is metal-rich and young implying external origin is very unlikely scenario. Hercules seems to be a transient phenomenon caused by dynamical perturbation.

Hyades-Pleiades stream : We studied 34 Hyades-Pleiades group members as given in the catalogue Famaey et al. (2005). Based on later study Famaey et al. (2008), we separated them into Hyades and pleiads stream members. Our sample containes (31 stars) predominantly of Hyades stream. The group lags the LSR by small amount ($V_{LSR} \sim$ 10-20 km s^{-1}), with a net radial outward motion. The member stars are very young with most of the stars having age less that 1 Gyr. They occupy a very narrow range in the angular momentum space of thin disc stars ($J_z \sim$ -1700 kpc km s^{-1}), with near circular orbits ($e \sim$ 0.10). Metallicity of the Hyades stream stars ranges from -0.12 dex to +0.36 dex, with a mean of +0.16 dex. Large range in metallity and ages, and large star-to-star scatter in the elemental abundances suggest that Hyades stream stars are not entirely from open cluster disruption. However, a small number of Hyades stream results are very similar to the results of Hyades cluster members. For this study we obtained results for the members of Hyades cluster. We conclude Hyades stream most probably the result of dynamical perturbation but one can't ignore the possibility of stars from the disrupted cluster such as Hyades super cluster.

Sirius stream : Sirius stream also known as Ursa Major stream is a group of stars. The group leads the LSR, although by small amount ($V_{LSR} \sim$ 10-15 km s^{-1}), with a net radial motion towards the Galactic center. Sirius stream members orbit the Galactic center in highly circular orbits ($e \sim 0.06$) and have high value of angular momentum ($J_z \sim$ -1970 kpc km s^{-1}).

In the literature, it has been suggested that Sirius stream stars might be from the UMa super cluster. Results show that the metallicity of Sirius stream members ranges from

[Fe/H] = -0.12 dex +0.28 dex, with a mean metallicity of +0.12 ± 0.11 dex. The age distribution peaks at ~ 400 Myr. We see a hint of clumping of stars in the age-metallicity plane close to the values of UMa cluster implying some kind of association between the stream and the UMa super cluster. In Tables 6.1 and 6.2, the mean properties of the streams studied here are summarized.

In summary, our results suggest that the cluster disruption is not responsible for the formation of any of the streams studied here, although we can't completely rule out their contribution. In the case of Arcturus, AF06 and Hercules streams we find no chemical homogeneity and no coevality which are characteristics of open clusters. In the case of Hyades and Sirius streams, we find some evidence that a fraction of stars in these streams seems to be associated with their respective clusters Hyades and UMa.

Also, we conclude from our results that the satellite accretion is the least likely scenario for the moving groups studied here. Main arguments against the scenario are: a) None of the known spheroidal galaxies are as young and metal-rich as the streams Hercules, Hyades-Pleaides and Sirius. Also, none of them have any similarity in their chemical abundance distribution with the distributions of the streams studied here. b)Streams show a range in age and metallicity which imply multiple episodes of star formation requiring enough mass to sustain long star formation process. Merger of such massive galaxies would have been a major merger and would have destroyed the thin disc component. Simulations and observations indicate there was no such major event in the recent past.

Finally, we conclude that the moving groups studied here most probably formed as a result of dynamical perturbations. The Galaxy is often modelled as an axisymmetric potential, though it has non-axisymmetric components such as the bar and the spiral arms. The non-axisymmetric components introduce dynamical perturbations in the disc which perturb the stellar orbits causing radial migration of the stars. Interactions of bar and/or spiral interact with orbits resonantly. At the resonance regions in the Galaxy one may find overdensities in the velocity space. These are transient in nature. The perturbations can move stars from different locations with different metallicities and ages to a particular orbit and hence can have similar velocities. Thus, the kinematic similarity but dissimilarity in ages and composition of the moving groups studied here suggests that these are formed due dynamical perturbations.

Table 6.1: The mean properties of the streams studied in this thesis

Quantity	Arcturus	AF06	Hercules	Hyades-Pleiades	Sirius
U_{LSR} (km s^{-1})	-6.48 ± 49.29	-41.55 ± 47.45	-44.25 ± 22.72	-24.61 ± 8.65	17.91 ± 5.78
V_{LSR} (km s^{-1})	-124.79 ± 8.92	-87.35 ± 7.83	-47.15 ± 12.54	-14.45 ± 3.90	10.38 ± 3.75
W_{LSR} (km s^{-1})	-11.5 ± 49.59	3.82 ± 54.34	-0.01 ± 13.86	4.19 ± 5.67	3.72 ± 4.50
e	0.59 ± 0.05	0.43 ± 0.03	0.27 ± 0.06	0.11 ± 0.02	0.06 ± 0.02
Z_{max} (kpc)	0.44 ± 0.37	0.49 ± 0.43	0.13 ± 0.09	0.11 ± 0.06	0.22 ± 0.23
R_{min} (kpc)	2.25 ± 0.31	3.56 ± 0.26	5.27 ± 0.54	7.10 ± 0.27	8.33 ± 0.20
R_{max} (kpc)	8.79 ± 0.32	9.09 ± 0.45	9.09 ± 0.44	8.89 ± 0.19	9.43 ± 0.43
R_{mean} (kpc)	5.52 ± 0.21	6.32 ± 0.25	7.18 ± 0.29	7.99 ± 0.14	8.88 ± 0.27
J_z (kpc km s^{-1})	-811 ± 77	-1130 ± 63	-1476 ± 107	-1754 ± 39	-1972 ± 53
$J_\perp$ (kpc km s^{-1})	347 ± 250	373 ± 268	99 ± 65	54 ± 33	68 ± 49.60
Age (Gyr)	12.28 ± 1.14	12.07 ± 1.18	1.41 ± 1.67	0.98 ± 0.90	0.90 ± 0.76

Table 6.2: The mean abundance ratios of the streams. (∗) The Ba abundance include λ6496 Å line also

Entity	Hercules (58)	Hyades-Pleiades(34)	Sirius (33)	Arcturus (18)	AF06 (26)
[Fe/H]	0.15 ± 0.14	0.16 ± 0.12	0.12 ± 0.11	-0.70 ± 0.26	-0.51 ± 0.43
[α/Fe]	0.02 ± 0.04	redo	-0.01 ± 0.04	0.18 ± 0.07	0.16 ± 0.09
[O/Fe](λ6300 Å)	-0.01 ± 0.06	−0.03 ± 0.07	−0.01 ± 0.07	...	...
[O/Fe](λ6363 Å)	0.05 ± 0.06	0.03 ± 0.06	0.01 ± 0.08	...	...
[O/Fe](triplet)	...	...	...	0.56 ± 0.18	0.46 ± 0.25
[Na/Fe]	0.14 ± 0.11	0.18 ± 0.09	0.12 ± 0.08	0.02 ± 0.0	0.05 ± 0.06
[Mg/Fe]	0.02 ± 0.06	−0.02 ± 0.06	−0.01 ± 0.06	0.22 ± 0.17	0.18 ± 0.12
[Al/Fe]	0.13 ± 0.06	0.08 ± 0.05	0.03 ± 0.06	0.19 ± 0.05	0.16 ± 0.10
[Si/Fe]	0.07 ± 0.03	0.06 ± 0.04	0.06 ± 0.05	0.13 ± 0.07	0.13 ± 0.08
[Ca/Fe]	0.01 ± 0.05	0.04 ± 0.05	−0.01 ± 0.07	0.15 ± 0.07	0.12 ± 0.10
[Sc/Fe]	0.05 ± 0.05	0.02 ± 0.04	0.01 ± 0.05	0.07 ± 0.09	0.05 ± 0.09
[TiI/Fe]	−0.01 ± 0.05	−0.01 ± 0.04	−0.05 ± 0.05	0.21 ± 0.06	0.19 ± 0.09
[TiII/Fe]	0.01 ± 0.06	0.02 ± 0.05	−0.02 ± 0.04	...	...
[V/Fe]	0.02 ± 0.05	0.01 ± 0.05	−0.02 ± 0.05	0.05 ± 0.13	0.11 ± 0.10
[CrI/Fe]	−0.00 ± 0.03	0.02 ± 0.02	−0.02 ± 0.03	-0.13 ± 0.03	-0.07 ± 0.05
[CrII/Fe]	...	...	...	-0.01 ± 0.05	-0.03 ± 0.07
[Mn/Fe]	−0.07 ± 0.04	−0.06 ± 0.04	−0.11 ± 0.05	-0.33 ± 0.07	-0.25 ± 0.10
[Co/Fe]	0.22 ± 0.10	0.16 ± 0.10	0.14 ± 0.09	0.10 ± 0.07	0.07 ± 0.07
[Ni/Fe]	0.05 ± 0.04	0.04 ± 0.04	−0.03 ± 0.04	-0.04 ± 0.04	:0.01 ± 0.04
[Cu/Fe]	...	...	...	-0.01 ± 0.14	0.09 ± 0.13
[Zn/Fe]	0.09 ± 0.07	0.04 ± 0.07	0.00 ± 0.09	0.21 ± 0.10	0.14 ± 0.09
[Y/Fe]	...	...	...	-0.02 ± 0.10	-0.03 ± 0.09
[Ba/Fe]	0.20 ± 0.10	0.29 ± 0.10	0.39 ± 0.10	-0.15 ± 0.08∗	-0.12 ± 0.09∗
[Ba/Fe](λ6496 Å)	0.35 ± 0.07	0.42 ± 0.08	0.51 ± 0.10		
[Ce/Fe]	...	...	...	0.07 ± 0.15	0.09 ± 0.11
[Nd/Fe]	...	...	...	0.22 ± 0.15	0.19 ± 0.12
[Eu/Fe]	...	...	...	0.29 ± 0.15	0.18 ± 0.14

6.2 Future Plans

It seems dynamical perturbations within the Galactic disc are playing a major role in the formation of moving groups. Though, we have not seen clear evidence of cluster disruption as the scenario for any of the five moving groups studied in this thesis, there are few moving groups which are found to be due to disruption of open clusters. It is quite straight forward to test the cluster disruption scenario with spectroscopy and kinematic data sets. However, the same thing can't be said about satellite accretion scenario. The merged satellites in the disc get dissolved relatively much faster and probably erase their past histrory. Searching for streams in the halo is one possibility to test the accretion hypothesis. Accreted satellites in the Galactic halo survive longer before getting mixed spatially. There are streams present in the Galactic halo (eg, Monoceros stream, Orphan stream) which are not spatially mixed yet. Simulations have shown that the remnants of accreted satellite can end up in the disc of the Galaxy and form streams. It would be interesting to study the halo streams by way of chemical tagging to check whether they exhibit any chemically distinct pattern similar to that of dwarf satellite galaxies. My immediate plan is to identify some well defined halo streams and analyse for chemical tagging and compare the results with dwarf spheroidals.

Further, to understand the Galaxy formation and its chronological evolution it is important to analyse as large sample as possible with much better astrometry and abundance data. Current studies are constrained by lack of large data sets and limited astrometry data for about one hundred thousand stars. Sample size with accuarate astrometry is going to be increased many fold with the GAIA mission which has been launched in 2013. GAIA is planned to measure as many as one billion stars which is about one percent of the total stellar population in the Galaxy. My plan is to devise sophisticated models to detect structures in the GAIA data and subject them to further studies such as high resolution spectroscopy.

Appendix A

Ages and Kinematical Parameters

Table A.1: Ages and kinematical properties of Arcturus stream

Star	V_r km s^{-1}	$U_{LSR} \pm 1\sigma$ km s^{-1}	$V_{LSR} \pm 1\sigma$ km s^{-1}	$W_{LSR} \pm 1\sigma$ km s^{-1}	R_m kpc	e	Z_{max} kpc	Age Gyr	P_{thick} %	J_z kpc km s^{-1}	$J_\perp$ kpc km s^{-1}
HIP 105888	−84.3	−23.9 ± 0.7	−122.4 ± 4.8	−40.0 ± 6.5	5.42	0.57	0.35	$10.8^{+0.9}_{-0.8}$	97 ± 0	−825	338
HIP 36710	−70.8	+45.8 ± 1.3	−107.3 ± 6.9	+45.3 ± 7.0	5.82	0.51	0.42	...	97 ± 1	−965	388
HIP 77637	−51.0	−26.9 ± 1.2	−134.0 ± 17.7	+15.8 ± 6.1	5.21	0.63	0.14	...	96 ± 0	−724	131
G 103−53	+10.0	+10.0 ± 1.8	−125.4 ± 19.1	−55.4 ± 9.6	5.44	0.58	0.54	...	96 ± 3	−813	476
G 72−12	−34.3	−13.7 ± 6.6	−118.7 ± 15.0	−62.9 ± 12.7	5.55	0.55	0.65	...	96 ± 2	−866	538
G 4−2	+38.8	−11.1 ± 1.2	−117.2 ± 19.8	−76.0 ± 8.1	5.60	0.54	0.90	...	95 ± 4	−880	650
HIP 53070	+65.8	−23.6 ± 0.71	−124.8 ± 4.84	+22.9 ± 2.1	5.41	0.59	0.19	...	95 ± 1	−811	194
G 204−30	−69.7	+58.9 ± 11.5	−130.4 ± 12.0	+46.9 ± 10.7	5.43	0.62	0.44	...	95 ± 3	−763	399
G 139−49	−94.1	−25.9 ± 5.5	−131.7 ± 11.8	−6.7 ± 1.9	5.24	0.62	0.06	...	95 ± 1	−742	57
G 241−7	−113.6	−45.5 ± 14.1	−134.1 ± 5.3	−20.4 ± 1.5	5.34	0.64	0.16	...	95 ± 0	−729	175
HIP 40613	+112.5	−31.6 ± 1.7	−139.0 ± 3.3	−32.7 ± 3.5	5.21	0.66	0.27	$12.9^{+0.5}_{-0.3}$	95 ± 1	−692	279
G42−34	+36.9	+8.4 ± 2.7	−126.5 ± 17.6	−7.1 ± 6.5	5.37	0.59	0.08	...	94 ± 6	−799	60
HIP 36491	+90.8	−47.7 ± 1.8	−118.9 ± 6.1	+1.2 ± 2.2	5.60	0.57	0.01	...	91 ± 4	−865	10
HIP 94931	−121.4	+65.9 ± 2.7	−120.7 ± 1.2	−79.2 ± 1.8	5.70	0.58	0.95	$13.4^{+3.2}_{-0.1}$	91 ± 1	−845	672
HIP 74033	−59.8	−111.7 ± 7.5	−132.7 ± 11.5	+42.3 ± 7.2	5.83	0.68	0.40	$12.0^{+1.6}_{-1.3}$	89 ± 5	−738	351
G 5−1	−22.4	+44.8 ± 2.4	−125.7 ± 15.5	−85.7 ± 13.2	5.56	0.59	1.07	...	89 ± 8	−810	737
G 102−44	−29.2	+73.6 ± 5.4	−130.5 ± 21.3	+88.1 ± 11.7	5.68	0.63	1.15	...	82 ± 14	−769	759
HIP 58253	+29.3	−62.5 ± 7.5	−106.2 ± 10.8	−3.4 ± 4.2	5.89	0.52	0.08	...	80 ± 16	−969	34

Table A.2: Ages and kinematical properties of AF06 stream

Star	V_r km s^{-1}	$U_{LSR} \pm 1\sigma$ km s^{-1}	$V_{LSR} \pm 1\sigma$ km s^{-1}	$W_{LSR} \pm 1\sigma$ km s^{-1}	R_m kpc	e	Z_{max} kpc	Age Gyr	P_{thick} %	J_z kpc km s^{-1}	$J_\perp$ kpc km s^{-1}
G 67−40	−29.2	−94.8 ± 15.3	−84.5 ± 10.2	−54.8 ± 12.2	6.61	0.48	0.57	...	97 ± 1	−1144	459
HIP 9080	−10.2	−92.8 ± 20.9	−91.2 ± 17.9	+54.2 ± 7.7	6.49	0.49	0.57	...	97 ± 1	−1098	469
G 66−51	−118.5	−86.1 ± 2.5	−79.8 ± 10.5	−66.9 ± 2.2	6.62	0.44	0.76	...	97 ± 0	−1183	571
G 106−8	+49.4	−16.3 ± 2.5	−92.2 ± 11.0	+85.9 ± 13.4	6.12	0.42	1.05	$14.0^{+1}_{-1.3}$	96 ± 2	−1097	737
HIP 10652	−20.9	−78.2 ± 7.7	−79.1 ± 5.7	+84.7 ± 4.9	6.68	0.42	1.08	...	96 ± 1	−1201	726
HIP 22020	+30.6	−74.3 ± 7.9	−85.6 ± 14.5	−52.9 ± 8.7	6.46	0.45	0.53	$11.8^{+1.2}_{-2}$	96 ± 3	−1151	455
HIP 26452	−35.8	+ 1.2 ± 4.6	−98.0 ± 10.3	+50.0 ± 6.7	5.91	0.45	0.47	...	96 ± 3	−1045	428
HIP 31740	+86.2	−94.8 ± 4.3	−107.5 ± 21.5	+49.6 ± 2.7	6.20	0.56	0.50	...	96 ± 2	−964	423
HIP 102923	−61.7	−12.2 ± 1.0	−92.0 ± 3.4	−52.6 ± 5.3	5.98	0.42	0.50	...	96 ± 2	−1084	446
G 146−76	−113.7	+50.3 ± 1.5	−80.6 ± 8.6	−90.6 ± 1.0	6.46	0.39	1.16	...	96 ± 1	−1189	770
HIP 34642	−28.1	−13.1 ± 5.4	−85.5 ± 9.4	−53.9 ± 5.6	6.19	0.39	0.52	$10.6^{+1.3}_{-1.6}$	95 ± 4	−1154	463
G 10−12	+133.0	−52.1 ± 6.5	−91.4 ± 4.8	+96.8 ± 3.8	6.24	0.43	1.29	...	94 ± 1	−1095	822
HIP 17147	+120.0	−101.3 ± 0.9	−83.8 ± 1.2	−34.2 ± 1.0	6.70	0.48	0.31	...	88 ± 1	−1160	290
HIP 24030	−15.9	+21.4 ± 1.2	−105.6 ± 23.5	+112.3 ± 20.5	5.94	0.47	1.65	...	85 ± 16	−984	966
HIP 11952	+24.0	+38.0 ± 6.47	−90.7 ± 15.3	−30.7 ± 2.9	6.11	0.43	0.29	...	72 ± 27	−1106	267
HIP 29814	+22.1	−43.2 ± 2.1	−92.8 ± 6.0	−20.9 ± 2.0	6.08	0.45	0.17	...	62 ± 13	−1087	179
G 197−45	+22.8	−67.0 ± 10.4	−76.9 ± 13.2	+32.1 ± 1.2	6.55	0.40	0.29	...	61 ± 24	−1219	268
HIP 104913	−64.5	−69.6 ± 5.4	−80.4 ± 1.8	+26.9 ± 1.9	6.47	0.42	0.23	$11.9^{+1.9}_{-2.6}$	58 ± 6	−1184	228
G 192−21	−18.6	+ 7.0 ± 3.2	−88.4 ± 13.1	+22.1 ± 3.0	6.08	0.41	0.18	$11.2^{+2.1}_{-2.9}$	47 ± 28	−1125	189
G 69−21	−15.8	−87.8 ± 15.6	−80.9 ± 11.1	+ 3.2 ± 2.0	6.63	0.45	0.06	...	45 ± 24	−1182	33
G 68−10	−40.6	−86.1 ± 8.6	−76.8 ± 4.6	−16.0 ± 4.4	6.67	0.43	0.14	$13.2^{+1.7}_{-1.5}$	45 ± 11	−1213	133
G 30−46	−22.9	−75.1 ± 13.4	−80.8 ± 10.6	−12.9 ± 5.5	6.50	0.43	0.13	...	42 ± 22	−1181	105
HIP 16169	+63.3	−47.4 ± 1.0	−87.5 ± 3.6	−10.5 ± 1.4	6.20	0.42	0.09	$12.85^{+1.05}_{-0.1}$	40 ± 7	−1131	88
G 6−16	+25.6	−31.4 ± 3.0	−85.4 ± 14.3	−15.9 ± 1.9	6.21	0.40	0.13	$11.0^{+1.1}_{-1.5}$	36 ± 27	−1154	135
G 78−41	−10.3	−18.7 ± 5.7	−88.7 ± 13.3	−3.3 ± 2.3	6.11	0.41	0.03	...	32 ± 25	−1127	28
G 25−5	−38.1	+44.2 ± 8.4	−85.0 ± 9.5	−2.4 ± 3.9	6.17	0.41	0.04	...	31 ± 17	−1143	23

Table A.3: Ages and space motion of Hercules stream

Star	V_r km s^{-1}	$U_{LSR} \pm \sigma$ km s^{-1}	$V_{LSR} \pm \sigma$ km s^{-1}	$W_{LSR} \pm \sigma$ km s^{-1}	Age Gyr
HIP 114742	−25.9	−70.8±6.47	-47.0±2.61	-9.8±2.53	$0.335^{+0.035}_{-0.042}$
HIP 22176	43.00	−32.3±1.03	-33.3±1.82	1.0±0.60	$1.73^{+0.32}_{-0.19}$
HIP 9517	28.8	−47.2±4.33	-49.9±6.99	-12.6±0.88	$0.95^{+0.25}_{-0.16}$
HIP 9307	−0.3	−45.0±2.82	-51.0±2.88	22.3±1.05	$0.41^{+0.06}_{-0.02}$
HIP 58654	23.9	−15.0±1.17	-45.7±2.91	28.1±1.05	$0.74^{+0.10}_{-0.04}$
HIP 52882	8.8	−41.8±3.64	-46.2±3.78	-16.4±2.54	$0.665^{+0.14}_{-0.1}$
HIP 50526	17.5	−64.1±5.42	-37.1±4.37	4.5±1.42	$0.65^{+0.135}_{-0.07}$
HIP 48140	28.3	−72.4±10.70	-40.9±9.14	-5.1±5.43	$0.86^{+0.49}_{-0.355}$
HIP 31039	40.4	−68.6±1.48	-50.8±1.99	-12.8±1.05	$1.385^{+0.085}_{-0.025}$
HIP 32844	60.5	−65.8±1.12	-54.0±1.77	-12.3±1.10	$0.695^{+0.075}_{-0.13}$
HIP 35146	24.6	−54.0±1.15	-42.9±1.17	-18.2±0.84	$1.00^{+0.15}_{-0.205}$
HIP 28677	39.2	−35.0±1.11	-39.3±2.99	25.0±0.77	$3.0^{+0.85}_{-0.44}$
HIP 20771	25.9	−8.3±0.97	-46.4±3.38	6.2±1.09	$0.68^{+0.09}_{-0.11}$
HIP 258	−17.6	−9.1±1.74	-53.0±3.46	-19.3±2.90	$0.58^{+0.12}_{-0.10}$
HIP 19287	53.9	−66.8±2.36	-43.0±5.45	-15.0±1.40	$2.8^{+0.8}_{-0.55}$
HIP 22765	−4.8	−31.5±5.36	-50.8±6.30	-7.3±1.66	$0.77^{+0.28}_{-0.21}$
HIP 7119	3.3	−101.5±74.23	-120.2±86.12	-7.9±9.11	$0.17^{+0.225}_{---}$
HIP 51047	12.6	−40.7±2.33	-43.7±2.50	-13.5±1.84	$1.65^{+0.31}_{-0.17}$
HIP 48417	72.6	−72.7±5.73	-38.4±3.31	24.1±5.46	12^{+7}_{-5}
HIP 504	−8.8	−69.3±11.48	-59.0±8.13	-20.8±4.72	$0.46^{+0.17}_{-0.095}$
HIP 3719	−2.8	−79.1±12.20	-46.5±6.80	18.0±1.45	$0.49^{+0.17}_{-0.11}$
HIP 37441	39.6	−49.6±2.41	-40.2±4.54	-4.6±2.78	$0.607^{+0.146}_{-0.045}$
HIP 116348	−38.6	−46.5±7.47	-51.8±2.89	14.0±1.31	$0.75^{+0.25}_{-0.15}$
HIP 20540	59.2	−51.1±1.35	-50.2±6.77	3.9±2.75	$0.76^{+0.155}_{-0.12}$
HIP 28168	40.8	−51.6±1.83	-33.0±3.37	7.7±0.85	$3.75^{+0.75}_{-0.95}$
HIP 29949	−2.7	−8.4±1.47	-63.5±3.54	-17.8±1.33	$1.50^{+0.24}_{-0.04}$
HIP 32261	19.5	−33.2±1.31	-60.1±2.53	4.4±0.64	$1.10^{+0.095}_{-0.11}$
HIP 96294	−60.9	−28.9±0.88	-42.0±1.07	0.0±1.62	$0.347^{+0.053}_{-0.067}$
HIP 87629	−64.7	−28.8±2.88	-45.8±1.17	-20.7±0.89	$1.33^{+0.21}_{-0.174}$
HIP 94576	−72.6	−41.5±1.20	-45.7±1.29	-24.9±1.15	$0.578^{+0.034}_{-0.023}$

Table A.3 – continued from previous page

Star	V_r km s^{-1}	$U_{LSR} \pm \sigma$ km s^{-1}	$V_{LSR} \pm \sigma$ km s^{-1}	$W_{LSR} \pm \sigma$ km s^{-1}	Age Gyr
HIP 95375	−58.2	10.8±0.50	-55.6±1.22	4.8±1.38	$1.56^{+0.24}_{-0.16}$
HIP 96028	−45.9	−78.7±3.64	-34.2±1.16	-6.8±0.53	$2.4^{+0.51}_{-0.35}$
HIP 115899	−27.9	−26.4±4.44	-39.4±2.11	3.1±0.94	$0.50^{+0.09}_{-0.10}$
HIP 116644	−24.9	−43.8±21.94	-63.3±19.41	-20.1±17.0	$0.35^{+0.52}_{-0.177}$
HIP 105502	−76.7	−40.0±0.52	-56.1±1.08	27.0±0.53	$0.51^{+0.04}_{-0.03}$
HIP 106551	−66.9	−44.4±1.54	-57.8±1.17	15.8±0.44	$0.76^{+0.11}_{-0.12}$
HIP 108914	−47.0	−22.2±3.13	-46.6±1.25	6.2±0.65	$0.83^{+0.18}_{-0.17}$
HIP 109387	−39.6	−29.1±2.51	-42.4±1.44	-9.8±2.65	$1.17^{+0.19}_{-0.062}$
HIP 109585	−29.9	−65.8±2.68	-44.1±1.32	1.9±0.43	$0.51^{+0.03}_{-0.02}$
HIP 113144	−45.3	−28.7±3.75	-50.5±1.61	4.5±1.69	$1.89^{+0.41}_{-0.16}$
HIP 102010	−73.4	−71.6±12.01	-32.9±4.51	1.3±10.85	$0.29^{+0.24}_{-0.118}$
HIP 104035	−49.6	−23.6±1.70	-40.5±1.32	0.9±3.42	$0.596^{+0.149}_{-0.072}$
HIP 22661	33.4	−42.8±4.62	-65.4±17.40	9.4±1.27	$1.40^{+1.5}_{-0.66}$
HIP 28417	100.4	−89.1±1.06	-42.6±3.47	-21.7±2.75	$1.09^{+0.16}_{-0.07}$
HIP 36647	62.3	−53.0±1.16	-44.0±3.51	-7.1±3.49	$2.30^{+0.70}_{-0.32}$
HIP 37049	44.7	−51.1±3.65	-40.7±8.58	22.7±1.30	$0.623^{+0.202}_{-0.135}$
HIP 107502	−47.5	−82.4±4.89	-36.0±1.12	-11.3±2.14	$1.21^{+0.24}_{-0.125}$
HIP 108012	−54.3	−54.1±3.84	-38.0±1.07	10.7±1.87	$1.7^{+0.5}_{-0.22}$
HIP 11117	14.8	−42.6±4.72	-43.8±5.57	16.6±2.41	$2.30^{+0.50}_{-0.55}$
HIP 111728	−42.3	−18.5±2.51	-48.5±1.69	-6.7±2.70	$2.6^{+0.69}_{-0.41}$
HIP 13786	−4.0	−6.4±1.50	-43.5±3.08	15.0±0.82	$2.6^{+0.6}_{-0.3}$
HIP 3546	−12.2	−35.0±12.25	-50.7±11.56	-5.5±4.85	$0.55^{+0.60}_{-0.24}$
HIP 6682	−4.3	−37.8±3.27	-38.8±2.76	11.2±0.56	$1.58^{+0.19}_{-0.185}$
HIP 8984	3.3	−44.9±5.65	-43.1±5.49	2.1±0.69	$1.90^{+0.7}_{-0.35}$
HIP 7710	−5.3	−23.9±2.82	-43.0±3.51	10.6±0.84	$2.8^{+0.75}_{-0.25}$
HIP 8926	−0.1	−32.2±5.94	-45.9±7.17	7.1±0.79	$0.60^{+0.15}_{-0.075}$
HIP 18865	2.2	−25.4±8.43	-45.6±13.02	1.0±1.92	$1.30^{+1}_{-0.56}$
HIP 4486	4.1	−33.0±2.78	-30.3±2.66	-3.4±0.93	$4.2^{+1.05}_{-0.5}$

Table A.4: Kinematical properties of Hercules stream

Star	R_{min} kpc	R_{max} kpc	e	Z_{max} kpc	J_z kpc km s^{-1}	$J_\perp$ kpc km s^{-1}	$P_{thin}\pm$ err %	σ_π/π %
HIP 114742	5.00	9.56	0.31	0.13	-1462.82	77.97	92±2	7.7
HIP 22176	6.09	8.86	0.19	0.02	-1601.40	10.32	98±1	4.5
HIP 9517	5.17	9.05	0.27	0.15	-1458.74	104.71	93±2	10.6
HIP 9307	5.12	8.98	0.27	0.20	-1446.32	194.99	89±2	4.9
HIP 58654	5.54	8.57	0.21	0.25	-1485.45	238.58	90±1	5.4
HIP 52882	5.41	8.94	0.25	0.22	-1491.96	150.05	94±1	7.4
HIP 50526	5.55	9.57	0.27	0.12	-1566.61	37.10	96±1	8.3
HIP 48140	5.33	9.78	0.29	0.16	-1540.62	60.34	94±3	16.5
HIP 31039	4.94	9.44	0.31	0.11	-1444.71	110.59	89±1	2.6
HIP 32844	4.87	9.40	0.32	0.11	-1428.29	107.95	88±1	2.6
HIP 35146	5.41	9.18	0.26	0.15	-1513.10	157.11	93±1	1.6
HIP 28677	5.76	8.86	0.21	0.20	-1546.63	213.77	93±1	5.7
HIP 20771	5.54	8.60	0.22	0.07	-1491.24	54.67	96±1	7.1
HIP 258	5.18	8.57	0.25	0.20	-1424.02	164.59	92±2	7.2
HIP 19287	5.31	9.58	0.29	0.12	-1523.07	128.70	92±2	7.8
HIP 22765	5.24	8.88	0.26	0.08	-1459.94	65.32	95±2	11.7
HIP 7119	2.22	10.19	0.64	0.48	-847.46	48.55	1±9	67.6
HIP 51047	5.51	8.93	0.24	0.16	-1510.21	121.46	95±1	5.0
HIP 48417	5.50	9.76	0.28	0.27	-1568.30	198.86	89±4	13.8
HIP 504	4.54	9.47	0.35	0.24	-1366.73	168.76	78±11	14.0
HIP 3719	4.98	9.88	0.33	0.22	-1479.12	167.02	87±5	13.5
HIP 37441	5.59	9.14	0.24	0.06	-1542.49	42.79	96±1	8.8
HIP 116348	5.02	9.00	0.28	0.14	-1429.37	123.80	92±1	11.3
HIP 20540	5.16	9.15	0.28	0.08	-1467.20	38.82	94±2	12.6
HIP 28168	5.90	9.30	0.22	0.07	-1605.46	64.85	97±1	6.2
HIP 29949	4.72	8.62	0.29	0.14	-1348.40	153.64	87±3	5.1
HIP 32261	4.78	8.77	0.29	0.05	-1369.84	36.93	91±1	3.4
HIP 96294	5.48	8.60	0.22	0.01	-1480.15	1.35	97±1	16.0
HIP 87629	5.39	8.68	0.23	0.19	-1469.39	178.85	93±1	10.7
HIP 94576	5.30	8.84	0.25	0.20	-1466.99	211.29	90±1	5.1

Table A.4 – continued from previous page

Star	R_{min} kpc	R_{max} kpc	e	Z_{max} kpc	J_z kpc km s^{-1}	$J_\perp$ kpc km s^{-1}	$P_{thin}\pm$ err %	σ_π/π %
HIP 95375	5.04	8.51	0.26	0.06	-1399.95	41.72	94±1	7.4
HIP 96028	5.42	9.94	0.29	0.06	-1569.51	60.59	95±1	4.2
HIP 115899	5.77	8.79	0.21	0.03	-1542.29	27.42	97±1	9.5
HIP 116644	4.51	8.97	0.33	0.34	-1326.02	164.23	81±25	38.4
HIP 105502	4.89	8.78	0.28	0.22	-1388.97	229.95	82±1	0.8
HIP 106551	4.78	8.87	0.30	0.12	-1375.15	134.70	88±1	3.0
HIP 108914	5.41	8.66	0.23	0.05	-1473.87	53.53	96±1	8.1
HIP 109387	5.57	8.70	0.22	0.09	-1503.69	82.22	96±1	7.3
HIP 109585	5.19	9.46	0.29	0.01	-1492.45	15.63	94±1	3.2
HIP 113144	5.19	8.70	0.25	0.05	-1440.27	40.03	95±1	8.3
HIP 102010	5.43	9.63	0.28	0.11	-1549.03	25.36	96±1	31.4
HIP 104035	5.64	8.58	0.21	0.08	-1505.21	17.09	97±1	13.1
HIP 22661	4.57	9.07	0.33	0.07	-1350.56	82.52	86±14	22.0
HIP 28417	5.14	10.23	0.33	0.19	-1533.97	188.10	83±3	8.1
HIP 36647	5.43	9.21	0.26	0.08	-1519.14	64.32	95±1	9.3
HIP 37049	5.60	9.31	0.25	0.22	-1553.96	192.21	92±3	14.5
HIP 107502	5.31	10.01	0.31	0.10	-1551.97	92.99	93±1	5.8
HIP 108012	5.51	9.18	0.25	0.12	-1530.89	96.16	96±1	7.6
HIP 11117	5.51	9.18	0.24	0.18	-1510.49	148.07	94±2	10.6
HIP 111728	5.34	8.59	0.23	0.07	-1456.14	56.42	96±1	8.3
HIP 13786	5.70	8.61	0.20	0.14	-1517.08	130.27	96±1	6.3
HIP 3546	5.19	8.98	0.27	0.23	-1457.45	53.41	95±3	24.2
HIP 6682	5.73	8.93	0.22	0.09	-1548.48	97.58	97±1	6.3
HIP 8984	5.47	9.09	0.25	0.04	-1517.23	20.12	96±1	10.6
HIP 7710	5.64	8.71	0.21	0.13	-1515.61	94.43	96±1	7.4
HIP 8926	5.46	8.88	0.24	0.13	-1498.60	67.27	96±1	13.9
HIP 18865	5.54	8.85	0.23	0.01	-1509.95	8.68	96±2	24.9
HIP 4486	6.19	8.88	0.18	0.08	-1618.86	29.86	98±1	6.6

Table A.5: Ages and space motion of Hyades-Pleiades stream

name	V_r km s^{-1}	$U_{LSR} \pm \sigma$ km s^{-1}	$V_{LSR} \pm \sigma$ km s^{-1}	$W_{\rm LSR} \pm \sigma$ km s^{-1}	Age Gyr
HIP 65366	-4.4	-51.5±10.34	-20.6±4.42	12.0±1.89	$0.43^{+0.22}_{-0.104}$
HIP 36739	49.6	-37.6±1.04	-15.9±0.80	5.9±1.56	$0.372^{+0.051}_{-0.039}$
HIP 1421	-9.3	-34.9±2.33	-20.0±1.30	11.7±0.96	$0.556^{+0.028}_{-0.03}$
HIP 88204	-44.2	-34.6±1.12	-13.7±0.96	12.4±1.27	$3.4^{+0.83}_{-0.53}$
HIP 80839	-37.8	-34.2±2.36	-12.7±0.98	-5.0±1.35	$0.51^{+0.055}_{-0.06}$
HIP 113635	-18.5	-33.4±6.04	-15.0±1.28	12.5±1.09	$0.365^{+0.085}_{-0.052}$
HIP 113084	-4.9	-31.9±1.81	-9.5±1.20	0.9±0.60	$1.29^{+0.205}_{-0.19}$
HIP 79867	-11.2	-31.6±2.26	-13.2±1.12	1.8±0.77	$1.28^{+0.25}_{-0.23}$
HIP 51224	9.2	-29.8±3.90	-18.1±3.02	0.0±1.81	$0.85^{+0.27}_{-0.144}$
HIP 49163	1.8	-29.6±2.55	-23.7±2.09	-0.4±0.95	$0.77^{+0.12}_{-0.085}$
HIP 24633	41.0	-27.9±1.04	-15.7±2.01	3.1±1.05	$0.362^{+0.068}_{-0.044}$
HIP 82219	-35.1	-27.4±2.00	-12.4±0.89	3.1±2.11	$0.776^{+0.144}_{-0.171}$
HIP 35317	35.9	-27.3±1.07	-12.6±1.69	11.1±1.06	$0.47^{+0.072}_{-0.073}$
HIP 117954	-3.8	-27.0±3.30	-15.3±1.82	11.0±0.56	$2.16^{+0.76}_{-0.51}$
HIP 18565	23.9	-24.3±1.17	-18.5±1.81	1.4±0.50	$0.41^{+0.056}_{-0.025}$
HIP 6939	8.4	-23.8±1.89	-10.7±1.53	9.5±0.84	$1.80^{+0.35}_{-0.33}$
HIP 17752	34.0	-23.5±1.31	-7.0±2.00	-3.7±1.58	$4.8^{+2.35}_{-1.42}$
HIP 51091	6.4	-23.2±3.84	-10.3±2.49	0.0±1.71	$1.58^{+0.58}_{-0.44}$
HIP 13887	21.2	-23.1±1.45	-11.5±2.18	-7.0±0.85	$0.66^{+0.10}_{-0.065}$
HIP 114565	-4.1	-22.9±3.44	-10.0±1.61	-1.8±1.22	$0.518^{+0.055}_{-0.083}$
HIP 62405	-2.9	-21.2±4.47	-15.7±2.89	4.1±1.01	$0.844^{+0.216}_{-0.144}$
HIP 2320	0.4	-20.5±2.22	-12.5±1.65	0.5±0.66	$0.93^{+0.19}_{-0.13}$
HIP 93589	-34.0	-20.5±0.93	-11.0±0.94	1.9±0.70	$1.2^{+0.23}_{-0.13}$
HIP 34043	28.4	-20.1±1.13	-12.4±2.29	3.0±1.92	$0.56^{+0.16}_{-0.125}$
HIP 19641	25.7	-19.5±1.19	-17.3±2.68	7.7±1.35	$0.47^{+0.068}_{-0.079}$
HIP 56756	12.2	-19.3±1.65	-9.7±0.95	10.8±1.07	$0.7^{+0.09}_{-0.10}$
HIP 19222	3.1	-18.3±1.38	-13.8±1.30	-5.5±0.78	$0.696^{+0.034}_{-0.04}$
HIP 41172	25.9	-18.3±1.14	-13.5±1.52	6.2±1.61	$0.78^{+0.135}_{-0.12}$
HIP 79647	-27.0	-16.5±3.48	-19.3±1.49	-0.1±2.15	$0.78^{+0.406}_{-0.26}$
HIP 85160	-28.0	-15.8±1.43	-15.8±1.00	3.8±1.22	$0.42^{+0.082}_{-0.04}$

Table A.5 – continued from previous page

name	V_r km s^{-1}	$U_{LSR} \pm \sigma$ km s^{-1}	$V_{LSR} \pm \sigma$ km s^{-1}	$W_{LSR} \pm \sigma$ km s^{-1}	Age Gyr
HIP 80656	-20.8	-13.4±2.38	-20.8±1.60	9.0±1.97	$0.565^{+0.165}_{-0.115}$
HIP 83289	-16.4	-12.0±0.77	-18.8±1.07	12.1±0.84	$0.68^{+0.05}_{-0.03}$
HIP 79164	-15.1	-11.1±0.90	-14.8±1.02	7.6±0.92	$1.04^{+0.15}_{-0.09}$
HIP 74080	-16.0	-10.6±1.00	-9.6±0.89	2.9±1.08	$1.05^{+0.13}_{-0.15}$

Table A.6: Kinematical properties of Hyades-Pleiades stream

name	R_{min} kpc	R_{max} kpc	e	Z_{max} kpc	J_z kpc km s^{-1}	$J_\perp$ kpc km s^{-1}	σ_π/π %
HIP 65366	6.40	9.35	0.19	0.34	-1687.12	105.27	16.9
HIP 36739	7.01	9.22	0.14	0.08	-1774.36	50.31	9.1
HIP 1421	6.67	9.00	0.15	0.14	-1701.11	105.47	4.9
HIP 88204	6.87	8.97	0.13	0.10	-1729.88	102.96	7.0
HIP 80839	6.92	9.02	0.13	0.13	-1742.70	53.31	8.0
HIP 113635	6.84	9.10	0.14	0.18	-1737.09	114.76	13.7
HIP 113084	7.19	9.11	0.12	0.03	-1789.45	10.19	4.1
HIP 79867	7.00	9.08	0.13	0.11	-1759.30	26.06	5.1
HIP 51224	6.90	9.00	0.13	0.15	-1736.30	30.47	11.0
HIP 49163	6.58	8.93	0.15	0.10	-1684.35	20.99	6.3
HIP 24633	7.15	9.03	0.12	0.06	-1776.22	29.72	13.4
HIP 82219	7.03	8.82	0.11	0.11	-1738.31	31.49	12.1
HIP 35317	7.27	9.02	0.11	0.10	-1791.13	94.82	8.4
HIP 117954	7.00	8.94	0.12	0.09	-1747.61	94.98	8.4
HIP 18565	6.96	8.89	0.12	0.02	-1735.77	13.76	5.1
HIP 6939	7.33	8.93	0.10	0.10	-1791.84	85.02	6.0
HIP 17752	7.61	9.01	0.08	0.10	-1837.62	35.31	14.4
HIP 51091	7.38	8.96	0.10	0.12	-1800.79	25.45	12.7
HIP 13887	7.33	8.94	0.10	0.06	-1792.62	60.19	7.1

Table A.6 – continued from previous page

name	R_{min} kpc	R_{max} kpc	e	Z_{max} kpc	J_z kpc km s^{-1}	$J_\perp$ kpc km s^{-1}	σ_π/π %
HIP 114565	7.30	8.92	0.10	0.06	-1788.44	18.81	10.1
HIP 62405	7.10	8.80	0.11	0.18	-1744.61	46.20	13.8
HIP 2320	7.26	8.86	0.10	0.00	-1776.20	4.20	7.0
HIP 93589	7.23	8.68	0.09	0.01	-1753.56	15.78	7.5
HIP 34043	7.43	8.91	0.09	0.06	-1804.24	27.36	13.2
HIP 19641	7.08	8.78	0.11	0.07	-1741.82	67.65	10.7
HIP 56756	7.48	8.73	0.08	0.13	-1790.80	92.79	5.7
HIP 19222	7.26	8.79	0.10	0.05	-1767.05	48.15	4.3
HIP 41172	7.36	8.80	0.09	0.10	-1782.47	54.51	9.4
HIP 79647	6.84	8.63	0.12	0.20	-1691.77	41.33	16.0
HIP 85160	7.02	8.60	0.10	0.12	-1715.03	37.68	8.6
HIP 80656	6.82	8.60	0.12	0.18	-1684.80	79.87	11.1
HIP 83289	6.99	8.59	0.10	0.11	-1709.56	102.46	3.0
HIP 79164	7.22	8.58	0.09	0.11	-1741.93	66.41	3.9
HIP 74080	7.53	8.57	0.06	0.10	-1780.96	31.40	5.5

Table A.7: Ages and space motion of Sirius stream

name	V_r km s^{-1}	$U_{LSR} \pm \sigma$ km s^{-1}	$V_{LSR} \pm \sigma$ km s^{-1}	$W_{LSR} \pm \sigma$ km s^{-1}	Age Gyr	Distance (d) pc
HIP 47719	-4.57	14.7±1.09	11.7±1.37	6.2±1.14	$0.64^{+0.41}_{-0.29}$	305± 53
HIP 52926	-10.24	13.0±0.92	6.2±1.05	-3.0±1.06	$0.42^{+0.17}_{-0.075}$	230± 40
HIP 67364	-7.90	23.4±5.28	11.9±2.77	-4.6±1.77	$0.45^{+0.74}_{-0.266}$	474± 159
HIP 68737	0.84	18.1±2.27	7.4±1.20	6.5±1.13	$1.47^{+1.17}_{-0.74}$	278± 71
HIP 49103	-5.20	11.2±0.84	14.2±1.20	3.9±0.96	$2.2^{+1.4}_{-0.7}$	222± 27
HIP 53710	-6.45	14.9±7.20	24.4±22.68	9.6±11.15	...	1235± 1646
HIP 66567	0.66	14.3±0.87	9.7±0.97	7.0±1.03	$1.73^{+0.72}_{-0.387}$	181± 24
HIP 68590	-3.05	17.2±4.01	7.9±2.61	2.7±1.48	$0.54^{+1.16}_{-0.316}$	467± 227
HIP 68828	4.82	11.7±1.15	10.1±1.41	10.4±1.12	$0.355^{+0.165}_{-0.086}$	407± 107

Table A.7 – continued from previous page

name	V_r km s^{-1}	$U_{LSR} \pm \sigma$ km s^{-1}	$V_{LSR} \pm \sigma$ km s^{-1}	$W_{LSR} \pm \sigma$ km s^{-1}	Age Gyr	Distance (d) pc
HIP 80211	5.66	17.6±2.15	10.9±1.37	8.5±1.39	$0.76^{+0.42}_{-0.24}$	344± 81
HIP 51825	-6.35	13.7±1.60	6.5±1.43	1.3±1.28	$0.366^{+0.176}_{-0.1}$	365± 105
HIP 53876	-5.83	11.2±0.80	10.2±1.12	0.5±1.02	$0.42^{+0.104}_{-0.06}$	220± 31
HIP 67021	-3.49	22.4±2.14	16.7±2.41	-1.0±1.32	$1.557^{+1.183}_{...}$	329± 55
HIP 68935	-1.43	19.6±1.08	9.8±0.90	2.9±1.07	$3.28^{+0.93}_{-0.51}$	127± 12
HIP 77401	3.44	10.4±1.19	11.2±1.42	6.7±1.25	$1.98^{+2.23}_{-1.09}$	388± 78
HIP 79326	12.77	27.5±2.80	8.9±1.70	5.5±3.32	$2.27^{+4.93}_{-1.47}$	351± 107
HIP 26711	-10.83	20.8±1.06	6.1±0.90	10.0±1.01	$0.37^{+0.16}_{-0.105}$	267± 44
HIP 28556	-14.55	24.5±1.05	8.5±0.92	0.4±1.80	$0.75^{+0.65}_{-0.35}$	246± 49
HIP 35431	-12.57	22.0±1.03	9.5±0.99	3.4±0.83	$0.43^{+0.083}_{-0.07}$	209± 29
HIP 117938	-7.20	32.8±3.96	3.3±1.34	4.3±1.41	$1.05^{+0.95}_{-0.502}$	300± 56
HIP 7668	-11.91	28.3±4.09	5.9±3.59	9.2±1.60	....	495± 176
HIP 37030	0.41	9.3±1.07	13.8±3.32	-0.2±2.93	$0.185^{+0.328}_{---}$	524± 181
HIP 7906	7.40	11.2±0.83	11.0±0.88	-2.0±0.73	$0.324^{+0.02}_{-0.02}$	158± 9
HIP 15554	-3.28	21.3±2.20	14.8±2.80	0.9±1.88	$0.58^{+0.49}_{-0.22}$	265± 58
HIP 44946	-8.86	15.8±0.83	8.0±0.74	1.0±0.81	$0.309^{+0.016}_{-0.019}$	114± 6
HIP 94156	7.26	16.6±0.69	10.1±1.11	9.2±0.53	$0.50^{+0.14}_{-0.14}$	262± 21
HIP 68418	-6.35	22.3±1.37	12.6±1.19	-2.9±1.10	$1.25^{+0.50}_{-0.35}$	217± 22
HIP 76366	2.14	26.2±1.65	9.3±0.93	1.6±1.17	$0.467^{+0.183}_{-0.138}$	266± 26
HIP 89065	5.74	15.2±0.92	11.4±0.84	-2.5±0.70	$0.500^{+0.055}_{-0.103}$	124± 6
HIP 64179	-0.85	17.9±0.52	10.9±0.69	5.6±1.03	$0.625^{+0.078}_{-0.040}$	95± 3
HIP 97282	6.25	15.3±0.73	11.9±1.16	1.2±0.93	$1.68^{+0.62}_{-0.71}$	216± 21
HIP 100116	6.46	17.7±1.77	9.1±1.35	10.8±1.84	$0.19^{+0.28}_{-0.10}$	485± 134
HIP 106771	3.11	12.9±0.58	8.7±1.17	9.5±0.55	$0.344^{+0.027}_{-0.024}$	165± 136

Table A.8: Kinematical properties of Sirius stream

name	R_{min} kpc	R_{max} kpc	e	Z_{max} kpc	J_z kpc km s^{-1}	$J_\perp$ kpc km s^{-1}	σ_π/π %
HIP 47719	8.49	9.60	0.06	0.25	-2014.15	78.57	17.4
HIP 52926	8.29	9.15	0.05	0.21	-1940.11	50.53	17.3

HIP 67364	8.10	9.57	0.08	0.50	-1947.82	110.63	33.6
HIP 68737	8.21	9.14	0.05	0.28	-1927.55	84.23	25.6
HIP 49103	8.52	9.63	0.06	0.19	-2020.14	54.89	12.2
HIP 53710	8.66	11.38	0.14	1.28	-2160.97	287.83	133.3
HIP 66567	8.24	9.19	0.05	0.19	-1938.33	72.64	13.0
HIP 68590	8.33	9.16	0.05	0.45	-1938.34	102.65	48.6
HIP 68828	8.44	9.18	0.04	0.40	-1955.31	125.40	26.4
HIP 80211	8.37	9.25	0.05	0.26	-1959.30	92.06	23.7
HIP 51825	8.24	9.30	0.06	0.29	-1947.81	65.85	28.8
HIP 53876	8.49	9.28	0.04	0.20	-1980.57	44.59	14.3
HIP 67021	8.38	9.90	0.08	0.30	-2027.88	67.56	16.8
HIP 68935	8.19	9.33	0.07	0.13	-1950.18	38.77	9.4
HIP 77401	8.44	9.15	0.04	0.31	-1957.32	89.10	20.2
HIP 79326	7.83	9.24	0.08	0.24	-1889.38	71.30	30.5
HIP 26711	8.32	9.48	0.07	0.08	-1982.35	87.84	16.5
HIP 28556	8.24	9.71	0.08	0.01	-1995.91	4.00	20.0
HIP 35431	8.31	9.62	0.07	0.09	-1995.78	35.58	13.8
HIP 117938	7.98	9.39	0.08	0.15	-1925.62	46.43	18.6
HIP 7668	8.43	9.53	0.06	0.16	-2001.22	84.29	35.6
HIP 37030	8.89	9.78	0.05	0.26	-2083.20	59.64	34.6
HIP 7906	8.52	9.29	0.04	0.08	-1986.56	26.29	5.8
HIP 15554	8.53	9.86	0.07	0.01	-2048.91	7.53	22.0
HIP 44946	8.29	9.27	0.06	0.07	-1955.87	19.42	5.6
HIP 94156	8.30	9.08	0.04	0.09	-1936.99	78.78	7.9
HIP 68418	8.21	9.56	0.08	0.22	-1974.56	52.10	10.0
HIP 76366	8.07	9.39	0.08	0.23	-1935.38	52.72	9.8
HIP 89065	8.25	9.21	0.06	0.03	-1943.48	21.05	4.7
HIP 64179	8.22	9.38	0.07	0.11	-1957.74	53.12	3.3
HIP 97282	8.38	9.24	0.05	0.04	-1965.11	13.74	9.9
HIP 100116	8.21	8.83	0.04	0.13	-1897.72	90.91	27.7
HIP 106771	8.43	9.06	0.04	0.07	-1950.92	80.86	7.6

Appendix B

Atmospheric Parameters and Elemental Abundances

Table B.1: Derived atmospheric parameters of Arcturus stream

Star	Photometry				Spectroscopy				
	$(T_{eff})_{V-K}$ K	$(T_{eff})_{b-y}$ K	log g ± error cm s^{-1}	$([M/H])_{b-y}$ dex	T_{eff} K	log g cm s^{-1}	$([Fe/H])_{model}$ dex	ξ_t km s^{-1}	N
HIP 105888	5798	5665	4.05 ± 0.05	−0.81	5790	4.30	−0.55	1.08	(42,7)
HIP 36710	5301	...	...	...	5340	4.63	−0.45	0.48	(46,6)
HIP 77637	5478	5550	4.31 ± 0.08	−0.94	5580	3.73	−0.85	0.90	(30,7)
G 103−53	5435	5340	4.16 ± 0.09	−0.66	5290	4.40	−0.65	0.52	(42,5)
G 72−12	5041	5094	...	−0.27	5060	4.64	−0.40	0.67	(43,5)
G 4−2	5258	5238	...	−0.61	5160	4.64	−0.70	0.48	(37,4)
HIP 53070	5962	5719	4.23 ± 0.04	−1.30	...	...	−1.40	1.36	(4,3)
G 204−30	5610	...	...	...	5550	4.42	−0.80	0.69	(27,5)
G 139−49	5331	...	...	...	5380	4.12	−0.75	0.47	(30,5)
G 241−7	5446	...	...	...	5320	4.00	−0.95	0.91	(25,4)
HIP 40613	5723	5670	4.16 ± 0.03	−0.64	5670	4.02	−0.55	0.90	(45,6)
G 42−34	4858	...	...	...	4920	4.22	−0.60	0.44	(47,4)
HIP 36491	5741	5681	4.41 ± 0.05	−0.96	5760	4.20	−0.85	1.10	(25,6)
HIP 94931	4964	5118	4.56 ± 0.01	−0.35	5120	4.58	−0 40	0.55	(48,6)
HIP 74033	5647	5574	4.02 ± 0.04	−0.92	5690	4.04	−0.70	1.06	(42,7)
G 5−1	5562	...	4.37 ± 0.08	...	5470	4.25	−1.05	0.45	(24,5)
G 102−44	5253	...	...	...	5260	4.43	−0.63	0.44	(45,5)
HIP 58253	5359	5351	...	−0.37	5280	4.38	−0.35	0.52	(41,4)

Table B.2: Derived atmospheric parameters of AF06 stream

Star	Photometry				Spectroscopy				
	$(T_{eff})_{V-K}$ K	$(T_{eff})_{b-y}$ K	log g ± error cm s^{-1}	$([M/H])_{b-y}$ dex	T_{eff} K	log g cm s^{-1}	$([Fe/H])_{model}$ dex	ξ_t km s^{-1}	N
G 67−40	5473	5326	...	−0.36	5370	4.42	−0.35	0.94	(48,6)
HIP 9080	5078	...	...	...	5250	4.45	−0.25	0.53	(51,7)
G 66−51	5420	...	...	...	5320	4.58	−0.80	0.79	(40,5)
G 106−8	5799	...	4.13 ± 0.10	...	5780	4.23	−0.40	1.00	(38,8)
HIP 10652	5607	5499	4.35 ± 0.03	−0.74	5580	4.42	−0.60	1.02	(38,5)
HIP 22020	5610	...	4.12 ± 0.08	...	5690	4.15	−0.20	0.95	(51,8)
HIP 26452	5837	...	...	...	5830	4.14	−0.68	0.70	(28,6)
HIP 31740	5293	5436	4.31 ± 0.12	−0.32	5430	4.45	−0.35	0.62	(44,7)
HIP 102923	4850	4933	4.61 ± 0.04	−0.19	4950	4.50	−0.25	0.69	(49,6)
G 146−76	5170	...	...	...	5090	2.67	−1.60	0.82	(16,5)
HIP 34642	5775	...	4.07 ± 0.05	...	5800	4.07	−0.40	1.00	(41,8)
G 10−12	4957	...	...	...	5120	3.98	−0.45	0.84	(50,7)
HIP 17147	5741	5722	4.22 ± 0.03	−0.83	5700	4.23	−0.85	0.71	(37,6)
HIP 24030	5915	5697	4.16 ± 0.11	−1.06	5730	4.20	−1.05	1.16	(15,6)
HIP 11952	6029	5785	4.24 ± 0.10	−1.57	...	...	...	1.38	(4,4)
HIP 29814	5160	5217	4.48 ± 0.01	−0.37	5230	4.48	−0.40	0.75	(51,6)
G 197−45	5176	...	...	...	5250	4.02	−0.60	0.85	(38,6)
HIP 104913	5355	...	4.40 ± 0.02	...	5380	4.48	−0.03	0.80	(51,8)
G 192−21	5790	5513	4.32 ± 0.10	−1.23	5820	4.20	−0.50	0.88	(36,6)
G 69−21	5562	5500	...	−0.30	5620	4.29	−0.20	1.07	(48,7)
G 68−10	5680	5589	4.36 ± 0.06	−0.57	5570	4.22	−0.50	0.73	(47,6)
G 30−46	5076	...	...	...	5150	4.65	+0.15	0.68	(48,6)
HIP 16169	5638	5575	4.34 ± 0.02	−0.56	5690	4.56	−0.48	1.10	(38,7)
G 6−16	5786	5655	4.16 ± 0.10	−0.19	5800	4.30	−0.05	1.10	(48,8)
G 78−41	5411	5494	4.37 ± 0.12	−0.38	5480	4.40	−0.40	0.74	(50,6)
G 25−5	5487	5508	...	−0.36	5560	4.50	−0.35	0.93	(50,7)

Table B.3: Derived atmospheric parameters of Hercules stream

Star	$(T_{eff})_{J-K}$ K	$(T_{eff})_{V-K}$ K	$(T_{eff})_{spec}$ K	$(\log g)_{phot}$ cm s^{-2}	$(\log g)_{spec}$ cm s^{-2}	ξ_t km s^{-1}	$([M/H])_{model}$ dex
HIP 22176	4460	4489	4660	2.73	2.90	1.51	+0.30
HIP 9517	4940	4799	4800	2.69	2.62	1.46	−0.01
HIP 9307	4896	5019	4920	2.72	2.85	1.51	+0.01
HIP 58654	4854	4564	4840	2.64	2.64	1.47	−0.02
HIP 52882	4780	4726	4670	2.25	2.58	1.51	−0.02
HIP 50526	4567	4820	4870	2.76	2.78	1.52	+0.06
HIP 48140	4489	4549	4680	2.50	2.65	1.46	+0.27
HIP 31039	5035	5170	5030	3.26	3.35	1.25	-0.05
HIP 32844	4561	4329	4480	2.04	2.34	1.61	+0.17
HIP 35146	4392	4747	4790	2.86	3.06	1.29	+0.26
HIP 28677	5323	4981	4910	3.09	3.10	1.30	−0.06
HIP 20771	4346	4966	4870	2.87	3.00	1.42	+0.31
HIP 258	4304	4953	4770	2.59	2.98	1.46	+0.27
HIP 19287	4552	4501	4690	2.61	2.65	1.54	+0.24
HIP 22765	4631	4710	4730	2.58	2.75	1.59	+0.20
HIP 7119	4699	4806	4960	2.32	3.00	1.46	+0.09
HIP 51047	4716	4673	4830	2.62	2.80	1.52	+0.12
HIP 48417	4493	4324	4440	2.33	2.33	1.41	+0.05
HIP 504	4833	4811	4830	2.60	2.80	1.50	+0.17
HIP 3719	4752	4706	4840	2.54	2.76	1.53	+0.04
HIP 37441	4683	4745	4930	2.73	2.75	1.62	−0.16
HIP 116348	4714	4833	4830	2.79	2.77	1.53	+0.10
HIP 20540	4797	5078	4965	3.12	3.20	1.26	+0.03
HIP 28168	4455	4511	4670	2.78	3.15	1.37	+0.40
HIP 29949	4510	4540	4710	2.58	2.70	1.53	+0.14
HIP 32261	4965	4747	4850	3.07	3.23	1.26	+0.32
HIP 96294	4601	4823	4880	2.61	3.00	1.48	+0.30
HIP 87629	5113	5013	5090	3.25	3.42	1.27	+0.08
HIP 94576	4949	4884	5050	2.95	3.20	1.45	+0.28
HIP 95375	4736	4786	4760	2.92	3.00	1.31	+0.15

Table B.3 – continued from previous page

Star	$(T_{eff})_{J-K}$ K	$(T_{eff})_{V-K}$ K	$(T_{eff})_{spec}$ K	$(\log g)_{phot}$ cm s^{-2}	$(\log g)_{spec}$ cm s^{-2}	ξ_t km s^{-1}	$([M/H])_{model}$ dex
HIP 96028	4535	4581	4700	2.76	2.93	1.29	+0.16
HIP 115899	5091	4840	4910	2.73	2.95	1.44	+0.12
HIP 116644	4605	4553	4760	2.42	2.88	1.45	+0.13
HIP 105502	4820	5021	4770	2.71	2.86	1.55	+0.17
HIP 106551	4464	4901	4840	2.65	2.88	1.59	+0.18
HIP 108914	4806	4785	4860	2.81	3.15	1.44	+0.42
HIP 109387	4864	5011	5000	3.26	3.40	1.27	+0.20
HIP 109585	4233	5249	4760	2.79	2.72	1.52	+0.18
HIP 113144	4735	4762	4980	3.16	3.40	1.19	+0.10
HIP 104035	4871	4966	5040	3.02	3.05	1.42	+0.20
HIP 22661	4488	4389	4630	2.36	2.77	1.70	+0.32
HIP 28417	4770	4758	4900	2.67	2.75	1.51	−0.09
HIP 36647	4766	4649	4680	2.81	2.65	1.45	+0.10
HIP 37049	4895	4820	4930	2.80	3.00	1.48	+0.10
HIP 107502	4380	4865	4610	2.57	2.75	1.38	+0.25
HIP 108012	4348	4459	4580	2.35	2.65	1.44	+0.14
HIP 11117	4575	4757	4820	3.16	3.34	1.23	+0.38
HIP 111728	4407	4569	4610	2.75	2.94	1.47	+0.33
HIP 13786	4306	4693	4650	2.59	2.60	1.62	+0.15
HIP 3546	4617	4572	4640	2.37	2.58	1.55	+0.25
HIP 6682	4858	4886	4920	3.29	3.32	1.22	+0.16
HIP 8984	4975	4656	4800	2.69	2.70	1.47	+0.05
HIP 7710	4486	4580	4650	2.54	2.65	1.35	−0.11
HIP 8926	4918	4997	5100	3.04	3.16	1.44	+0.23
HIP 18865	4737	4555	4960	2.99	3.10	1.42	+0.30
HIP 4486	4138	4649	4770	2.92	3.08	1.25	+0.17
HIP 102010	4376	4720	4710	2.46	2.70	1.56	+0.13
HIP 114742	...	...	4750	2.52	2.93	1.63	+0.35

Table B.4: Derived atmospheric parameters of Hyades-Pleiades stream

Star	$(T_{eff})_{J-K}$ K	$(T_{eff})_{V-K}$ K	$(T_{eff})_{spec}$ K	$(\log g)_{phot}$ cm s^{-2}	$(\log g)_{spec}$ cm s^{-2}	ξ_t km s^{-1}	[M/H]$_{model}$ dex
HIP 65366	4793	4725	4900	2.52	2.87	1.50	−0.03
HIP 36739	4923	4847	4900	2.56	2.80	1.47	+0.05
HIP 1421	4450	5257	5200	2.98	3.30	1.49	+0.15
HIP 88204	4559	4494	4800	2.62	2.90	1.64	+0.22
HIP 80839	4977	4926	5070	2.87	3.08	1.44	+0.27
HIP 113635	4844	4915	4680	2.62	2.60	1.43	+0.05
HIP 113084	4570	4892	4760	2.66	2.85	1.54	+0.24
HIP 79867	4149	4459	4510	2.01	2.57	1.65	+0.28
HIP 51224	4187	4745	4850	2.54	2.60	1.48	-0.10
HIP 49163	4042	4759	4940	2.73	3.03	1.41	+0.08
HIP 24633	5107	5208	5020	2.76	2.93	1.53	+0.18
HIP 82219	4966	4949	5030	3.02	3.03	1.42	+0.07
HIP 35317	5170	4944	4990	2.83	2.93	1.47	+0.06
HIP 117954	4235	4456	4600	2.45	2.56	1.45	+0.17
HIP 18565	4329	5124	4840	2.78	2.87	1.42	+0.11
HIP 6939	4238	4651	4700	2.64	2.76	1.57	+0.34
HIP 17752	4737	4689	4850	2.82	2.80	1.47	−0.12
HIP 51091	4691	4697	4840	2.82	2.86	1.50	+0.28
HIP 13887	4920	4898	5080	2.95	3.00	1.51	+0.12
HIP 114565	5145	4946	5080	2.91	3.15	1.42	+0.30
HIP 62405	5103	5052	5150	3.22	3.17	1.19	+0.20
HIP 2320	4725	4735	4940	2.91	3.08	1.42	+0.37
HIP 93589	5371	4862	4800	2.85	2.64	1.48	+0.04
HIP 34043	4738	4959	4970	2.85	2.80	1.65	+0.26
HIP 19641	4989	5131	4920	2.90	3.00	1.49	+0.20
HIP 56756	4447	4794	4880	2.75	3.00	1.47	+0.27
HIP 19222	4261	5030	5070	3.08	3.21	1.38	+0.27
HIP 41172	4917	4932	5000	3.01	3.20	1.44	+0.30
HIP 79647	4686	4657	4830	2.62	2.96	1.35	+0.16
HIP 85160	4969	4958	5080	2.84	3.12	1.34	+0.12

Table B.4 – continued from previous page

Star	$(T_{eff})_{J-K}$ K	$(T_{eff})_{V-K}$ K	$(T_{eff})_{spec}$ K	$(\log g)_{phot}$ cm s^{-2}	$(\log g)_{spec}$ cm s^{-2}	ξ_t km s^{-1}	$[M/H]_{model}$ dex
HIP 80656	4808	4795	4940	2.64	2.90	1.52	+0.10
HIP 83289	3788	4904	5000	2.97	3.15	1.45	+0.27
HIP 79164	3741	4674	4870	2.71	2.86	1.51	+0.12
HIP 74080	4470	4911	5060	2.99	3.15	1.43	+0.12

Table B.5: Derived atmospheric parameters of Sirius stream

Star	$(T_{eff})_{J-K}$ K	$(T_{eff})_{V-K}$ K	$(T_{eff})_{spec}$ K	$(\log g)_{phot}$ cm s^{-2}	$(\log g)_{spec}$ cm s^{-2}	ξ_t km s^{-1}	$([M/H])_{model}$ dex
HIP 47719	4598	4450	4620	2.19	2.55	1.49	+0.21
HIP 52926	4843	4813	4990	2.68	2.96	1.43	+0.07
HIP 67364	4525	4510	4630	2.20	2.60	1.45	+0.16
HIP 68737	4790	4751	4920	2.78	2.90	1.48	+0.15
HIP 49103	4189	4357	4480	1.99	2.30	1.59	+0.15
HIP 53710	4312	4220	4420	...	2.35	1.54	+0.20
HIP 66567	4657	4755	4950	2.96	3.20	1.31	+0.05
HIP 68590	4770	4758	4950	2.67	2.90	1.51	+0.05
HIP 68828	4961	4969	5150	2.71	3.14	1.49	+0.12
HIP 80211	4848	4870	5030	2.90	2.90	1.52	−0.05
HIP 51825	4822	5010	5180	2.73	3.10	1.55	+0.16
HIP 53876	5059	5031	5240	2.83	3.15	1.41	+0.16
HIP 67021	3867	4228	4370	...	2.15	1.52	+0.12
HIP 68935	4694	4710	4870	2.80	2.86	1.33	−0.10
HIP 77401	4320	4208	4310	1.88	2.07	1.57	+0.16
HIP 79326	4183	4294	4370	1.91	2.15	1.43	−0.10
HIP 26711	4617	4512	5090	2.43	2.65	1.72	+0.17
HIP 28556	4486	4563	4590	2.36	2.52	1.48	+0.14

Table B.5 – continued from previous page

Star	$(T_{eff})_{J-K}$ K	$(T_{eff})_{V-K}$ K	$(T_{eff})_{spec}$ K	$(\log g)_{phot}$ cm s^{-2}	$(\log g)_{spec}$ cm s^{-2}	ξ_t km s^{-1}	$([M/H])_{model}$ dex
HIP 35431	4964	5081	5200	2.83	3.00	1.41	+0.05
HIP 117938	4377	4297	4480	2.08	2.40	1.48	+0.20
HIP 7668	4284	4276	4330	...	2.05	1.75	+0.01
HIP 37030	4415	4410	4590	...	2.32	1.61	+0.03
HIP 7906	5430	5031	5140	2.63	3.11	1.59	+0.28
HIP 100116	3989	4441	4420	1.64	1.82	1.77	−0.03
HIP 106771	4646	4801	4700	2.69	2.55	1.14	+0.18
HIP 15554	4184	4472	4780	2.33	2.60	1.37	−0.12
HIP 44946	4793	5007	5160	2.68	2.82	1.61	+0.24
HIP 94156	4048	4455	4510	1.98	2.24	1.60	+0.22
HIP 68418	4561	4424	4450	2.04	2.22	1.55	+0.20
HIP 76366	4005	4344	4460	1.86	2.22	1.51	+0.20
HIP 89065	4351	4368	4710	2.35	2.71	1.52	+0.30
HIP 64179	4846	4923	4960	2.87	2.93	1.39	+0.24
HIP 97282	4519	4461	4725	2.42	2.88	1.43	+0.25

Table B.6: Abundance ratios ([X/Fe]) of the member stars of Arcturus stream

Star	[Fe I/H]	[O/Fe]	[Na/Fe]	[Mg/Fe]	[Al/Fe]	[Si/Fe]	[Ca/Fe]	[Sc/Fe]	[Ti/Fe]	[V/Fe]
HIP 105888	−0.56	0.58	0.10	0.25	0.20	0.16	0.12	0.17	0.24	0.08
HIP 36710	−0.42	0.32	0.03	0.02	0.16	0.10	0.10	0.16	0.23	0.18
HIP 77637	−0.82	0.69	−0.04	0.38	0.17	0.22	0.17	−0.09	0.15	−0.06
G 103−53	−0.65	0.61	0.00	0.03	0.18	0.19	0.17	0.11	0.17	0.07
G 72−12	−0.37	0.29	0.05	−0.01	0.12	0.14	0.01	0.16	0.13	0.21
G 4−2	−0.70	0.38	−0.07	0.10	0.13	0.17	0.06	0.21	0.16	0.06
HIP 53070	−1.40	0.84	...	...	...	...	0.27	...	...	...
G 204−30	−0.81	0.60	0.11	0.30	0.19	0.22	0.19	0.11	0.24	0.07
G 139−49	−0.75	0.69	−0.18	0.37	0.22	0.09	0.12	0.03	0.12	−0.18
G 241−7	−0.94	0.92	0.22	0.51	0.20	0.18	0.30	0.00	0.28	−0.01
HIP 40613	−0.54	0.61	0.09	0.37	0.27	0.16	0.17	0.03	0.23	0.01
G 42−34	−0.60	0.26	0.03	0.09	0.16	−0.05	0.24	0.03	0.29	0.24
HIP 36491	−0.86	0.56	0.11	0.43	0.27	0.19	0.19	0.12	0.19	—
HIP 94931	−0.42	0.39	−0.01	0.12	0.14	0.11	0.10	0.18	0.21	0.23
HIP 74033	−0.70	0.60	0.09	0.35	0.20	0.16	0.13	0.11	0.19	−0.03
G 5−1	−1.04	0.62	−0.05	0.31	0.30	0.00	0.11	−0.03	0.19	−0.20
G 102−44	−0.61	0.55	−0.03	0.03	0.17	0.08	0.16	−0.06	0.25	0.03
HIP 58253	−0.38	0.61	−0.08	0.09	0.16	0.19	0.12	−0.05	0.15	0.18

Table B.7: Abundance ratios ([X/Fe]) of the the member stars of Arcturus stream

Star	[Cr I/Fe]	[Cr II/Fe]	[Mn/Fe]	[Co/Fe]	[Ni/Fe]	[Cu/Fe]	[Zn/Fe]	[Y/Fe]	[Ba/Fe]	[Ce/Fe]	[Nd/Fe]	[Eu/Fe]
HIP 105888	−0.10	0.02	−0.34	0.13	−0.01	−0.05	0.30	0.02	−0.17	−0.02	0.16	0.36
HIP 36710	−0.17	−0.04	−0.28	0.09	−0.04	0.07	0.21	−0.08	−0.22	0.15	...	0.41
HIP 77637	−0.17	−0.06	−0.37	−0.01	−0.09	−0.20	0.26	0.09	0.01	−0.11	0.18	0.21
G 103−53	−0.14	−0.10	−0.35	0.16	−0.05	0.13	0.26	−0.11	−0.19	0.14	0.26	0.10
G 72−12	−0.11	−0.04	−0.24	0.10	−0.06	0.09	0.17	−0.01	−0.19	0.10	0.38	0.16
G 4−2	−0.14	0.04	−0.31	0.09	−0.07	0.06	0.12	−0.15	−0.24	...	...	0.49
HIP 53070	...	...	...	...	−0.06	...	0.12	0.19	0.03	...	...	...
G 204−30	−0.17	...	−0.27	0.08	0.05	−0.08	0.14	0.05	−0.09	...	...	0.37
G 139−49	−0.14	...	−0.37	0.05	−0.14	0.05	0.36	−0.15	−0.15	...	...	...
G 241−7	−0.05	0.06	−0.48	0.07	0.01	0.01	0.43	0.05	−0.20	0.02	...	...
HIP 40613	−0.18	0.00	−0.32	0.06	−0.04	−0.01	0.28	−0.07	−0.15	−0.26	0.03	0.24
G 42−34	−0.11	...	−0.31	0.21	−0.10	0.16	0.02	−0.14	−0.23	0.33	0.05	0.47
HIP 36491	−0.14	−0.06	−0.37	0.24	0.02	−0.12	0.20	−0.03	−0.17	0.15	0.46	0.34
HIP 94931	−0.14	0.04	−0.20	0.06	−0.05	0.17	0.16	0.05	−0.21	0.17	0.16	0.43
HIP 74033	−0.12	0.01	−0.30	0.10	−0.03	−0.02	0.32	0.11	−0.08	−0.04	0.16	0.33
G 5−1	−0.18	−0.05	−0.43	0.07	−0.07	−0.40	0.08	−0.08	−0.22	0.13	...	0.29
G 102−44	−0.10	0.02	−0.35	0.04	−0.07	−0.05	0.20	−0.09	−0.14	0.11	0.40	−0.01
HIP 58253	−0.14	−0.01	−0.31	0.23	−0.00	0.01	0.13	−0.02	−0.09	...	...	0.13

Table B.8: Abundance ratios ([X/Fe]) of the member stars of AF06 stream

Star	[Fe I/H]	[O/Fe]	[Na/Fe]	[Mg/Fe]	[Al/Fe]	[Si/Fe]	[Ca/Fe]	[Sc/Fe]	[Ti/Fe]	[V/Fe]
G 67−40	−0.38	0.37	0.08	0.21	0.22	0.18	0.16	0.08	0.21	0.22
HIP 9080	−0.17	0.24	−0.03	0.08	0.04	0.03	0.01	−0.00	0.13	0.14
G 66−51	−0.80	0.46	−0.01	0.27	0.21	0.14	0.21	0.03	0.29	0.18
G 106−8	−0.41	0.42	0.08	0.28	0.16	0.15	0.13	0.09	0.21	0.11
HIP 10652	−0.59	0.55	0.09	0.29	0.30	0.22	0.22	0.04	0.25	0.06
HIP 22020	−0.22	0.36	0.01	0.21	0.21	0.14	0.10	0.09	0.22	0.01
HIP 26452	−0.70	0.46	0.15	0.23	0.20	0.11	0.11	−0.05	0.16	0.02
HIP 31740	−0.36	0.47	0.10	0.13	0.20	0.16	0.15	0.19	0.27	0.14
HIP 102923	−0.29	0.32	0.14	0.11	0.06	0.11	0.12	0.16	0.29	0.47
G 146−76	−1.59	0.86	...	0.28	...	0.31	0.12	−0.20	−0.01	...
HIP 34642	−0.42	0.38	0.03	0.25	0.20	0.11	0.10	0.10	0.17	0.09
G 10−12	−0.43	0.55	0.07	0.25	0.22	0.19	0.18	0.20	0.30	0.18
HIP 17147	−0.86	0.75	0.08	0.42	0.28	0.22	0.22	0.08	0.23	−0.03
HIP 24030	−1.07	0.73	0.06	0.37	0.27	0.24	0.24	−0.07	0.26	...
HIP 11952	−1.69	1.25	...	...	...	...	0.33	...	...	...
HIP 29814	−0.40	0.36	0.02	0.04	0.16	0.11	0.12	0.08	0.20	0.16
G 197−45	−0.58	0.48	0.11	0.11	0.24	0.16	0.24	−0.10	0.24	0.10
HIP 104913	−0.02	0.16	−0.05	0.09	−0.02	0.00	−0.05	0.08	0.02	0.04
G 192−21	−0.50	0.49	0.11	0.30	0.19	0.07	0.15	0.06	0.26	0.10
G 69−21	−0.22	0.27	0.01	0.12	0.11	0.04	0.04	−0.00	0.08	0.04
G 68−10	−0.50	0.56	0.08	0.14	0.21	0.14	0.19	0.01	0.25	0.03
G 30−46	+0.22	−0.03	−0.09	−0.10	−0.09	−0.05	−0.13	0.01	0.11	0.22
HIP 16169	−0.44	0.49	0.05	0.31	0.21	0.17	0.11	0.16	0.20	0.09
G 6−16	−0.02	0.09	−0.08	0.07	0.02	−0.03	−0.03	0.01	0.03	−0.03
G 78−41	−0.40	0.55	0.04	0.09	0.20	0.16	0.11	0.10	0.25	0.11
G 25−5	−0.32	0.35	0.12	0.03	0.18	0.14	0.11	0.11	0.23	0.16

Table B.9: Abundance ratios ([X/Fe]) of the member stars of AF06 stream

Star	[Cr I/Fe]	[Cr II/Fe]	[Mn/Fe]	[Co/Fe]	[Ni/Fe]	[Cu/Fe]	[Zn/Fe]	[Y/Fe]	[Ba/Fe]	[Ce/Fe]	[Nd/Fe]	[Eu/Fe]
G 67−40	−0.11	−0.06	−0.28	0.08	0.04	0.14	0.15	−0.02	−0.23	0.17	...	0.36
HIP 9080	−0.07	−0.06	−0.18	0.03	−0.02	0.23	0.08	0.07	−0.10	0.29	0.22	−0.01
G 66−51	−0.02	...	−0.26	0.12	−0.02	0.05	0.05	0.08	−0.17	0.25	...	...
G 106−8	−0.11	−0.04	−0.25	0.13	0.00	0.06	0.20	−0.07	−0.08	0.14	0.12	0.18
HIP 10652	−0.07	−0.01	−0.30	0.08	0.07	0.05	0.12	0.01	−0.20	0.03	0.22	0.22
HIP 22020	−0.03	0.02	−0.23	0.12	0.03	0.16	0.21	−0.05	−0.07	0.04	0.17	0.14
HIP 26452	−0.09	0.01	−0.29	−0.04	−0.02	−0.19	0.14	−0.07	−0.05	0.22	0.48	0.09
HIP 31740	−0.05	0.03	−0.26	0.04	0.04	0.21	0.25	0.07	−0.13	0.02	0.15	0.45
HIP 102923	−0.02	0.01	−0.08	0.17	0.02	0.27	0.22	−0.11	−0.21	0.19	...	0.39
G 146−76	−0.25	...	−0.56	...	−0.06	...	0.02	−0.23	0.05	...	...	0.23
HIP 34642	−0.10	−0.06	−0.19	0.16	0.05	0.07	0.16	−0.04	0.00	−0.09	0.28	0.22
G 10−12	−0.05	0.10	−0.26	0.15	0.05	0.17	0.25	0.06	−0.12	−0.01	0.24	0.41
HIP 17147	−0.12	0.02	−0.41	0.08	0.01	−0.18	0.27	0.14	0.09	0.03	0.10	0.30
HIP 24030	−0.03	...	−0.42	0.12	−0.01	−0.26	0.28	0.01	−0.03	...	...	−0.02
HIP 11952	...	...	...	...	...	...	0.21	0.10	−0.15	...	...	...
HIP 29814	−0.06	−0.20	−0.18	0.08	0.01	0.15	0.19	−0.05	−0.14	0.18	0.22	...
G 197−45	0.03	0.02	−0.26	−0.03	0.02	0.15	0.09	−0.23	−0.28	0.14	...	0.10
HIP 104913	−0.14	−0.13	−0.17	0.00	−0.06	0.13	0.10	−0.03	−0.11	0.16	0.27	0.18
G 192−21	−0.08	−0.17	−0.38	0.12	0.05	0.10	0.15	−0.03	−0.08	...	...	0.12
G 69−21	−0.08	0.01	−0.16	0.05	−0.01	0.13	0.09	−0.02	−0.08	0.09	0.29	0.15
G 68−10	−0.08	−0.06	−0.31	0.11	0.02	0.05	0.29	−0.05	−0.16	−0.16	−0.07	−0.03
G 30−46	−0.10	−0.03	−0.13	−0.02	−0.10	0.15	−0.08	−0.09	−0.26	0.08	0.12	0.07
HIP 16169	−0.09	−0.02	−0.23	0.14	0.03	0.06	0.07	0.01	−0.19	0.16	0.04	0.07
G 6−16	−0.04	0.03	−0.14	−0.10	−0.05	0.11	−0.02	−0.12	−0.07	0.00	0.10	−0.01
G 78−41	−0.09	−0.03	−0.29	0.08	0.01	0.21	0.20	−0.04	−0.18	0.07	0.18	0.28
G 25−5	−0.04	0.03	−0.19	0.09	0.03	0.12	0.12	−0.04	−0.14	0.05	0.36	0.29

Table B.10: Abundance ratios ([X/Fe]) of elements O, Na, Mg and Al for the member stars of Hercules stream

Star	[Fe/H]	[O/Fe] (λ6300 Å)	[O/Fe] Å) (λ6363 Å)	[Na/Fe]	[Mg/Fe]	[Al/Fe]
HIP 107502	0.23	-0.05	0.01	0.11	0.06	0.12
HIP 108012	0.15	-0.08	0.04	0.20	0.08	0.12
HIP 11117	0.38	-0.13	-0.01	0.22	0.04	0.17
HIP 111728	0.31	0.02	0.10	0.34	0.07	0.22
HIP 114742	0.36	-0.05	0.11	0.33	0.04	0.21
HIP 116348	0.08	-0.01	0.03	0.06	0.03	0.15
HIP 13786	0.13	0.03	0.01	0.24	-0.06	0.30
HIP 18865	0.33	-0.10	0.06	0.29	-0.03	0.06
HIP 19287	0.23	-0.04	0.03	0.17	0.01	0.12
HIP 20540	0.03	0.02	0.06	0.12	0.00	0.09
HIP 20771	0.29	-0.05	-0.03	0.17	-0.12	0.06
HIP 22176	0.31	0.03	-0.01	0.40	-0.05	0.14
HIP 22661	0.32	0.02	0.07	0.38	0.04	0.20
HIP 22765	0.19	-0.16	-0.01	0.15	-0.05	0.12
HIP 258	0.26	-0.01	0.17	0.25	-0.04	0.18
HIP 28168	0.43	-0.07	0.07	0.18	-0.07	0.13
HIP 28417	-0.11	0.06	0.15	0.02	0.11	0.16
HIP 28677	-0.08	0.08	0.14	0.05	0.07	0.15
HIP 29949	0.12	0.10	0.16	0.17	0.17	0.22
HIP 31039	-0.03	-0.02	0.20	0.04	0.00	0.08
HIP 32261	0.30	-0.03	0.02	0.25	-0.01	0.15
HIP 32844	0.18	-0.10	0.00	0.10	-0.04	0.12
HIP 35146	0.27	-0.09	-0.02	0.06	-0.04	0.08
HIP 3546	0.24	-0.14	0.02	0.27	0.00	0.13
HIP 36647	0.11	0.07	0.09	0.08	0.13	0.15
HIP 37049	0.09	-0.02	0.10	0.11	-0.04	0.09
HIP 3719	0.03	0.05	0.05	0.07	0.07	0.12
HIP 37441	-0.17	0.10	0.05	0.10	0.07	0.14
HIP 4486	0.15	0.04	0.13	0.09	0.01	0.16

Table B.10 – continued from previous page

Star	[Fe/H]	[O/Fe] (λ6300 Å)	[O/Fe] (λ6363 Å)	[Na/Fe]	[Mg/Fe]	[Al/Fe]
HIP 48140	0.30	-0.02	0.06	0.21	0.01	0.12
HIP 48417	0.04	-0.08	-0.01	0.12	0.05	0.19
HIP 504	0.17	-0.03	0.03	0.09	0.02	0.12
HIP 50526	0.05	-0.07	0.11	0.08	0.01	0.11
HIP 51047	0.11	-0.03	0.02	0.12	0.02	0.15
HIP 52882	-0.03	0.05	0.11	0.17	0.03	0.11
HIP 58654	-0.02	-0.01	0.02	0.10	0.07	0.18
HIP 6682	0.14	0.01	0.00	0.00	-0.02	0.06
HIP 7119	0.07	0.06	0.10	0.09	-0.01	0.03
HIP 7710	-0.13	0.10	0.10	0.03	0.11	0.21
HIP 8926	0.21	-0.06	-0.08	0.16	-0.06	0.04
HIP 8984	0.03	0.01	-0.01	0.07	0.05	0.13
HIP 9307	0.01	0.07	0.11	0.07	0.04	0.12
HIP 9517	-0.01	0.03	-0.08	0.02	0.05	0.23
HIP 102010	0.11	...	0.13	0.11	0.18	0.20
HIP 104035	0.17	-0.06	-0.03	0.07	-0.02	0.00
HIP 105502	0.18	...	-0.09	-0.01	0.03	0.13
HIP 106551	0.18	...	0.10	0.17	-0.08	0.11
HIP 108914	0.42	...	0.02	0.29	-0.08	0.14
HIP 109387	0.21	-0.02	0.08	0.07	0.06	0.07
HIP 109585	0.20	0.00	0.06	0.15	0.10	0.14
HIP 113144	0.09	...	0.13	-0.01	0.05	0.09
HIP 115899	0.10	0.00	0.06	0.04	0.01	0.03
HIP 116644	0.14	0.01	0.04	0.09	-0.01	0.00
HIP 87629	0.05	...	0.13	-0.02	-0.02	0.01
HIP 94576	0.26	...	0.05	0.44	0.10	0.21
HIP 95375	0.13	...	0.08	0.09	0.06	0.08
HIP 96028	0.17	-0.04	0.05	0.05	0.00	0.10
HIP 96294	0.28	-0.01	0.10	0.23	-0.06	0.06

Table B.11: Abundance ratios ([X/Fe]) of elements Si, Ca, Sc, Ti, V and Cr for the member stars of Hercules stream

Star	[Si/Fe]	[Ca/Fe]	[Sc/Fe]	[Ti I/Fe]	[Ti II/Fe]	[V/Fe]	[Cr/Fe]
HIP 107502	0.06	-0.02	0.05	0.01	-0.01	0.02	-0.01
HIP 108012	0.10	-0.01	0.04	0.01	-0.08	-0.01	-0.01
HIP 11117	0.05	-0.05	0.06	-0.03	-0.06	0.02	-0.01
HIP 111728	0.10	-0.06	0.11	0.06	-0.10	0.09	0.04
HIP 114742	0.13	-0.06	0.12	-0.03	-0.03	0.01	0.02
HIP 116348	0.08	0.03	0.04	0.00	0.02	-0.01	-0.01
HIP 13786	0.09	0.04	0.04	0.10	-0.08	0.11	0.08
HIP 18865	0.08	0.02	0.04	-0.03	-0.06	0.04	0.04
HIP 19287	0.06	0.00	-0.01	-0.01	-0.08	-0.01	0.01
HIP 20540	0.04	0.07	0.04	0.01	0.01	0.05	0.00
HIP 20771	0.03	-0.01	-0.01	-0.07	0.01	-0.03	0.01
HIP 22176	0.06	-0.02	0.09	0.02	-0.10	0.11	0.06
HIP 22661	0.14	-0.12	0.05	0.01	-0.11	0.08	0.01
HIP 22765	0.10	-0.03	-0.03	-0.06	-0.05	-0.03	-0.02
HIP 258	0.09	-0.05	0.08	-0.05	-0.01	-0.03	0.02
HIP 28168	0.02	-0.11	0.11	-0.02	-0.06	0.05	-0.01
HIP 28417	0.10	0.08	0.11	0.04	0.11	0.08	-0.03
HIP 28677	0.06	0.07	0.04	0.06	0.05	0.07	0.00
HIP 29949	0.12	0.05	0.04	0.07	0.03	0.08	0.03
HIP 31039	0.05	0.06	-0.01	0.01	0.04	0.02	0.00
HIP 32261	0.06	-0.02	0.07	-0.01	0.01	0.01	0.03
HIP 32844	0.10	-0.10	0.03	-0.12	-0.02	-0.06	-0.02
HIP 35146	0.02	-0.06	-0.02	-0.12	-0.08	-0.08	-0.09
HIP 3546	0.11	-0.03	-0.03	-0.09	-0.15	-0.06	0.01
HIP 36647	0.12	0.00	0.02	0.01	0.06	-0.01	-0.06
HIP 37049	0.05	0.02	0.05	-0.01	0.09	0.01	-0.02
HIP 3719	0.08	0.06	0.06	0.01	0.05	0.01	-0.01
HIP 37441	0.11	0.09	0.10	0.06	0.08	0.10	-0.01
HIP 4486	0.07	0.02	0.08	0.02	0.07	0.04	0.01
HIP 48140	0.02	-0.08	-0.05	-0.11	-0.01	-0.10	-0.07

Table B.11 – continued from previous page

Star	[Si/Fe]	[Ca/Fe]	[Sc/Fe]	[Ti I/Fe]	[Ti II/Fe]	[V/Fe]	[Cr/Fe]
HIP 48417	0.09	-0.01	0.05	-0.04	-0.05	-0.01	-0.06
HIP 504	0.06	0.03	0.01	-0.05	-0.01	-0.01	-0.01
HIP 50526	0.09	0.05	-0.01	0.01	0.06	-0.01	-0.01
HIP 51047	0.05	0.03	0.02	-0.01	0.03	0.03	0.03
HIP 52882	0.06	0.02	0.09	0.03	0.06	0.04	-0.01
HIP 58654	0.07	0.09	0.02	0.03	0.00	0.08	0.03
HIP 6682	0.03	0.01	0.05	0.00	0.06	0.03	0.00
HIP 7119	0.05	0.05	0.04	-0.01	0.06	0.03	0.00
HIP 7710	0.12	0.08	0.08	0.07	0.10	0.02	0.01
HIP 8926	0.04	0.06	-0.02	0.01	0.01	0.01	-0.01
HIP 8984	0.10	0.03	0.06	-0.03	0.07	0.01	-0.01
HIP 9307	0.05	0.05	0.06	0.03	0.07	0.06	-0.01
HIP 9517	0.07	0.10	-0.08	0.14	0.07	0.08	0.06
HIP 102010	0.13	-0.01	0.10	0.01	0.09	0.05	-0.02
HIP 104035	0.02	0.08	-0.01	-0.01	0.06	0.01	0.01
HIP 105502	0.06	-0.03	0.10	-0.08	0.06	-0.06	-0.04
HIP 106551	0.06	-0.04	0.09	-0.08	-0.01	0.03	-0.05
HIP 108914	0.07	-0.06	0.11	-0.06	-0.02	0.01	0.01
HIP 109387	0.03	-0.04	0.00	0.00	0.02	0.01	0.00
HIP 109585	0.07	0.01	0.03	-0.01	0.01	0.06	0.00
HIP 113144	0.03	0.04	0.11	0.04	0.11	0.05	-0.02
HIP 115899	0.06	0.04	0.07	-0.02	0.09	-0.02	-0.03
HIP 116644	0.07	-0.05	0.04	-0.07	0.04	-0.04	-0.03
HIP 87629	0.03	0.05	0.03	-0.03	0.04	0.03	0.03
HIP 94576	0.03	0.06	0.06	0.04	-0.01	0.08	0.08
HIP 95375	0.06	-0.02	0.05	-0.06	-0.02	-0.01	0.01
HIP 96028	0.06	-0.01	0.07	-0.03	0.02	-0.02	-0.03
HIP 96294	0.02	0.00	0.08	-0.02	0.06	0.04	0.02

Table B.12: Abundance ratios ([X/Fe]) of elements Mn, Co, Ni, Zn and Ba for the member stars of Hercules stream. [Ba/Fe] (second last column) is the mean barium abundance from two lines λ 5853.68 Å and λ 6141.73 Å

Star	[Mn/Fe]	[Co/Fe]	[Ni/Fe]	[Zn/Fe]	[Ba/Fe]	[Ba/Fe](λ6496 Å)
HIP 107502	-0.02	0.29	0.06	0.09	0.25	0.42
HIP 108012	-0.02	0.29	0.06	0.11	0.27	0.39
HIP 11117	-0.03	0.37	0.13	0.18	0.06	0.27
HIP 111728	-0.01	0.43	0.16	0.19	0.05	0.28
HIP 114742	-0.11	0.40	0.10	0.18	0.12	0.36
HIP 116348	-0.07	0.18	0.04	0.00	0.26	0.36
HIP 13786	-0.13	0.31	0.07	0.08	0.17	0.33
HIP 18865	-0.04	0.25	0.10	0.13	0.01	0.39
HIP 19287	-0.09	0.32	0.08	0.13	0.11	0.32
HIP 20540	-0.08	0.11	0.03	0.05	0.25	0.36
HIP 20771	-0.06	0.21	0.05	0.05	0.23	0.42
HIP 22176	-0.05	0.39	0.11	0.13	0.04	0.29
HIP 22661	-0.06	0.46	0.14	0.24	-0.07	0.29
HIP 22765	-0.04	0.29	0.08	0.14	0.13	0.26
HIP 258	0.03	0.33	0.11	0.14	0.06	0.29
HIP 28168	-0.02	0.37	0.08	0.15	0.07	0.30
HIP 28417	-0.09	0.13	0.04	0.14	0.19	0.31
HIP 28677	-0.07	0.13	0.03	0.06	0.11	0.24
HIP 29949	-0.08	0.36	0.08	0.20	0.18	0.29
HIP 31039	-0.09	0.05	0.02	0.08	0.21	0.35
HIP 32261	-0.02	0.34	0.12	0.09	0.18	0.30
HIP 32844	-0.08	0.20	0.03	0.08	0.26	0.40
HIP 35146	-0.07	0.18	0.04	0.03	0.25	0.37
HIP 3546	-0.09	0.34	0.10	0.17	0.05	0.24
HIP 36647	-0.18	0.26	0.04	0.24	0.19	0.29
HIP 37049	-0.07	0.16	0.03	0.05	0.26	0.41
HIP 3719	-0.10	0.12	0.03	0.03	0.35	0.44
HIP 37441	-0.07	0.13	0.01	0.02	0.30	0.42
HIP 4486	-0.02	0.27	0.08	0.09	0.21	0.33

Table B.12 – continued from previous page

Star	[Mn/Fe]	[Co/Fe]	[Ni/Fe]	[Zn/Fe]	[Ba/Fe]	[Ba/Fe](λ6496 Å)
HIP 48140	-0.09	0.31	0.03	0.08	0.17	0.34
HIP 48417	-0.05	0.24	0.06	0.14	0.17	0.32
HIP 504	-0.03	0.23	0.05	0.05	0.23	0.39
HIP 50526	-0.05	0.13	0.04	0.03	0.22	0.36
HIP 51047	-0.04	0.23	0.08	0.08	0.23	0.32
HIP 52882	-0.08	0.20	0.03	0.09	0.25	0.38
HIP 58654	-0.07	0.16	0.03	0.07	0.19	0.35
HIP 6682	-0.06	0.16	0.03	0.02	0.25	0.27
HIP 7119	-0.06	0.09	0.01	0.00	0.37	0.50
HIP 7710	-0.08	0.17	0.04	0.08	0.17	0.27
HIP 8926	-0.07	0.10	0.02	-0.05	0.32	0.44
HIP 8984	-0.11	0.19	0.05	0.09	0.25	0.37
HIP 9307	-0.05	0.13	0.02	0.06	0.28	0.43
HIP 9517	-0.13	0.09	0.01	...	0.34	0.45
HIP 102010	-0.11	0.29	0.06	0.18	0.09	...
HIP 104035	-0.10	0.07	-0.01	-0.08	0.38	0.44
HIP 105502	-0.15	0.12	0.02	0.04	0.18	0.29
HIP 106551	-0.10	0.17	0.03	0.14	0.12	0.18
HIP 108914	-0.04	0.35	0.10	0.11	0.12	...
HIP 109387	-0.07	0.12	0.03	0.06	0.20	0.29
HIP 109585	-0.02	0.30	0.07	0.17	0.19	0.38
HIP 113144	-0.05	0.19	0.04	0.04	0.29	...
HIP 115899	-0.06	0.13	0.01	0.02	0.40	0.51
HIP 116644	-0.13	0.14	0.01	0.05	0.29	0.41
HIP 87629	-0.04	0.05	0.02	0.02	0.27	...
HIP 94576	0.04	0.23	0.08	0.13	0.17	...
HIP 95375	-0.01	0.22	0.07	0.17	0.17	...
HIP 96028	-0.12	0.28	0.04	0.07	0.17	...
HIP 96294	-0.06	0.26	0.06	0.08	0.23	...

Table B.13: Abundance ratios ([X/Fe]) of elements O, Na, Mg and Al for the member stars of Hyades-Pleiades stream. The starred [Mg/Fe] value is estimated from one single line λ 5711.09 Å, but reliable beacuase of the quality of the line

Star	[Fe/H]	[O I/Fe] (λ6300 Å)	[O/Fe] (λ6363 Å)	[Na/Fe]	[Mg/Fe]	[Al/Fe]
HIP 65366	-0.03	0.04	0.08	0.04	0.03	0.12
HIP 36739	0.06	-0.04	-0.03	0.15	-0.09	0.08
HIP 1421	0.14	0.07	0.11	0.24	-0.02	0.03
HIP 88204	0.20	0.00	0.14	0.28	0.02$\star$	0.17
HIP 80839	0.26	...	-0.04	0.24	-0.07	0.01
HIP 113635	0.05	0.07	0.04	0.05	0.19	0.22
HIP 113084	0.25	-0.04	0.06	0.19	-0.01	0.09
HIP 79867	0.30	-0.04	0.08	0.26	-0.06	0.15
HIP 51224	-0.10	0.05	0.07	0.09	0.01	0.11
HIP 49163	0.06	0.12	0.13	0.11	0.02	0.08
HIP 24633	0.18	-0.06	0.00	0.33	-0.06	0.03
HIP 82219	0.08	...	-0.01	0.09	-0.08	0.01
HIP 35317	0.06	-0.05	0.03	0.14	-0.01	0.06
HIP 117954	0.16	-0.02	0.02	0.16	-0.01	0.05
HIP 18565	0.11	0.03	0.04	0.18	-0.11	0.05
HIP 6939	0.34	-0.06	0.02	0.30	0.01	0.16
HIP 17752	-0.12	0.11	0.12	0.06	-0.05	0.08
HIP 51091	0.28	-0.09	0.00	0.26	-0.02	0.13
HIP 13887	0.11	-0.05	-0.01	0.18	-0.03	0.04
HIP 114565	0.30	-0.11	-0.07	0.20	-0.04	0.05
HIP 62405	0.21	-0.12	-0.01	0.21	0.02	0.07
HIP 2320	0.36	-0.13	0.01	0.23	-0.03	0.09
HIP 93589	0.03	...	-0.04	0.08	0.10	0.15
HIP 34043	0.24	-0.09	-0.08	0.29	-0.04	0.01
HIP 19641	0.18	0.08	0.05	0.11	-0.03	0.07
HIP 56756	0.26	-0.03	0.05	0.20	-0.08	0.09
HIP 19222	0.26	-0.16	0.03	0.17	-0.05	0.09
HIP 41172	0.28	-0.01	0.09	0.37	-0.03	0.10

Table B.13 – continued from previous page

Star	[Fe/H]	[O I/Fe] (λ6300 Å)	[O/Fe] (λ6363 Å)	[Na/Fe]	[Mg/Fe]	[Al/Fe]
HIP 79647	0.16	0.02	0.06	0.10	-0.03	0.01
HIP 85160	0.12	-0.05	0.01	0.11	-0.04	0.03
HIP 80656	0.09	-0.03	-0.05	0.07	-0.01	0.06
HIP 83289	0.24	-0.10	0.07	0.25	0.02	0.05
HIP 79164	0.12	-0.04	0.07	0.13	0.02	0.12
HIP 74080	0.11	-0.08	0.09	0.18	-0.05	0.03

Table B.14: Abundance ratios ([X/Fe]) of elements Si, Ca, Sc, Ti, V and Cr for the member stars of Hyades-Pleiades stream

Star	[Si/Fe]	[Ca/Fe]	[Sc/Fe]	[Ti I/Fe]	[Ti II/Fe]	[V/Fe]	[Cr/Fe]
HIP 65366	0.09	0.06	0.11	0.02	0.11	0.05	0.01
HIP 36739	0.03	0.09	0.00	0.03	0.04	0.03	0.04
HIP 1421	0.02	0.08	0.03	0.01	0.04	0.05	0.03
HIP 88204	0.10	0.01	0.08	0.05	0.03	0.11	0.04
HIP 80839	0.05	0.01	-0.02	-0.11	0.02	-0.02	0.01
HIP 113635	0.18	0.07	0.02	0.08	0.17	0.01	0.03
HIP 113084	0.06	-0.03	-0.02	-0.07	-0.07	-0.01	0.02
HIP 79867	0.13	-0.10	0.05	-0.03	-0.01	0.08	0.04
HIP 51224	0.10	0.11	0.03	0.04	0.04	0.00	0.00
HIP 49163	0.06	0.07	0.10	0.01	0.11	0.09	0.03
HIP 24633	0.05	0.02	-0.01	-0.09	0.03	-0.05	-0.03
HIP 82219	0.03	0.03	-0.02	-0.06	0.03	-0.05	-0.02
HIP 35317	0.06	0.10	0.03	0.00	0.07	0.00	0.01
HIP 117954	0.05	-0.02	-0.02	-0.04	-0.08	-0.01	0.02
HIP 18565	0.03	0.03	-0.02	-0.03	0.02	-0.01	0.01
HIP 6939	0.07	-0.05	0.03	-0.04	-0.09	0.05	0.02

Table B.14 – continued from previous page

Star	[Si/Fe]	[Ca/Fe]	[Sc/Fe]	[Ti I/Fe]	[Ti II/Fe]	[V/Fe]	[Cr/Fe]
HIP 17752	0.07	0.10	0.06	0.06	0.09	0.05	-0.03
HIP 51091	0.07	0.04	0.04	-0.01	0.01	0.03	0.05
HIP 13887	0.04	0.08	-0.09	0.01	-0.01	-0.02	0.00
HIP 114565	-0.01	0.06	-0.05	-0.05	-0.02	-0.04	0.04
HIP 62405	-0.03	0.13	-0.01	0.07	0.01	0.10	0.06
HIP 2320	0.06	0.02	-0.01	-0.04	-0.03	-0.03	0.04
HIP 93589	0.09	0.04	0.04	-0.02	0.05	-0.05	-0.03
HIP 34043	0.04	0.03	-0.04	-0.04	-0.03	-0.04	0.01
HIP 19641	0.05	0.06	0.04	0.03	0.04	0.08	0.05
HIP 56756	0.04	0.04	0.05	0.01	0.03	0.04	0.05
HIP 19222	0.04	0.05	0.01	-0.03	0.01	-0.02	0.02
HIP 41172	0.06	0.04	0.08	-0.01	0.01	0.07	0.01
HIP 79647	0.03	0.01	0.00	-0.04	0.05	-0.04	-0.02
HIP 85160	0.04	0.08	-0.02	-0.02	0.05	0.01	0.01
HIP 80656	0.06	0.04	0.03	-0.01	0.06	0.00	0.00
HIP 83289	0.09	0.02	0.03	-0.05	-0.04	-0.01	0.01
HIP 79164	0.07	0.04	0.05	0.00	0.03	0.00	0.00
HIP 74080	0.05	0.04	-0.01	-0.05	0.06	-0.02	-0.01

Table B.15: Abundance ratios ([X/Fe]) of elements Mn, Co, Ni, Zn and Ba for the member stars of Hyades-Pelaides stream. [Ba/Fe](second last column) is the mean barium abundance from two lines λ 5853.68 Å and λ 6141.73 Å

Star	[Mn/Fe]	[Co/Fe]	[Ni/Fe]	[Zn/Fe]	[Ba/Fe]	[Ba/Fe](λ6496 Å)
HIP 65366	-0.07	0.14	0.04	0.07	0.31	0.40
HIP 36739	-0.09	0.07	0.00	-0.03	0.48	0.62
HIP 1421	-0.04	0.05	0.01	-0.05	0.38	0.41
HIP 88204	-0.06	0.32	0.10	0.18	0.11	0.35

Table B.15 – continued from previous page

Star	[Mn/Fe]	[Co/Fe]	[Ni/Fe]	[Zn/Fe]	[Ba/Fe]	[Ba/Fe](λ6496 Å)
HIP 80839	-0.01	0.13	0.03	0.03	0.28	....
HIP 113635	-0.16	0.28	0.09	0.17	0.22	0.30
HIP 113084	-0.02	0.31	0.12	0.10	0.11	0.33
HIP 79867	-0.09	0.36	0.08	0.20	0.21	0.30
HIP 51224	-0.05	0.14	0.03	0.08	0.31	0.45
HIP 49163	-0.04	0.15	0.05	0.10	0.45	0.56
HIP 24633	-0.08	0.09	0.02	0.02	0.28	0.43
HIP 82219	-0.14	0.03	-0.03	0.03	0.36	...
HIP 35317	-0.09	0.05	0.01	-0.02	0.40	0.49
HIP 117954	-0.07	0.26	0.05	0.06	0.21	0.36
HIP 18565	-0.06	0.14	0.01	0.01	0.32	0.44
HIP 6939	-0.05	0.37	0.12	0.20	0.04	0.31
HIP 17752	-0.05	0.08	-0.01	-0.05	0.42	0.51
HIP 51091	-0.04	0.27	0.08	0.09	0.22	0.47
HIP 13887	-0.06	0.01	0.02	-0.04	0.33	0.48
HIP 114565	-0.11	0.08	0.04	-0.08	0.32	0.41
HIP 62405	0.01	0.10	0.06	0.01	0.39	0.48
HIP 2320	-0.06	0.23	0.08	0.01	0.24	0.38
HIP 93589	-0.11	0.14	0.03	0.08	0.23	0.43
HIP 34043	-0.10	0.07	0.03	-0.01	0.27	0.44
HIP 19641	-0.02	0.18	0.04	-0.03	0.37	0.45
HIP 56756	-0.04	0.25	0.10	0.09	0.25	0.41
HIP 19222	-0.06	0.15	0.06	-0.04	0.28	0.38
HIP 41172	0.02	0.26	0.10	0.12	0.17	0.34
HIP 79647	-0.04	0.15	0.00	0.08	0.31	0.42
HIP 85160	-0.09	0.05	-0.02	-0.01	0.43	0.67
HIP 80656	-0.01	0.08	0.01	-0.02	0.32	0.40
HIP 83289	-0.08	0.17	0.07	0.08	0.17	0.30
HIP 79164	0.00	0.16	0.01	0.03	0.28	0.41
HIP 74080	-0.08	0.05	-0.01	0.06	0.33	0.42

Table B.16: Abundance ratios ([X/Fe]) of elements O, Na, Mg and Al for the member stars of Sirius stream. The starred [Mg/Fe] values are estimated from one single line λ 5711.09 Å, but reliable because of the quality of the line

Star	[Fe/H]	[O/Fe] (λ6300 Å)	[O/Fe] (λ6363 Å)	[Na/Fe]	[Mg/Fe]	[Al/Fe]
HIP 117938	0.21	0.02	0.01	0.16	-0.07	0.03
HIP 26711	0.17	-0.16	-0.07	0.20	-0.07	-0.01
HIP 28556	0.14	0.01	0.02	0.06	-0.08	-0.02
HIP 35431	0.04	-0.18	-0.01	0.17	-0.09	-0.06
HIP 37030	0.00	0.03	0.10	0.11	-0.06	-0.02
HIP 47719	0.18	-0.03	0.01	0.06	-0.06	-0.05
HIP 49103	0.14	0.02	0.08	0.19	0.04	0.12
HIP 51825	0.17	-0.04	0.01	0.21	-0.06	-0.04
HIP 52926	0.07	0.02	0.02	0.09	-0.04	0.01
HIP 53710	0.21	0.07	0.03	0.10	-0.05	0.06
HIP 53876	0.16	-0.09	-0.08	0.17	-0.06	-0.06
HIP 66567	0.05	0.07	0.14	0.03	0.02	0.05
HIP 67021	0.11	0.01	0.04	0.25	0.03	0.14
HIP 67364	0.17	-0.06	0.03	0.13	-0.05	0.03
HIP 68590	0.02	0.08	0.15	0.09	0.03	0.05
HIP 68737	0.15	0.01	0.11	0.16	-0.03	0.07
HIP 68828	0.12	-0.06	-0.12	0.11	-0.04	-0.03
HIP 68935	-0.08	0.07	0.09	0.10	0.10	0.12
HIP 7668	0.01	0.04	0.00	0.18	-0.09	-0.02
HIP 77401	0.14	-0.05	-0.06	-0.02	0.02	0.06
HIP 79326	-0.11	0.06	0.07	0.03	0.10	0.14
HIP 80211	-0.06	0.05	0.05	0.05	0.02	0.05
HIP 7906	0.27	...	0.05	0.19	...	0.03
HIP 15554	-0.12	...	0.18	0.07	0.00$\star$	0.07
HIP 44946	0.25	...	-0.15	0.30	0.10	0.14
HIP 94156	0.22	...	0.02	0.11	0.02$\star$	-0.05
HIP 68418	0.21	...	-0.07	0.08	0.08$\star$	0.12
HIP 76366	0.20	...	-0.03	0.05	-0.04$\star$	0.00

Table B.16 – continued from previous page

Star	[Fe/H]	[O/Fe] (λ6300 Å)	[O/Fe] (λ6363 Å)	[Na/Fe]	[Mg/Fe]	[Al/Fe]
HIP 89065	0.28	...	-0.04	0.03	-0.03$\star$	-0.01
HIP 64179	0.23	...	-0.13	0.04	-0.03$\star$	0.02
HIP 97282	0.25	...	0.01	0.07	....	-0.03
HIP 100116	-0.03	...	0.03	0.28	0.06	0.10
HIP 106771	0.18	...	-0.05	0.08	-0.04$\star$	0.05

Table B.17: Abundance ratios ([X/Fe]) of elements Si, Ca, Sc, Ti, V and Cr for the member stars of Sirius stream

Star	[Si/Fe]	[Ca/Fe]	[Sc/Fe]	[TiI/Fe]	[TiII/Fe]	[V/Fe]	[Cr/Fe]
HIP 117938	0.06	-0.07	0.01	-0.09	-0.07	-0.06	0.00
HIP 26711	0.01	0.05	-0.07	-0.06	-0.05	-0.04	-0.03
HIP 28556	0.05	-0.03	-0.01	-0.08	-0.02	-0.06	-0.03
HIP 35431	-0.04	0.08	-0.05	-0.04	0.05	0.01	-0.01
HIP 37030	0.06	-0.02	0.06	-0.06	-0.03	-0.06	-0.06
HIP 47719	-0.01	-0.06	-0.04	-0.09	-0.06	-0.08	-0.02
HIP 49103	0.08	-0.02	0.03	-0.04	-0.06	-0.02	-0.01
HIP 51825	-0.03	0.05	0.01	-0.03	0.01	-0.03	-0.02
HIP 52926	0.02	0.07	-0.01	0.00	0.02	0.01	0.02
HIP 53710	0.06	-0.07	0.04	-0.03	-0.05	-0.02	0.00
HIP 53876	-0.06	0.05	-0.07	-0.02	-0.01	0.02	-0.01
HIP 66567	0.02	0.04	0.03	0.02	0.03	0.04	0.02
HIP 67021	0.11	-0.02	0.01	-0.02	-0.08	0.03	0.07
HIP 67364	0.06	-0.03	-0.01	-0.12	-0.06	-0.09	-0.01
HIP 68590	0.06	0.06	0.07	0.02	0.04	0.05	0.01
HIP 68737	0.04	0.03	0.05	-0.06	-0.01	-0.02	-0.01
HIP 68828	0.02	0.06	-0.02	-0.06	0.01	-0.05	-0.03

Table B.17 – continued from previous page

Star	[Si/Fe]	[Ca/Fe]	[Sc/Fe]	[TiI/Fe]	[TiII/Fe]	[V/Fe]	[Cr/Fe]
HIP 68935	0.04	0.10	0.01	0.06	0.03	0.07	0.03
HIP 7668	0.12	-0.10	0.02	-0.11	0.00	-0.08	-0.05
HIP 77401	0.13	-0.14	-0.06	-0.10	-0.03	-0.08	-0.03
HIP 79326	0.12	-0.01	0.05	0.00	0.04	0.01	-0.02
HIP 80211	0.07	0.09	0.05	0.02	0.05	0.03	0.01
HIP 7906	0.03	-0.02	0.10	-0.06	0.03	0.02	-0.05
HIP 15554	0.09	0.07	0.04	0.03	0.03	-0.02	-0.04
HIP 44946	0.07	0.05	-0.05	-0.08	-0.01	0.07	0.01
HIP 94156	0.07	-0.12	-0.01	-0.18	-0.06	-0.17	-0.08
HIP 68418	0.13	-0.06	0.03	-0.09	-0.09	-0.03	-0.05
HIP 76366	0.06	-0.07	-0.01	-0.06	0.00	-0.07	-0.05
HIP 89065	0.07	-0.10	0.09	-0.11	-0.02	-0.09	-0.06
HIP 64179	0.08	-0.01	0.04	-0.13	-0.04	-0.03	-0.03
HIP 97282	...	-0.06	0.06	-0.10	0.03	-0.04	-0.04
HIP 100116	0.12	0.00	0.06	-0.01	-0.01	0.01	0.04
HIP 106771	0.07	-0.01	-0.05	-0.12	-0.12	-0.05	-0.01

Table B.18: Abundance ratios ([X/Fe]) of elements Mn, Co, Ni, Zn and Ba for the member stars of Sirius stream. [Ba/Fe] (second last column) is the mean barium abundance from two lines λ 5853.68 Å and λ 6141.73 Å

Star	[Mn/Fe]	[Co/Fe]	[Ni/Fe]	[Zn/Fe]	[Ba/Fe]	[Ba/Fe](λ6496 Å)
HIP 117938	-0.17	0.23	0.02	0.09	0.32	0.43
HIP 26711	-0.08	-0.02	-0.06	-0.08	0.45	0.59
HIP 28556	-0.12	0.19	-0.05	0.04	0.39	0.56
HIP 35431	-0.15	0.01	-0.09	-0.09	0.58	0.635
HIP 37030	-0.12	0.11	-0.04	-0.01	0.52	0.58
HIP 47719	-0.11	0.13	-0.02	0.02	0.35	0.47

Table B.18 – continued from previous page

Star	[Mn/Fe]	[Co/Fe]	[Ni/Fe]	[Zn/Fe]	[Ba/Fe]	[Ba/Fe](λ6496 Å)
HIP 49103	-0.08	0.28	0.04	0.05	0.31	0.49
HIP 51825	-0.06	-0.01	-0.05	-0.05	0.38	0.62
HIP 52926	-0.07	0.05	-0.02	-0.06	0.43	0.51
HIP 53710	-0.19	0.24	0.02	-0.02	0.47	0.59
HIP 53876	-0.06	0.00	-0.07	-0.10	0.45	0.60
HIP 66567	-0.07	0.11	-0.01	-0.04	0.27	0.35
HIP 67021	-0.11	0.30	0.03	0.15	0.32	0.46
HIP 67364	-0.09	0.20	0.02	0.10	0.25	0.37
HIP 68590	-0.08	0.12	0.02	0.02	0.35	0.46
HIP 68737	-0.05	0.14	0.04	0.07	0.24	0.38
HIP 68828	-0.13	-0.02	-0.05	-0.06	0.42	0.56
HIP 68935	-0.07	0.13	0.02	0.03	0.23	0.32
HIP 7668	-0.20	0.17	-0.01	...	0.55	0.55
HIP 77401	-0.19	0.23	0.02	0.09	0.27	0.38
HIP 79326	-0.17	0.23	-0.01	0.18	0.19	0.31
HIP 80211	-0.08	0.03	-0.03	-0.04	0.44	0.52
HIP 7906	-0.07	0.08	-0.08	-0.09	0.51	0.59
HIP 15554	-0.12	0.14	-0.05	0.07	0.39	0.54
HIP 44946	-0.04	0.06	-0.06	-0.18	0.38	0.72
HIP 94156	-0.20	0.15	-0.10	0.17	0.47	0.56
HIP 68418	-0.09	0.29	-0.01	0.07	0.34	0.47
HIP 76366	-0.09	0.16	-0.10	...	0.55	0.61
HIP 89065	-0.12	0.19	-0.05	-0.09	0.44	0.56
HIP 64179	-0.07	0.11	-0.07	-0.10	0.37	0.41
HIP 97282	-0.06	0.25	-0.02	0.07	0.37	0.47
HIP 100116	-0.06	0.16	-0.08	-0.09	0.55	0.62
HIP 106771	-0.15	0.19	-0.07	-0.10	0.44	0.54

REFERENCES

Abadi M. G., Navarro J. F., Steinmetz M., Eke V. R., 2003a, ApJ, 591, 499

Abadi M. G., Navarro J. F., Steinmetz M., Eke V. R., 2003b, ApJ, 597, 21

Ali A., 1940, MNRAS, 100, 570

Allende Prieto C., Barklem P. S., Lambert D. L., Cunha K., 2004, A&A, 420, 183

Allende Prieto C., Lambert D. L., Asplund M., 2001, ApJ, 556, L63

Alonso A., Arribas S., Martinez-Roger C., 1996, A&A, 313, 873

Alonso A., Arribas S., Martínez-Roger C., 1999, A&AS, 140, 261

Amaral L. H., Lepine J. R. D., 1997, MNRAS, 286, 885

Ammler-von Eiff M., Guenther E. W., 2009, A&A, 508, 677

Antoja T., Figueras F., Fernández D., Torra J., 2008, A&A, 490, 135

Antoja T., Figueras F., Torra J., Valenzuela O., Pichardo B., 2010, Lecture Notes and Essays in Astrophysics, 4, 13

Antoja T., Valenzuela O., Pichardo B., Moreno E., Figueras F., Fernández D., 2009, ApJ, 700, L78

Arce H. G., Goodman A. A., 1999, ApJ, 512, L135

Arifyanto M. I., Fuchs B., 2006, A&A, 449, 533

Arnold R., Gilmore G., 1992, MNRAS, 257, 225

Asiain R., Figueras F., Torra J., Chen B., 1999, A&A, 341, 427

Asplund M., Grevesse N., Sauval A. J., Scott P., 2009, ARA&A, 47, 481

Baade W., 1944, ApJ, 100, 137

Baranne A., Mayor M., Poncet J. L., 1979, Vistas in Astronomy, 23, 279

Beers T. C., Chiba M., Yoshii Y., Platais I., Hanson R. B., Fuchs B., Rossi S., 2000, AJ, 119, 2866

Belokurov V., Zucker D. B., 2006, ApJ, 642, L137

Bensby T., Feltzing S., Lundström I., 2003, A&A, 410, 527

Bensby T., Feltzing S., Lundström I., 2004, A&A, 415, 155

Bensby T., Feltzing S., Lundström I., Ilyin I., 2005, A&A, 433, 185

Bensby T., Oey M. S., Feltzing S., Gustafsson B., 2007, ApJ, 655, L89

Bessell M. S., 2005, ARA&A, 43, 293

Biazzo K., D'Orazi V., Desidera S., Covino E., Alcalá J. M., Zusi M., 2012, MNRAS, 427, 2905

Bienaymé O., 1999, A&A, 341, 86

Blaauw A., 1964, ARA&A, 2, 213

Blumenthal G. R., Faber S. M., Primack J. R., Rees M. J., 1984, Nature, 311, 517

Boesgaard A. M., Budge K. G., Burck E. E., 1988, ApJ, 325, 749

Boesgaard A. M., Friel E. D., 1990, ApJ, 351, 467

Bonifacio P., Monai S., Beers T. C., 2000, AJ, 120, 2065

BOSS L. J., 1908, AJ, 26, 31

Bovy J., Hogg D. W., Roweis S. T., 2009, ApJ, 700, 1794

Briceño C., 2009, in Revista Mexicana de Astronomia y Astrofisica Conference Series Vol. 35 of Revista Mexicana de Astronomia y Astrofisica Conference Series, OB Associations: new insights from large scale surveys. pp 27–32

Bullock J. S., Johnston K. V., 2005, ApJ, 635, 931

Burstein D., 1979, ApJ, 234, 829

Carney B. W., Latham D. W., Laird J. B., Aguilar L. A., 1994, AJ, 107, 2240

Cayrel R., 1988, in Cayrel de Strobel G., Spite M., eds, The Impact of Very High S/N Spectroscopy on Stellar Physics. Kluwer Dordrecht, p.345

Carraro G., Beletsky Y., Marconi G., 2013a, MNRAS, 428, 502

Carraro G., Beletsky Y., Marconi G., 2013b, MNRAS, 428, 502

Carrera R., Pancino E., 2011, A&A, 535, A30

Castelli F., Gratton R. G., Kurucz R. L., 1997, A&A, 318, 841

Chaboyer B., Green E. M., Liebert J., 1999, AJ, 117, 1360

Chakrabarty D., 2007, A&A, 467, 145

Chen B., Asiain R., Figueras F., Torra J., 1997, A&A, 318, 29

Chereul E., Creze M., Bienayme O., 1998, A&A, 340, 384

Chereul E., Crézé M., Bienaymé O., 1999, A&AS, 135, 5

Cutri R. M., Skrutskie M. F., van Dyk S., Beichman C. A., Carpenter J. M., 2003, 2MASS All Sky Catalog of point sources.

D'Antona F., Caloi V., D'Ercole A., Tailo M., Vesperini E., Ventura P., Di Criscienzo M., 2013, MNRAS, 434, 1138

De Silva G. M., Freeman K. C., Bland-Hawthorn J., Asplund M., Bessell M. S., 2007, AJ, 133, 694

de Silva G. M., Freeman K. C., Bland-Hawthorn J., Asplund M., Williams M., Holmberg J., 2011, MNRAS, 415, 563

De Silva G. M., Sneden C., Paulson D. B., Asplund M., Bland-Hawthorn J., Bessell M. S., Freeman K. C., 2006, AJ, 131, 455

De Simone R., Wu X., Tremaine S., 2004, MNRAS, 350, 627

Dehnen W., 1998, AJ, 115, 2384

Dehnen W., 1999, ApJ, 524, L35

Dehnen W., 2000, AJ, 119, 800

Dehnen W., Binney J. J., 1998, MNRAS, 298, 387

Demarque P., Woo J.-H., Kim Y.-C., Yi S. K., 2004, ApJS, 155, 667

Dettbarn C., Fuchs B., Flynn C., Williams M., 2007, A&A, 474, 857

Doinidis S. P., Beers T. C., 1989, ApJ, 340, L57

D'Orazi V., Biazzo K., Desidera S., Covino E., Andrievsky S. M., Gratton R. G., 2012, MNRAS, 423, 2789

Drimmel R., Spergel D. N., 2001, ApJ, 556, 181

Eggen O. J., 1957, The Observatory, 77, 229

Eggen O. J., 1958a, MNRAS, 118, 65

Eggen O. J., 1958b, MNRAS, 118, 154

Eggen O. J., 1959, The Observatory, 79, 182

Eggen O. J., 1960, MNRAS, 120, 563

Eggen O. J., 1971a, ApJS, 22, 389

Eggen O. J., 1971b, ApJ, 165, 317

Eggen O. J., 1971c, PASP, 83, 271

Eggen O. J., 1971d, PASP, 83, 251

Eggen O. J., 1977, ApJ, 215, 812

Eggen O. J., 1984, AJ, 89, 830

Eggen O. J., 1986, AJ, 92, 910

Eggen O. J., 1992a, AJ, 104, 1482

Eggen O. J., 1992b, AJ, 104, 1493

Wilson G, 1990, PhD Thesis, Australian National University. Eggen O. J., 1994, in Galactic and Solar System Optical Astrometry, 191

Eggen O. J., 1995, AJ, 110, 2862

Eggen O. J., 1996, AJ, 112, 1595

Eggen O. J., 1997, AJ, 114, 825

Eggen O. J., 1998a, AJ, 115, 2435

Eggen O. J., 1998b, AJ, 115, 2397

Eggen O. J., 1998c, AJ, 115, 2453

Eggen O. J., 1998d, AJ, 116, 1810

Eggen O. J., 1998e, AJ, 116, 782

Famaey B., Jorissen A., Luri X., Mayor M., Udry S., Dejonghe H., Turon C., 2005, A&A, 430, 165

Famaey B., Pont F., Luri X., Udry S., Mayor M., Jorissen A., 2007, A&A, 461, 957

Famaey B., Siebert A., Jorissen A., 2008, A&A, 483, 453

Figueras F., Gomez A. E., Asiain R., Chen B., Comeron F., Grenier S., Lebreton Y., Moreno M., Sabas V., Torra J., 1997, in Bonnet R. M., Hg E., Bernacca P. L., Emiliani L., Blaauw A., Turon C., Kovalevsky J., Lindegren L., Hassan H., Bouffard M., Strim B., Heger D., Perryman M. A. C., Woltjer L., eds, Hipparcos - Venice '97 Vol. 402 of ESA Special Publication, Identification of Moving Groups in a Sample of Early-Type Main-Sequence Stars. pp 519–524

Freeman K., Bland-Hawthorn J., 2002, ARA&A, 40, 487

Fuhrmann K., 2004, Astronomische Nachrichten, 325, 3

Fux R., 2000, in Combes F., Mamon G. A., Charmandaris V., eds, Dynamics of Galaxies: from the Early Universe to the Present Vol. 197 of Astronomical Society of the Pacific Conference Series, Stellar Streams in the Solar Neighbourhood from High Resolution N-Body Simulations. p. 27

Fux R., 2001, A&A, 373, 511

Gardner E., Flynn C., 2010, MNRAS, 405, 545

Giannuzzi M. A., 1979, A&A, 77, 214

Gilmore G., Reid N., 1983, MNRAS, 202, 1025

Gomez A. E., Delhaye J., Grenier S., Jaschek C., Arenou F., Jaschek M., 1990, A&A, 236, 95

Gómez F. A., Minchev I., O'Shea B. W., Lee Y. S., Beers T. C., An D., Bullock J. S., Purcell C. W., Villalobos Á., 2012, MNRAS, 423, 3727

Gould A., 2003, ApJ, 592, L63

Gratton R., Sneden C., Carretta E., 2004, ARA&A, 42, 385

Gratton R. G., Carretta E., Claudi R., Lucatello S., Barbieri M., 2003, A&A, 404, 187

Gustafsson B., Bell R. A., Eriksson K., Nordlund A., 1975, A&A, 42, 407

Gustafsson B., Edvardsson B., Eriksson K., Jrgensen U. G., Nordlund ., Plez B., 2008, A&A, 486, 951

Hauck B., Mermilliod M., 1998, A&AS, 129, 431

Helmi A., 2008, A&A Rev., 15, 145

Helmi A., de Zeeuw P. T., 2000, MNRAS, 319, 657

Helmi A., Navarro J. F., Meza A., Steinmetz M., Eke V. R., 2003, ApJ, 592, L25

Helmi A., Navarro J. F., Nordström B., Holmberg J., Abadi M. G., Steinmetz M., 2006, MNRAS, 365, 1309

Helmi A., White S. D. M., 1999, MNRAS, 307, 495

Herschel W., 1784, Royal Society of London Philosophical Transactions Series I, 74, 437

Herschel W., 1785, Royal Society of London Philosophical Transactions Series I, 75, 213

Hertzsprung E., 1909, ApJ, 30, 135

Hinkle K., Wallace L., Valenti J., & Harmer D. (ed.) 2000, Visible and Near Infrared Atlas of the Arcturus Spectrum 3727−9300 (San Francisco, CA:ASP)

Huggins W., 1871, Royal Society of London Proceedings Series I, 20, 379

Ibata R., Lewis G. F., Irwin M., Totten E., Quinn T., 2001, ApJ, 551, 294

Ibata R. A., Gilmore G., Irwin M. J., 1994, Nature, 370, 194

Ivezić Ž., Beers T. C., Jurić M., 2012, ARA&A, 50, 251

Johnson D. R. H., Soderblom D. R., 1987, AJ, 93, 864

Kalnajs A. J., 1991, in Sundelius B., ed., Dynamics of Disc Galaxies Pattern Speeds of Density Waves. p. 323

Kapteyn J. C., 1914, ApJ, 40, 43

Kapteyn J. C., 1922, ApJ, 55, 302

Kapteyn J. C., van Rhijn P. J., 1920, ApJ, 52, 23

Kazantzidis S., Bullock J. S., Zentner A. R., Kravtsov A. V., Moustakas L. A., 2008, ApJ, 688, 254

Kharchenko N. V., 2001, Kinematika i Fizika Nebesnykh Tel, 17, 409

King J. R., Schuler S. C., 2005, PASP, 117, 911

King J. R., Villarreal A. R., Soderblom D. R., Gulliver A. F., Adelman S. J., 2003, AJ, 125, 1980

Kirby E. N., Guhathakurta P., Simon J. D., Geha M. C., Rockosi C. M., Sneden C., Cohen J. G., Sohn S. T., Majewski S. R., Siegel M., 2010, ApJS, 191, 352

Klement R., Fuchs B., Rix H.-W., 2008, ApJ, 685, 261

Klement R., Rix H.-W., Flynn C., Fuchs B., Beers T. C., Allende Prieto C., Bizyaev D., Brewington H., Lee Y. S., Malanushenko E., Malanushenko V., Oravetz D., Pan K., Re Fiorentin P., Simmons A., Snedden S., 2009, ApJ, 698, 865

Klement R. J., 2010, A&A Rev., 18, 567

König B., Fuhrmann K., Neuhäuser R., Charbonneau D., Jayawardhana R., 2002, A&A, 394, L43

Kurucz R.L., 1998, http://kurucz.harvard.edu/ (online data)

Lada C. J., 2010, Royal Society of London Philosophical Transactions Series A, 368, 713

Lada C. J., Lada E. A., 2003, ARA&A, 41, 57

Lambert D. L., 1978, MNRAS, 182, 249

Levato H., Abt H. A., 1978, PASP, 90, 429

Lin C. C., Yuan C., Shu F. H., 1969, ApJ, 155, 721

Lindblad B., 1925, ApJ, 62, 191

Mädler J. H., 1846, Astronomische Nachrichten, 24, 213

Majewski S. R., Munn J. A., Hawley S. L., 1996, ApJ, 459, L73

Majewski S. R., Skrutskie M. F., Weinberg M. D., Ostheimer J. C., 2003, ApJ, 599, 1082

Maldonado J., Martínez-Arnáiz R. M., Eiroa C., Montes D., Montesinos B., 2010, A&A, 521, A12

Mayor M., 1972, A&A, 18, 97

Mayor M., 1985, in Philip A. G. D., Latham D. W., eds, Stellar Radial Velocities Cross-correlation spectroscopy using CORAVEL.. pp 35–48

McWilliam A., 1990, ApJS, 74, 1075

Meza A., Navarro J. F., Abadi M. G., Steinmetz M., 2005, MNRAS, 359, 93

Minchev I., Famaey B., 2010, ApJ, 722, 112

Minchev I., Quillen A. C., Williams M., Freeman K. C., Nordhaus J., Siebert A., Bienaymé O., 2009, MNRAS, 396, L56

Mishenina T. V., Soubiran C., Kovtyukh V. V., Korotin S. A., 2004, A&A, 418, 551

Monaco L., Bellazzini M., Bonifacio P., Ferraro F. R., Marconi G., Pancino E., Sbordone L., Zaggia S., 2005, A&A, 441, 141

Monari G., Antoja T., Helmi A., 2013, ArXiv e-prints

Montes D., López-Santiago J., Gálvez M. C., Fernández-Figueroa M. J., De Castro E., Cornide M., 2001, MNRAS, 328, 45

Navarro J. F., 2004, in Block D. L., Puerari I., Freeman K. C., Groess R., Block E. K., eds, Penetrating Bars Through Masks of Cosmic Dust Vol. 319 of Astrophysics and Space Science Library, The Hierarchical Formation of the Galactic Disk. p. 655

Navarro J. F., Helmi A., Freeman K. C., 2004, ApJ, 601, L43

Newberg H. J., Yanny B., Rockosi C., Grebel E. K., Rix H.-W., Brinkmann J., Csabai I., Hennessy G., Hindsley R. B., Ibata R., Ivezić Z., Lamb D., Nash E. T., Odenkirchen M., Rave H. A., Schneider D. P., Smith J. A., Stolte A., York D. G., 2002, ApJ, 569, 245

Nordström B., Mayor M., Andersen J., Holmberg J., Pont F., J*rgensenB. R.*, *OlsenE. H.*, *UdryS.*, *MowlaviN.*, 2004, *A&A*, 418, 989

Ojha D. K., Bienaymé O., Mohan V., Robin A. C., 1999, A&A, 351, 945

Ojha D. K., Bienayme O., Robin A. C., Creze M., Mohan V., 1996, A&A, 311, 456

Pakhomov Y. V., Antipova L. I., Boyarchuk A. A., 2011, Astronomy Reports, 55, 256

Pancino E., Rejkuba M., Zoccali M., Carrera R., 2010, A&A, 524, A44

Paulson D. B., Yelda S., 2006, PASP, 118, 706

Paunzen E., Heiter U., Netopil M., Soubiran C., 2010, A&A, 517, A32

Peebles P. J. E., 1974, ApJ, 189, L51

Perryman M. A. C., Brown A. G. A., Lebreton Y., Gomez A., Turon C., Cayrel de Strobel G., Mermilliod J. C., Robichon N., Kovalevsky J., Crifo F., 1998, A&A, 331, 81

Perryman M. A. C., Lindegren L., Kovalevsky J., Hoeg E., Bastian U., Bernacca P. L., Crézé M., Donati F., Grenon M., Grewing 1997, A&A, 323, L49

Peterson R. C., Dalle Ore C. M., Kurucz R. L., 1993, ApJ, 404, 333

Petrie R. M., 1953, JRASC, 47, 185

Phelps R. L., 1997, ApJ, 483, 826

Pompéia L., Masseron T., Famaey B., van Eck S., Jorissen A., Minchev I., Siebert A., Sneden C., 2011, MNRAS, 415, 1138

Proctor R. A., 1869, Royal Society of London Proceedings Series I, 18, 169

Quillen A. C., 2003, AJ, 125, 785

Quillen A. C., Minchev I., 2005, AJ, 130, 576

Raboud D., Grenon M., Martinet L., Fux R., Udry S., 1998, A&A, 335, L61

Ramírez I., Allende Prieto C., 2011, ApJ, 743, 135

Ramírez I., Meléndez J., 2005, ApJ, 626, 446

Rao N. K., Sriram S., Jayakumar K., Gabriel F., 2005, Journal of Astrophysics and Astronomy, 26, 331

Reddy B. E., 2010, in Cunha K., Spite M., Barbuy B., eds, IAU Symposium Vol. 265 of IAU Symposium, The Galactic Thick Disk: An Observational Perspective. pp 289–299

Reddy B. E., Lambert D. L., Allende Prieto C., 2006, MNRAS, 367, 1329

Reddy B. E., Tomkin J., Lambert D. L., Allende Prieto C., 2003, MNRAS, 340, 304

Robin A. C., Reylé C., Derrière S., Picaud S., 2003, A&A, 409, 523

Roman N. G., 1949, ApJ, 110, 205

Sarajedini A., von Hippel T., Kozhurina-Platais V., Demarque P., 1999, AJ, 118, 2894

Schlegel D. J., Finkbeiner D. P., Davis M., 1998, ApJ, 500, 525

Schuster W. J., Nissen P. E., 1989, A&A, 221, 65

Seabroke G. M., Gilmore G., Siebert A., Bienaymé O., Binney J., Bland-Hawthorn J., Campbell R., 2008, MNRAS, 384, 11

Sellwood J. A., Binney J. J., 2002, MNRAS, 336, 785

Shapley H., Shapley M. B., 1919, ApJ, 50, 107

Skrutskie M. F., Cutri R. M., Stiening R., Weinberg M. D., Schneider S., Carpenter J. M., Beichman C., 2006, AJ, 131, 1163

Skuljan J., Hearnshaw J. B., Cottrell P. L., 1999, MNRAS, 308, 731

Smart W. M., 1939, MNRAS, 99, 441

Smiljanic R., 2012, MNRAS, 422, 1562

Sneden C., 1973, PhD Thesis, University of Texas, Austin

Sneden C., McWilliam A., Preston G. W., Cowan J. J., Burris D. L., Armosky B. J., 1996, ApJ, 467, 819

Soderblom D. R., Mayor M., 1993, AJ, 105, 226

Soubiran C., Bienaymé O., Siebert A., 2003, A&A, 398, 141

Steinmetz M., Zwitter T., Siebert A., Watson F. G., Freeman K. C., Munari U., Campbell R., Williams M., Seabroke G. M., Wyse R. F. G., 2006, AJ, 132, 1645

Stoughton C., Lupton R. H., Bernardi M., Blanton M. R., Burles S., Castander F. J., Connolly A. J., Eisenstein D. J., Frieman J. A., Hennessy G. S., Hindsley R. B., Ivezić Ž., Kent S., 2002, AJ, 123, 485

Tabernero H. M., Montes D., González Hernández J. I., 2012, A&A, 547, A13

Tolstoy E., Hill V., Tosi M., 2009, ARA&A, 47, 371

Trumpler R. J., 1930, Lick Observatory Bulletin, 14, 154

Tull R. G., MacQueen P. J., Sneden C., Lambert D. L., 1995, PASP, 107, 251

Vallée J. P., 2002, ApJ, 566, 261

van Leeuwen F., 2007, A&A, 474, 653

van Leeuwen F., 2009, A&A, 497, 209

Venn K. A., Irwin M., Shetrone M. D., Tout C. A., Hill V., Tolstoy E., 2004, AJ, 128, 1177

Villalobos Á., Helmi A., 2009, MNRAS, 399, 166

von Hoerner S., 1957, ZAp, 42, 273

White S. D. M., Rees M. J., 1978, MNRAS, 183, 341

Wielen R., 1971, A&A, 13, 309

Wielen R., 1978, in Bulletin of the American Astronomical Society Vol. 10 of Bulletin of the American Astronomical Society, Kinematics and Structure of the Ursa Major Star Cluster. p. 408

Williams M. E. K., Freeman K. C., Helmi A., RAVE Collaboration 2009, in J. Andersen, J. Bland-Hawthorn, & B. Nordström ed., IAU Symposium Vol. 254 of IAU Symposium, The Arcturus Moving Group: Its Place in the Galaxy. pp 139–144

Wilson G, 1990, PhD Thesis, Australian National University.

Wilson R. E., 1932, AJ, 42, 49

Woolley R., 1961, The Observatory, 81, 203

Woosley S. E., Heger A., Weaver T. A., 2002, Reviews of Modern Physics, 74, 1015

Wyse R. F. G., Gilmore G., Franx M., 1997, ARA&A, 35, 637

Yanny B., Newberg H. J., Grebel E. K., Kent S., Odenkirchen M., Rockosi C. M., Schlegel D., Subbarao M., Brinkmann J., Fukugita M., Ivezic Ž., Lamb D. Q., Schneider D. P., York D. G., 2003, ApJ, 588, 824

Yanny B., Rockosi C., Newberg H. J., Knapp G. R., Adelman-McCarthy J. K., Alcorn B., Allam S., 2009, AJ, 137, 4377

Zhao J., Zhao G., Chen Y., 2009, ApJ, 692, L113